THE BIOGEOCHEMISTRY, BIOPHYSICS, RADIOBIOLOGY, AND TECHNICAL CHALLENGES OF DEEP SUBSURFACE RESEARCH

EDITED BY: Geoffrey Battle Smith, Maria Antonella Tabocchini and Carlos Peña Garay

PUBLISHED IN: Frontiers in Public Health, Frontiers in Earth Science, Frontiers in Microbiology, Frontiers in Physics and Frontiers in Astronomy and Space Sciences

frontiers Research Topics

ISSN 1664-8714
ISBN 978-2-88966-892-2
DOI 10.3389/978-2-88966-892-2

About Frontiers

Frontiers is more than just an open-access publisher of scholarly articles: it is a pioneering approach to the world of academia, radically improving the way scholarly research is managed. The grand vision of Frontiers is a world where all people have an equal opportunity to seek, share and generate knowledge. Frontiers provides immediate and permanent online open access to all its publications, but this alone is not enough to realize our grand goals.

Frontiers Journal Series

The Frontiers Journal Series is a multi-tier and interdisciplinary set of open-access, online journals, promising a paradigm shift from the current review, selection and dissemination processes in academic publishing. All Frontiers journals are driven by researchers for researchers; therefore, they constitute a service to the scholarly community. At the same time, the Frontiers Journal Series operates on a revolutionary invention, the tiered publishing system, initially addressing specific communities of scholars, and gradually climbing up to broader public understanding, thus serving the interests of the lay society, too.

Dedication to Quality

Each Frontiers article is a landmark of the highest quality, thanks to genuinely collaborative interactions between authors and review editors, who include some of the world's best academicians. Research must be certified by peers before entering a stream of knowledge that may eventually reach the public - and shape society; therefore, Frontiers only applies the most rigorous and unbiased reviews.
Frontiers revolutionizes research publishing by freely delivering the most outstanding research, evaluated with no bias from both the academic and social point of view. By applying the most advanced information technologies, Frontiers is catapulting scholarly publishing into a new generation.

What are Frontiers Research Topics?

Frontiers Research Topics are very popular trademarks of the Frontiers Journals Series: they are collections of at least ten articles, all centered on a particular subject. With their unique mix of varied contributions from Original Research to Review Articles, Frontiers Research Topics unify the most influential researchers, the latest key findings and historical advances in a hot research area! Find out more on how to host your own Frontiers Research Topic or contribute to one as an author by contacting the Frontiers Editorial Office: frontiersin.org/about/contact

THE BIOGEOCHEMISTRY, BIOPHYSICS, RADIOBIOLOGY, AND TECHNICAL CHALLENGES OF DEEP SUBSURFACE RESEARCH

Topic Editors:
Geoffrey Battle Smith, New Mexico State University, United States
Maria Antonella Tabocchini, National Institute of Health (ISS), Italy
Carlos Peña Garay, Laboratorio Subterráneo de Canfranc, Spain

Citation: Smith, G. B., Tabocchini, M. A., Garay, C. P., eds. (2021). The Biogeochemistry, Biophysics, Radiobiology, and Technical Challenges of Deep Subsurface Research. Lausanne: Frontiers Media SA. doi: 10.3389/978-2-88966-892-2

Table of Contents

4. RADIOBIOLOGY

frontiers in Earth Science

EDITORIAL
published: 13 May 2021
doi: 10.3389/feart.2021.678034

Editorial: The Biogeochemistry, Biophysics, Radiobiology, and Technical Challenges of Deep Subsurface Research

Geoffrey Battle Smith[1]*, *Maria Antonella Tabocchini*[2,3] *and Carlos Peña Garay*[4]

[1] Department of Biology, New Mexico State University, Las Cruces, NM, United States, [2] Istituto Superiore di Sanità (ISS), Rome, Italy, [3] Istituto Nazionale di Fisica Nucleare (INFN) Sezione Roma 1, Rome, Italy, [4] Laboratorio Subterráneo de Canfranc, Canfranc, Spain

Keywords: subsurface science, radiation biology, biogeochemistry, below background radiation, biophysics, radiation health effects

Editorial on the Research Topic

The Biogeochemistry, Biophysics, Radiobiology, and Technical Challenges of Deep Subsurface Research

Numerous earth science projects are being carried out worldwide in the underground in both natural settings and laboratories. Life in the deep subsurface is dominated by microbes, which in turn directly impact the subsurface physicochemistry. The diversity of subsurface environments and interfaces that are able to sustain life, and the range of lifestyles that organisms have developed to exploit these systems give insight on how life has adapted to these unusual conditions, and this in turn illuminates potential conditions for life on other planets. As more labs, mines and other commercial facilities are installed internationally, the impacts of subsurface conditions on humans have become increasingly important. Model organisms from the surface ranging from bacterium to fly to fish and worm are brought underground to test the benefits or consequences to life underground. The absence of natural levels of radiation in the subsurface allows for the experimental testing of the hypothesis that background, surface levels of radiation maintain fitness. In this Research Topic, some articles document subsurface prokaryotic life extremes and others focus on the biological response and adaptation to deep subsurface environments as well as on the technical challenges associated with this research. This is a highly cross-disciplinary collection, reflecting the expertise required in Biology, Physics and Geochemistry to successfully work in this field.

The cover photos for this Research Topic show a researcher in the Italian cave, *Grotta Grande dei Cervi*, and a microbial consortium of iron oxidizers that colonize pyrite in Spain's Iberian Pyrite Belt (details reported in Vacarelli et al., and Escudero et al., respectively). The photos thus represent two of the many scales used in deep subsurface research, which utilizes measurements ranging from astronomical to subatomic. As an indication of the vitality of the discipline we note 14 deep underground laboratories worldwide (Ianni), with two international astroparticle physics labs (UK's Boulby and Canada's SNOLAB) recently starting up new underground Biology laboratories (Boulby Astrobiology Lab, "BISAL" reported by Wadsworth et al. and the REPAIR project at SNOLAB, reported by Pirkkanen et al.).

Papers on biogeochemistry, radiation biology, astrobiology, and methods in mitigating background radiation are covered in this collection. Escudero et al. report on the influence of pyrite on the distribution of the iron-oxidizing *Acidovorax* bacterial group using an innovative approach combining catalyzed reporter deposition fluorescence *in-situ* hybridization and fluorescence plus

OPEN ACCESS

Edited and reviewed by:
Alexandra V. Turchyn, University of Cambridge, United Kingdom

***Correspondence:**
Geoffrey Battle Smith
gsmith@nmsu.edu

Specialty section:
This article was submitted to Biogeoscience, a section of the journal Frontiers in Earth Science

Received: *08 March 2021*
Accepted: *09 April 2021*
Published: *13 May 2021*

Citation:
Smith GB, Tabocchini MA and Garay CP (2021) Editorial: The Biogeochemistry, Biophysics, Radiobiology, and Technical Challenges of Deep Subsurface Research. Front. Earth Sci. 9:678034. doi: 10.3389/feart.2021.678034

confocal Raman microscopy. Intriguing evidence that the *Acidovorax* species in these deep subsurface samples may oxidize pyrite mineral is presented. Vaccarelli et al. combine electron dispersive spectroscopy and scanning microscopy with DNA analysis to report on the association of cave manganese laminae and microbial biosignatures. These reports have application to identifying conditions that may support life in other planetary systems. A biogeochemistry paper with industrial application by Ren et al., reports on the microbial communities in oil production wells, demonstrating by pyrosequencing analysis that different methods of oil extraction significantly shift the oil field microflora.

A number of the radiation biology papers report on the remarkable biological response to below background radiation. Statistically significant responses of mammalian tissue culture (Liu et al.), whitefish (Pirkkanen et al.), fruit fly (Esposito et al.) and nematode (Van Voorhies et al.) provide evidence that multiple organismal models "notice" minute differences in radiation fields and respond to sub-background radiation levels at the proteomic, transcriptomic and physiological levels.

Some papers show how underground biology studies are relevant not only for improving our knowledge on life evolution, but also for assessing the robustness of the present radiation protection system that currently assumes that public health risk is linearly related to the radiation dose. The review by Belli and Indovina describes the mechanisms involved in the biological response to low dose and protracted exposures, particularly to natural background radiation and emphasizes how cell response to low doses appears more complex than that assumed for radiation protection purposes and is not always detrimental. Overall, data suggest the hypothesis that environmental radiation contributes to the development and maintenance of homeostatic balance and defense response in living organisms.

Further studies on pKZ1 A11 mouse hybridoma cells (Fischietti et al.) analyzed proliferation and expression of key proteins involved in stress response, apoptosis, and autophagy in underground and above ground environments. The results showed differential response to growth-stress conditions with a switch from apoptosis to autophagy, correlated with activation of p53, in the underground environment. They also suggest a scarce contribution of the gamma component of environmental radiation in triggering the biological response. This is an issue presently under investigation at the Laboratori Nazionali del Gran Sasso (LNGS, Esposito et al.). The RENOIR experiment, recently launched, is aimed at improving knowledge on the environmental radiation spectrum and to investigate the specific role of the gamma component on the biological response of *Drosophila melanogaster*.

Future low background biological experiments will require better control on the radioactive backgrounds. Underground laboratories provide a natural reduction of cosmic radiation, while radioactive decays from potassium-40 and the naturally occurring decay chains from uranium-238, uranium-235 and thorium-232 should be reduced by experimental design. Current most sensitive ultra-low background detection techniques and best level of background reduction are discussed by Laubenstein and Lawson, who coordinate a worldwide germanium detectors cross-calibration program. The gamma background is dominated by radon emanation, which is generally larger underground and should be reduced by ventilation. Further reduction requires the use of low radon cleanrooms. A detailed discussion of prototyping this installation is presented by Štekl et al., who discussed both the control of radon concentration in air and radon decay products on surfaces. Potassium-40 is singular among the radioactive isotopes because it is necessary for the function of all living cells. Tomasi discusses the interesting proposal for the therapeutic use of potassium enriched in the K-40 isotope for patients suffering from diseases caused by mitochondrial dysfunctions.

AUTHOR CONTRIBUTIONS

All authors listed have made a substantial, direct and intellectual contribution to the work, and approved it for publication.

Conflict of Interest: The authors declare that the research was conducted in the absence of any commercial or financial relationships that could be construed as a potential conflict of interest.

frontiers in Physics

MINI REVIEW
published: 23 February 2021
doi: 10.3389/fphy.2021.612417

Science in Underground Laboratories and DULIA-Bio

*Aldo Ianni**

LNGS-INFN, L'Aquila, Italy

This paper reports a brief introduction to Deep Underground Laboratories (DULs) and the connection they have with research on biology in extreme environments and the effect of radiation in life. Presently, there are 14 DULs in operation worldwide. Although the main research activity in these infrastructures concerns the search for rare events in astroparticle physics and neutrino physics, DULs offer a unique opportunity to undertake experiments in astrobiology and biology in extreme environments. This is the main motivation of Deep Underground Laboratory Integrated Activity in biology (DULIA-bio) 2019 Workshop, which was held at the Gran Sasso (Italy) underground laboratory. This paper aims to give an introduction to the subject of the Workshop by reviewing the main features of DULs.

Keywords: underground laboratories, low radioactivity environment, underground biology, DULIA-bio, LNGS

OPEN ACCESS

Edited by:
Geoffrey Battle Smith,
New Mexico State University,
United States

Reviewed by:
Kate Scholberg,
Duke University, United States
Annarita Margiotta,
University of Bologna, Italy

***Correspondence:**
Aldo Ianni
aldo.ianni@lngs.infn.it

Specialty section:
This article was submitted to High-Energy and Astroparticle Physics, a section of the journal Frontiers in Physics

Received: *21 October 2020*
Accepted: *04 January 2021*
Published: *23 February 2021*

Citation:
Ianni A (2021) Science in Underground Laboratories and DULIA-Bio. Front. Phys. 9:612417. doi: 10.3389/fphy.2021.612417

INTRODUCTION: DEEP UNDERGROUND LABORATORIES

Deep Underground Laboratories (DULs) are research infrastructures built under a rock overburden greater than about 1,000 m of water equivalent (m.w.e). The larger the overburden the greater the reduction of the muon flux from primary cosmic rays. This is a key feature for DULs. A reduced muon flux by a factor larger than 10^5 allows the probing of rare events such as low energy (~MeV) neutrino interactions, neutrinoless double beta decay, and dark matter particle interactions. At present, 14 DULs are in operation and three underway in a time scale of 1–7 years (the ANDES is foreseen in 2027). In **Figure 1** we show the distribution of DULs around the world, updated from [1]. We notice that at present there is no DUL in operation in the Southern hemisphere. A DUL in the Southern hemisphere is of great relevance due to the atmospheric muon flux dependence on the season. The seasonal effect depends on the temperature of the atmosphere. As a matter of fact, a positive correlation between the temperature and the muon flux has been measured in several DULs. Therefore, in summer time the atmospheric muon flux on surface is larger. This effect could induce a seasonal dependence of the atmospheric muon-induced backgrounds in DULs. A comprehensive study of the atmospheric muon flux and temperature correlation has been carried out by the LVD collaboration from data taken from 1994 to 2017 [2]. The comparison of measurements of the seasonal effect induced by atmospheric muons in DULs located in the Northern and Southern hemisphere is crucial, as an example, in the evaluation of the expected annual modulation of dark matter particle interaction rate, which is a model-independent signature of dark matter. In fact, the motion of the Earth in the galactic halo produces an annual dependence of the rate with a maximum in early June. This dependence is expected to not change from one hemisphere to the other. On the contrary, any muon related background will change moving from one hemisphere to the other. Therefore, a comparison of measurements from detectors deployed in DULs in the Northern and Southern hemispheres will disentangle physics signals against backgrounds.

The muon flux in DULs as a function of the depth is shown in **Figure 2**. The solid line shows the muon flux for a flat surface. For some of the DULs the mountain profile affects significantly the muon flux underground, which has a characteristic angular distribution in these cases. This effect is shown

FIGURE 1 | Deep underground laboratories around the World. Geographic location of deep underground laboratories worldwide is shown for existing and future ones. Stawell underground physics laboratory (SUPL) in Australia and the new Yangyang (Y2L) in South Korea are under construction. ANDES in South America is a long-term project.

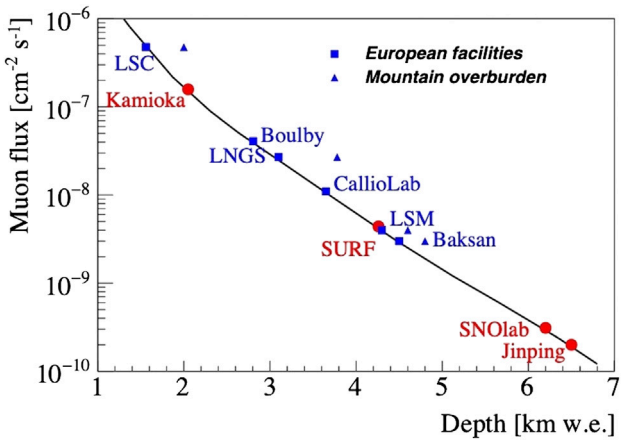

FIGURE 2 | Muon flux in underground laboratories. The muon flux in DULS is given against depth. The solid line shows the muon flux under a flat surface profile. Triangles show the maximum depth taking into account the real mountain profile.

for the Laboratorio Subterraneo de Canfranc (LSC), the Gran Sasso Laboratory (LNGS), Modane Underground Laboratory (LSM), and Baksan in the same figure.

Important and unique facilities are installed in DULs to support experimental activities. Of particular interest are the low background installations, which are mainly made by high purity germanium detectors for gamma spectroscopy. They are used for radiopurity assay of materials to be used in experimental projects. In addition, the development of experimental activities in DULs in the last 30 years has brought a significant boost in the search for rare events.

Science in DULs not Related to Biology

The main research activity in DULs concerns the search for rare events such as solar neutrino interactions, neutrinoless double beta decay, and dark matter particle interactions. In addition, nuclear interactions at low energy (~keV scale) between light nuclei are studied underground due to the very low cross sections. These nuclear interactions are relevant to understand energy production processes taking place inside stars [3]. Neutrinos produced by beta radioactive decays from U and Th in the interior of the Earth, so-called geo-neutrinos, are also detected in DULs [4, 5].

The scientific effort made in DULs has been awarded with two Nobel prizes in Physics in 2002 and 2015, respectively. In particular, in 2002 for the observation of neutrinos from the Sun [6, 7] and in 2015 for the discovery of neutrino oscillations [8, 9].

The Sun is a huge source of electron neutrinos in the MeV energy range. These neutrinos carry information directly from the core of the star. Massive (100–1,000 ton) water Cherenkov [8, 10] or scintillator [11] detectors with extreme radio-purity are

needed to detect solar neutrinos. Solar neutrinos in DULs have been studied for 50 years. From this experimental activity we have learnt about neutrino oscillations, neutrino propagation in matter, and about the inner properties of energy production inside stars [12].

The neutrino can be its own antiparticle, the so-called Majorana neutrino. This property could offer an explanation for the matter-antimatter asymmetry in the Universe. Only eleven nuclei can undergo a double beta decay: two electrons and two neutrinos are emitted during the decay on the contrary of a standard beta decay, where only one electron and one neutrino are emitted. Yet, if the neutrino is a Majorana particle no neutrinos will be emitted. These nuclei offer a unique opportunity to understand whether a neutrino is a Majorana particle. A number of experiments are underway to search for a neutrinoless double beta decay. Presently, the sensitivity to this extreme rare event is of the order of 10^{26} years [13]. These experiments require an environment where the natural radioactivity level and the cosmic ray background are extremely low.

There are strong arguments to believe that our galaxy, as much as other galaxies, contains a dominant amount of dark matter [14]. Dark matter has been observed only through gravitational effects, such as the rotation curves of stars moving in the outer region of galaxies. Yet, in DULs it is possible to directly observe interactions of dark matter particles. This opportunity would be crucial to understand what dark matter is made of.

Besides these main research topics, in recent years DULs have become multidisciplinary infrastructures. The underground environment in DULs allows for high sensitivity studies in teleseismic and other rare phenomena, such as solid Earth tides and water effects deep below surface. The LSC, as an example, is equipped with two 70 m-long laser interferometers [15] and a network of seismometers to characterize Newtonian noise underground.

Finally and recently, in Kamioka (Japan) an experiment to search for gravitational waves (KAGRA) has been installed in an underground environment due to the reduced background noise with respect to ground-based detectors [16].

Biology in DULs and DULIA-Bio

Life on Earth extends into deep subsurface and extreme environments, where bacteria and archaea tend to be the main living organisms. Subterranean microorganisms have been described in some detail, but most reports refer to samples taken centimeters to few meters below the surface. The literature describing microorganism inhabiting the very inside of rocks are still scarce and show a rather high diversity of microbial taxa and metabolic pathways [17]. Repeated and/or long-term sampling substantially simplifies in the neighborhood or inside of a DUL. On the contrary, the majority of data describing the influence of deep underground conditions on life have been derived from experiments carried out in DULs. In particular, the exploration of changes in living organisms exposed to low radioactivity has been challenging the initial belief of a decrease in biological risk. Multiple experiments with a variety of methods and organisms sampled on surface and in DULs have demonstrated a significant negative impact on life due to the lack of radiation. However, for a conclusive understanding more studies are needed. Therefore, DULs offer an opportunity to advance in these scientific quests in a multidisciplinary environment, helped by experienced physicists that have been working in low background characterization for several decades. In this spirit, the first DULIA-bio conference was organized by the Canfranc Underground Laboratory (Spain) in 2015 (https://indico.cern.ch/event/436589/). In the second meeting, hosted by the Underground Laboratory at Gran Sasso (Italy) in 2019 (https://agenda.infn.it/event/19116/), new experiments, installed in underground laboratories at Sudbury, Modane, Canfranc, Boulby, and Sichuan, showed an increased research effort in this framework with respect to the pioneering works done at LNGS and WIPP [18, 19]. The Boulby laboratory in the United Kingdom agreed to host the next DULIA-bio conference, likely in 2021.

DISCUSSION

DULs are large and unique infrastructures equipped with a number of ancillary facilities to support research activity. For years the main topic of research in DULs has been focused on astroparticle physics (dark matter, nuclear astrophysics, neutrino astrophysics) and neutrino physics (neutrinoless double beta decay and neutrino oscillations). However, in recent years DULs are diversifying the research activities to include geophysics and biology. As it has been mentioned above, DULs offer a unique opportunity to support research on astrobiology, biology in extreme environments, and radiation effects on life. The above discussed Workshops, named DULIA-bio, offered a forum where progress achieved and major needs to go further in this framework could be identified and addressed. Among current requirements, there is a need for consistent methods and conditions to improve the control on all the environmental conditions in order to reduce systematic uncertainties. In particular, materials where biological samples are stored underground should be well characterized, placed inside lead and polyethylene shields with radon free air atmosphere, so that an accurate background model can determine the nature and levels of radioactivity and also, very importantly, the energy spectra of the different sources. The impact of low radioactivity on life may well be diverse. In addition, standardization among laboratories is needed, and toward this goal the model organism *Drosophila* is being discussed as a common model organism. Also, standard methods would make results more comparable in different laboratories. In conclusion, these improvements and synergy with DULs may well allow this community to further understand the impact of natural radioactivity in life, which addresses the deeper question of the influence of randomness in life. We believe that evolution at some level involves randomness. The rate of interaction of

an organism with external factors, such as ionizing radiation, as an example, could be a source of randomness. Due to a substantial reduction in muon-induced ionization and muon-induced radioactivity deep underground, DULs, by comparison with exposure on surface, offer a unique opportunity to study how, at least, this factor plays a role in the concept of random processes, which might affect the reproduction of cells and the development of organisms. The role which could be played by DULs is crucial. Therefore, we aim for future DULIA-bio meetings to reinforce synergies between DULs and the community involved in this specific research topic.

AUTHOR CONTRIBUTIONS

The author confirms being the sole contributor of this work and has approved it for publication.

ACKNOWLEDGMENTS

The author would like to thank LNGS and all technical Services for the support in the organization of the DULIA-bio 2019 Workshop. The author would like to thank Carlos Peña-Garay for comments and suggestions.

REFERENCES

1. Ianni A. Review of technical features in underground laboratories. *Int J Mod Phys A* (2017) 32:1743001. doi:10.1142/S0217751X17430011
2. Agafonova NY, Aglietta M, Antonioli P, Ashikhmin VV, Bari G, Bruno, et al. The LVD collaboration, characterization of the varying flux of atmospheric muons measured with the large volume detector for 24 years. *Phys Rev D* (2019) 100:062002. doi:10.1103/PhysRevD.100.062002
3. Formicola A, Imbriani G. Introduction to experimental nuclear astrophysics. *Eur Phys J Plus* (2019) 134(3):89. doi:10.1140/epjp/i2019-12497-1
4. Gando A, Gando Y, Hanakago H, Ikeda H, Inoue K, Ishidoshiro, et al. Reactor on-off antineutrino measurments with KamLAND. *Phys Rev D* (2013) 88:033001. doi:10.1103/PhysRevD.88.033001
5. Agostini M, Altenmuller K, Appel S, Atroshchenko V, Bagdasarian Z, Basilico D, et al. Comprehensive geoneutrino analysis with Borexino. *Phys Rev D* (2020) 101:012009. doi:10.1103/PhysRevD.101.012009
6. Cleveland BT, Daily T, Davis R, Distel JR, Lande K, Lee CK, et al. Measurement of the solar electron neutrino flux with the Homestake chlorine experiment. *Astrophys J* (1998) 496:505–26. doi:10.1086/305343
7. Hirata KS, Kajita T, Kifune T, Kihara K, NakahataNakamura M, et al. Observation of 8B solar neutrinos in the Kamiokande-II detector. *Phys Rev Lett* (1989) 63:16–9. doi:10.1103/PhysRevLett.63.16
8. Abe K, Haga Y, Hayato Y, Ikeda M, Iyogi K, Kameda J, et al. The super-kamiokande collaboration, Solar neutrino measurements in super-kamiokande IV. *Phys Rev D* (2016) 94:052010. doi:10.1103/PhysRevD.94.052010
9. Aharmim B, Ahmed SN, Anthony AE, Barros N, Beier EW, Bellerive A, et al. The SNO Collaboration, combined analysis of all three phases of solar neutrino data from the sudbury neutrino observatory. *Phys Rev C* (2013) 88:025501. doi:10.1103/PhysRevC.88.025501
10. Aharmim B, Ahmed SN, Anthony AE, Barros N, Beier EW, Bellerive A, et al. The SNO collaboration. *Nucl Instrum Methods* (2000) 449:172. doi:10.1016/S0168-9002(99)01469-2
11. Agostini M, Altenmuller K, Appel S, Atroshchenko V, Bagdasarian Z, Basilico D, et al. The borexino collaboration. *Astropart Phys* (2002) 16:205–34. doi:10.1016/S0927-6505(01)00179-7
12. Oberauer L, Ianni A, Serenelli A. *Solar neutrino physics*. Berlin: Wiley VCH (2020). 240 p.
13. Kim Y-H. *Neutrinoless double beta decay experiment*. Available from: arXiv:2004.02510v1 (Accessed April 6, 2020).
14. Profumo S, Giani L, Piattella OF An introduction to dark matter particles. *Universe* (2019) 5:213. doi:10.3390/universe5100213
15. Amoruso A, Crescentini L Free core resonant parameters from diurnal strain tides recorded by the Gran Sasso (Italy) and Canfranc (Spain) underground geodetic interferometers. *Geophys J Int* (2020) 198:923–36. doi:10.1111/j.1365-246X.2012.05440.x
16. Akutsu T, Ando M, Arai K, Arai Y, Araki S, Araya A, et al. KAGRA Collaboration, KAGRA: 2.5 generation interferometric gravitational wave detector. *Nature Astron* (2019) 3(1):35–40. doi:10.1038/s41550-018-0658-y
17. Wilkins M, Daly RA, Mouser PJ, Trexler R, Sharma S, Cole DR, et al. Trends and future challenges in sampling the deep terrestrial biosphere. *Front Microbiol* (2014) 5:481. doi:10.3389/fmicb.2014.00481
18. Castillo H, Smith GB. Below-background ionizing radiation as an environmental cue for bacteria. *Front Microbiol* (2017) 8:177. doi:10.3389/fmicb.2017.00177
19. Morciano P, Cipressa F, Porrazzo A, Esposito G, Tabocchini MA, Cenci G. Fruit flies provide new insights in low-radiation background biology at the INFN LNGS. *Radiat Res* (2018) 3:217. doi:10.1667/RR15083.1

Conflict of Interest: The author declares that the research was conducted in the absence of any commercial or financial relationships that could be construed as a potential conflict of interest.

frontiers in Public Health

REVIEW
published: 15 December 2020
doi: 10.3389/fpubh.2020.601711

The Response of Living Organisms to Low Radiation Environment and Its Implications in Radiation Protection

Mauro Belli[1]* *and Luca Indovina*[2]

[1] *Independent Researcher, Rome, Italy,* [2] *Dipartimento di Diagnostica per Immagini, Radioterapia Oncologica ed Ematologia, Fondazione Policlinico Universitario A. Gemelli IRCCS, Rome, Italy*

Life has evolved on Earth for about 4 billion years in the presence of the natural background of ionizing radiation. It is extremely likely that it contributed, and still contributes, to shaping present form of life. Today the natural background radiation is extremely small (few mSv/y), however it may be significant enough for living organisms to respond to it, perhaps keeping memory of this exposure. A better understanding of this response is relevant not only for improving our knowledge on life evolution, but also for assessing the robustness of the present radiation protection system at low doses, such as those typically encountered in everyday life. Given the large uncertainties in epidemiological data below 100 mSv, quantitative evaluation of these health risk is currently obtained with the aid of radiobiological models. These predict a health detriment, caused by radiation-induced genetic mutations, linearly related to the dose. However a number of studies challenged this paradigm by demonstrating the occurrence of non-linear responses at low doses, and of radioinduced epigenetic effects, i.e., heritable changes in genes expression not related to changes in DNA sequence. This review is focused on the role that epigenetic mechanisms, besides the genetic ones, can have in the responses to low dose and protracted exposures, particularly to natural background radiation. Many lines of evidence show that epigenetic modifications are involved in non-linear responses relevant to low doses, such as non-targeted effects and adaptive response, and that genetic and epigenetic effects share, in part, a common origin: the reactive oxygen species generated by ionizing radiation. Cell response to low doses of ionizing radiation appears more complex than that assumed for radiation protection purposes and that it is not always detrimental. Experiments conducted in underground laboratories with very low background radiation have even suggested positive effects of this background. Studying the changes occurring in various living organisms at reduced radiation background, besides giving information on the life evolution, have opened a new avenue to answer whether low doses are detrimental or beneficial, and to understand the relevance of radiobiological results to radiation protection.

Keywords: ionizing radiation, radiation protection, radiobiology, low dose effects of radiation, background radiation, epigenetics (MeSH), underground experiments

OPEN ACCESS

Edited by:
Geoffrey Battle Smith, New Mexico State University, United States

Reviewed by:
Lorenzo Manti, University of Naples Federico II, Italy
Narongchai Autsavapromporn, Chiang Mai University, Thailand

***Correspondence:**
Mauro Belli
mau.belli1@gmail.com

Specialty section:
This article was submitted to Radiation and Health, a section of the journal Frontiers in Public Health

Received: *01 September 2020*
Accepted: *25 November 2020*
Published: *15 December 2020*

Citation:
Belli M and Indovina L (2020) The Response of Living Organisms to Low Radiation Environment and Its Implications in Radiation Protection. Front. Public Health 8:601711. doi: 10.3389/fpubh.2020.601711

INTRODUCTION

Living organisms have evolved on Earth for about 4 billion years in the presence of the natural background of ionizing radiation even if it was not always the same as today. Without it, life on Earth could not have existed or would not exist in the present form. Not only the Earth's crust contains radionuclides, but also the Earth is continuously bombarded by high-energy particles originating in outer space and by the Sun (cosmic radiation).

In the late 20s, it was suggested that variations in cosmic radiation, in addition to possible contribution to organic evolution, could have affected the evolution of organic compounds and, eventually, of life on earth (1). It should be considered that probably in the past the cosmic rays on Earth have experienced many fluctuations due to explosions of supernovae in the nearby interstellar space and to variations in solar wind.

Today life is shielded against cosmic particles by the Earth's magnetic field and by the atmosphere layer but some radiation reaches the biosphere as a consequence of the primary particle interactions that generate secondary particles in the atmosphere. Understanding its role is important for improving our knowledge about life evolution on Earth and about the health effects of low dose ionizing radiation exposure, a hot topic in radiation protection. In this review the role of background radiation is considered in the perspective of the low dose issue in radiation protection.

THE NATURAL BACKGROUND OF IONIZING RADIATION

Exposure of organisms to ionizing radiation from natural background is an unavoidable feature of life on Earth. The background radiation is intended as the radiation that is already in a location, when no source is deliberately introduced (2). The resulting doses to human beings have been evaluated for many years by international bodies, notably by the United Nations Scientific Committee on the Effects of Atomic Radiation (UNSCEAR), on the report of which the data here presented are based (3), with some integrations from the report issued by the U.S. National Academy of Sciences Biologic Effects of Ionizing Radiation, BEIR (4).

The main contribution to radiation background exposure of the public comes from natural sources of both low- and high-LET[1], i.e., from cosmic radiation, external terrestrial radiation, inhalation and ingestion of radionuclides (**Table 1**), while the contribution due to man-made sources is today relatively small, mostly coming from the fall-out (now only about 0.005 mSv/year[2] on average) of the nuclear weapons testing in the atmosphere occurred between 1945 and 1980.

TABLE 1 | Average annual effective dose of public due to natural background exposure [based on data from UNSCEAR (3)] and BEIR (4).

Source of exposure	World average (mSv)	Typical range (mSv)	Remark
Cosmic radiation	0.39 (0.16%)	0.3–1.0	Depends on altitude, includes cosmogenic radionuclides
External terrestrial radiation	0.48 (0.20%)	0.3–1.0	Depends on soil and building material
Inhalation of air	1.26 (0.52%)	0.2–10	Mainly from radon, depends on indoor accumulation
Ingestion of food and water	0.29 (0.12%)	0.2–1.0	Depends on food and drinking water composition, includes K-40
Total (natural)	2.40	1.0–13	Depends strongly on the geographical site

Cosmic radiation originates by bombardment of the Earth by high-energy particles arising from outer space (galactic radiation) and by solar radiation (mainly protons, especially during solar flares). These particles interact with the nuclei of the atmosphere to produce a cascade of interactions and secondary reaction products that constitute the cosmic radiation on the Earth surface. These interactions also produce a number of radioactive nuclei known as cosmogenic radionuclides, such as C-14, that eventually reach the Earth's surface and can be incorporated into living organisms.

Besides the shielding provided by the earth's magnetic field, life is shielded against cosmic radiation by an air layer which is comparable at sea level to a 10 m thick water layer (3). Therefore, fluence and energy of these particles strongly depend on both latitude (the number of particles penetrating the atmosphere is higher close to the earth's poles) and altitude. At ground level, the cosmic ray field is largely from muons, neutrons, and electrons, with muons constituting the dominant component. In other words, it is made of various radiation qualities: roughly speaking, neutrons are high-LET particles, while muons, and other directly ionizing charged particles and photons, are low-LET radiation. Studying the effects of cosmic radiation on human organisms,

Abbreviations: UNSCEAR, United Nations Scientific Committee on the Effects of Atomic Radiation; ICRP, International Commission on Radiological Protection; DSB, Double strand break; LET, Linear energy transfer; LNT, Linear No-Threshold; NTE, Non-targeted effects; AR, Adaptive response; BE, Bystander effect; GI, Genomic instability; C, G, Cytosine, Guanine; CpG, 5'—C—phosphate—G—3'; DNMT, DNA methyltransferase; ncRNA, Non-coding RNA; miRNA, Micro RNA; ROS, Reactive oxygen species; RNS, Reactive nitrogen species; TE, Transposable element; HNBR, High natural background radiation.

[1]LET stands for Linear Energy Transfer, defined as the ratio between the energy ΔE deposited by a charged particle in a very short track element, and its length Δx. It also corresponds to the linear collision stopping power of a charged particle in a medium. For radiation other than charged particles (e.g., X- or γ-rays, neutrons) it is often conventionally defined by the average LET of their charged secondaries. More details are found in the Report 85 of the International Commission on Radiation Units and Measurements, ICRU (5). Since the biological effectiveness of radiation is related to ionization density, LET is currently considered as an index of it. However, as LET is a measure of linear ionization density, not of spatial density, the terms "sparsely ionizing/densely ionizing radiation" are sometimes preferred instead of "low-/high-LET radiation."

[2]The sievert (Sv) is the unit of equivalent dose obtained by the unit of absorbed dose, gray (Gy), by applying (a) the radiation weighing factors to take into account the biological effectiveness of the different radiation qualities, and (b) the tissue weighing factors to take into account the inhomogeneity of the exposure. For the special case of uniform total-body exposure to low-LET radiation: 1 Sv = 1 Gy.

even outside the protection offered by the earth's atmosphere and magnetic field, has presently a great importance for assessing the radiation risks during human space travel (6).

The main contribution to external terrestrial exposure comes from gamma-emitting radionuclides present in trace amounts in the soil, whose amount varies geographically.

Internal exposures arise from the intake of terrestrial radionuclides by inhalation and ingestion. Inhalation of radon gas and its decay products constitutes the majority of human exposure to background ionizing radiation. It results in lung irradiation by high-LET alpha particles, but also low-LET radiation is emitted. There are large differences in indoor radon concentration depending on the site, building characteristics, etc. Exposures from ingestion are mainly due to K-40 and to the U-238 and Th-232 series radionuclides present in food and drinking water and in the human body itself.

Today the annual dose due to external exposure from natural background on average approaches 1 mSv/y, with cosmic contributions slightly less than the terrestrial one. Contribution from inhalation is higher than external exposure (**Table 1**). It is worth noting here that: (i) the average annual dose from natural background of 2.4 mSv, corresponds to a low dose rate of ≈ 0.27 μSv/h; (ii) several areas of the world, such as Guarapan in Brazil, Ramsar in Iran, Yangjiang in China and Kerala in India, are found to have levels of natural background radiation that are in excess of those considered to be "normal background" (3)so that they are defined as High Natural Background Radiation (HNBR) areas (7); (iii) the evaluation of inhalation and ingestion exposures are strictly related to human beings and may not hold for different organisms, certainly not for the cultured cells often used in radiobiology experiments.

THE LOW DOSE ISSUE IN RADIATION PROTECTION

Epidemiological Approaches to Health Risks

Despite the fact that the natural radiation background is extremely small, nevertheless it may be significant enough for living organisms to sense it and respond to it, keeping memory of this exposure. Our knowledge about the response of living organisms to low and protracted doses of ionizing radiation is mainly related to radiation protection needs, where the focus is on detrimental effects. However, the response of living organisms to these levels of exposures is still a matter of debate.

Our scientific community has become aware of ionizing radiation just a little over a century ago, after the discovery of X-rays (1895) and of natural radioactivity (1896). Compared to other disciplines, radiation science is a quite recent field. Even if harmful effects were reported soon after the X-rays discovery, scientists were slow to understand them, probably because they were overshadowed by the enthusiastic attempts to treat with them nearly any kind of illness or discomfort.

In 1926, the American geneticist Muller discovered that, by exposing the fruit fly Drosophila melanogaster to high levels of radiation (such as X- or gamma-rays), the mutation rate in their offspring can be increased by as much as 150 times (8, 9). For this discovery he was awarded the 1946 Nobel Prize in medicine and physiology. His work convinced him that the vast majority of mutations were deleterious and consequently that exposure to radiation should be strictly controlled. However, the primary focus for radiation protection remained for long time the acute/deterministic radiation syndromes. It was only some years after the atomic bombing of Hiroshima and Nagasaki that increased radiation risks have been documented for malignant diseases among survivors, in particular leukemia (10). Since these health effects appeared as stochastic events, ICRP updated their recommendations, until then intended to keep exposures below the relevant thresholds for induction of deterministic effects, by introducing the concept of reducing exposure to the lowest possible level, a terminology today changed in "as low as reasonably achievable" (ALARA) level and included in the optimization principle.

Epidemiological studies consistently show that the main health risk at moderate and low doses (i.e., doses not causing acute/deterministic effects) is induction of solid tumors and leukemias and even today the most important long-term evaluation of populations exposed to radiation remains the epidemiological study of the Hiroshima and Nagasaki survivors of the atomic bombing (Life Span Study, LSS) with a cohort of about 120,000 subjects followed since 1950 (11). LSS also showed increased radiation risks for malignant diseases among survivors exposed *in utero*, and possible risks for some non-cancer diseases. Evidence for health effects of moderate/high-dose radiation ($\geq$100 mSv), mostly consisting in linear dose-response relationship for cancer development, are conclusive, but the effects at lower dose levels are still uncertain (11).

Indeed, for two perfectly matched populations of 100,000 people, the minimum detectable excess relative risk (ERR) is calculated to be around 0.05 for all cancers for whole population (12). Using the ERR for cancer induction derived from LSS of about 0.50 Gy-1 (13) the lowest dose with significant risk results to be about 100 mGy for this epidemiological study. Also, some recent epidemiological investigation have suggested possible cancer induction below this dose, but analytical limitations and other difficulties generated several controversies about their ability to provide firm epidemiological evidence of excess cancers at low doses (14). Given the limited statistical power and the large uncertainties in epidemiological data below 100 mGy, different plausible dose–response relationships could be considered for the risk of cancer from exposures at low and moderate doses (12) (**Figure 1**).

What Is a "Low Dose" of Ionizing Radiation?

The term "low dose" has different definitions depending on the contexts. In the field of microdosimetry it is an absorbed dose such that a single cell or nucleus is very unlikely to be traversed by more than 1 track so that the number of affected nuclei or cells is proportional to the absorbed dose. However, the definition of "unlikely" is subjective so that, according to a more precise and conservative definition used in some radiobiological context, it

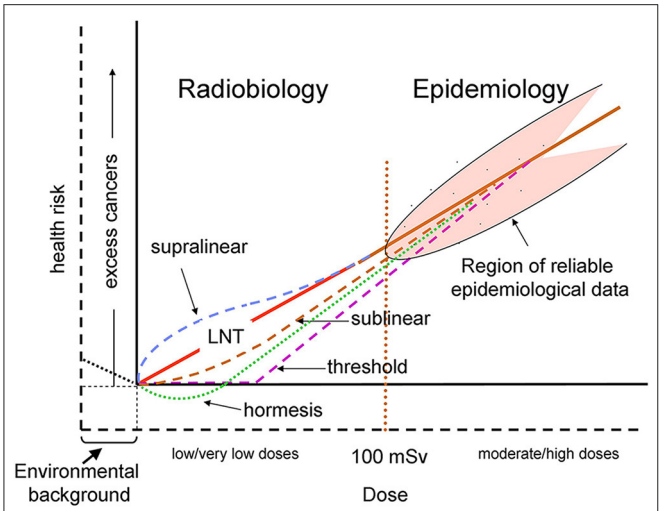

FIGURE 1 | Schematic representation of possible dose–response relationships for radiation-induced cancer risk. The doses are effective doses in addition to the natural background exposure. The solid axes correspond to the current representation where doses are those above the natural background and the cancer risk is the corresponding excess risk (12), while the dashed axes also take into account the natural background. The vertical red dotted line at 100 mSv represents a rough separation between the regions of reliable (> ∼100 mSv) and unreliable (< ∼100 mSv) epidemiological data. The solid red line represents the conventional linear no-threshold (LNT) relationship. Hormetic response, represented by the dotted green line, corresponds to the hypothetical responses driven by doses above background, according to the usual representation. The dotted black line below background represents a hypothetical protective response driven by the background radiation. The other dashed colored lines represent various proposed dose–response relationships, that could take into account various non-linear responses, such as BE (often considered to induce a supralinear response), and AR (sublinear).

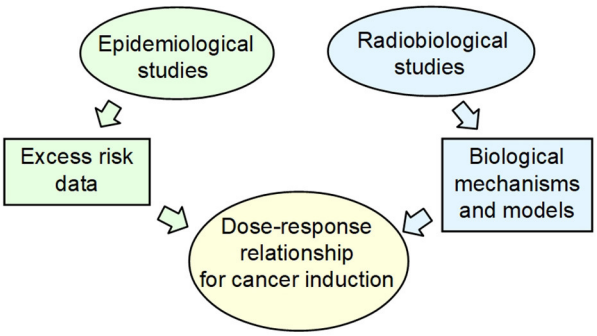

FIGURE 2 | The current approach for health risk assessment at low and protracted dose, in particular for cancer induction, is a combination of epidemiological data and radiobiological mechanistic models.

corresponds to a mean number of 0.2 tracks per nucleus or cell (15), meaning that <2% of the cells will be subject to traversals by more than one radiation track. This would correspond to a dose of only 0.2 mGy of low-LET radiation (16). Using an epidemiology-based definition a low dose is a dose below which it is not possible to detect adverse health effects (17). For radiation protection purposes the International Commission for Radiation Protection, ICRP (18) defines low doses as those of 100 mSv or less for low-LET radiation, a value also consistent with that used by UNSCEAR (3) and by the U.S. National Academy of Sciences Biologic Effects of Ionizing Radiation (4). In practice, the doses typically encountered in the workplace, in the environment and in diagnostic medicine fall in the low dose range; also irradiation of normal tissues in radiotherapy may be included in this type of exposure. Moreover, in view of protracted exposures, a low dose rate has been defined as 0.1 mGy/min or less for low-LET radiation (19).

Radiobiology Is Needed to Extrapolate Epidemiological Data to Low Doses

Due to limitations of epidemiological data for excess of stochastic risk at low and protracted doses, radiobiological knowledge is recognized to provide a framework for the analysis of risks at low-dose and low-dose-rate exposures (20) and to establish causal relationships from correlations found by observational studies (21). The need of an integration between biological mechanisms and epidemiological approaches is invoked for assessing the shape of the dose–response relationship for cancer induction at low doses (19). In principle, radiobiology data and models can identify the relevant radiobiological mechanisms, thus providing a rationale for the extrapolation to low and protracted doses of the epidemiological data obtained at moderate and high doses (**Figure 2**).

Indeed, a wealth of radiobiological information has been obtained after just over a century of research about the response of living organisms to low dose of ionizing radiation. Since this research was stimulated by radiation protection needs, it is not surprising that the focus was on detrimental.

THE RADIOBIOLOGICAL BASES OF HEALTH RISK ASSESSMENT

The Conventional Paradigm of Radiobiology and the LNT Assumption

It is well-known that ionizing radiation, being defined as radiation capable to ionize biological matter (whose ionization threshold is ∼12.4 eV), can break the chemical bonds of the cell components, the DNA being the most important cell target. Ionizing radiation can cause DNA lesion by direct deposition of energy in the DNA as well as by the indirect action through reactive chemical species (mostly free radicals) formed by radiolysis of water molecules near the DNA (22–24). Indirect DNA damage is the most frequent mechanisms for low-LET radiation while direct DNA damage is predominant for high-LET radiation (25, 26). The free radicals formed through the radiolysis of water molecules are converted, in aerobic conditions, to reactive oxygen species (ROS) that include free radicals as well as non-free radicals. Ionizing radiation can also generate reactive nitrogen species (RNS) through up-regulation of several enzymes, including inducible nitric oxide synthetase. The yield and spatial distribution of ROS and RNS is strongly modulated

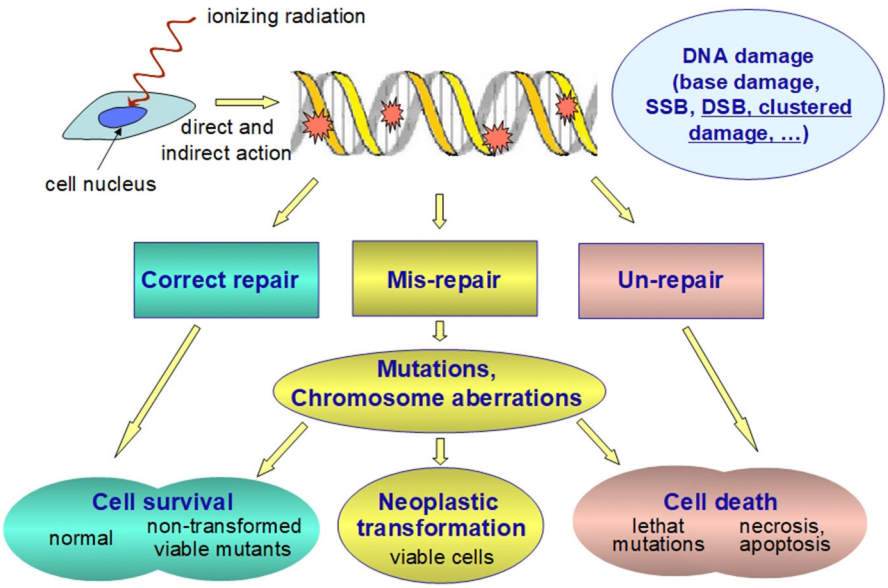

FIGURE 3 | Schematic representation of the fate of radiation-induced DNA damage. Ionizing radiation can damage nuclear DNA by direct and indirect (i.e., through reactive chemical species formed as a result of the water radiolysis near the DNA) action. Clustered DNA lesions (defined as two or more lesions within one or two helical turns of DNA) are considered to be the most biologically relevant DNA damage since they are expected to be less readily repaired as compared to other damage. Unrepaired or misrepaired DNA lesions causes genetic mutations and/or chromosome aberrations, which are very likely detrimental. Even at low doses they are assumed to increase both the probability of developing cancer and the rates of hereditary diseases. Therefore, the health risk for stochastic effects arises not from the killed cells, but from the surviving cells bearing important genetic damage.

by radiation quality as a consequence of the specific track structure of each quality (27). ROS and RNS can attack the DNA resulting in several alterations, including DNA single strand and double strand breaks (SSB and DSB, respectively), base damage and destruction of sugars. The most biologically relevant radiation-induced DNA damage, both directly and indirectly, is the clustered DNA damage, defined as two or more DNA lesions formed within one or two helical turns of DNA (22, 24, 28, 29). Particularly relevant are complex DSB and non-DSB clusters (29–32). A complex DSB is a DSB with additional lesions within 10 bp. The proportion of complex DSB and the degree of complexity increase with increasing radiation LET (33). Indeed, ionizing radiation is uniquely very efficient at inducing clustered DNA lesions (34) compared to endogenous or metabolism-related cellular damage. At low doses, even the passage of a single particle can produce clustered DNA lesions (24, 29, 35). The degree of complexity is assumed to be an index of severity of the radiation-induced damage, since complex lesions are not repaired with high fidelity by the repair machinery of the cells. Unrepair or mis-repair may lead to genetic mutations in surviving cells (**Figure 3**). It is generally assumed that a vast majority of mutations are neutral or detrimental, as in many circumstances gene mutation is a process which acts contrary to natural selection and which burdens each population with a load of harmful genes (36). Cancer development is described as a multistep process originating from single cells that have sustained mutations through DNA damage and radiation is judged to act most commonly by inducing initiating mutations in proto-oncogenes or in tumor suppressor genes (12).

Based on the above considerations, the following overall picture has been developed, sometimes called "conventional paradigm of radiobiology" as described by Goodhead (37): (a) the DNA damage in directly exposed cells is the main event for biological effects; (b) the DNA damage occurs during, or very shortly after, irradiation of the nuclei in targeted cells; (c) the potential for biological consequences can be expressed within one or two cell generations; (d) at low doses the biological effect is in direct proportion to the energy deposited in nuclear DNA.

This paradigm implies that genetic mutations consequent to radiation-induced damage to the cellular DNA are the main event leading to deleterious biological effects and that they are linearly related to the absorbed dose. It provides therefore the rational basis for the assuming the LNT relationship between excess cancer risk and dose also at low doses. As far as this aspect is concerned, the internationally agreed system for radiation protection has developed from this paradigm, although with many simplifications and assumptions (18). LNT assumption makes radiation protection relatively easy and manageable (doses are additive, dose can be used as an index of risk).

In the last 15 years a lively debate developed on the health effects at low dose (14, 38–40), and consequently the LNT relationship was questioned using various arguments (41–45). In the following, the radiobiological bases relevant to this issue will be considered.

Limitations of the Conventional Paradigm

The current approach in estimating health risks at low doses substantially uses a model centered on detrimental effects, arising from DNA damage and gene mutations, with a linear dose-response, similarly to that observed for the high-dose response. However, this model has been challenged since the end of 1980s from *in vitro* and *in vivo* studies that demonstrated the occurrence of biological responses inconsistent with it, in particular of non-linear dose-responses and non-genetic effects, such as those mentioned in the following.

Biological Response Is Different Between High- and Low-Doses

Evidence is accumulated that living organisms, including humans, respond to low and protracted doses in a way that is not only quantitatively, but also qualitatively, different from that to high and acute dose. For example, low doses may be insufficient to induce an efficient DSB repair *in vitro* (46, 47), differences in gene expression profiles have been found in a human myeloid tumor cell line (48) and subsequently many other data were accumulated for a variety of biological systems (49–51), including human tissue models (52) and human tissue irradiated *in vivo* (53). These observations raise the question whether the dose-dependent biological response is reflected in non-linear relationship between health effects and dose. Moreover, in some circumstances human cellular responses to low doses of radiation were shown to induce lower levels of chromosomal damage than that occurring spontaneously at the basal level [(54) and refs therein (14) and refs therein], giving support to the assumption, based on studies with *in vitro* and animal models, that low-dose radiation has beneficial effects (55).

Non-targeted and Adaptive Responses

A number of non-linear responses have been described in details in the last decades, such as the so-called non-targeted effects (NTE), i.e., effects that are not consequent to the DNA damage in the irradiated cells, and the adaptive response (AR). Remarkable NTE are the bystander effect (BE) (56, 57), the genomic instability (GI) (58–63), the low dose hypersensitivity (HRS) (64, 65), and delayed reproductive death (58) and induction of genes by radiation (66).

Particularly interesting and extensively studied NTE are the BE and the GI discovered between the end of the 1980s and the beginning of the 1990s (67–70) In general a BE describes the ability of cells affected by an agent to convey manifestations of damage to other cells not directly targeted by the agent or not necessarily susceptible to it *per se* (71). Thus, radiation induced BE is an effect manifesting in cells that were non-irradiated, neighbors of irradiated cells or that received factors secreted or shed by irradiated cells. Abscopal, or out-of-field, effects, defined in radiotherapy as radiation-induced effects observed outside the irradiated volume, are currently considered as a special type of BE (72–74).

GI is a delayed radiation effect, observed both *in vitro* and *in vivo* models, an all-embracing term to describe the increased rate of acquisition of alterations in the genome (62, 63). Radiation-induced genomic instability is characterized by an increased rate of genetic alterations ranging from simple DNA sequence changes to structural and numerical abnormalities at the chromosomal level in the progeny of irradiated cells multiple generations after the initial insult. It is measured, e.g., as enhanced death rate, chromosomal alterations, changes in ploidy, micronucleus formation, specific gene mutations.

AR can be regarded as a quite general phenomenon that can occur with various harmful agents. AR to radiation exposure is a transient phenomenon that has been observed in cells, tissues and organisms when a small conditioning radiation dose, called "priming dose," reduces the biological effects of a subsequent (usually higher) radiation dose called "challenging dose" [see for a review (75)]. Early evidence of this effect was shown in human lymphocytes even earlier than NTE (76, 77).

In this review we will denote with BE and AR only those effects that are radiation-induced. NTE and AR have been observed in many *in-vitro and in-vivo* experiments, and also in *ex-vivo* experiments with blood samples from irradiated humans (63, 69). These phenomena have been seen using a variety of cell and tissue types, of biological end-points and of radiation qualities (69, 78–80), however they have not been universally observed (70, 81–83), an intriguing aspect that is not yet fully elucidated. All NTE can be described as the expression of inter- or intra-cellular signaling (84) and are deemed to be particularly relevant to cell response to low doses.

These studies, especially those on BE, support the notion that, in general, the cellular system responds as a whole and therefore, especially at low dose, the cell population must be seen as a single entity perturbed by radiation, and the response comes from the whole population in a coordinated way (85, 86). Interestingly, there is evidence that NTE and AR are inter-related (78, 87, 88) and likely related, at least in part, to non-DNA damage, so that epigenetic mechanisms may have a role in them (89, 90).

Radiation-Induced Epigenetic Effects

Epigenetic changes are meiotically heritable and mitotically stable alterations in gene expression without alteration in DNA sequences and the "epigenome" can be intended as the complete set of the epigenetic trait of an organism. By the second half of the last century, it has been recognized that DNA by itself does not determine all characteristics of an organism, including the human one. Epigenetic regulation play an important role in various biological processes including embryonic development, genetic imprinting, and X-chromosome inactivation, therefore explaining how cells carrying identical DNA differentiate into different cell types, and how they maintain differentiated cellular states (91). Deregulation of these processes causes aberrant gene function and altered gene expression that play critical role in cancer initiation and development and, indeed, alterations of one or more of these processes are observed in various human cancers (92–96).

Environmental stimuli or stressors, including ionizing radiation, can trigger phenotype changes through epigenetic alterations [see the reviews in (97) and in (98)]. An interesting aspect is that some of them can be reversed after removal of the stressor (epigenetic plasticity) but some epigenetic modifications can persist (99, 100). A heritable change in gene expression

induced by a previous stimulus is often called "epigenetic memory" (101).

Since the phenotype of a cell or individual is affected by which of its genes are transcribed, epigenetics is considered a bridge between genotype and phenotype. Genetic changes, such as mutations, are heritable, but not very affected by environmental influence (even if mutations can be induced by the environmental radiation, they are relatively rare events). At the other extreme there are the metabolic processes, susceptible to environmental changes, but not heritable. Epigenetic modifications, instead, are susceptible to environmental changes and are heritable at the same time (99).

The three key epigenetic processes are changes in DNA methylation, histones alteration leading to chromatin modification, and post-translational gene regulation by non-coding RNAs (ncRNAs).

DNA methylation represents the best characterized form of epigenetic modification. It is a covalent modification of the cytosine ring by addition of a methyl group at the $5'$ position resulting in 5-metylcytosine (5 mC). In mammals, cytosine methylation is found almost exclusively in the context of CpG dinucleotides (97) and DNA methylation patterns are maintained or established by a family of enzymes, the DNA methyltransferases (DNMTs). DNA methylation establishes and maintains an inactive state of a gene by keeping the chromatin structure compact and inaccessible to the transcription machinery (102). However, it must be considered that 5 mC is inherently mutagenic because it can spontaneously undergo deamination, leading to $C \rightarrow T$ transitions. Typical alterations in DNA methylation consists in hypermethylation in specific genes, potentially leading to their transcriptional silencing, or in global hypomethylation, leading to genomic instability when transposable elements are de-methylated (103, 104). Although 5 mC was discovered in calf thymus DNA around the middle of the last century, it was only around 1980 that DNA methylation was demonstrated to be involved in gene regulation and cell differentiation (105). Not many years later, early findings indicated that exposure to ^{60}Co γ-radiation causes a dose-dependent decreases in DNA methylation in several cultured cell lines (106). Since then, considerably amount of research carried out both *in vitro* and *in vivo* showed that exposure to ionizing radiation can change the DNA methylation pattern, both in terms of specific hypermethylation and/or global hypomethylation [see the reviews in (107, 108, 110)]. Such studies are relevant to a better understanding of radiation-induced cancer, as hypermethylation in the promoter region of a tumor-suppressor gene can cause its silencing, therefore contributing to the oncogenic process (103, 107–109, 111–113) while global DNA hypomethylation induces DNA hypomethylation, which plays critical roles in both cancer initiation and progression (114) being the first epigenetic alteration detected in several human cancers [see the reviews in (107) and (110)]. Indeed, hypermethylation of tumor-suppressor genes was observed in lung cancers of occupationally exposed workers at the Russian MAYAK plutonium plant [(115, 116) and references therein] and in an appreciable fraction of patients with renal cell carcinomas living in radiocontaminated areas after the Chernobyl accident (117). A link between radiation-induced global genomic hypomethylation and carcinogenesis was established in rats with radiation-induced mammary tumors [(118) see also the review in (108)].

In addition to DNA methylation changes, ionizing radiation was shown to induce a variety of histone modifications both *in vitro* and *in vivo*. Histones, as essential constituents of the chromatin in eukaryotic cells, were regarded for years as having a merely structural role. However, now they are recognized to control the organization of chromatin and hence transcriptional responses (119) In cultured cells and in mouse models exposure to ionizing radiation is shown to induce post-translational modification on histones, such as acetylation, methylation, phosphorylation, that are crucial in DNA repair, cell cycle regulation, apoptosis and genome stability (120–122). A well-known radiation-induced histone modification is phosphorylation of histone H2AX, often used as a measure of radiation-induced DSBs, which is crucially important for the repair of DNA double strand breaks (DSB) and for the maintenance of genome stability.

The third type of epigenetic radiation-induced modification involves non-coding RNAs (ncRNAs), in particular microRNA (miRNAs). Since their discovery in 1993 (123) miRNAs, which are small RNA molecules, usually 21–23 nucleotides, are emerging as important modulators in many cellular pathways, including gene expression. *In vitro* and *in vivo* studies demonstrate that miRNA expression levels change in response to radiation, and that certain miRNAs alter radiation sensitivity (124–127). Expression levels of a variety of miRNAs after low-LET ionizing radiation are reviewed and listed in Marta et al. (128).

Many findings indicate that DNA methylation, histone modification and miRNA expression are not separate and independent events, but that there is a strong interplay between them. A cross-talk between DNA methylation and histone modification occurs in specific gene loci in a variety of organisms, and DNA methylation can be regulated by miRNAs and vice versa, achieving a sort of mutual regulation [see also the review in (110)]. Also other non-coding RNAs were found to interact with DNA methylation and histones (129).

Interestingly, there is evidence that epigenome may be differently affected by low- and high-LET radiation. Indeed, a number of studies show that exposure to high-LET radiation can result in lasting changes in the total levels of DNA methylation and in the miRNA expression that may be different from those induced by equivalent doses of low-LET radiation (89, 130–135). Some of these studies were focussed on the effect of high energy Fe-ions, as they are representative of the most detrimental component of space radiation for astronauts in deep space. Overall, these experiments show a complex picture, as the observed differences may likely be related not only to radiation quality, but also to differences in biological system, doses/dose rates, time of observation, and assay used [see the reviews in (107, 110)].

In general, irradiation with protons and high-LET heavy ions (Si-, Fe-, Ti-ion) often, though not always, causes hypermethylation in global and/or repetitive element and alterations at specific genes [as reviewed in (135)]. It is interesting to note that, since protons of relatively low-LET gave an effect similar to that caused by high-LET Fe-ions, it appears that epigenetic responses may be related to radiation quality (i.e., to properties in their track structure) rather than to LET (130). Experiments with human primary lung cancers suggested that exposure to these particle "creates a DNA methylation 'signature' that uniquely reflects cancer-specific methylation patterns" (135). The difference between sparsely and densely ionizing radiation has been ascribed to the possible difference in oxidative stress (130). It was also speculated that an increased DNA methylation might occur because of the higher persistence of lesions in heterochromatin related to inefficient repair of clustered lesions along the particle trajectory of densely ionizing radiation (135).

An important question concerns the possibility of transgenerational epigenetic effects in organisms exposed to ionizing radiation. In cells, relatively stable epigenetic modifications were observed that are heritable through mitosis, and can manifest in the progeny of the irradiated cells for many divisions (63). In plants and in some animals, such as nematodes, transgenerational epigenetic inheritance is relatively common and many examples are reported (136) but in mammals epigenetic patterns are largely erased and then remodeled during germ cell development and early embryonic development (epigenetic reprogramming) (137, 138). Nevertheless, transgenerational induction of chromosomal instability has been documented in irradiated rodents (63, 139, 140) but the occurrence of transgenerational radiation effects is highly controversial in humans [see the review in (110)].

LINKS BETWEEN RADIATION-INDUCED OXIDATIVE STRESS, EPIGENETIC CHANGES, NON-TARGETED EFFECTS AND ADAPTIVE RESPONSE

Ionizing radiation induces oxidative stress when excess of ROS/RNS are not compensated by the scavenging mechanisms of the cell. ROS can be directly generated by radiation exposure and indirectly through the damage of mitochondria (141).

Besides the well-known mutagenic action of ROS and RNS, there is also evidence that oxidative stress can modify the epigenome by multiple mechanisms, the most important of which involve oxidation of DNA bases and/or mitochondria-mediated changes, with the main target being the CpG sites, especially in the CpG islands (142, 143).

Oxidative stress are also known to play an important role in NTE and AR (144, 145). For example, they contribute to genomic instability (146) and may spread to neighboring, non-targeted bystander cells (27). It appears therefore that they share the radiation-induced oxidative stress as a common origin with the radiation-induced epigenetic changes.

The existence of inter-relations between BE, GI, and AR, from one side, and of those between DNA methylation, histone modifications and ncRNA expression, from the other side, along with the existence of interactions among all these processes, speaks in favor of a picture where the biological response to ionizing radiation is a complex response to a variety of signals at the cellular and supracellular levels. In this picture, epigenetic changes have become increasingly recognized as important aspects besides the genetic ones, especially at low doses (**Figure 4**). It is then plausible that this complex response explains the observation of non-linear phenomena. These considerations strongly suggest that the assumption of a linear dose-response, at least at low doses, for radiation- induced cancer is an oversimplification. Developing more realistic radiobiological models is not only relevant to radiation biology, but is also important in radiation protection to guide extrapolations to low doses and low dose rates of epidemiological data on exposed human populations, and also to identify the factors determining individual radiation sensitivity/susceptibility. Realistic models, focused on biological end-points relevant to health effects in humans, could also settle the long-standing dispute about possible "beneficial" effects of low doses, such as "radiation hormesis," i.e., an induction of beneficial health effects by stimulation of defense mechanisms by low-dose radiation.

UNDERGROUND RADIOBIOLOGY EXPERIMENTS

Understanding the role of natural background radiation on living organisms is essential to complete the above mentioned scenario, given that this background contributes to the basal biological state on which the response to additional (man-made) exposures superimposes. It is recognized that studies of low-dose-rate exposure from environmental sources can potentially contribute to a better understanding of the risks of radiation-induced cancer (7). It is interesting to note that the background radiation shows large geographical variations (3) and that residents in high natural background radiation (HNBR) areas were the subject of several epidemiological studies in the attempt to find possible differences between them and people living in normal background areas. Overall, these studies did not show any increase in cancer risk, but since they are subjected to the already mentioned typical limitations of epidemiological studies (mainly lack of statistical power and biases and confounding factors) it was recognized that improvements would be needed (7). Residents in HNBR areas were also the subject of cytogenetic investigations. For example, in the Ramsar area of northern Iran, one of the areas with the highest radiation background in the world, preliminary findings suggested no significant difference in cytogenetic parameters in the residents there compared to people living in normal background areas (148), but subsequent studies showed a higher incidence of chromosomal aberrations (149) and of spontaneous levels of DNA damage and radiosensitivity in the study group compared to the control groups (150, 151). In spite of the recognized potential contribution of HNBR studies to a better understanding of the risks of radiation-induced cancer (7), the data so far obtained are far from providing a consistent picture and a solid contribution to the matter, so that various hypotheses

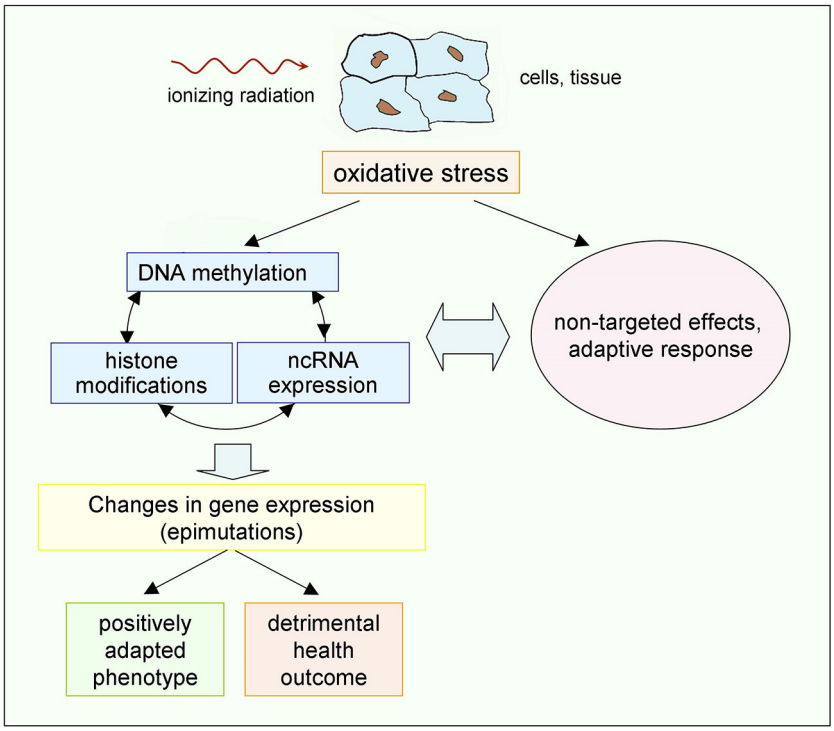

FIGURE 4 | Possible chain of events driven by low doses of ionizing radiation. Epigenetic mechanisms, on the one hand, and non-targeted effects and adaptive response, on the other hand, share as a common origin the radiation-induced oxidative stress, and interplay exists between them (89, 90). The resulting effects may, in principle, either provide a positively adapted phenotype or a detrimental outcome (45). Occurrence of additional radiation-induced genetic effects, not shown here, cannot be excluded, but gene mutations are much less frequent than epimutations [see the review in (147)].

are still on the table. For example, lack of proven detrimental health effects in the Ramsar residents was hypothesized as due to induction of adaptive response and, consequently, to the induction of non-linear responses (152).

Controlled long-term experiments with model organisms, conducted in underground laboratories where conditions with no or largely reduced radiation background are realized, compared with normal conditions at natural background radiation, can provide basic information for understanding the role of this background [see the review in (153)].

From the radiobiological point of view, these experiments provide an original approach to the low dose issue, since they aim at investigating the effect on biological systems after removing or decreasing the radiation dose, rather than observing the effect after exposing them to small doses that superimpose to the background. The latter case implies an exposure increase over the (local) natural background and, if the dose increments used in these conventional experiments are comparable to the dose coming from the natural radiation background, its geographical variations may make inappropriate any comparison between different laboratories.

Underground laboratories were mainly built to host experiments in fundamental Physics and Astrophysics searching for rare events such as neutrino interactions, thus requiring a very low radioactivity environment to decrease the experimental noise (154). The overburden provides a shield that strongly reduces the cosmic ray flux and in several cases additional measures were undertaken to reduce other components of the radiation background. A list with the relevant characteristics of these underground laboratories around the world can be found in Morciano et al. (155). Only quite recently their unique opportunities for radiobiology experiments were exploited in some of them. For a survey of deep-underground laboratories focusing on biological research see the review in Liu et al. (156). So far, a number of studies have been carried out in several underground laboratories set up in various countries using a variety of cell and organisms, i.e., bacteria, protozoa, yeasts, rodent and human cells, fruit flies (153).

Pioneering works carried out in a low-radiation environmental laboratory in the Pyrenees Mountains, have shown that the growth rate of paramecium cells was decreased when they were cultured in low background radiation. Normal growth was restored upon the addition of a radiation source equivalent to control levels (157, 158).

Two bacterial species, *S. oneidensis* and *D. radiodurans*, grown under reduced radiation environmental conditions at the Waste Isolation Pilot Plant in New Mexico, have shown upregulation of oxidative stress-related genes and of heath-shock protein genes, respectively, and reduction of growth rate for both species, suggesting that a stress response is triggered in the absence

of normal levels of radiation. Interestingly, these changes were restored after the recovery of radiation (159). Also, up-regulation of oxidative stress related proteins was observed in human lung fibroblast cells and bronchial epithelial cells grown in low radiation background (160, 161). Transcriptome analysis in *S. oneidensis* deprived of background radiation showed down-regulation of ribosomal proteins, indicating a marked decrease in protein translation, and a genome-wide gene regulation response that was interpreted as due to a lower intracellular radiolysis products concentration because of a reduced hit rate by radiation tracks (162).

In the 1990s a series of experiments were started in the Gran Sasso underground Laboratory of the Italian National Institute of Nuclear Physics, shielded by about 1,400 m of rocks. The first study, carried out on the yeast strain *S. cerevisiae,* showed that permanence in the low radiation laboratory decreased the cell defense ability against genotoxic and radio-mimetic agents (163). Subsequent experiments, using rodent and human cell lines, cultured for 9 months and over, showed that cultures kept in this strongly reduced background, when compared with similar cultures in normal background, showed less ROS scavenging ability, down-regulation in genes involved in protection from oxidative damage, and higher susceptibility to subsequent radiation-induced damage (164–166). As a step forward the study of more complex organisms, the investigators started studying the fruit fly *D. melanogaster*, providing the first evidence of the influence of the radiation environment on life span, fertility and response to genotoxic stress at the organism level (167). Interestingly, permanence in low radiation environment increased the fly life span, but decreased male and female fertility, and trans-generational effects were demonstrated.

Despite the difficulties of ruling out confounder factors when comparing the underground situations to the normal ones (i.e., factors such as temperature, humidity, atmospheric pressure, etc.), on the whole these results suggest that the natural background radiation is capable to stimulate defense mechanisms against stress, including further exposure to ionizing radiation. The observed effects on oxidative stress genes, and the restoration after radiation recovery, are consistent with the hypothesis that epigenetic mechanisms are involved in setting up or reinforcing these defense mechanisms. It is worth noting that in some of the mentioned experiments (165, 166) the possibility was ruled out, through parallel analysis of multiple samples, that the results were affected by random selection of (genetic) mutants, which corroborates a possible involvement of epigenetic mechanisms.

CONCLUSIONS AND PERSPECTIVES

Awareness that we live in a world in which natural background radiation is present everywhere has raised several fundamental questions, from the general one "does life need low level radiation ?" to the more specific issues "is natural background radiation a damaging or stimulatory agent ?" and "are epigenetic mechanisms important to the biological response to this background ?"

Observation of radiation-induced biological phenomena such as non-linear responses at low doses (in particular NTE and AR), of epigenetic mechanisms capable to respond to changes in environmental ionizing radiation, and of possible stimulation of cell defense mechanisms by natural background radiation speaks in favor of the following two lines of conclusions that are inter-related.

The first one is the general observation that natural background radiation was, and likely continues to be, essential for evolution of life on Earth by, e.g., stabilizing the genome and, at the same time, allowing the necessary adaptation of organisms to environmental changes. Radiation-induced epigenetic modifications are important players in these processes as it is known that, in general, the epimutation rates can be much faster than rates of (genetic) mutations and the epimutations are more easily reversible (168).

The second and more specific one is related to radiation protection issues. Biological response at low doses appears to be more complex then that taken as a basis for the LNT relationship between health risk and dose, whereby ionizing radiation always induces harmful gene mutations in direct proportion to the energy deposited by radiation. Linear dependence of the health risk on doses above natural background must be seen as an oversimplification. Besides the possibility that radiation-induced epigenetic mechanisms contribute to cancer induction, also the possibility must be considered that this same background triggers a hormetic response, as shown in **Figure 1**.

The latter consideration highlights some practical drawbacks in the current system, derived from the conclusion that, whatever the real dose-response relationship will be, it is unreasonable assuming a linear one. An important example is in the "optimization of protection," one of the three fundamental principles of radiation protection (18), where different options, in the current system, could be compared based on collective dose, irrespective of the fact that it can be made of many small individual doses or of few larger ones. At the same time the problem is posed of how health risk can be assessed not only for workers and members of the public exposed to low doses above the background, but also for people working in underground sites at reduced natural background radiation, so that a special branch of medicine ("underground medicine") has been envisaged (156).

The complex biological response to low and protracted doses, such as those involved in exposure to natural background, calls for a revision of the relevant radioprotection approach as currently assumed by the International regulatory bodies. It can be noted that even though non-linear, epigenetic-mediated, responses such as the GI, BE and AR, are already incorporated in epidemiological measures of risk (18, 68), nevertheless these responses, as well as epigenetic mechanisms in general, may be relevant at low doses where the epidemiological data are very uncertain. In this region any realistic radiobiological model used for extrapolating the epidemiological data should include both genetic and epigenetic effects induced by ionizing radiation. Development of such new models requires, besides *in vitro* studies that continue to be important for a better understanding of the mechanisms of radiation action, also *in vivo* investigation on model organisms suitable for plausible

extrapolation of the results to the human beings. In this research area "underground biology" appears as a new and exciting area for improving our knowledge in evolutionary biology and fundamental radiobiology, as well as in its practical applications, such as radiation protection. More relevant information is expected to be gained from the ongoing research in the already mentioned laboratories (France, USA, Italy) and in others in Canada, Spain and China [see the review in (156)]. An interesting aspect that could be addressed by these investigations concerns the role of the high-LET component of background radiation, exploiting the possibility of simulating the dose-rate at the surface using weak gamma-sources which, however, lacks the high-LET cosmic component. Moreover, underground experiments could be combined with observations coming from HBRAs to get information on the role of background radiation and its various components by comparing exposures spanning from well below the average background dose-rate to several times it.

It is expected that such developments can settle the long-standing controversy about the detrimental or beneficial effects of low-level exposures. Indeed, this is not a trivial question, as every coin has two sides. Although stimulation of defense reactions is evocative of a positive outcome, it could not be the case if, for example, cells damaged by protracted exposures at low doses escape apoptosis, a situation that could enhance tumor promotion by increasing the probability of survival of cells with accumulating damage or mutation (49). Therefore, settling this controversy needs deeper insights of those radiobiological genetic and epigenetic mechanisms that dominate at low doses and at the same time are relevant to health effects on humans, so as to avoid biased, and even opposite, conclusions based on "cherry picking" of published data. It should also be considered that in human studies the individual radiosensitivity/susceptibility can be a source of large variability around the average responses as those represented in **Figure 1**.

As a final consideration about the process of improving the current system of radiation protection, we cannot overlook that the latter has the advantage of being manageable since, e.g., a given dose can be used as a direct index of risk and different doses can be summed up to evaluate the overall risk. Keeping an acceptable level of manageability is an important constraint in the process of replacing the current paradigm with a new and more realistic one.

AUTHOR CONTRIBUTIONS

MB: conceptualization of the work, writing the original draft, and manuscript supervision. LI: bibliographic resources and revising the manuscript. All authors have read and agreed to the published version of the manuscript.

ACKNOWLEDGMENTS

MB acknowledges the support of the Multidisciplinary European Low Dose Initiative (MELODI) for participation, as a member of its Scientific Committee, in several MELODI Workshops where subjects relevant to this review were discussed. The authors apologize to scientists whose relevant publications were not cited due to space limitation. MB thanks his friend Matisse for his continued encouragement in writing the first draft.

REFERENCES

1. Atri D, Melott AL. Cosmic rays and terrestrial life: a brief review. *Astropart Phys*. (2014) 53:186–90. doi: 10.1016/j.astropartphys.2013.03.001
2. IAEA, International Atomic Energy Agency. *IAEA Safety Glossary: Terminology Used in Nuclear Safety and Radiation Protection*. Vienna: IAEA (2007).
3. UNSCEAR (United Nations Scientific Committee on the Effects of Atomic Radiation). *Sources and Effects of Ionizing Radiation*. 2008 Report to the General Assembly. Vol. I. Annex A. New York, NY: United Nations (2010).
4. National Research Council. *Health Risks from Exposure to Low Levels of Ionizing Radiation: BEIR VII Phase 2*. Washington, DC: The National Academies Press (2006).
5. ICRU, International Commission on Radiation Units and Measurements. *Report 85: Fundamental Quantities and Units for Ionizing Radiation*. International Commission on Radiation Units and Measurements [Journal of the ICRU Volume 11, No. 1] (2011).
6. Cucinotta FA, Durante M. Cancer risk from exposure to galactic cosmic rays: implications for space exploration by human beings. *Lancet Oncol*. (2006) 7:431–5. doi: 10.1016/S1470-2045(06)70695-7
7. UNSCEAR (United Nations Scientific Committee on the Effects of Atomic Radiation). *Sources, Effects and Risks of Ionizing Radiation, UNSCEAR 2017 Report to the General Assembly, With Scientific Annexes*. New York, NY: United Nations (2018).
8. Muller H. Evolution by mutation. *Bull Amer Math Soc*. (1958) 64:137–60. doi: 10.1090/S0002-9904-1958-10191-3
9. Gleason KM. *Hermann Joseph Muller's Study of X-Rays as a Mutagen, (1926-1927)*. Embryo Project Encyclopedia (2017). Available online at: http://embryo.asu.edu/handle/10776/11441
10. Folley J, Borges W, Yamawaki T. Incidence of leukemia in survivors of the atomic bomb in Hiroshima and Nagasaki, Japan. *Am J Med*. (1952) 13:311–21. doi: 10.1016/0002-9343(52)90285-4
11. Ozasa K, Cullings HM, Ohishi W, Ayumi H, Grant E. Epidemiological studies of atomic bomb radiation at the radiation effects research foundation. *Int J Radiat Biol*. (2019) 95:879–91. doi: 10.1080/09553002.2019.1569778
12. UNSCEAR (United Nations Scientific Committee on the Effects of Atomic Radiation). *Sources, Effects and Risks of Ionizing Radiation*. 136 Report to the General Assembly with Scientific Annexes. New York, NY: United Nations (2015).
13. Grant E, Brenner A, Sugiyama H, Sakata R, Sadakane A, Utada M, et al. Solid cancer incidence among the life span study of atomic bomb survivors: 1958-2009. *Radiat Res*. (2017) 187:513–37. doi: 10.1667/RR14492.1
14. Vaiserman A, Koliada A, Zabuga O, Socol Y. Health impacts of low-dose ionizing radiation: current scientific debates and regulatory issues. *Dose Response*. (2018) 16:1559325818796331. doi: 10.1177/1559325818796331
15. Goodhead D. Spatial and temporal distribution of energy. *Health Phys*. (1988) 55:231–40. doi: 10.1097/00004032-198808000-00015
16. UNSCEAR (United Nations Scientific Committee on the Effects of Atomic Radiation). *Sources and Effects of Ionizing Radiation*. 14 Report to the General Assembly With Scientific Annexes. New York, NY: United Nations (1993).
17. UNSCEAR (United Nations Scientific Committee on the Effects of Atomic Radiation). *Sources and Effects of Ionizing Radiation*. 15 Report to the General Assembly with Scientific Annexes. New York, NY: United Nations (2000).
18. ICRP. ICRP Publication 103: the 2007 recommendations of the international commission on radiological protection. *Ann ICRP*. (2007) 37:1–332. doi: 10.1016/j.icrp.2008.07.001

19. MELODI, Multidisciplinary European Low Dose Initiative. *SRA Working Group: 2019 Strategic Research Agenda of MELODI.* (2019). Available online at: http://www.melodi-online.eu/m_docs_sra.html17
20. Valentin J. Low-dose extrapolation of radiation-related cancer risk. *Ann ICRP.* (2005) 35:1–140. doi: 10.1016/j.icrp.2005.11.002
21. Wojcik A, Harms-Ringdahl M. Radiation protection biology then and now. *Int J Radiat Biol.* (2019) 95:841–50. doi: 10.1080/09553002.2019.1589027
22. Ward JF. Biochemistry of DNA lesions. *Radiat Res.* (1985) 104:S103–11. doi: 10.2307/3576637
23. Ward J. DNA damage produced by ionizing radiation in mammalian cells: identities, mechanisms of formation, and reparability. *Prog Nucleic Acid Res Mol Biol.* (1988) 35:95–125. doi: 10.1016/S0079-6603(08)60611-X
24. Ward J. The complexity of DNA damage: relevance to biological consequences. *Int J Radiat Biol.* (1994) 66:427–32. doi: 10.1080/09553009414551401
25. O'Neill P, Fielden E. Primary free radical processes in DNA. *Adv Radiat Biol.* (1993) 17:53–120. doi: 10.1016/B978-0-12-035417-7.50005-2
26. de Lara C, Jenner T, Townsend KM, Marsden S, O'Neill P. The effect of dimethyl sulfoxide on the induction of DNA double-strand breaks in V79-4 mammalian cells by alpha particles. *Radiat Res.* (1995) 144:43–49. doi: 10.2307/3579234
27. Azzam EI, Jay-Gerin JP, Pain D. Ionizing radiation-induced metabolic oxidative stress and prolonged cell injury. *Cancer Lett.* (2012) 327:48–60. doi: 10.1016/j.canlet.2011.12.012
28. Goodhead D, Thacker J, Cox R. Weiss lecture. Effects of radiations of different qualities on cells: molecular mechanisms of damage and repair. *Int J Radiat Biol.* (1993) 63:543–56. doi: 10.1080/09553009314450721
29. Goodhead D. Initial events in the cellular effects of ionising radiation: clustered damage in DNA. *Int J Radiat Biol.* (1994) 65:7–17. doi: 10.1080/09553009414550021
30. Nikjoo H, O'Neill P, Goodhead D. Computational modelling of low-energy electron-induced DNA damage by early physical and chemical events. *Int J Radiat Biol.* (1997) 71:467–83. doi: 10.1080/095530097143798
31. O'Neill P, Wardman P. Radiation chemistry comes before radiation biology. *Int J Radiat Biol.* (2009) 85:9–25. doi: 10.1080/09553000802640401
32. Georgakilas A, O'Neill P, Stewart R. Induction and repair of clustered DNA lesions: what do we know so far?. *Radiat Res.* (2013) 180:100–9. doi: 10.1667/RR3041.1
33. Nikjoo H, O'Neill P, Wilson W, Goodhead D. Computational approach for determining the spectrum of DNA damage induced by ionizing radiation. *Radiat Res.* (2001) 156:577–83. doi: 10.1667/0033-7587(2001)156[0577:CAFDTS]2.0.CO;2
34. Hill M. Radiation track structure: how the spatial distribution of energy deposition drives biological response. *Clin Oncolol.* (2001) 32:75–83. doi: 10.1016/j.clon.2019.08.006
35. Prise K, Pinto M, Newman H, Michael B. A review of studies of ionizing radiation-induced double-strand break clustering. *Radiat Res.* (2001) 156:572–6. doi: 10.1667/0033-7587(2001)156[0572:AROSOI]2.0.CO;2
36. UNSCEAR (United Nations Scientific Committee on the Effects of Atomic Radiation). *1988 Report. Sources, Effects and Risks of Ionizing Radiation*. New York, NY: United Nations (1988).
37. Goodhead D. New radiobiological, radiation risk and radiation protection paradigms. *Mutat Res.* (2010) 687:13–16. doi: 10.1016/j.mrfmmm.2010.01.006
38. Tubiana M, Aurengo A, Averbeck D, Masse R. Recent reports on the effect of low doses of ionizing radiation and its doseŰeffect relationship. *Radiat Environ Biophys.* (2006) 44:245–51. doi: 10.1007/s00411-006-0032-9
39. Dauer L, Brooks A, Hoel D, Morgan W, Stram D, Tran P. Review and evaluation of updated research on the health effects associated with low-dose ionising radiation. *Radiat Protect Dosimetry.* (2010) 140:103–36. doi: 10.1093/rpd/ncq141
40. Siegel J, Stabin M. RADAR commentary: use of linear no-threshold hypothesis in radiation protection regulation in the United States. *Health Phys.* (2012) 102:90–9. doi: 10.1097/HP.0b013e318228e5b4
41. Averbeck D. Does scientific evidence support a change from the LNT model for low-dose radiation risk extrapolation?. *Health Phys.* (2009) 97:493–504. doi: 10.1097/HP.0b013e3181b08a20
42. Cuttler J. Commentary on using LNT for radiation protection and risk assessment. *Dose Response.* (2010) 8:378–83. doi: 10.2203/dose-response.10-003.Cuttler
43. Calabrese EJ, O'Connor MK. Estimating risk of low radiation doses – a critical review of the BEIR VII report and its use of the linear no-threshold (LNT) hypothesis. *Radiat Res.* (2014) 182:463–74. doi: 10.1667/RR13829.1
44. Siegel J, Greenspan B, Maurer A, Taylor AT, Phillips WT, Van Nostrand D, et al. The BEIR VII estimates of low-dose radiation health risks are based on faulty assumptions and data analyses: a call for reassessment. *J Nucl Med.* (2018) 59:1017–9. doi: 10.2967/jnumed.117.206219
45. Tharmalingam S, Sreetharan S, Kulesza A, Boreham D, Tai T. Low-dose ionizing radiation exposure, oxidative stress and epigenetic programing of health and disease. *Radiat Res.* (2017) 188:525–38. doi: 10.1667/RR14587.1
46. Rothkamm K, Löbrich M. Evidence for a lack of DNA double-strand break repair in human cells exposed to very low x-ray doses. *Proc Natl Acad Sci USA.* (2003) 100:5057–62. doi: 10.1073/pnas.0830918100
47. Grudzenski S, Raths A, Conrad S, Rübe C, Löbrich M. Inducible response required for repair of low-dose radiation damage in human fibroblasts. *Proc Natl Acad Sci USA.* (2010) 107:14205–10. doi: 10.1073/pnas.1002213107
48. Amundson SA, Do KT, Fornace AJ. Induction of stress genes by low doses of gamma rays. *Radiat Res.* (1999) 152:225–31. doi: 10.2307/3580321
49. Amundson SA, Lee RA, Koch-Paiz CA, Bittner ML, Meltzer P, Trent JM, et al. Differential responses of stress genes to low dose-rate γ irradiation. *Mol Cancer Res.* (2003) 1:445–52.
50. Ding L, Shingyoji M, Chen F, Hwang J, Burma S, Lee C, et al. Gene expression profiles of normal human fibroblasts after exposure to ionizing radiation: a comparative study of low and high doses. *Radiat Res.* (2005) 164:17–26. doi: 10.1667/RR3354
51. Sokolov M, Neumann R. Global gene expression alterations as a crucial constituent of human cell response to low doses of ionizing radiation exposure. *Int J Mol Sci.* (2016) 17:55. doi: 10.3390/ijms17010055
52. Mezentsev A, Amundson S. Global gene expression responses to low- or high-dose radiation in a human three-dimensional tissue model. *Radiat Res.* (2011) 175:677–88. doi: 10.1667/RR2483.1
53. Goldberg Z, Rocke D, Schwietert C, Berglund S, Santana A, Jones A, et al. Human *in vivo* dose-response to controlled, low-dose low linear energy transfer ionizing radiation exposure. *Clin Cancer Res.* (2006) 12:3723–9. doi: 10.1158/1078-0432.CCR-05-2625
54. Azzam EI, Colangelo NW, Domogauer JD, Sharma N, de Toledo SM. Is ionizing radiation harmful at any exposure? *An echo that continues to vibrate. Health Phys.* (2016) 110:249–51. doi: 10.1097/HP.0000000000000450
55. Feinendegen L. Evidence for beneficial low level radiation effects and radiation hormesis. *Br J Radiol.* (2005) 78:3–7. doi: 10.1259/bjr/63353075
56. Nagasawa H, Little JB. Induction of sister chromatid exchanges by extremely low doses of α-particles. *Cancer Res.* (1992) 52:6394–6.
57. Mothersill C, Seymour C. Medium from irradiated human epithelial cells but not human fibroblasts reduces the clonogenic survival of unirradiated cells. *Int J Radiat Biol.* (1997) 71:421–7. doi: 10.1080/095530097144030
58. Seymour C, Mothersill C, Alper T. High yields of lethal mutations in somatic mammalian cells that survive ionizing radiation. *Int J Radiat Biol Relat Stud Phys Chem Med.* (1986) 50:167–79. doi: 10.1080/09553008614550541
59. Kadhim M, Macdonald D, Goodhead D, Lorimore S, Marsden S, Wright E. Transmission of chromosomal instability after plutonium alpha-particle irradiation. *Nature.* (1992) 355:738–40. doi: 10.1038/355738a0
60. Lorimore S, Kadhim M, Pocock DA, Papworth D, Stevens DL, Goodhead DT, et al. Chromosomal instability in the descendants of unirradiated surviving cells after alpha-particle irradiation. *Proc Natl Acad Sci USA.* (1998) 95:5730–3. doi: 10.1073/pnas.95.10.5730
61. Marder B, Morgan W. Delayed chromosomal instability induced by DNA damage. *Mol Cell Biol.* (1993) 13:6667–77. doi: 10.1128/MCB.13.11.6667
62. Morgan W. Non-targeted and delayed effects of exposure to ionizing radiation: I. Radiation-induced genomic instability and bystander effects *in vitro*. *Radiat Res.* (2003) 159:567–80. doi: 10.1667/0033-7587(2003)159[0567:NADEOE]2.0.CO;2
63. Morgan W. Non-targeted and delayed effects of exposure to ionizing radiation: II. Radiation-induced genomic instability and bystander effects *in vivo*, clastogenic factors and transgenerational effects. *Radiat Res.* (2003) 159:581–96. doi: 10.1667/0033-7587(2003)159[0581:NADEOE]2.0.CO;2

64. Joiner M, Denekamp J, Maughan R. The use of 'top-up' experiments to investigate the effect of very small doses per fraction in mouse skin. *Int J Radiat Biol.* (1986) 49:565–80. doi: 10.1080/09553008514552811
65. Joiner M, Marples B, Lambin P, Short S, Turesson I. Low-dose hypersensitivity: current status and possible mechanisms. *Int J Radiat Oncol Biol Phys*. (2001) 49:379–89. doi: 10.1016/S0360-3016(00)01471-1
66. Amundson SA, Bittner M, Meltzer P, Trent J, Fornace AJ. Induction of gene expression as a monitor of exposure to ionizing radiation. *Radiat Res.* (2001) 156:657–61. doi: 10.1667/0033-7587(2001)156[0657:IOGEAA]2.0.CO;2
67. Snyder A. Review of radiation-induced bystander effects. *Hum Exp Toxicol.* (2004) 23:87–9. doi: 10.1191/0960327104ht423oa
68. UNSCEAR (United Nations Scientific Committee on the Effects of Atomic Radiation). *66 Report, vol. II, Annex C, Non-Targeted and Delayed Effects of Exposure to Ionizing Radiation*. New York, NY: United Nations (2006). p. 1–79.
69. Kadhim M, Salomaa S, Wright E, Hildebrandt G, Belyakov O, Prise K, et al. Non-targeted effects of ionising radiation-implications for low dose risk. *Mutat Res*. (2013) 752:84–98. doi: 10.1016/j.mrrev.2012.12.001
70. Campa A, Balduzzi M, Dini V, Esposito G, Tabocchini MA. The complex interactions between radiation induced non-targeted effects and cancer. *Cancer Lett*. (2015) 356:126–36. doi: 10.1016/j.canlet.2013.09.030
71. Djordjevic B. Bystander effects: a concept in need of clarification. *Bioessays.* (2000) 22:286–90 doi: 10.1002/(SICI)1521-1878(200003)22:3<286::AID-BIES10>3.0.CO;2-S
72. Koturbash I, Boyko A, Rodriguez-Juarez R, McDonald R, Tryndyak V, Kovalchuk I, et al. Role of epigenetic effectors in maintenance of the long-term persistent bystander effect in spleen *in vivo*. *Carcinogenesis.* (2007) 28:1831–8. doi: 10.1093/carcin/bgm053
73. Blyth BJ, Sykes PJ. Radiation-Induced bystander effects: what are they, and how relevant are they to human radiation exposures? *Radiat Res*. (2011) 176:139–57. doi: 10.1667/RR2548.1
74. Mancuso M, Pasquali E, Leonardi S, Tanori M, Rebessi S, Di Majo V, et al. Oncogenic bystander radiation effects in Patched heterozygous mouse cerebellum. *Proc Natl Acad Sci USA*. (2008) 105:12445–50. doi: 10.1073/pnas.0804186105
75. Tapio S, Jacob V. Radioadaptive response revisited. *Radiat Environ Biophys*. (2007) 46:1–12. doi: 10.1007/s00411-006-0078-8
76. Olivieri G, Bodycote J, Wolff S. Adaptive response of human lymphocytes to low concentrations of radioactive thymidine. *Science.* (1984) 223:594–7. doi: 10.1126/science.6695170
77. Wolff S. The adaptive response in radiobiology: evolving insights and implications. *Environ Health Perspect*. (1998) 106:277–83. doi: 10.1289/ehp.98106s1277
78. Schwartz J. Variability: the common factor linking low dose-induced genomic instability, adaptation and bystander effects. *Mutat Res*. (2007) 616:196–200. doi: 10.1016/j.mrfmmm.2006.11.016
79. Mothersill C, Seymour C. Changing paradigms in radiobiology. *Mutat Res Rev Mutat Res*. (2012) 750:85–95. doi: 10.1016/j.mrrev.2011.12.007
80. Morgan W, Sowa M. Non-targeted effects induced by ionizing radiation: mechanisms and potential impact on radiation induced health effects. *Cancer Lett*. (2015) 356:17–21. doi: 10.1016/j.canlet.2013.09.009
81. Hall EJ. The bystander effect. *Health Phys*. (2003) 85:31–35. doi: 10.1097/00004032-200307000-00008
82. Sowa M, Goetz W, Baulch J, Pyles D, Dziegielewski J, Yovino S, et al. Lack of evidence for low-LET radiation induced bystander response in normal human fibroblasts and colon carcinoma cells. *Int J Radiat Biol*. (2010) 86:102–13. doi: 10.3109/09553000903419957
83. Sowa M, Goetz W, Baulch J, Lewis A, Morgan W. No evidence for a low linear energy transfer adaptive response in irradiated RKO cells. *Radiat Prot Dos*. (2011) 143:311–14. doi: 10.1093/rpd/ncq487
84. Azzam EI, Toledo SM, Gooding T, Little JB. Intercellular communication is involved in the bystander regulation of gene expression in human cells exposed to very low fluences of alpha particles. *Radiat Res*. (1998) 150:497–504. doi: 10.2307/3579865
85. Barcellos-Hoff MH, Brooks AL. Extracellular signaling through the microenvironment: a hypothesis relating carcinogenesis, bystander effects, and genomic instability. *Radiat Res*. (2001) 156:618–27. doi: 10.1667/0033-7587(2001)156[0618:ESTTMA]2.0.CO;2
86. Brooks AL, Dauer LT. Advances in radiation biology: effect on nuclear medicine. *Semin Nucl Med.* (2014) 44:179–86. doi: 10.1053/j.semnuclmed.2014.03.004
87. Lorimore S, Coates P, Wright E. Radiation-induced genomic instability and bystander effects: inter-related nontargeted effects of exposure to ionizing radiation. *Oncogene.* (2003) 22:7058–69. doi: 10.1038/sj.onc.1207044
88. Huang L, Kim P, Nickoloff J, Morgan W. Targeted and nontargeted effects of low-dose ionizing radiation on delayed genomic instability in human cells. *Cancer Res*. (2007) 67:1099–104. doi: 10.1158/0008-5472.CAN-06-3697
89. Aypar U, Morgan WF, Baulch JE. Radiation-induced epigenetic alterations after low and high LET irradiations. *Mutat Res*. (2011) 707:24–33. doi: 10.1016/j.mrfmmm.2010.12.003
90. Ilnytskyy Y, Kovalchuk O. Non-targeted radiation effects-an epigenetic connection. *Mutat Res*. (2011) 714:113–25. doi: 10.1016/j.mrfmmm.2011.06.014
91. Reik W. Stability and flexibility of epigenetic gene regulation in mammalian development. *Nature.* (2007) 447:425–32. doi: 10.1038/nature05918
92. Jones P, Gonzalgo M. Altered DNA methylation and genome instability: a new pathway to cancer? *Proc Natl Acad Sci USA*. (1997) 94:2103–5. doi: 10.1073/pnas.94.6.2103
93. Kanwal R, Gupta S. Epigenetics and cancer. *J Appl Physiol*. (2010) 109:598–605. doi: 10.1152/japplphysiol.00066.2010
94. Sharma S, Kelly T, Jones P. Epigenetics in cancer. *Carcinogenesis.* (2010) 31:27–36. doi: 10.1093/carcin/bgp220
95. Kanwal R, Gupta K, Gupta S. Cancer epigenetics: an introduction. *Methods Mol Biol*. (2015) 1238:3–25. doi: 10.1007/978-1-4939-1804-1_1
96. Madakashira B, Sadler K. DNA methylation, nuclear organization, and cancer. *Front Genet*. (2017) 8:76. doi: 10.3389/fgene.2017.00076
97. Feil R, Fraga MF. Epigenetics and the environment: emerging patterns and implications. *Nat Rev Genet.* (2012) 13:97–109. doi: 10.1038/nrg3142
98. Romani M, Pistillo M, Banelli B. Environmental epigenetics: crossroad between public health, lifestyle, and cancer prevention. *Biomed Res Int*. (2015) 2015:587983. doi: 10.1155/2015/587983
99. Head J, Dolinoy D, Basu N. Epigenetics for ecotoxicologists. *Environ Toxicol Chem*. (2012) 31:221–7. doi: 10.1002/etc.1707
100. Tompkins J, Hall C, Chen V, et al. Epigenetic stability, adaptability, and reversibility in human embryonic stem cells. *Proc Natl Acad Sci USA*. (2012) 109:12544–9. doi: 10.1073/pnas.1209620109
101. D'Urso A, Brickner JH. Mechanisms of epigenetic memory. *Trends Genet*. (2014) 30:230–6. doi: 10.1016/j.tig.2014.04.004
102. Razin, A. CpG methylation, chromatin structure and gene silencing-a three-way connection. *EMBO J.* (1998) 17:4905–8. doi: 10.1093/emboj/17.17.4905
103. Jones P. Functions of DNA methylation: islands, start sites, gene bodies and beyond. *Nat Rev Genet*. (2012) 13:484–92. doi: 10.1038/nrg3230
104. Miousse I, Chalbot M, Lumen A, Ferguson A, Kavouras I, Koturbash I. Response of transposable elements to environmental stressors. *Mutat Res Rev Mutat Res*. (2015) 765:19–39. doi: 10.1016/j.mrrev.2015.05.003
105. Razin A, Riggs A. DNA methylation and gene function. *Science.* (1980) 210:604–10. doi: 10.1126/science.6254144
106. Kalinich J, Catravas G, Snyder S. The effect of gamma radiation on DNA methylation. *Radiat Res.* (1989) 117:185–97. doi: 10.2307/3577319
107. Miousse I, Kutanzi K, Koturbash I. Effects of ionizing radiation on DNA methylation: from experimental biology to clinical applications. *Int J Radiat Biol.* (2017) 93:457–69. doi: 10.1080/09553002.2017.1287454
108. Miousse I, Ewing L, Kutanzi K, Griffin R, Koturbash I. DNA methylation in radiation-induced carcinogenesis: experimental evidence and clinical perspectives. *Crit Rev Oncogen*. (2018) 23:1–11. doi: 10.1615/CritRevOncog.2018025687
109. Baylin SB, Jones PA. A decade of exploring the cancer epigenome-biological and translational implications. *Nat Rev Cancer.* (2012) 11:726–34. doi: 10.1038/nrc3130
110. Belli M, Tabocchini MA. Ionizing radiation-induced epigenetic modifications and their relevance to radiation protection. *Int J Mol Sci.* (2020) 21:5993. doi: 10.3390/ijms21175993
111. Mendonca M, Antoniono R, Redpath J. Delayed heritable damage and epigenetics in radiation-induced neoplastic transformation of human hybrid cells. *Radiat Res.* (1993) 134:209–16. doi: 10.2307/3578461

112. Hoffmann M, Schulz W. Causes and consequences of DNA hypomethylation in human cancer. *Biochem Cell Biol*. (2005) 83:296–321. doi: 10.1139/o05-036
113. Toyota M, Issa J. The role of DNA hypermethylation in human neoplasia. *Electrophoresis*. (2000) 21:329–33. doi: 10.1002/(SICI)1522-2683(20000101)21:2<329::AID-ELPS329>3.0.CO;2-9
114. Feinberg A, Vogelstein B. Hypomethylation distinguishes genes of some human cancers from their normal counterparts. *Nature*. (1983) 301:89–92. doi: 10.1038/301089a0
115. Lyon C, Klinge D, Liechty K, Gentry F, March T, Kang T, et al. Radiation-induced lung adenocarcinoma is associated with increased frequency of genes inactivated by promoter hypermethylation. *Radiat Res*. (2007) 168:409–14. doi: 10.1667/RR0825.1
116. Christensen BC, Marsit CJ. Epigenomics in environmental health. *Front Genet*. (2011) 2:84. doi: 10.3389/fgene.2011.00084
117. Romanenko A, Morell-Quadreny L, Lopez-Guerrero J, Pellin A, Nepomnyaschy V, Vozianov A, et al. The INK4a/ARF locus: role in cell cycle control for renal cell epithelial tumor growth after the chernobyl accident. *Virchows Arch*. (2004) 445:298–304. doi: 10.1007/s00428-004-1056-7
118. Takabatake M, Blyth B, Daino K, Imaoka T, Nishimura M, Fukushi M, et al. DNA methylation patterns in rat mammary carcinomas induced by pre- and post-pubertal irradiation. *PLoS ONE*. (2016) 11:e0164194. doi: 10.1371/journal.pone.0164194
119. Margueron R, Trojer P, Reinberg D. The key to development: interpreting the histone code? *Curr Opin Genet Dev*. (2005) 15:163–76. doi: 10.1016/j.gde.2005.01.005
120. Mendez-Acuna L, Di Tomaso M, Palitti F, Martinez-Lopez W. Histone posttranslational modifications in DNA damage response. *Cytogenet Genome Res*. (2010) 128:28–36. doi: 10.1159/000296275
121. Averbeck NB, Durante M. Protein acetylation within the cellular response to radiation. *J Cell Physiol*. (2011) 226:962–7. doi: 10.1002/jcp.22466
122. Tharmalingam S, Sreetharan S, Brooks A, Boreham D. Re-evaluation of the linear no-threshold (LNT) model using new paradigms and modern molecular studies. *Chem Biol Interact*. (2019) 301:54–67. doi: 10.1016/j.cbi.2018.11.013
123. Lee R, Feinbaum R, Ambros V. The *C. elegans* heterochronic gene lin-4 encodes small RNAs with antisense complementarity to lin-14. *Cell*. (1993) 75:843–54. doi: 10.1016/0092-8674(93)90529-Y
124. Halimi M, Asghari S, Sariri R, Moslemi D, Parsian H. Cellular response to ionizing radiation: a MicroRNA story. *Int J Mol Cell Med*. (2012) 1:178–84.
125. Metheetrairut C, Slack F. MicroRNAs in the ionizing radiation response and in radiotherapy. *Curr Opin Genet Dev*. (2013) 23:12–19. doi: 10.1016/j.gde.2013.01.002
126. Chaudhry MA. Radiation-induced microRNA: discovery, functional analysis, and cancer radiotherapy. *J Cell Biochem*. (2014) 115:436–49. doi: 10.1002/jcb.24694
127. Cellini F, Morganti AG, Genovesi D, Silvestris N, Valentini V. Role of microRNA in response to ionizing radiations: evidences and potential impact on clinical practice for radiotherapy. *Molecules*. (2014) 19:5379–401. doi: 10.3390/molecules19045379
128. Marta G, Garicochea B, Carvalho A, Real J, Kowalski L. MicroRNAs, cancer and ionizing radiation: where are we? *Rev Assoc Med Bras*. (2015) 61:275–81. doi: 10.1590/1806-9282.61.03.275
129. O'Leary V, Hain S, Maugg D, Smida J, Azimzadeh O, Tapio S, et al. Long non-coding RNA PARTICLE bridges histone and DNA methylation. *Sci Rep*. (2017) 7:1790. doi: 10.1038/s41598-017-01875-1
130. Goetz W, Morgan MN, Baulch J. The effect of radiation quality on genomic DNA methylation profiles in irradiated human cell lines. *Radiat Res*. (2011) 175:575–87. doi: 10.1667/RR2390.1
131. Lima F, Ding D, Goetz W, Yang A, Baulch J. High LET 56Fe ion irradiation induces tissue-specific changes in DNA methylation in the mouse. *Environ Mol Mutagen*. (2014) 55:266–77. doi: 10.1002/em.21832
132. Nzabarushimana E, Miousse I, Shao L, Chang J, Allen A, Turner J, et al. Long-term epigenetic effects of exposure to low doses of 56Fe in the mouse lung. *J Radiat Res*. (2014) 55:823–8. doi: 10.1093/jrr/rru010
133. Miousse I, Shao L, Chang J, Feng W, Wang Y, Allen A. Exposure to low-dose Fe-56-ion radiation induces long-term epigenetic alterations in mouse bone marrow hematopoietic progenitor and stem cells. *Radiat Res*. (2014) 182:92–101. doi: 10.1667/RR13580.1
134. Kennedy E, Conneely K, Vertino P. *Epigenetic Memory of Space Radiation Exposure*. (2014). Available online at: https://three.jsc.nasa.gov/articles/Vertino.pdf (accessed July 30, 2014).
135. Kennedy E, Powell D, Li Z, Bell JS, Barwick B, Feng H, et al. Galactic cosmic radiation induces persistent epigenome alterations relevant to human lung cancer. *Sci Rep*. (2018) 8:6709. doi: 10.1038/s41598-018-24755-8
136. Heard E, Martienssen R. Transgenerational epigenetic inheritance: myths and mechanisms. *Cell*. (2014) 157:95–109. doi: 10.1016/j.cell.2014.02.045
137. Reik W, Dean W, Walter J. Epigenetic reprogramming in mammalian development. *Science*. (2001) 293:1089. doi: 10.1126/science.1063443
138. Zeng Y, Chen T. DNA methylation reprogramming during mammalian development. *Genes*. (2019) 10:257. doi: 10.3390/genes10040257
139. Dubrova Y, Plumb M. Ionising radiation and mutation induction at mouse minisatellite loci. The story of the two generations. *Mutat Res*. (2002) 499:143–50. doi: 10.1016/S0027-5107(01)00284-6
140. UNSCEAR (United Nations Scientific Committee on the Effects of Atomic Radiation). *Biological Mechanisms of Radiation Actions at Low Doses*. New York, NY: United Nations (2012).
141. Szumiel I. Ionizing radiation-induced oxidative stress, epigenetic changes and genomic instability: the pivotal role of mitochondria. *Int J Radiat Biol*. (2015) 91:1–12. doi: 10.3109/09553002.2014.934929
142. Franco R, Schoneveld O, Georgakilas A, Panayiotidis M. Oxidative stress, DNA methylation and carcinogenesis. *Cancer Lett*. (2008) 266:6–11. doi: 10.1016/j.canlet.2008.02.026
143. Ziech D, Franco R, Pappa A, Panayiotidis M. Reactive oxygen species (ROS)-induced genetic and epigenetic alterations in human carcinogenesis. *Mutat Res*. (2011) 711:167–73. doi: 10.1016/j.mrfmmm.2011.02.015
144. Sprung C, Ivashkevich A, Forrester H, Redon CE, Georgakilas A, Martin OA. Oxidative DNA damage caused by inflammation may link to stress-induced non-targeted effects. *Cancer Lett*. (2015) 356:72–81. doi: 10.1016/j.canlet.2013.09.008
145. Sisakht M, Darabian M, Mahmoodzadeh A, Bazi A, Shafiee S, Mokarram P, et al. The role of radiation induced oxidative stress as a regulator of radio-adaptive responses. *Int J Radiat Biol*. (2020) 96:561–76. doi: 10.1080/09553002.2020.1721597
146. Clutton S, Townsend KM, Walker C, Ansell J, Wright E. Radiation-induced genomic instability and persisting oxidative stress in primary bone marrow cultures. *Carcinogenesis*. (1996) 17:1633–9. doi: 10.1093/carcin/17.8.1633
147. Sarkies P. Molecular mechanisms of epigenetic inheritance: possible evolutionary implications. *Semin Cell Dev Biol*. (2019) 97:106–15. doi: 10.1016/j.semcdb.2019.06.005
148. Ghiassi-Nejad M, Mortazavi S, Cameron J, Niroomand-Rad A, Karam P. Very high background radiation areas of Ramsar, Iran: preliminary biological studies. *Health Phys*. (2002) 82:87–93. doi: 10.1097/00004032-200201000-00011
149. Ghiassi-Nejad M, Zakeri F, Assaei R, Kariminia A. Long-term immune and cytogenetic effects of high level natural radiation on Ramsar inhabitants in Iran. *J Environ Radioact*. (2004) 74:107–16. doi: 10.1016/j.jenvrad.2003.12.001
150. Masoomi J, Mohammadi SH, Amini M, Ghiassi-Nejad M. High background radiation areas of Ramsar in Iran: evaluation of DNA damage by alkaline single cell gel electrophoresis (SCGE). *J Environ Radioact*. (2006) 86:176–86. doi: 10.1016/j.jenvrad.2005.08.005
151. Zakeri F, Rajabpour M, Haeri S, Kanda R, Hayata I, Nakamura S, et al. Chromosome aberrations in peripheral blood lymphocytes of individuals living in high background radiation areas of Ramsar, Iran. *Radiat Environ Biophys*. (2011) 50:571–8. doi: 10.1007/s00411-011-0381-x
152. Mortazavi S, Mozdarani H. Non-linear phenomena in biological findings of the residents of high background radiation areas of Ramsar. *Int J Radiat Res*. (2013) 11:3–9. Available online at: http://ijrr.com/article-1-1004-en.html
153. Lampe N, Breton V, Sarramia D, Sime-Ngando T, Biron D. Understanding low radiation background biology through controlled evolution experiments. *Evol Appl*. (2017) 10:658–66. doi: 10.1111/eva.12491
154. Smith NJ. The development of deep underground science facilities. *Nucl Phys B Proc Suppl*. (2012) 229:333–41. doi: 10.1016/j.nuclphysbps.2012.09.052

155. Morciano P, Cipressa F, Porrazzo A, Esposito G, Tabocchini M, Cenci G. Fruit flies provide new insights in low radiation background biology at the INFN underground Gran Sasso national laboratory (LNGS). *Radiat Res.* (2018) 190:217–25. doi: 10.1667/RR15083.1
156. Liu J, Ma T, Liu Y, Zou J, Gao M, Zhang R, et al. History, advancements, and perspective of biological research in deep-underground laboratories: a brief review. *Environ Int*. (2018) 120:207–14. doi: 10.1016/j.envint.2018.07.031
157. Planel H, Soleilhavoup J, Tixador R, Richoilley G. Demonstration of a stimulating effect of natural ionizing radiation and of very low radiation doses on cell multiplication. In: IAEA, editor. *Symposiumon Biological Effects of Low-Level Radiation Pertinent to Protection of Man and His Environment*. Vienna: International Atomic Energy Agency (1976). p. 127–39.
158. Planel H, Soleilhavoup J, Tixador R, Richoilley G, Conter A, Croute F, et al. Influence on cell proliferation of background radiation or exposure to very low, chronic radiation. *Health Phys.* (1987) 52:571–8. doi: 10.1097/00004032-198705000-00007
159. Castillo H, Smith GB. Below-background ionizing radiation as an environmental cue for bacteria. *Front Microbiol.* (2017) 8:177. doi: 10.3389/fmicb.2017.00177
160. Smith G, Grof Y, Navarrette A, Guilmette R. Exploring biological effects of low background radiation from the other side of the background. *Health Phys*. (2011) 100:263–5. doi: 10.1097/HP.0b013e318208cd44
161. Castillo H, Schoderbek D, Dulal S, Escobar G, Wood J, Nelson R, et al. Stress induction in the bacteria shewanella oneidensis and deinococcus radiodurans in response to below-background ionizing radiation. *Int J Radiat Biol*. (2015) 91:749–56. doi: 10.3109/09553002.2015.1062571
162. Castillo H, Li X, Schilkey F, Smith GB. Transcriptome analysis reveals a stress response of *Shewanella oneidensis* deprived of background levels of ionizing radiation. *PLoS ONE.* (2018) 13:e0196472. doi: 10.1371/journal.pone.0196472
163. Satta L, Augusti-Tocco G, Ceccarelli R, Esposito A, Fiore M, Paggi P, et al. Low environmental radiation background impairs biological defence of the yeast saccharomyces cerevisiae to chemical radiomimetic agents. *Mutat Res*. (1995) 347:129–33. doi: 10.1016/0165-7992(95)00031-3
164. Satta L, Antonelli F, Belli M, Sapora O, Simone G, Sorrentino E, et al. Influence of a low background radiation environment on biochemical and biological responses in V79 cells. *Radiat Environ Biophys.* (2002) 41:217–24. doi: 10.1007/s00411-002-0159-2
165. Carbone MC, Pinto M, Antonelli F, Amicarelli F, Balata M, Belli M, et al. Effects of deprivation of background environmental radiation on cultured human cells. *Il Nuovo Cimento.* (2010) 4:469–77. doi: 10.1393/ncb/i2010-10889-y
166. Fratini E, Carbone C, Capece D, Esposito G, Simone G, Tabocchini M, et al. Low-radiation environment affects the development of protection mechanisms in V79 cells. *Radiat Environ Biophys*. (2015) 54:183–94. doi: 10.1007/s00411-015-0587-4
167. Morciano P, Iorio R, Iovino D, Cipressa F, Esposito G, Porrazzo A, et al. Effects of reduced natural background radiation on drosophila melanogaster growth and development as revealed by the FLYINGLOW program. *J Cell Physiol*. (2018) 233:23–9. doi: 10.1002/jcp.25889
168. Rando O, Verstrepen K. Timescales of genetic and epigenetic inheritance. *Cell.* (2007) 128:655–68. doi: 10.1016/j.cell.2007.01.023

Conflict of Interest: The authors declare that the research was conducted in the absence of any commercial or financial relationships that could be construed as a potential conflict of interest.

frontiers in Public Health

PERSPECTIVE
published: 07 December 2020
doi: 10.3389/fpubh.2020.611146

Underground Radiobiology: A Perspective at Gran Sasso National Laboratory

*Giuseppe Esposito[1,2], Pasquale Anello[1], Marco Ampollini[1], Emanuela Bortolin[1], Cinzia De Angelis[1], Giulia D'Imperio[2], Valentina Dini[1,2], Cristina Nuccetelli[1,2], Maria Cristina Quattrini[1], Claudia Tomei[2], Aldo Ianni[3], Marco Balata[3], Giuseppe Carinci[4], Maurizio Chiti[4], Oscar Frasciello[4], Giovanni Cenci[5], Francesca Cipressa[5], Alex De Gregorio[5], Antonella Porrazzo[5], Maria Antonella Tabocchini[1,2,6], Luigi Satta[7] and Patrizia Morciano[3]**

[1] Istituto Superiore di Sanità (ISS), Rome, Italy, [2] Istituto Nazionale di Fisica Nucleare (INFN) Sezione Roma 1, Rome, Italy, [3] Laboratori Nazionali del Gran Sasso-INFN, Assergi, L'Aquila, Italy, [4] Laboratori Nazionali di Frascati-INFN, Frascati, Italy, [5] SAPIENZA Università di Roma, Rome, Italy, [6] Museo storico della Fisica e Centro Studi e Ricerche "Enrico Fermi", Rome, Italy, [7] Independent Researcher, Rome, Italy

OPEN ACCESS

Edited by:
Shinji Tokonami, Hirosaki University, Japan

Reviewed by:
Ikuo Kashiwakura, Hirosaki University, Japan
Alexey Moskalev, Komi Scientific Center (RAS), Russia

***Correspondence:**
Patrizia Morciano
patrizia.morciano@lngs.infn.it

Specialty section:
This article was submitted to Radiation and Health, a section of the journal Frontiers in Public Health

Received: *28 September 2020*
Accepted: *16 November 2020*
Published: *07 December 2020*

Citation:
Esposito G, Anello P, Ampollini M, Bortolin E, De Angelis C, D'Imperio G, Dini V, Nuccetelli C, Quattrini MC, Tomei C, Ianni A, Balata M, Carinci G, Chiti M, Frasciello O, Cenci G, Cipressa F, De Gregorio A, Porrazzo A, Tabocchini MA, Satta L and Morciano P (2020) Underground Radiobiology: A Perspective at Gran Sasso National Laboratory. Front. Public Health 8:611146. doi: 10.3389/fpubh.2020.611146

Scientific community and institutions (e. g., ICRP) consider that the Linear No-Threshold (LNT) model, which extrapolates stochastic risk at low dose/low dose rate from the risk at moderate/high doses, provides a prudent basis for practical purposes of radiological protection. However, biological low dose/dose rate responses that challenge the LNT model have been highlighted and important dowels came from radiobiology studies conducted in Deep Underground Laboratories (DULs). These extreme ultra-low radiation environments are ideal locations to conduct below-background radiobiology experiments, interesting from basic and applied science. The INFN Gran Sasso National Laboratory (LNGS) (Italy) is the site where most of the underground radiobiological data has been collected so far and where the first *in vivo* underground experiment was carried out using *Drosophila melanogaster* as model organism. Presently, many DULs around the world have implemented dedicated programs, meetings and proposals. The general message coming from studies conducted in DULs using protozoan, bacteria, mammalian cells and organisms (flies, worms, fishes) is that environmental radiation may trigger biological mechanisms that can increase the capability to cope against stress. However, several issues are still open, among them: the role of the quality of the radiation spectrum in modulating the biological response, the dependence on the biological endpoint and on the model system considered, the overall effect at organism level (detrimental or beneficial). At LNGS, we recently launched the RENOIR experiment aimed at improving knowledge on the environmental radiation spectrum and to investigate the specific role of the gamma component on the biological response of *Drosophila melanogaster.*

Keywords: low radiation environment, underground biology, radiobiology, *Drosophila melanogaster*, DULIA-*bio*, LNGS, RENOIR

INTRODUCTION

Understanding the impact of natural background radiation on metabolism of living organisms is an open puzzling issue. For about 4 billion years, life on Earth has experienced differing levels of natural radiation, of cosmic and Earth origin. Environmental radiation is believed to have played a relevant role during the evolution of living organisms, contributing to the development of still poorly characterized defense mechanisms to minimize oxidative stress (1) In addition to issues of fundamental interest, these studies also have practical implications in radiation protection and medicine. The United Nations Scientific Committee on the Effects of Atomic Radiation (UNSCEAR) "*encourage*(s) *research into the mechanistic understanding of low-dose radiation action that may contribute to disease in humans*," and fosters studies "*to assess the health risk related to the environmental radiation exposure*" (2, 3). In this framework, underground biology is a new and very exciting area of investigation. The definition is referred to as the biological studies conducted in Deep Underground Laboratories (DULs), originally built to host particle, astro-particle and nuclear physics experiments searching for rare events such as proton or neutrino-less double decays that require a very low radioactivity environment (4, 5). These unique and extreme settings are now being exploited in other disciplines, including biology with its applications in radiobiology, making it possible to investigate if and how a substantial reduction of the exposure to environmental ionizing radiation background affects living organisms.

The Gran Sasso National Laboratory (LNGS), L'Aquila, Italy, is one of the largest DUL in the world and where most biological investigations have been conducted so far. The results of the first LNGS experiment, named Pulex, showed that the permanence in the low radiation underground laboratory decreases the defense mechanisms against chemical radio-mimetic compounds in yeasts (6). More recently, the PULEX-COSMIC SILENCE experiments get more insight into the role of environmental radiation in the biological response of different *in vitro* mammalian cellular systems of rodent (7–9) and human origin (10, 11). In 2018, we obtained the first evidence of the influence of environmental radiation on the response of a complex organism, namely *Drosophila melanogaster* (12, 13).

Interestingly, similar evidence has been obtained from experiments conducted in other DULs using protozoan, bacteria, and mammalian cells (14–18).

The general message coming from all these studies is that environmental radiation may trigger biological mechanisms that increase the capability to cope against stress.

However, several issues are still open, among them: the role of the quality of the radiation spectrum in modulating the biological response, the dependence on the biological endpoint and on the model system considered, the role of genetic/epigenetic modifications (19), the overall effect at organism level (detrimental or beneficial).

The growing interest in underground radiobiology is testified by the establishment of several projects, like LBRE that is being conducted at WIPP (USA) since 2011 (15), the more recent REPAIR at SNOLAB (Canada) (20), the Deep-underground Medicine studies at CJEML (China) (21) and SELLR at Boulby Underground Laboratory (UK) (22).

This scenario has driven the organization of a series of dedicated Workshops, named DULIA-*bio* (Deep Underground Laboratory Integrated Activity in biology), with the purpose to establish a common path for European/International underground laboratories in deep life studies and its application to astrobiology, biophysics, human health and radiation protection. The first one was held in Canfranc, Spain, in October 2015,[1] the second at the LNGS, Italy, in November 2019.[2] The next DULIA-*bio* Workshop is expected to be organized in Boulby, UK.

In this Perspective paper, after a brief summary of the LNGS experience in conducting underground radiobiological studies, we report on our approach to get more insight in the field of extremely low dose rate radiobiology. In our opinion, a crucial point is to elucidate the role of the different components of the environmental radiation field on the response of living organisms. With this aim, we recently started the RENOIR (*Radiation ENvirOnment triggers bIological Responses in flies: physical and biological mechanisms*) experiment, using *Drosophila melanogaster* as *in vivo* model system. We will describe the challenges faced, the strategies to overcome them and the first dosimetric and biological results finalized to optimize the experimental set up.

THE UNDERGROUND RADIOBIOLOGY EXPERIENCE AT LNGS: HISTORY, ACHIEVEMENTS AND CHALLENGES

During the construction of the LNGS, a group of physicists was involved in the measurements of the radiation field inside the experimental halls that were being built. One of them, Luigi Satta, was "*struck by the numbers*," as he uses to say. Indeed, it was immediately clear that, thanks to the 1400 m-coverage of dolomitic rocks poor of uranium and thorium, the underground radiation field was considerably reduced with respect to the external environment. Luigi Satta's pioneering idea of conducting underground experiments with biological systems soon took shape and a multidisciplinary group of scientists launched the first biological experiment on yeasts. Since then, biological investigation has continued for many years using different *in vitro* and *in vivo* model systems and most recently the fruit fly *Drosophila melanogaster*.

Although *in vitro* studies are continuing to provide important mechanistic answers, *in vivo* investigation remains a top priority for the underground radiobiology community seeking a "robust" model organism suitable for studies in these extreme environments.

In our experience, *Drosophila melanogaster* has proven to be particularly responsive to changes in environmental radiation promptly modifying its physiological responses. However, in

[1] https://indico.cern.ch/event/436589/overview
[2] https://agenda.infn.it/event/19116/timetable/

addition to flies, other organisms are currently being investigated, namely fishes at the SNOLAB (23) and nematodes at WIPP (24). The comparison between the responses of the organisms placed at different levels of the phylogenetic tree will provide interesting insights to understand the role of natural radiations in the adaptation and evolution of living organisms.

Since the pilot yeast study, the LNGS experience demonstrated that a fruitful approach is to conduct parallel tests in underground Low Radiation Environment (LRE) and in above ground Reference Radiation Environment (RRE), keeping working conditions and environmental parameters as much as possible the same, except for the ionizing radiation background. Since the visible solar spectrum at LRE can influence the circadian rhythms of flies, we decided to eliminate this source of variability using two identical *Drosophila* incubators (one at LRE and the other at RRE) in which flies live under the same conditions of light, temperature and humidity.

A close monitoring of the experimental parameters is mandatory for the interpretation of the results. As for the biological tests, reagents from the same batch should always be used. Furthermore, the presence of specialized facilities, e.g., Mechanical Workshop, Electronics, Chemistry & Chemical Plants Services, can be extremely useful for any experimental need.

LNGS, being located in a tunnel under a mountain, has some favorable features. There is no significant difference in terms of atmospheric pressure; moreover, an easy horizontal access to the LRE and the proximity of the RRE and the LRE labs allows the same operator to conduct measurements in both locations during the same day, minimizing other possible sources of variability.

Over many years of researches, the multidisciplinary Cosmic Silence Collaboration has developed and improved strategies and implemented facilities to further optimize the working conditions at LNGS. The new Cosmic Silence facility dedicated to *in vivo* studies was recently built and equipped, next the Pulex one, dedicated to *in vitro* studies. A key goal of the research group is to continuously improve the characterization of the radiation field in the environments where the experiments are conducted. In particular, during the biological tests, radon is continuously monitored as well as the gamma dose-rate. Furthermore, especially designed devices are under implementation to modulate the gamma component, in order to evaluate this specific contribution on the observed biological responses (see below "The RENOIR Experiment").

THE RENOIR EXPERIMENT: A FIRST STEP IN THE EVALUATION OF THE ROLE OF RADIATION QUALITY

It is interesting to note that *Drosophila melanogaster,* well-known to be a radioresistant organism, responds so promptly to changes in the environmental radiation. The doses/fluences of concern are so low that we should speculate about the triggering of bystander mechanisms, typical of the so-called ≪non-targeted effects≫, that involve cell-cell communication phenomena for amplifying such small signal(s) (25).

In the attempt to understand whether the biological response is related to an overall increase of the dose-rate exposure or to the contribution of specific component(s) of the radiation field, the three-year RENOIR experiment recently started at LNGS. We adopt a step by step approach; the first phase will consists in modulating the gamma component using shielding or naturally occurring gamma-emitters.

RENOIR has two main aims: 1. to improve the knowledge of the radiation field at RRE and at LRE; 2. to obtain information about the involvement of the gamma component of the environmental radiation field on the fertility and gene expression of fruit flies.

Characterization of the Radiation Field

Different components contribute to the overall environmental dose/dose rate in the different experimental sites. As evaluated on the basis of the UNSCEAR Report (26), at RRE the cosmic rays (mostly muons) contribution to the dose rate is of about 41 nSv/h, that of cosmic-ray neutrons of about 21 nSv/h; the terrestrial gamma rays contribution, measured by LNGS colleagues, is of about 22 nSv/h (Di Carlo personal communication). At LRE, the dose rates due to cosmic rays and neutrons are strongly reduced with respect to those at RRE (27), while the gamma dose rate is comparable (about 20 nSv/h, as obtained by us in Reuter Stokes, Automess and TLD measurements).

Another contribution to the environmental dose/dose rate comes from the radon (^{222}Rn) decay products. In the underground Pulex-Cosmic Silence facilities, an efficient ventilation system is running to maintain radon concentration comparable to that at RRE. Hourly and daily variations of indoor radon activity concentration in air are routinely monitored by the AlphaGUARD active device. We are currently able to have average values of ∼15 Bq/m^3 and ∼20.43 Bq/m^3, at LRE and RRE, respectively.

One of the first goals of the RENOIR Project is to further characterize the radiation field by semi-quantitative *in-situ* gamma spectroscopic measurements using a high-efficiency commercial portable spectrometer (80% HpGe). With this technique, already successfully applied in indoor environments since the 80' (28, 29), we will collect and elaborate the gamma spectra to gain information about the gamma fluxes in the experimental sites. Moreover, the gamma dose rates will be measured at RRE and LRE laboratories with organic scintillator dose rate meters, Reuter Stokes high pressure ionization chamber and high sensitivity thermo-luminescent detectors (TLD).

To detect thermal neutrons, we will subtract the gamma contribution measured by TLD-700H from the TLD-600H gross reading, these latter also exhibiting a large thermal neutron absorption cross section. To perform a dosimetric and spectroscopic investigation of the neutron field in a wider energy range, we will use a BF3 proportional tube in particular a Boron trifluoride detector (Centronic) and the DIAMON spectrometer, a low energy resolution neutron spectrometer developed by the Nuclear Measurements group (Energy department, PoliMi, Italy) in collaboration with RAYLAB (30).

Finally, in order to characterize radiation field components that are not directly detectable by our instrumentations (e.g.,

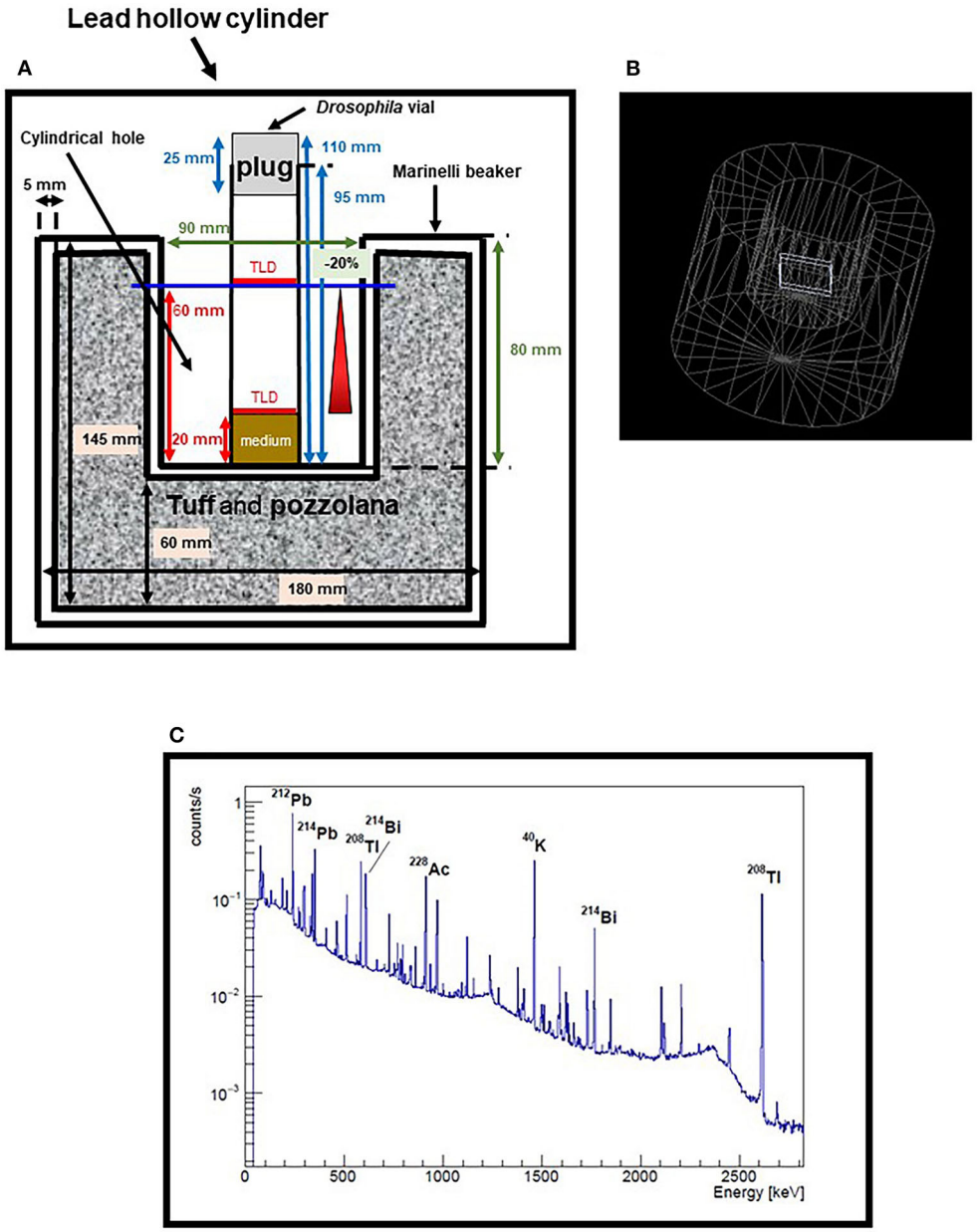

FIGURE 1 | Measurements and simulations for the optimization of the Marinelli beaker. **(A)** Scheme of Marinelli beaker currently in use, placed inside the 10 cm thick lead hollow cylinder. Only the *Drosophila* vial in the center of the cylindrical hole is shown, with two sets of TLDs positioned at two different heights. Dimensions of Marinelli are in black, dimensions of *Drosophila* vial are in blue, dimensions of the cylindrical hole are in green and the heights of TLDs are indicated in red. **(B)** Geometry of the Marinelli beaker implemented in the simulation. The TLDs were simulated with dimensions 40 × 40 × 4 mm^3, that is with the same thickness but much wider surface area than the real detectors, to get a reasonable compromise between statistics and computation time. **(C)** Spectrum of a tuff/pozzolana sample, measured with an HPGe detector. Some of the major peaks are shown as examples of the heterogeneity of the emitters in the sample.

muons) and to arrange a suitable dose model inside both LRE and RRE, we will conduct Monte Carlo simulations. Simulations will also help in the design and realization of the devices we are implementing for decreasing or increasing the gamma dose rate. Indeed, the modulation of the gamma component of radiation field is linked to the second major goal of RENOIR.

Implementation and Optimization of Devices for Modulating the Gamma Component of the Radiation Spectrum

In order to reduce of several hundred times the gamma component at RRE, we are adapting to our purposes a Gamma spectrometry shield. The 10 cm thick lead hollow cylinder will be

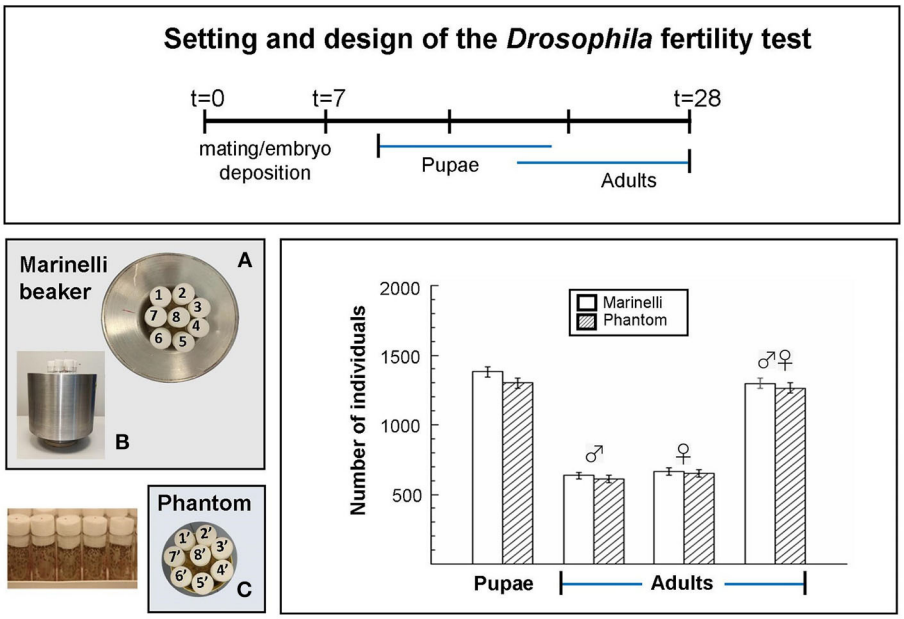

FIGURE 2 | Benchmark *Drosophila* fertility test, carried out in the reference external LNGS laboratory, aimed at checking the irradiation configuration and getting information for optimizing the design of the new device. Setting and design of the *Drosophila* fertility test: After mating and embryo deposition, pupae and adults were counted for the periods indicated by the blue lines. **(A)** Top view and **(B)** lateral view of eight tubes containing flies inside the Marinelli; **(C)** top view of eight tubes containing flies inside the phantom. Columns indicate the total number of pupae and adults (males and females) from five replicates (tubes) obtained in three independent experiments. Error bars represent the square root of the total counts. Statistical differences between the results obtained inside and outside the Marinelli beaker were analyzed using the Student's t test ($p < 0.05$). No significant differences were observed.

equipped with a properly designed ventilation system to prevent the accumulation of radon and with a temperature and light control system for proper *Drosophila* maintenance.

To increase the gamma component at LRE, we will use especially designed Marinelli beakers filled with natural gamma-emitter building material (tuff and pozzolana), and sealed to avoid any radon exposure. This approach has been proposed for the first time by the WIPP group who used gamma from ^{40}K to increase the dose rate underground in bacteria experiments (16).

The increase of the dose rate with the gamma rays from the decay of the different emitters present in our tuff/pozzolana mix (see **Figure 1C**) is a first step in the attempt to simulate the low LET component of the background radiation spectrum. Starting from the measured value of about 20 nGy/h for gamma rays at LRE (i.e., the only low LET radiation type in this environment), we will gradually increase this contribution up to the total dose rate value of the low LET components at RRE (i.e., gamma rays plus muons) and even beyond. We will use TLD to monitor the dose rate inside and outside the shield and the Marinelli beaker.

Presently, we have launched a series of gamma radiation measurements using TLD-700H inside the cylindrical hole of a large size standard Marinelli beaker placed into the 10 cm thick lead cylinder (**Figure 1A**). A first set of measurements was performed during a period of 41 days with the aim to verify the vertical and horizontal variations in the dose distribution experienced by flies. Several vials containing five TLDs each, were placed at the perimeter of the Marinelli internal hole, at the same height. An additional vial was placed in the center of the hole in which two sets of TLDs were positioned at two different heights, i.e., 20 mm e 60 mm respectively (representing the base of the nutrient medium and the max height reached by the flies). Preliminary results gave a dose rate of ∼122 nGy/h, with a variation coefficient within 2.5% for the dosimeters placed in the same plane and a difference of about 20% between the dosimeters located at the two different heights. In order to reduce this difference below 10%, a value acceptable to our purposes, we decided to design new Marinelli beakers.

Simulations by means of the Geant 4 code (31) were performed where the geometry of the Marinelli beaker was implemented and its dimensions parameterized, keeping the internal hole fixed (**Figure 1B**). The volume of the Marinelli was assigned a material with the chemical composition and density of a standard rock. Then, gamma rays were generated and uniformly distributed within this volume, with isotropic direction distribution and energy randomly extracted from a spectrum of a tuff/pozzolana sample, as measured by an HPGe detector (**Figure 1C**).

As expected, the variation between the dosimeters located at the two aforementioned heights was mainly due to the irradiation coming from the bottom part of the Marinelli. Therefore, we simulated only the upper part of the Marinelli, a cylindrical shell with an inner and outer diameter of 90 mm and 180 mm, respectively, and performed a scan of the simulated dose rate by

varying the position of the TLD. We found that in the central region between 20 and 60 mm the dose rate is constant within 5%, a condition that is suitable for our purposes.

Simulations also indicate that increasing the outer diameter to 280 mm, the dose rate at the position of 20 mm height could be increased up to 40%.

Feasibility Test of *Drosophila* Irradiation Using Marinelli Beaker

Taking advantage of our previous results (12), to test the Marinelli as exposure device we conducted at RRE a benchmark test on fertility, being this end point robust and less time consuming than life span. Wild-type *Drosophila* was put inside the Marinelli beaker and also inside a phantom, having the same geometry as the Marinelli, in the absence of naturally occurring gamma-emitters. Both were placed on the bench in the same fly-room two meters apart each other in order to significantly reduce the gamma irradiation from Marinelli to the phantom. Temperature, relative humidity and day/night light cycle were the same. Briefly, five young wild-type males and five virgin wild-type females were crossed for 1 week, parents were removed and progeny was left to develop to adults. The number of pupae was counted along with the number of hatched adults until 21 days. No significant differences were observed in the number of pupae or hatched adults per cross in the two exposure scenarios (**Figure 2**), suggesting that *Drosophila* fertility is not affected by ∼5 times increasing of the gamma component at RRE (∼122 nGy/h vs. ∼22 nGy/h).

The experiment was useful to check the irradiation configuration and confirmed the feasibility of the test in the conditions we are setting.

CONCLUSIONS

Underground biology is becoming a field in constant and considerable expansion. The last few years showed a growing interest from several worldwide DULs for biological studies and increasing efforts to implement in loco underground radiobiology. Although a limited number of research groups are involved in this field of investigation, due to the limited number of DULs worldwide and the difficulties of working in such extreme places, the information that comes from controlled studies in underground environments can be extremely interesting from basic and applied science.

Experiments conducted in DULs have shown changes compared to above ground laboratories in the responses of bacteria, protozoa and mammalian cells, as well as in more complex organisms, i.e., flies, fishes and worms. Experimental evidence indicates that despite natural radiation background is presently extremely small nevertheless it may be significant enough for living organisms to sense it and respond to it, keeping memory of this continuous exposure.

Moreover, observation of a lower stress response below the average environmental background, associated to the non-linear responses observed at low dose/dose rate, further challenges the radioprotection assumption that stochastic risk is directly proportional to dose (the LNT model) (32, 33).

The search for valid multicellular model systems and robust endpoints, the definition of efficient strategies and the need of deep radiation environment characterization for radiation quality studies are some of the objectives pursued by the underground biology groups (DULIA-bio community).

In this framework, RENOIR's results are expected to help take a step forward this direction, especially if properly integrated with data coming from above ground laboratories at increasing dose rates.

To conclude, investigation in DULs can help to understand the molecular mechanisms underlying biological effects observed at very low radiation dose/dose-rate (e.g., adaptive response and bystander effect), their interrelationship, their dependence on radiation type, total dose and dose rate and, even more importantly, their possible role in human health risks.

DATA AVAILABILITY STATEMENT

The original contributions presented in the study are included in the article/supplementary materials, further inquiries can be directed to the corresponding author/s.

AUTHOR CONTRIBUTIONS

GE, MT, and PM designed and wrote the article. GE, CT, and PM designed the figures. PM performed the *Drosophila* experiments. CT and GD'I performed simulations. MA, EB, CD, CN, and MQ designed and performed dosimetric analysis. GE performed biological data statistical analysis. All the authors contributed to manuscript editing, revision and approved the submitted version.

FUNDING

This work, carried out in the framework of the INFN-ISS Operative Agreement for R&D activities in the field of Radiobiology, was supported by INFN-CSN5 (RENOIR Experiment). We additionally thank Museo Storico della Fisica e Centro Studi e Ricerche Enrico Fermi, Rome, Italy and INFN-CSN5 for the support given to the COSMIC SILENCE project.

ACKNOWLEDGMENTS

The authors would like to thank LNGS and all technical Services for their skilled assistance and support for the experiments. Thank are due to G. Di Carlo for sharing his data on the gamma dose rate at the LNGS. We are also indebted to M. Belli for the critical review of the manuscript.

REFERENCES

1. Lampe N, Breton V, Sarramia D, Sime-Ngando T, Biron DG. Understanding low radiation background biology through controlled evolution experiments. *Evol Appl*. (2017) 10:658–66. doi: 10.1111/eva.12491
2. UNSCEAR. *Biological Mechanisms of Radiation Actions at Low Doses. A White Paper to Guide the Scientific Committee's Future Programme of Work*. New York, NY: United Nations (2012).
3. UNSCEAR. *Sources, Effects and Risks of Ionizing Radiation. UNSCEAR 2017. Report to the General Assembly. Scientific Annexes A and B*. New York, NY: United Nations (2018).
4. Smith NJT. The development of deep underground science facilities. *Nuclear Phys B*. (2012) 229–232, 333–341. doi: 10.1016/j.nuclphysbps.2012.09.052
5. Best A, Caciolli A, Fülöp Z, Gyürky G, Laubenstein M, Napolitani E, et al. Underground nuclear astrophysics: why and how (Review). *Eur. Phys. J. A*. (2016) 52:72. doi: 10.1140/epja/i2016-16072-7
6. Satta L, Augusti-Tocco G, Ceccarelli R, Esposito A, Fiore. Low environmental radiation background impairs biological defence of the yeast *Saccharomyces cerevisiae* to chemical radiomimetic agents. *Mutat Res*. (1995) 347:129–33. doi: 10.1016/0165-7992(95)00031-3
7. Antonelli F, Belli M, Sapora O, Simone G, Sorrentino E, Tabocchini MA, et al. Radiation biophysics at the Gran Sasso laboratory: influence of a low background radiation environment on the adpative response of living cells. *Nuclear Phys B Proc Suppl*. (2000) 87:508–9. doi: 10.1016/S0920-5632(00)00735-0
8. Satta L, Antonelli F, Belli M, Sapora O, Simone G, Sorrentino E, et al. Influence of a low background radiation environment on biochemical and biological responses in V79 cells. *Radiat Environ Biophys*. (2002) 41:217–24. doi: 10.1007/s00411-002-0159-2
9. Fratini E, Carbone C, Capece D, Esposito G, Simone G, Tabocchini MA, et al. Low-radiation environment affects the development of protection mechanisms in V79 cells. *Radiat Environ Biophys*. (2015) 54:183–94. doi: 10.1007/s00411-015-0587-4
10. Carbone MC, Pinto M, Antonelli F, Amicarelli F, Balata M, Belli M, et al. The cosmic silence experiment: on the putative adaptive role of environmental ionizing radiation. *Radiat Environ Biophys*. (2009) 48:189–96. doi: 10.1007/s00411-008-0208-6
11. Carbone MC, Pinto M, Antonelli F, Balata M, Belli M, Devirgiliis LC, et al. Effects of deprivation of background environmental radiation on cultured human cells. *Nuovo Cimento Della Soc Italiana Fisica B Basic Topics Phys*. (2010) 125:469–77. doi: 10.1393/ncb/i2010-10889-y
12. Morciano P, Iorio R, Iovino D, Cipressa F, Esposito G, Porrazzo A, et al. Effects of reduced natural background radiation on Drosophila melanogaster growth and development as revealed by the FLYINGLOW program. *J Cell Physiol*. (2018) 233:23–9. doi: 10.1002/jcp.25889
13. Morciano P, Cipressa F, Porrazzo A, Esposito G, Tabocchini MA, Cenci G. Fruit flies provide new insights in low-radiation background biology at the INFN underground Gran Sasso national laboratory (LNGS). *Radiat Res*. (2018) 190:217–25. doi: 10.1667/RR15083.1
14. Planel G, Soleilhavoup JP, Tixador R, Croute F, Richoilley G. *Demonstration of a Stimulating Effect of Natural Ionizing Radiation and of Very Low Radiation Doses on Cell Multiplication*. Vienna: International Atomic Energy Agency (IAEA) (1976).
15. Smith GB, Grof Y, Navarrette A, Guilmette RA. Exploring biological effects of low level radiation from the other side of background. *Health Phys*. (2011) 100:263–5. doi: 10.1097/HP.0b013e318208cd44
16. Castillo H, Schoderbek D, Dulal S, Escobar G, Wood J, Nelson R, et al. Stress induction in the bacteria *Shewanella oneidensis* and *Deinococcus radiodurans* in response to below-background ionizing radiation. *Int J Radiat Biol*. (2015) 91:749–56. doi: 10.3109/09553002.2015.1062571
17. Castillo H, Li X, Schilkey F, Smith GB. Transcriptome analysis reveals a stress response of Shewanella oneidensis deprived of background levels of ionizing radiation. *PLoS ONE*. (2018) 13:e0196472. doi: 10.1371/journal.pone.0196472
18. Liu J, Ma T, Liu Y, Zou J, Gao M, Zhang R, et al. History, advancements, and perspective of biological research in deep-underground laboratories: a brief review. *Environ Int*. (2018) 120:207–14. doi: 10.1016/j.envint.2018.07.031
19. Belli M, Tabocchini MA. Ionizing radiation-induced epigenetic modifications and their relevance to radiation protection. *Int J Mol Sci*. (2020) 21:5993. doi: 10.3390/ijms21175993
20. Thome C, Tharmalingam S, Pirkkanen J, Zarnke A, Laframboise T, Boreham DR. The REPAIR project: examining the biological impacts of sub-background radiation exposure within SNOLAB, a deep underground laboratory. *Radiat Res*. (2017) 188:470–4. doi: 10.1667/RR14654.1
21. Xie HP, Liu JF, Gao MZ, Wan XH, Liu SX, Zou J, et al. The research advancement and conception of the deep-underground medicine. *Sichuan Da Xue Xue Bao Yi Xue Ban*. (2018) 49:163–8.
22. Wadsworth J, Cockell CS, Murphy A, St J, Nilima A, Paling S, et al. There's plenty of room at the bottom: low radiation as a biological extreme. *Front Astron Space Sci*. (2020) 7:50. doi: 10.3389/fspas.2020.00050
23. Pirkkanen J, Zarnke AM, Laframboise T, Lees SJ, Tai TC, Boreham D R, et al. A research environment 2 km deep-underground impacts embryonic development in lake whitefish (*Coregonus clupeaformis*). *Front Earth Sci*. (2020) 8:327. doi: 10.3389/feart.2020.00327
24. Van Voorhies WA, Castillo HA, Thawng CN, Smith GB. The phenotypic and transcriptomic response of the caenorhabditis elegans nematode to background and below-background radiation levels. *Front Public Health*. (2020) 8:581796. doi: 10.3389/fpubh.2020.581796
25. Campa A, Balduzzi M, Dini V, Esposito G, Tabocchini MA. The complex interactions between radiation induced non-targeted effects and cancer. *Cancer Lett*. (2015) 356:126–36. doi: 10.1016/j.canlet.2013.09.030
26. UNSCEAR. *Sources and Effects of Ionizing Radiation. UNSCEAR 2008 Report. Vol. I*. New York, NY: United Nations (2008).
27. Best A, Görres J, Junker M, Krat KL, Laubenstein M, Long A, et al. Low energy neutron background in deep underground laboratories. *Nuclear Instrum Methods Phys Res A*. (2016) 812:1–6. doi: 10.1016/j.nima.2015.12.034
28. Miller KM. *A Spectral Stripping Method for a Ge Spectrometer Used for Indoor Gamma Exposure Rate Measurements. Report EML-419*. New York, NY: Environmental Measurement Laboratory, USDOE (1984). doi: 10.2172/6984023
29. Miller KM, Beck HL. Indoor gamma and cosmic ray exposure rate measurements using a Ge spectrometer and pressurised ionisation chamber. *Radiat Prot Dosim*. (1984) 7:185–9. doi: 10.1093/rpd/7.1-4.185
30. Pola A, Rastelli D, Treccani M, Pasquato S, Bortot D. DIAMON: a portable, real-time and direction-aware neutron spectrometer for field characterization and dosimetry. *Nuclear Instrum Methods Phys Res*. (2020) 969:164078. doi: 10.1016/j.nima.2020.164078
31. Agostinelli S, Allison J, Amako K, Apostolakis J, Araujo H, Arce P, et al. Geant4—a simulation toolkit. *Nucl Instr Meth A*. (2003) 506:250–303. doi: 10.1016/S0168-9002(03)01368-8
32. Morgan FW, Bair WJ. Issues in low dose radiation biology: the controversy continues. *A Perspect Radiat Res*. (2013) 179:501–10. doi: 10.1667/RR3306.1
33. Morgan WF, Sowa MB. Non-targeted effects induced by ionizing radiation: mechanisms and potential impact on radiation induced health effects. *Cancer Lett*. (2015) 356:17–21. doi: 10.1016/j.canlet.2013.09.009

Conflict of Interest: The authors declare that the research was conducted in the absence of any commercial or financial relationships that could be construed as a potential conflict of interest.

frontiers in Public Health

OPINION
published: 09 October 2020
doi: 10.3389/fpubh.2020.578392

Potassium Radioisotope 40 as Component of Mitochondria Physiology: Therapy Proposal for Mitochondrial Disfunction Diseases

*Maurizio Tomasi**

Department of Biology, New Mexico State University, Las Cruces, NM, United States

Keywords: background ionizing radiations, Auger electrons, electron transport chain, mitochondria, hydrogen peroxide signaling, Coenzyme Q_{10}, mitochondrial dysfunction

INTRODUCTION

Huge quantities of energy poured onto the still-crusting earth. Solar storms, supernova explosions, volcanic eruptions, geysers were very frequent events in the Archaeozoic period, $3.5{\cdot}10^9$ years ago. A melting pot of electrons, protons, free radicals, methane, ammonia, hydrogen, water, and carbon dioxide whose meeting and collision has produced billions of compounds. And together they made up the primordial soup. A broth where matter aggregated into orderly structures that allowed life and its expansion. Alternative to the primordial soup, the iron-sulfur world hypothesis has been advanced: the mineral surfaces of iron sulphides provided the catalytic conditions for giving rise to life (1). However both hypothesis can be complementary if the ocean had been a relatively small sea portion. The slow depletion of the nutrients selected the cyanobacteria, which thanks to the chlorophyll synthesis required only a few very common elements to reproduce: sun, water, and minerals. The expanding plant world has provided the nutrients which allowed the birth of the animal world. The environment and the living organisms changed each other. The atmosphere turned into oxidative from a reducing agent. Through the chlorophyll synthesis solar energy has been transformed in chemical bonds so that all the anabolism and catabolism were determined by energy exchanges provided by electron and proton movements. Among all types of natural ionizing radiation (NIR), which scattered the energy of electrons and protons in all directions, light radiations have become the energy unique source by channeling electrons and protons on strictly defined paths. Life has grown in complexity and refinement, and this has kept the memory of the previous state of complexity (2). For example, the common characteristics of the electron transport chains of mitochondria and chloroplasts represent the inheritance received from the same ancestor.

Currently, NIR refers only to ionizing radiation from the cosmos and radioactive minerals, which are toxic in high concentrations causing irreversible genetic and metabolic damage. Toxicity is related to the average of the energy deposited in the recipient organism (energy defined as LET, Linear Energy Transfer). Initially the toxicity of the NIR on the earth's surface was predicted by extrapolating LET. Therefore, even small doses of NIR should have been harmful, and if an organism had managed to grow in an environment with reduced quantities of NIR, the organism would have had to benefit from it. The hypothesis was first tested by shielding Paramecium Tetraurelia cultures with lead plates (3). Subsequently prof. Luigi Satta, with a brilliant intuition, promoted the construction of a biology section in the National Nuclear Physics laboratories inside the Gran Sasso tunnel (LNGS). The results showed that the NIR at surface level are stimulating rather than inhibiting, showing a two-phase trend of hormesis, i.e., linear only in high energy (4, 5). The effect does not seem due to the involvement of genetic mutation, since an evolutionary experiment on *E. coli* cultures followed for 500 generations both in surface (SL) and underground (UL) laboratories, excludes it (6). Other research has indicated that NIR regulates metabolic homeostasis. A study on *Drosophila melanogaster* showed less fertility and greater longevity when midges grow in an underground laboratory (UL) than those grown on

OPEN ACCESS

Edited by:
Shinji Tokonami,
Hirosaki University, Japan

Reviewed by:
Lorenzo Manti,
University of Naples Federico II, Italy
Tomisato Miura,
Hirosaki University, Japan

***Correspondence:**
Maurizio Tomasi
mauriziotomasi46@gmail.com

Specialty section:
This article was submitted to Radiation and Health, a section of the journal Frontiers in Public Health

Received: *01 July 2020*
Accepted: *24 August 2020*
Published: *09 October 2020*

Citation:
Tomasi M (2020) Potassium Radioisotope 40 as Component of Mitochondria Physiology: Therapy Proposal for Mitochondrial Disfunction Diseases. Front. Public Health 8:578392. doi: 10.3389/fpubh.2020.578392

the surface (SL) (7). Data from *Shewanella oneidensis* transcriptome analysis also suggest that NIR are involved in metabolic homeostasis. In fact, UL cultures show a marked decrease in ribosomal protein synthesis, and in respiratory chain proteins as well (8). However, in energy terms, not all radiation has the same toxicity. Photons at 20 KeV are not toxic as a dose of ray x at 20 KeV. And ray x at 20 KeV affect quite differently a *Deinococcus radiodurans* or one belonging to the Flavobacterium species. The former is an extremophilic bacterium that resists cold, dehydration, vacuum, and even an acidic environment, on the contrary the latter is sensitive to any environmental variations.

At odd there are bacteria as *Candidatus Desulforudis audaxviator*, which lives in areas without light and obtain energy from the radioactivity of Uranium, Thorium and Potassium (9).

DISCUSSION

The use of toxic radiations as a source of energy, suggested to review the data analysis on the radioisotope 40 of Potassium (^{40}K) which prompted Moore and Sastry (10) to speculate that ^{40}K was the "primordial gene irradiator." Hypothesis which was later discarded as reported in (11). However, the analysis on the possible biological role of ^{40}K, performed by Moore and Sastry, has such consistency as to suggest that it is worth considering an alternative biological role with respect to the mutagenetic one. The hypothesis, presented here, considers that the beta decays of ^{40}K could rather play an energetic role, which, although tiny, could intervene in very special situations. It is important to stress that ^{40}K beta decay includes the Auger and Coster-Kronig electrons (ACKE), which travel few nanometers distances and can be deposited on molecules very close to K. The ACKE cannot be measured as ambient radioactivity because of their very low energy content, still these beta decays are the most effective, thanks to the drastic changes induced on molecules acquiring an electron outside their metabolic context.

Actually the ^{40}K is the main source of radioactivity within living organisms. In the early stages of evolution, about $3.5{\cdot}10^9$ years ago, it was seven times higher than now, but likely has been well-tolerated or even integrated into living organisms. The maintenance of unbalanced concentrations is guaranteed by specific channels for K (Kcls). Inside the mitochondria Kcls finely modulate apoptosis, respiratory activity, volume, signal transmission and anti-stress action.

To date there is no data on ACKE target molecules, therefore on the matter there is wide space for speculations. If oxygen O_2 were a target molecule, superoxide is formed, which before and immediately afterwards, would spawn hydrogen peroxide (H_2O_2). A chemical compound that in small concentration, acts as signaling molecule in a wide variety of processes, spanning from embryonic development to cell death, and in the nervous system can modulate both neuronal excitability and dopamine neuronal firing (12). Since H_2O_2 rapidly diffuses because of its membrane permeability, its signals must act in fractions of a second (13). Therefore, opening and closing of the Kcls could modulate both timing and sites of the H_2O_2 production through dynamic gradient of ^{40}K.

Another hypothesis predicts that ^{40}K is somehow involved in the mitochondria respiratory chain. The rationale is as follows: K with its isotope ^{40}K, 3.5 billion years ago, had a radioactivity seven times greater than the present time, the continuous and conspicuous emission of ACKE could therefore have contributed to the construction of a primitive transport chain. Over the course of time ^{40}K has gradually lost the power of radioactivity and its role has become residual, but always able to contribute to the functioning of the mitochondrial respiratory chain in restricted and determined circumstances. In addition there is another molecule of the mitochondria, which like K is practically ubiquitous in all living organisms: the ubiquinone, also known as Coenzyme Q_{10} (CoQ_{10}), which play a crucial role in electronic transport. In fact, CoQ_{10} is an amphoteric lipid molecule that with its great mobility transfers electrons between complexes I, II and III. Complexes which are proteins with the tendency to form rather rigid structures unable to get electrons without a proper provider. In mitochondria, CoQ_{10} also acts as an antioxidant and as free radical scavenger. Thus CoQ_{10} protects lipid integrity, in particular that of cardiolipin, from attack by free radicals (14). A role that other antioxidants, such as glutathione or manganese superoxide dismutase, would not be able to play being in mitochondrial matrix (15). In addition CoQ_{10} membrane localization makes it close to K, precisely where its concentration is higher. It is therefore probable that part of ACKE are captured by CoQ_{10} and recycled in the respiratory chain. Under this visual angle the ACKE would supply a constant, albeit minuscule, amount of energy to the electronic transport system. However, this energy, more similar to a spark than a flame, could be useful when the respiratory chain slows down drastically, or even stops for physiological or pathological reasons, such as in the transient cases of hypoxia and lack of nutrients. In these situations the ACKE would autonomously provide those electrons which could avoid the consequences of a complete stop of mitochondrial activity. Something that should behave like the very tiny flame, constantly lit, of a switched off boiler, which, on command, allows it to be ignited.

Even if ^{40}K will prove irrelevant to biological systems, the idea that ^{40}K can supply electrons to CoQ_{10} could have important application in medicine, for the following reasons:

If CoQ_{10} were given in combination with ^{40}K enriched K, the increase in available ACKE, once captured and transported by CoQ_{10} into the respiratory chain, should have to improve the energy efficiency of the mitochondrial system. And significant, if not synergistic, therapeutic effects should be observed. The list of pathologies caused by mitochondrial dysfunctions is quite long, only a few are mentioned here: epilepsy, aging and degenerative diseases of the nervous system. It is important to stress that CoQ_{10} is already on the market as widely established dietary supplement, which has been shown to be beneficial in a variety of clinical cases: recovery after heart failure, in treating statin myopathy, in neurological disorders, aging (16). To give an extra spurt to mitochondria should be the very reason, worthy to try, for using the CoQ_{10}—K enriched ^{40}K. Finally

it should be emphasized that to understand the importance of ^{40}K in biology there is no other way than to develop research lines that foresee the use in the culture media of K without ^{40}K, but also in parallel with K enriched with ^{40}K. If the experiments were carried out in underground biological laboratories, such as the WIPP in Carlsbad, New Mexico, USA, which are shielded from environmental NIR, an environment almost completely free of radioactivity would be obtained. The experimental conditions would be suitable for evaluating not only the contribution of the ^{40}K but also that of the NIR on living organisms.

CONCLUSIONS

In this work, the hypothesis is advanced that the K isotope 40 plays a role in cellular homeostasis. In particular, its beta radiations, which includes low energy electrons with high ionization potential, ACKE, could produce micro quantities of H_2O_2 and directly and indirectly supply electrons to the mitochondrial respiratory chain. CoQ_{10} would be responsible for the electronic transfer, which in addition to having the role of transfering electrons in the respiratory chain also has the role of free radical scavenger. Although the amounts of energy produced through ACKE appear insignificant in situations of normal metabolism, their production in the event of temporary blockage of mitochondrial activity could avoid irreversible damage and therefore help recovery.

The hypothesis has the non-secondary purpose of stimulating ^{40}K research and its effects in biology and medicine.

It is important to underline that the rationale behind a scientific research proposal has been presented here: the purpose of the research is to determine whether the combined administration of CoQ_{10} and potassium enriched with radioisotope 40 can be used in the therapy of patients suffering from diseases caused by mitochondria dysfunctions.

AUTHOR CONTRIBUTIONS

The author confirms being the sole contributor of this work and has approved it for publication.

ACKNOWLEDGMENTS

MT would like to thank prof. Geoffrey B. Smith very much for not only hosting me in the Biological Laboratory at Waste Isolation Pilot Plant (WIPP), but also allowing me to perform experiments on the influence of background radiation on the growth of vegetable seeds. The idea reported in this article has been generated during that lab work.

REFERENCES

1. Wächtershäuser G. On the chemistry and evolution of the pioneer organism. *Chem Biodivers.* (2007) 4:584–602. doi: 10.1002/cbdv.200790052
2. Prigogine I. Time, structure, and fluctuations. *Science.* (1978) 201:777–85.
3. Tixador R, Richoilley G, Monrozies E, Planel H, Tap G. Effects of very low doses of ionizing radiation on the clonal life-span in paramecium tetraurelia. *Int J Radiat Biol Relat Stud Phys Chem Med.* (1981) 39:47–54.
4. Satta L, Augusti-Tocco G, Ceccarelli R, Esposito A, Fiore M, Paggi P, et al. Low environmental radiation background impairs biological defense of the yeast *Saccharomyces cerevisiae* to chemical radiomimetic agents. *Mutat. Res.* (1995) 347:129–33.
5. Fratini E, Carbone C, Capece D, Esposito G, Simone G, Tabocchini MA, et al. Low-radiation environment affects the development of protection mechanisms in V79 cells. *Radiat Environ Biophys.* (2015) 54:183–94. doi: 10.1007/s00411-015-0587-4
6. Lampe N, Marin P, Coulon M, Micheau P, Maigne L, Sarramia D, et al. Reducing the ionizing radiation background does not significantly affect the evolution of *Escherichia coli* populations over 500 generations. *Sci Rep.* (2019) 9:14891–7. doi: 10.1038/s41598-019-51519-9
7. Morciano P, Cipressa F, Porrazzo A, Esposito G, Tabocchini MA, Cenci G. Fruit flies provide new insights in low-radiation background biology at the INFN Underground Gran Sasso National Laboratory (LNGS). *Radiat Res.* (2018) 190:217–25. doi: 10.1667/RR15083.1
8. Castillo H, Xioping L, Schilkey F, Smith GB. Transcriptome analysis reveals a stress response of *Shewanella oneidensis* deprived of background levels of ionizing radiation. *PLoS ONE.* (2018) 13:e0196472. doi: 10.1371/journal.pone.0196472
9. Atri D. On the possibility of galactic cosmic ray-induced radiolysis-powered life in subsurface environments in the Universe. *J R Soc Interface.* (2016) 13:20160459. doi: 10.1098/rsif.2016.0459
10. Moore FD, Sastry KSR. Intracellular potassium: ^{40}K as a primordial gene irradiator. *Proc. Natl Acad Sci USA.* (1982) 79:3556–9.
11. Gevertz D, Friedman AM, Katz JJ, Kubitshek HE. Biological effects of background radiation: Mutagenicity of ^{40}K. *Proc Natl Acad Sci USA.* (1985) 82:8602–5.
12. Lee CR, Patel JC, O'Neil B, Rice ME. Inhibitory and excitatory neuromodulation by hydrogen peroxide: translating energetics to information. *J Physiol.* (2015) 593:3431–46. doi: 10.1113/jphysiol.2014.273839
13. Rice ME. H_2O_2: a dynamic neuromodulator. *Neuroscientist.* (2011) 7:389–406. doi: 10.1177/1073858411404531
14. Ernster L, Forsmark P, Nordenbrand K. The mode of action of lipid-soluble antioxidants in biological membranes: relationship between the effects of ubiquinol and vitamin E as inhibitors of lipid peroxidation in submitochondrial particles. *J. Nutr. Sci. Vitaminol.* (1992) 548:1–51. doi: 10.3177/jnsv.38.special_548
15. Holley AK, Bakthavatchalu V, Velez-Roman JM, St Clair DK. Manganes superoxide dismutase: guardian of the powerhouse. *Int. J. Mol. Sci.* 12:7114–62. doi: 10.3390/ijms12107114
16. Hernández-Camacho JD, Bernier M, López-Lluch G, Plácido Navas P. Coenzyme Q_{10} supplementation in aging and disease. *Front Physiol.* (2018) 9:44. doi: 10.3389/fphys.2018.00044

Conflict of Interest: The author declares that the research was conducted in the absence of any commercial or financial relationships that could be construed as a potential conflict of interest.

frontiers in Physics

BRIEF RESEARCH REPORT
published: 06 November 2020
doi: 10.3389/fphy.2020.577734

Low Background Radiation Detection Techniques and Mitigation of Radioactive Backgrounds

Matthias Laubenstein[1]* *and Ian Lawson*[2]*

[1]INFN-Laboratori Nazionali del Gran Sasso, L'Aquila, Italy, [2]SNOLAB, Sudbury, ON, Canada

The study of rare fundamental physics phenomena, such as double-beta decay, rare nuclear decays and dark matter, requires very low levels of background radiation in order to observe a signal. To achieve the required background levels, experiments are located deep underground as these facilities provide significant rock overburden and commensurate reduction in the cosmic ray flux and cosmic ray-spallation induced products. An overview of the sources of these backgrounds will be presented. Taking advantage of the deep underground laboratory spaces, there have been a growing number of underground measurements in other fields, including environmental monitoring, benchmarking of other physical techniques, Life Science studies in low background environments, and material selection. The exceptional sensitivity and high resolution of high-purity germanium detectors allows for very sensitive measurements using gamma-ray spectrometry. Their use has been increasing as they allow for non-destructive measurements of experiment components, which can be directly used if they meet specified background requirements. This paper will discuss the current most sensitive ultra-low background germanium detectors in operation and explain how to achieve the best level of background reduction to attain the best sensitivities. In addition, an overview of several complementary low background measurement methods will be discussed. A proposed program to cross calibrate germanium detectors at several laboratories will be described and a searchable database used to store radioactivity measurements of experimental materials will be introduced.

Keywords: gamma-ray spectrometry, ultra-low background, germanium detectors, alpha spectrometry, backgrounds

OPEN ACCESS

Edited by:
Maria Antonella Tabocchini, National Institute of Health (ISS), Italy

Reviewed by:
Cristina Nuccetelli, National Institute of Health (ISS), Italy
Jiri Hulka, National Radiation Protection Institute, Czechia

***Correspondence:**
Matthias Laubenstein
matthias.laubenstein@lngs.infn.it
Ian Lawson
lawson@snolab.ca

Specialty section:
This article was submitted to High-Energy and Astroparticle Physics, a section of the journal Frontiers in Physics

Received: *01 July 2020*
Accepted: *30 September 2020*
Published: *06 November 2020*

Citation:
Laubenstein M and Lawson I (2020) Low Background Radiation Detection Techniques and Mitigation of Radioactive Backgrounds. Front. Phys. 8:577734. doi: 10.3389/fphy.2020.577734

1 INTRODUCTION

The study of radioactive backgrounds has been ongoing for several decades, it began in the 1950's with the search for little-known backgrounds in materials surrounding particle accelerators to determine if those materials were activated from the accelerator itself. Counting facilities were then developed to measure the materials and then to search for lesser known backgrounds. This involved building dedicated facilities with the appropriate construction materials to shield the counters from local backgrounds. Once sufficient local backgrounds were removed from the counters, dedicated background experiments were gradually developed as the need arose. The counters were then developed for local use quantifying radionuclides in basic materials such as rock, concrete and steel. This led to a natural transition to low background material assays for nuclear and particle physics

experiments as these became more sensitive to backgrounds from their construction materials. The initial counting facilities were usually developed by the individual experiments as their needs arose. Gradually these counters were developed into permanent facilities and improved to increase sensitivity (see for example Refs. 1 and 2).

It was realized that to increase sensitivity and to remove cosmogenic backgrounds, moving the background counters to underground laboratories would be very beneficial. For these early low background counting facilities shallow underground labs were developed with depths up to 100 m. As experiments required lower background materials to observe rare event searches, the materials to build the counter were improved and to further remove atmospheric backgrounds the counters were moved to deep underground laboratories. The search for low background materials continues with a particular emphasis on the search to find materials which have low concentrations of the radioactive chain elements, ^{238}U, ^{232}Th, and ^{40}K, often well below mBq kg^{-1}. These concentrations are below what is generally accessible by standard chemical and analytical techniques, therefore assay methods are often performed through radiation counting or through very sensitive non radiometric techniques like mass spectrometry.

The backgrounds of interest can include muons, alphas, betas, gammas or neutrons, depending upon the experiment and component in question (see Refs. 3 and 4). The radiation could be direct or via leaching or emanation, thus, several different detector technologies are used to estimate radioactive contamination levels. In addition, the counting detectors themselves must be very low in background contamination levels, which requires them to be radioactively clean and underground, and fabricated and shielded with low background materials. Several complementary methods are used to measure the backgrounds, which depend on the material, if the material itself is going to be used in the experiment or if some of the material can be sacrificed for the assay (see for example Ref. 5). These methods and their advantages and drawbacks will be discussed in **Section 3**.

2 BACKGROUND SOURCES

The energy range of the expected signals in experiments searching for rare events is approximately 1–5 MeV, the same range as that of the decay of radionuclides and other nuclear reactions. The background induced by cosmic rays, especially muons, is diminished by going underground. The rock overburden reduces efficiently their intensity and their reaction products through interaction with matter (mainly neutrons). The muon flux at LNGS is for example suppressed by more than six orders of magnitude to less than 1 muon m^{-2} h^{-1} for energies up to 1 TeV.

However, just having an experiment deep underground is not enough to reduce the backgrounds to levels required for the current generation of experiments. All materials contain traces of radioactive nuclides and the most important task is to bring down the intrinsic background of the detector set-up. In general, materials contain radioactive impurities because either they are not radio-pure or they come into contact with radio impurities during their production process. Other substances such as copper are intrinsically very radio-pure, but can contain radio impurities by being exposed to cosmic rays after manufacturing.

2.1 Primordial Radionuclides and Natural Decay Chains

All nuclides that still exist since they were produced in stellar nucleosynthesis are called primordial; ^{40}K, ^{232}Th, ^{235}U, and ^{238}U, the latter three are the starting nuclides of the three naturally occurring decay chains, belong to this group. In addition to these four ubiquitous radionuclides usually identified in gamma-ray spectra, there are a lot more elements with primordial radioisotopes (e.g., ^{87}Rb, ^{113}Cd, ^{115}In, ^{190}Pt, ^{144}Nd, ^{176}Lu, ^{138}La and many more) (see Ref. 6), but they are only relevant as a background source in very specific cases, for example, in scintillating crystals like lanthanum bromide (^{138}La), sodium iodide (^{87}Rb), and cadmium tungstate (^{113}Cd). Primordial ^{232}Th, ^{235}U, and ^{238}U can be found in all natural occurring mineral materials. In nature the isotope ratio ^{238}U/^{235}U is 137.88, thus in samples with low radioactivity concentration often only the ^{238}U concentration is assessed. Therefore, in the following the focus will be set only to ^{238}U. The elemental abundance of thorium and uranium in the Earth's crust is very variable and different average values have been determined (see, e.g., Refs. 4, 7, 8]), which are for Th and U in the range of (17–60) and (16–110) Bq kg^{-1}, respectively. All their decay products are present in the materials as well, unless chemical or physical separation will take place. Each of these decay chains stops with a stable lead isotope. If any separation occurred in a material, the chain is not anymore in secular equilibrium. Primordial ^{40}K is also present everywhere. Its concentration varies very much from levels of few hundreds to thousands of Bq kg^{-1} as in soil samples down to tenths of mBq or even less in pure materials like copper, lead and special plastic products. It is often considered as less problematic as it can rather easily be identified, but nevertheless, in some cases its presence can be limiting to the experimental sensitivity [9]. Many radionuclide activities in the three decay chains can not be assessed right-away using gamma-ray spectrometry, due to no or very faint emission of gamma-rays (e.g., ^{232}Th and ^{238}U themselves). Other methods are necessary to determine their concentration (e.g., neutron activation, mass spectrometry, see, for example, Ref. 10).

2.2 Cosmogenic Radionuclides

This group of radionuclides is produced through interaction with matter of secondary and tertiary cosmic ray particles [6]. For example ^{3}H, ^{14}C, and ^{7}Be are produced through interactions in the upper atmosphere between high energy cosmic ray particles and oxygen and nitrogen. Their production rate is approximately constant and they are present in the atmosphere and in living animals and plants. In addition, there are many more radionuclides which are produced by neutron and muon capture from cosmic radiation in the atmosphere; several of these isotopes are extremely important as possible background sources in metals (e.g., ^{108m}Ag and ^{110m}Ag in silver, ^{57}Co, ^{58}Co, and ^{60}Co in copper, iron and many alloys [11]).

TABLE 1 | Techniques used to measure radioactive backgrounds.

Measurement method	Background detected	Sensitivity (for U/Th assumed to be in secular equilibrium)
Ge spectrometry	γ emitting nuclides	10 – 100 μBq/kg
Rn assay measurements	^{226}Ra (through ^{222}Rn), ^{228}Th (through ^{220}Rn)	0.1 – 10 μBq/kg
Neutron activation	primordial parents	0.01 μBq/kg
Mass spectrometry	primordial parents	1 – 100 μBq/kg
Röntgen excitation	primordial parents	10 mBq/kg
α spectrometry	α emitting nuclides (e.g., ^{210}Po, ^{212}Bi, ^{224}Ra)	1 mBq

2.3 Anthropogenic Radionuclides

These are man-made radionuclides i.e., artificially produced through nuclear reactions either in nuclear power and reprocessing plants, nuclear weapons testing, and production of radioactive sources for industrial and medical applications. The radionuclides belonging to this group are for example ^{60}Co, ^{137}Cs, ^{238}Pu, and ^{241}Am. They are present in the environment, because they are and were freed either in nuclear incidents (in nuclear power plants and by accidental melting of high activity sources), in nuclear weapons testing (until the late 50s) and as emission from reprocessing plants. For example, ^{60}Co is used as a tracer to ensure the integrity of the melting furnaces, thus steel may contain notable amounts of this isotope, which exceeds the naturally present concentration of cosmogenic ^{60}Co by up to two orders of magnitude [12].

3 RADIO-ASSAY TECHNIQUES

There are several different techniques available to assay materials. Each technique has its advantages and drawbacks. For example, some techniques require the sample to be destroyed while other techniques may only allow a small fraction of the material to be sampled. **Table 1** lists the most common counting techniques used, the type of background each method is best suited for and the current sensitivity of each method. Several of these common counting techniques will be described in the following sections.

3.1 Gamma-Ray Spectrometry

Gamma-ray spectrometry (GRS) with high purity germanium (HPGe) detectors is an all-important tool for material screening in rare event experiments. In order to achieve the best sensitivity, the most important prerequisite for these detectors is that near the sample and inside the detector itself the radioactivity concentration is as low as possible. In comparison to other methods (e.g., mass spectrometry or neutron activation) GRS provides a more inclusive method of radionuclide detection. The information about all contributing gamma-ray emitting radionuclides is combined in a single energy spectrum. The excellent energy resolution of HPGe detectors allows for a highly efficient separation of different gamma-ray lines and for the best way to identify the various radionuclides present. One further very important advantage is that material screening can be performed non-destructively, and no elaborate sample treatment is needed.

As previously discussed, the primordial radionuclides ^{40}K, ^{238}U, and ^{232}Th represent the most important sources of radioactivity in ordinary materials. Only GRS is capable of measuring the concentration of all progenies that emit gamma-rays in the uranium and thorium decay chains. This also makes it possible to assess whether secular equilibrium is broken in the respective decay chains. Furthermore, if this is the case, the actual state of equilibrium can be investigated by comparing the concentrations of the gamma-active progenies in the decay chains. Within the ^{232}Th chain one has two sub-chains that can be out of secular equilibrium, one starting with ^{228}Ra (half-life 5.75 y) and the other with ^{228}Th (half life 1.9126 y). For the first sub-chain, we need to assess ^{228}Ac as direct progeny of ^{228}Ra. For the second sub-chain, we measure the progenies of ^{228}Th, i.e., ^{212}Pb, ^{212}Bi, and ^{208}Tl. In the ^{238}U chain one has again two sub-chains of interest for GRS, ^{238}U (half life 4.468×10^9 y) itself and ^{226}Ra (half life 1600 y). In the first case, the sub-chain can be assessed through ^{234}Th (direct progeny of uranium) and ^{234m}Pa (progeny of ^{234}Th). For the second sub-chain, one measures the gamma-active progenies of ^{226}Ra, i.e., ^{214}Pb and ^{214}Bi.

Ultra-Low Background (ULB) HPGe spectrometers are specially developed detectors that use carefully selected materials (e.g., very pure copper, not exposed or at least only very shortly exposed to cosmic rays, ultrapure aluminium) as construction materials and very low radioactivity containing electronic components inside the detector end cap close to the germanium crystal. When operated deep underground [13], or even at rather shallow depths but with efficient active shielding [14], ULB HPGe detectors can reach sensitivities on the order of 10 – 100 μBq kg^{-1}. This, however, requires long counting periods, sometimes even of up to 100 days, and rather bulky samples (up to several tens of kg). Consequently, it is recommended to run simultaneously several spectrometers in order to not prolong the counting time needed for screening samples. These detectors usually have rather elaborate shielding composed of graded lead with the innermost parts made of ancient or ultra-high purity lead followed by high-purity low-Z material (usually very pure copper) to absorb bremsstrahlung radiation from residual radioactivity in the lead. Moreover, radon gas (coming from the surrounding material or entering through diffusion from the outside) is removed through encapsulation of the experimental set-up and flushing with radon-free gas (e.g., boil-off nitrogen). Since these ULB detectors have very low count rates compared to normal systems (on the order of 100 counts per day in the energy

range of interest between 40 and 2.7 MeV compared to several hundred to several thousands of counts per day in normal detectors) it is mandatory to perform regularly long background measurements (on the order of several weeks) and energy calibrations in order to check for possible changes in background performance or electronic problems (worsening of resolution, shift in energy etc.).

3.2 ICP-MS Mass Spectrometry

Inductively coupled plasma mass spectrometry (ICP-MS) is a type of mass spectrometry which uses inductively coupled plasma to ionize the sample [15, 16, 17, 18]. The sample is atomized creating atomic and small polyatomic ions, which can then be detected. It is often used to detect metals and some non-metals which are dissolved in liquids at very low concentrations. The ions are then separated on the basis of their mass-to-charge ratio and a mass spectrometer then detects the ion signal, which is proportional to the concentration of the isotope, for this it is a non radiometric technique as it does not look for radioactive decay in itself, but for the concentration of the radioactive isotope. The absolute concentration in the sample can be determined through calibrations with certified reference materials. ICP-MS screening is useful for small samples or when a piece of a large sample can be used. The sensitivity of current methods down to nBq per kg levels for U and Th can now be achieved, so this method is very important in finding low background materials as it is one of the most sensitive background detection method currently used [19, 20]. The main drawback of this method is the condition that the sample preparation is destructive and only small samples of larger materials can be measured.

3.3 Alpha Spectrometry

Many isotopes can decay via alpha particle emission, these alpha particles can then be detected and counted using alpha spectrometry to identify and quantify the isotope based on properties of the emitted alpha particle. Similar to gamma spectrometry, energy spectra are detected with high precision alpha detectors and electronics and analyzed to determine the nuclide. Samples are often measured following chemical separation to isolate the radionuclides of concern due to the complexity associated with correcting for interferences since alpha particle energies are often very close together. Alpha spectrometry is widely used in several applications, including: environmental radioactivity monitoring, health physics personnel monitoring, materials testing, geology and mineralogy, forensics and nuclear fuel processing, see for example Ref. 21.

Alpha counting is often used for material testing as a complementary method to gamma counting. Samples are generally machined into thin disks, or a liquid solution is placed on a metal disk and then allowed to dry to give a uniform coating. If the thickness of the layer or of the sample is too thick then the detected energy line spectra are broadened to lower energies, due to some of the energy of the alpha particles being lost during their interactions through the layer of active material [22]. The samples can be measured with various types of detectors, some of the most sensitive detectors currently used are

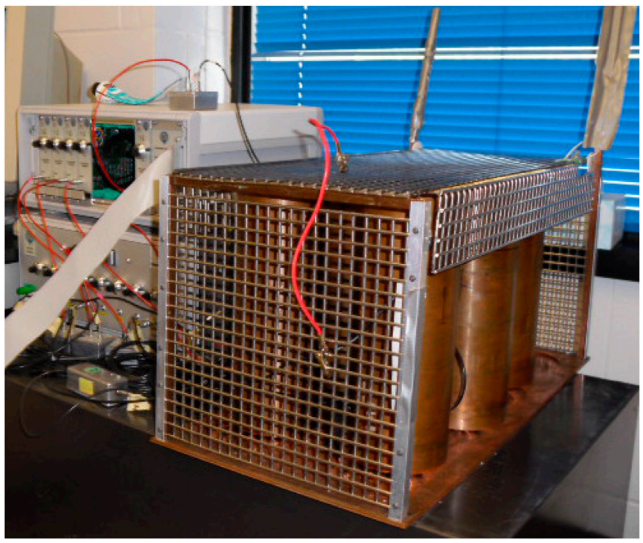

FIGURE 1 | A photograph of a custom built alpha beta coincidence liquid scintillation detector located at SNOLAB.

ionization chambers with or without sensor wires. The current detectors can detect alphas over an energy range of 1 to 10 MeV with a sensitivity better than 100 nBq cm^{-2}. Semiconductor detectors such as the Passivated Implanted Planar Silicon (PIPS) are improvements from the silicon surface barrier (SSB) detectors and diffused junction detectors, which were both designed in the 1960's. The PIPS detector was designed with thin windows to improve sensitivity and resolution and backgrounds for these detectors are usually less then 0.05 counts/hr/cm^2 [23].

A second method of alpha spectrometry is to use internal liquid scintillation counting, in which the sample is mixed with or dissolved into a scintillation cocktail. The light emissions are then counted using photomultipliers and the signal is then analyzed using a combination of pulse shape discrimination and coincidence counting for identifying alpha beta coincidence events. The sensitivity of this method is on the order of 1 mBq/kg for ^{238}U and ^{232}Th assuming that the chains are in equilibrium. A custom built system is shown in **Figure 1**, this system is built using low background copper housings and photomultipliers to reduce internal backgrounds. Drawbacks to this method include the failure of all photons to be detected, cloudy or colored samples which can be difficult to count and the fact that random quenching can reduce the number of photons generated per radioactive decay.

3.4 Radon Assay Measurements

Radon emanation of a material is the process in which the radon atoms formed from the decay of ^{226}Ra escape from the decaying isotopes and move into the pore spaces of the molecule. Diffusion and advective flow then cause the movement of the radon atoms throughout the material and subsequently to the surface. Once the radon atoms reach the surface, they can be exhaled from the material (see, e.g., Ref. 24). These radon atoms and their progeny

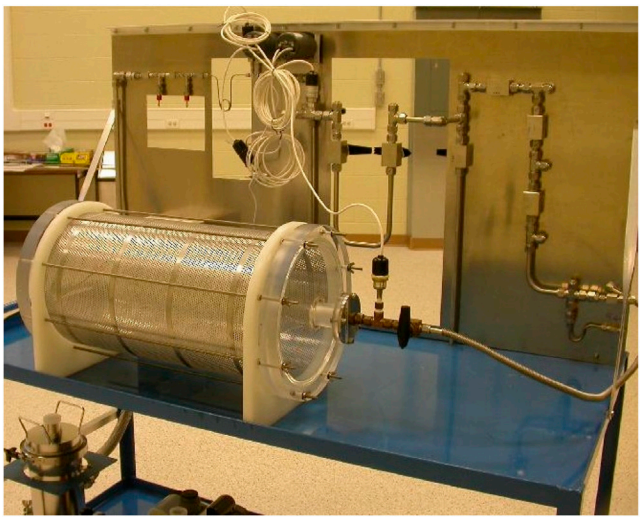

FIGURE 2 | A photograph of a typical radon exhalation chamber at SNOLAB. The sample material is placed in the cylindrical chamber where the radon progeny are accumulated for several ^{222}Rn half-lives after which the progeny are collected in a Lucas cell which is then used to count the photons from the alpha interactions [30].

can be collected inside a radon exhalation chamber for several half-lives of the ^{222}Rn and then counted directly with a radon detector (e.g., Durridge RAD7 [25]) or using alpha spectrometry. These measurements provide radon exhalation rates in units of Bq m^{-2} s^{-1} or Bq kg^{-1} s^{-1}. A typical radon exhalation collection chamber system is shown in **Figure 2**. The exhalation rates of typical construction materials for underground laboratories are shown in **Table 2**, as can be observed, the rates can vary a lot, so one should choose their materials with the exhalation rate in mind when constructing a low background experiment.

3.5 Neutron Activation

A sample which is not normally radioactive can be activated with neutrons causing its components to form radioactive isotopes which can then be detected using the methods described above. The process involves neutrons inducing radioactivity in the sample in which the nuclei capture free neutrons, thus becoming heavier and entering into excited states. The excited nucleus then decays by emitting gamma rays, beta and alpha particles, fission products and neutrons. The main drawback of this method is that the activation products could have long half-lives, thus making the sample unusable for the immediate deployment in an experiment. The main advantage of this method is that the sample usually does not need to be destroyed to complete the measurement, so this method is very useful if the activated isotopes have half-lives of at most a few days or months. This method is not used as much as in the past due the limited opportunities to irradiate samples as suitable activation reactors are in declining use. A very good overview on this method, its application in the field of rare events physics experiments and its actual sensitivity is given in Ref. 26.

TABLE 2 | Typical radon exhalation rates for some common construction materials used in underground experiments.

Sample	Rate		Reference
Shotcrete	1.7 – 4.2	mBq m^{-2} s^{-1}	[31]
Concrete	1.0 – 70.0	mBq kg^{-1} hr^{-1}	[32]
Copper foil	1.2 – 1.7	μBq m^{-2} s^{-1}	[33]
Stainless steel	4.6 – 10.2	μBq m^{-2} s^{-1}	[33]
De-ionized water	15.0 – 23.2	mBq m^{-3}	[33]
Silicon rubber	196.0	mBq m^{-2} s^{-1}	[34]
Aluminium laminated foil	1.8 – 2.3	Bq m^{-2} h^{-1}	[31]
Gray polypropylene pipe	15.0 – 23.2	Bq m^{-2} h^{-1}	[31]
White polypropylene pipe	0.7 – 1.1	Bq m^{-2} h^{-1}	[31]
Acrylic	< 0.1	Bq m^{-2} h^{-1}	[31]

3.6 Röntgen Excitation Analysis

Röntgen excitation analysis or X-ray fluorescence involves the emission of characteristic "secondary" (or fluorescent) X-rays from a material that has been excited by being bombarded with high-energy X-rays or gamma-rays. This method was first proposed by Glocker and Shreiber in 1928 [27]. This technique is used for elemental and chemical analysis in the composition of materials, such as metals, glass and ceramics, building materials, forensic science, archaeology and others. It can be used to determine U and Th in different matrices (see, e.g., Refs. 28, 29).

4 GERMANIUM DETECTOR CALIBRATIONS

Several underground laboratories operate germanium detectors which are used for low background counting. These detectors may be operated by the laboratories themselves or directly by various experiments. Each detector group has developed their own analysis method based on their experience with their particular detectors and analysis techniques. This makes it difficult to compare samples counted on different detectors without cross calibrations to take into account the different detector characteristics and analysis methods. Different research groups are currently taking a lead role in comparing as many germanium detectors as possible to determine the best detectors to measure the large number of samples expected to be counted to find the best possible materials to build their experiments.

The detector comparison is using calibration sources created from NIST and IAEA standards containing several isotopes in known quantities at very low levels. The sources are prepared in a container which can be fit most detectors to simplify the comparisons between the detectors. The detector groups will be sent the calibration sources without knowing the composition and will then report their results. The different groups will keep their results confidential until each laboratory has counted the calibration sources to avoid biases. The results from the different detectors will then be compared to determine the consistency of the results and if the measurements returned the expected concentration levels of the isotopes contained in the sources,

this will allow the different analysis methods to be compared and to determine if there are any fundamental differences between the various analysis techniques. In addition, the detector sensitivities will be made available such that one can select which detector will be best suited for particular samples to make the best use of the detectors to count samples as efficiently as possible. For example, known high background materials should be counted on higher background detectors and materials expected to be low background should be counted on lower background detectors to maximize the number of samples counted.

5 MATERIAL ASSAY DATABASE

The low background community has an ongoing effort to bring together all relevant low background counting results from around the world to create a central database. The database is a useful tool in tabulating data from many laboratories into one place so that those searching for new materials have a central repository to search for their materials. The database is currently hosted at SNOLAB and is maintained by an international collaboration of scientists who are responsible for developing the database application, defining the material assay data format and encouraging laboratories and experiments to contribute their data. The database is located at the following web site: www.radiopurity.org.

The project began at Lawrence Berkeley National Laboratory and has grown with the support of the wider low-background community, in particular the Assay and Acquisition of Radiopure Materials (AARM) collaboration and the ILIAS program which created a database of radio-pure materials from data collected at several European laboratories. The new database incorporated all of the data from the ILIAS database as its starting point and has continued to add new data from ongoing experiments. Currently, improvements are being planned to upgrade the software and databases to keep them current and to allow new data to be more easily added to keep the database relevant for the next generation of low background experiments.

6 FUTURE PROSPECTS

To further improve the low background detection counting techniques, the background levels of the existing counting systems must be reduced by at least an order of magnitude from current levels. To accomplish this large task, a program to find cleaner materials to build the counters themselves will be required. This includes, for example, finding the raw materials such as copper and lead with even lower internal backgrounds as these will be required to better shield the current suite of experiments.

One such proposed low background facility is being developed at SNOLAB which will includes its own supply of radon-reduced air to allow detector development in the underground lab. In addition it is being proposed to build a general purpose shielding tank with its own veto system to identify muon spallation events from cosmic rays. The tank would contain an inner acrylic tank and a photomultiplier array counter. Such a tank may prove critical to find cleaner materials for future experiment construction.

7 SUMMARY

There are many different techniques employed to measure radioactive backgrounds, the techniques can depend on several factors, such as the sample size, whether or not the sample itself will be used in the final experiment, can the sample be sacrificed, etc. To fully understand a material background, often it can be counted using several techniques, where one can use germanium spectrometry to measure the bulk background of a material while using alpha spectrometry to measure the surface backgrounds. A program to cross calibrate low background detectors at several laboratories around the world is in progress which will allow a comparison of the different detectors and the different analysis techniques used by each experimental group. Finally, an improved database to collate the low background results for common materials will be further improved to enhance the user experience and to include data from many more underground laboratories.

DATA AVAILABILITY STATEMENT

The original contributions presented in the study are included in the article/supplementary material, further inquiries can be directed to the corresponding author/s.

AUTHOR CONTRIBUTIONS

ML and IL jointly contributed to this review of the low background radiation techniques by researching the topic and jointly writing and reviewing the text. IL created the tables and the figures.

FUNDING

SNOLAB operations are supported by the Canada Foundation for Innovation and the Province of Ontario, with underground access provided by Vale Canada Limited at the Creighton mine site.

ACKNOWLEDGMENTS

We would like to thank LNGS and SNOLAB and their staff for support through underground space, logistical and technical services.

REFERENCES

1. Hult M, Preusse W, Gasparro J, Köhler M. Underground gamma-ray spectrometry. *Acta Chim Slov* (2006) **53**:1–7.
2. Laubenstein M, Hult M, Gasparro J, Arnold D, Neumaier S, Heusser G, et al. Underground measurements of radioactivity. *Appl Radiat Isot* (2004) **61**: 167–72. doi:10.1016/j.apradiso.2004.03.039
3. Formaggio JA, Martoff CJ. Backgrounds to sensitive experiments underground. *Annu Rev Nucl Part Sci* (2004) **54**:361–412. doi:10.1146/annurev.nucl.54.070103.181248
4. Heusser G. Low-radioactivity background techniques. *Annu Rev Nucl Part Sci* (1995) **45**:543–90. doi:10.1146/annurev.ns.45.120195.002551
5. BOREXINO. Measurements of extremely low radioactivity levels in BOREXINO. *Astropart Phys* (2002) **18**:1–25. doi:10.1016/S0927-6505(01)00179-7
6. L'Annunziata M. Radiation physics and radionuclide decay In: M L'Annunziata, editor *Handbook of radioactivity analysis*. Amsterdam, Netherlands: Elsevier, Academic Press (2012). p 1–162.
7. Plant JA, Saunders AD. The radioactive earth. *Radiat Protect Dosim* (1996) **68**: 25–36. doi:10.1093/oxfordjournals.rpd.a031847
8. UNSCEAR. Sources and effects of ionizing radiation. In United Nations Scientific Committee on the Effects of Atomic Radiation, editor *UNSCEAR 2008 report to the general assembly with scientific annexes, volume I: sources*. New York, NY: United Nations (2008). p 1–463.
9. Pradler J, Singh B, Yavin I. On an unverified nuclear decay and its role in the dama experiment. *Phys Lett B* (2013) **720**:399–404. doi:10.1016/j.physletb.2013.02.033.
10. Nisi S, Di Vacri A, Di Vacri ML, Stramenga A, Laubenstein M. Comparison of inductively coupled mass spectrometry and ultra low-level gamma-ray spectroscopy for ultra low background material selection. *Appl Radiat Isot* (2009) **67**:828–32. doi:10.1016/j.apradiso.2009.01.021.
11. Maneschg W, Laubenstein M, Budjáš D, Hampel W, Heusser G, Knöpfle KT, et al. Measurements of extremely low radioactivity levels in stainless steel for GERDA. *Nucl Instrum Methods Phys Res Sect A Accel Spectrom Detect Assoc Equip* (2008) **593**:448–53. doi:10.1016/j.nima.2008.05.036
12. Köhler M, Hult M, Arnold D, Laubenstein M, Reyss JL. Reference measurements of low levels of 60Co in steel. *Appl Radiat Isot* (2004) **61**: 207–11. doi:10.1016/j.apradiso.2004.03.047
13. Heusser G, Laubenstein M, Neder N. Low-level germanium gamma-ray spectrometry at the μbq/kg level and future developments towards higher sensitivity In: P Povinec J Sanchez-Cabeza, editors *Radionuclides in the environment*. Amsterdam, Netherlands: Elsevier (2006). p. 495–510.
14. Heusser G, Weber M, Hakenmüller J, Laubenstein M, Lindner M, Maneschg W, et al. Giove: a new detector setup for high sensitivity germanium spectroscopy at shallow depth. *Eur Phys J C* (2015) **75**:531. doi:10.1140/epjc/s10052-015-3704-2
15. Gray AL, Date AR. Inductively coupled plasma source mass spectrometry using continuum flow ion extraction. *Analyst* (1983) **108**:1033–50. doi:10.1039/AN9830801033
16. Houk RS. Mass spectrometry of inductively coupled plasmas. *Anal Chem* (1986) **58**:97A–105A. doi:10.1021/ac00292a003
17. Meermann B, Nischwitz V. ICP-MS for the analysis at the nanoscale–a tutorial review. *J Anal At Spectrom* (2018) **33**:1432–68. doi:10.1039/C8JA00037A
18. Tanner SD, Baranov VI, Bandura DR. Reaction cells and collision cells for icp-ms: A tutorial review. *Spectrochim Acta B Atom Spectrosc* (2002) **57**:1361–452. doi:10.1016/S0584-8547(02)00069-1.
19. Dobson J, Ghag C, Manenti L. Ultra-low background mass spectrometry for rare-event searches. *Nucl Instrum Methods Phys Res Sect A Accel Spectrom Detect Assoc Equip* (2018) **879**:25–30. doi:10.1016/j.nima.2017.10.014
20. Povinec PP. New ultra-sensitive radioanalytical technologies for new science. *J Radioanal Nucl Chem* (2018) **316**:893–931. doi:10.1007/s10967-018-5787-3
21. Aggarwal SK. Alpha-particle spectrometry for the determination of alpha emitting isotopes in nuclear, environmental and biological samples: Past, present and future. *Anal Methods* (2016) **8**:5353–71. doi:10.1039/c6ay00920d
22. Knoll G. *Radiation detection and measurement*. 4th ed. Hoboken, NJ: John Wiley and Sons (2010).
23. Mirion Technologies. *Passivated implanted planar silicon (PIPS) detectors*. Smyrna, GA: Mirion Technology Inc (2020). Available at: https://www.mirion.com/products/passivated-implanted-planar-silicon-detectors (Accessed November 4, 2019).
24. Sakoda A, Ishimori Y. Mechanisms and modeling approaches of radon emanation for natural materials. *Jpn J Health Phys* (2017) **52**:296–306. doi:10.5453/jhps.52.296.
25. Durridge. *RAD7 radon detector user manual*. Boston, MA: Durridge Company Inc. (2020). Available at: www.durridge.com/support/product-manuals
26. Clemenza M. Low background neutron activation: a high sensitivity technique for long-lived radionuclides determination in rare events physics experiments. *J Radioanal Nucl Chem* (2018) **318**:1765–72doi:10.1007/s10967-018-6333-z.
27. Glocker R, Schreiber H. Quantitative Röntgenspektralanalyse mit Kalterregung des Spektrums. *Ann Phys* (1928) **390**:1089–102. doi:10.1002/andp.19283900805
28. Kazy SK, D'Souza SF, Sar P. Uranium and thorium sequestration by a pseudomonas sp: Mechanism and chemical characterization. *J Hazard Mater* (2009) **163**:65–72. doi:10.1016/j.jhazmat.2008.06.076.
29. Park JY, Lim JM, Ji YY, Lim CS, Jang BU, Chung KH, et al. Rapid screening of naturally occurring radioactive nuclides (238U,232Th) in raw materials and by-Products samples using XRF. *J Radiat Prot Res* (2016) **41**:359–67. doi:10.14407/jrpr.2016.41.4.359
30. Lucas HF. Improved low-level alpha-scintillation counter for radon. *Rev Sci Instrum* (1957) **28**:680–3. doi:10.1063/1.1715975
31. Bigu J, Hallman E. Radon emanation from shotcrete (1992). p. 1–2. SNO Technical Report SNO-STR-92-064.
32. Trevisi R, Leonardi F, Risica S, Nuccetelli C. Updated database on natural radioactivity in building materials in europe. *J Environ Radioact* (2018) **187**: 90–105. doi:10.1016/j.jenvrad.2018.01.024.
33. Zuzel G, Simgen H. High sensitivity radon emanation measurements. In: D. Arnold, S. Jerome, and M. Hult, editors. 5th international conference on radionuclide metrology–low-level radioactivity measurement techniques ICRM-LLRMT'08; Elsevier Applied Radiation and Isotopes (2009). September 22–26, 2008. (Braunschweig, Germany). p. 889–93. doi:10.1016/j.apradiso.2009.01.052
34. Zuzel G. Highly sensitive measurements of 222-radon diffusion and emanation. In: R. Ford, B. Cleveland M Chen, editors *Topical workshop on low radioactivity techniques: LRT 2004*. AIP Conference Proceedings (2005). Vol. 785, p 142–9. Sudbury, Ontario, Canada, December 12–14, 2004. (Melville, New York). doi:10.1063/1.2060465

Conflict of Interest: The authors declare that the research was conducted in the absence of any commercial or financial relationships that could be construed as a potential conflict of interest.

frontiers in Public Health

TECHNOLOGY AND CODE
published: 02 February 2021
doi: 10.3389/fpubh.2020.589891

Low Radon Cleanroom for Underground Laboratories

Ivan Štekl[1], Jirí Hůlka[2], Fadahat Mamedov[1], Pavel Fojtík[2], Eva Čermáková[2], Karel Jílek[2], Miroslav Havelka[2], Rastislav Hodák[1] and Miroslav Hýža[2]*

[1] *Institute of Experimental and Applied Physics, Czech Technical University in Prague, Prague, Czechia,* [2] *SÚRO, Prague, Czechia*

Aim of a low radon cleanroom technology is to minimize at the same time radon, radon decay products concentration and aerosol concentration and to minimize deposition of radon decay products on the surfaces. The technology placed in a deep underground laboratory such as LSM Modane with suppressed muon flux and shielded against external gamma radiation and neutrons provides "Zero dose" space for basic research in radiobiology (validity of the LNT hypothesis for very low doses) and for the fabrication of nanoelectronic circuits to avoid undesirable "single event effects." Two prototypes of a low radon cleanroom were built with the aim to achieve radon concentration lower than 100 mBq·m^3 in an interior space where only radon-free air is delivered into the cleanroom technology from a radon trapping facility. The first prototype, built in the laboratory of SÚRO Prague, is equipped with a standard filter-ventilation system on the top of the cleanroom with improved leakproofness. In an experiment, radon concentration of some 50 mBq·m^{-3} was achieved with the filter-ventilation system switched out. However, it was not possible to seal the system of pipes and fans against negative-pressure air leakage into the cleanroom during a high volume ventilation with the rate of 3,500 m^3·h^{-1}. From that reason more sophisticated second prototype of the cleanroom designed in the LSM Modane uses the filter-ventilation system which is completely covered in a further improved leakproof sealed metal box placed on the top of the cleanroom. Preliminary experiments carried out in the SÚRO cleanroom with a high radon activity injection and intensive filter-ventilation (corresponding to room filtration rate every 13 s) showed extremely low radon decay products equilibrium factor of 0.002, the majority of activity being in the form of an "unattached fraction" (nanoparticles) of ^{218}Po and a surface deposition rate of some 0.05 mBq· m^{-2}·s^{-1} per Bq·m^{-3}. Radon exhalation from persons may affect the radon concentration in a low radon interior space. Balance and time course of the radon exhalation from the human body is therefore discussed for persons that are about to enter the cleanroom.

Keywords: radon, cleanroom, underground laboratory, nanotechnology, zero dose, equilibrium factor

OPEN ACCESS

Edited by:
Carlos Peña Garay, Laboratorio Subterráneo de Canfranc, Spain

Reviewed by:
Qiuju Guo, Peking University, China
Rakesh C. Ramola, Hemwati Nandan Bahuguna Garhwal University, India

****Correspondence:***
Jirí Hůlka
jiri.hulka@suro.cz

Specialty section:
This article was submitted to Radiation and Health, a section of the journal Frontiers in Public Health

Received: *20 August 2020*
Accepted: *30 December 2020*
Published: *02 February 2021*

Citation:
Štekl I, Hůlka J, Mamedov F, Fojtík P, Čermáková E, Jílek K, Havelka M, Hodák R and Hýža M (2021) Low Radon Cleanroom for Underground Laboratories. Front. Public Health 8:589891. doi: 10.3389/fpubh.2020.589891

INTRODUCTION

Only recently, the need has been recognized in both nanotechnology (e.g., CCD image sensor, pixel detectors fabrication) and fundamental biological research (verification of LNT hypothesis for very low doses and without pollutants) to achieve at the same time very low radon and minimum aerosol concentrations in the air of laboratories, in so-called low radon cleanrooms (1). Radon

and its decay products in the air or deposited on the surfaces emit alpha particles (with relatively high energy) which can cause undesirable "single event effects" in nanoelectronic circuits. In the fundamental research of biological cells response carried out in the radiation free environment (Zero dose in underground laboratories) radon and its decay products can adversely affect the experiment. Radon air concentrations are required to be as low as possible in such special cases. However, since levels of radon concentration in the outdoor atmosphere range normally from units to tens of $Bq{\cdot}m^{-3}$ and in buildings from tens to thousands $Bq{\cdot}m^{-3}$ the achievement of indoor radon air concentration in the laboratory at the level of some tens of $mBq{\cdot}m^{-3}$ requires advanced systems able to reduce radon concentration at least by a factor 1,000 in comparison to the outdoor environment. We present realization of the complex technology able to achieve at the same time low radon concentration levels of 10–100 $mBq{\cdot}m^{-3}$ for radon, about $mBq{\cdot}m^{-3}$ for radon decay products and the minimum aerosol concentrations in the air of the cleanroom as well as radon decay product ^{218}Po deposition rate of some $\mu Bq{\cdot}m^{-2}{\cdot}s^{-1}$. In addition, if the technology is placed in a deep underground laboratory such as LSM Modane with suppressed muon flux and the technology or at least a part of the inner space inside the cleanroom are shielded against external gamma radiation and neutrons, a complex suppression of the all above-mentioned components of external radiation can be achieved for Zero dose basic research.

PROTOTYPE SETUP

Experimental Low Radon Cleanroom Technology—Prototype Development

Cleanroom is defined (ISO14644-1) as a room in which the concentration of airborne particles is controlled, and which is constructed and used in a manner to minimize the introduction, generation, and retention of particles inside the room and in which other relevant parameters, e.g., temperature, humidity, and pressure, are controlled as necessary. A clean room is generally based on several rooms in a row including e.g., room for person undressing, clean dressing room, air-shower where a strong air stream cleans the work clothes from adhering dust particles before entering to the clean room, and one clean room. The rooms are separately ventilated and filtrated. The person entering the cleanroom has to respect time required for air regeneration in each room. The doors are equipped with an alarm to indicate the current opening, the air shower door is equipped with a lock, preventing simultaneous opening. Thanks to all these procedures higher degree of purity is gradually achieved in adjoining rooms and the highest class of cleanliness is reached in the cleanroom intensively filtered by HEPA filters. The lowest aerosol concentration, however, is reached only in part of cleanroom just under air outlet from HEPA filtration system where the laminar flow is ensured. Standard commercial cleanrooms technologies don't deal with radon and therefore filtration system uses ambient air with outdoor background radon concentration.

The new technology developed to minimize radon and radon decay products in the cleanroom is based on following innovations: (a) the filter ventilation system is closed, it means the air from cleanroom returns back through HEPA filter into the cleanroom to avoid mixing with outdoor air, (b) the cleanroom uses air delivered from an external radon trapping facility, where adsorption of radon on charcoal takes place (2, 3), (c) radon exhalation from human body is taken into account. To reach minimal radon concentration in the cleanroom the "radon-free air" has to be delivered from radon trapping facility in a sufficient amount for two reasons: to ensure both sufficient air exchange rate for persons in the cleanroom and to ensure reasonable over-pressure to suppress potential radon entry from outer space. Commercial radon trapping facilities available today are able to deliver typically from 20 $m^3{\cdot}h^{-1}$ up to 300 $m^3{\cdot}h^{-1}$ "radon free air" with radon concentration in range 10–100 $mBq{\cdot}m^{-3}{\cdot}h^{-1}$. From that reason they are often used in underground laboratories for suppression of background radon concentration particularly for detectors in fundamental physical research, neutrino physics, astrophysics, such as NEMO-3 experiment (4). The low radon concentration in the air supplied from the radon trapping facility determines the achievable radon concentration in low radon cleanroom together with system leakproofness. An experimental prototype of the low radon cleanroom was built at SÚRO Prague laboratory. The prototype consists of four rooms (**Figure 1**), a room for person undressing (1), a clean dressing room (2), an air-shower (3), and a low radon cleanroom (4) intensively filtered by a closed filter-ventilation system (3,600 $m^3{\cdot}h^{-1}$) with HEPA filters. The used experimental radon trapping facility is located out of the cleanroom and is able to provide to the cleanroom up to 20 $m^3{\cdot}h^{-1}$ of radon-free compressed air by means of a cooper manifolds The air leaks out from the room through the air shower as well as in the ventilation system. Radon-free air is supplied directly into the cleanroom filtration system and allows to reach indoor overpressure at least 5 Pa. The air leaks out from the room through the air shower as well as in the ventilation system. Volume of the cleanroom is 13 m^3 and the delivery of 20 m^3 h^{-1} radon free air corresponds to the air exchange rate of $\sim$1.5 h^{-1}. Clean room meets the requirement of ISO 14644-1 (5) Class 5 (maximum concentration limits particles/m^3 of air for particles equal to and larger than the considered sizes, it means 3 520 p/m^3 $< 0.5\,\mu m$, 832 p/m^3 $< 1\,\mu m$, 29 p/m^3 $< 5\,\mu m$). The standard room temperature is 20° C and can be changed, the standard relative humidity in the clean room is very low (<5% due to the dried air supplied from the anti-radon facility), but can be increased by humidifier with radon-free water.

The goal of the prototype design was to reach indoor radon concentration in range 10–100 $mBq{\cdot}m^{-3}$. From that reason attention was paid to reduce so far as possible radon penetration from subsoil and ambient outdoor air and its emanation from building material. Hence, the whole room is built from metal (iron) and surface treated sandwich panels with thermal polystyrene insulation inside (total panel thickness of 62 mm). The panels are joined and sealed with sealant. To reduce penetration of ambient outdoor radon the panels are additionally sealed by a membrane with low diffusion coefficient (the TROPAC® foil). To reduce radon entry from subsoil,

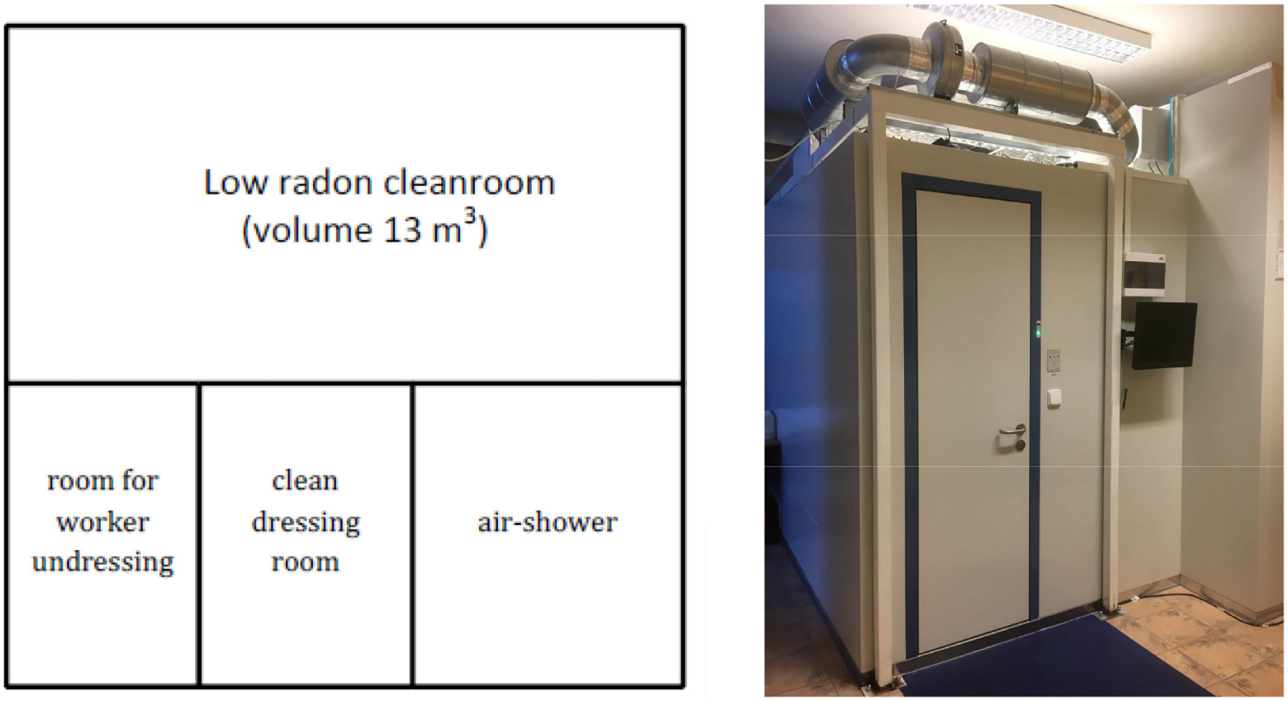

FIGURE 1 | Radon Cleanroom at SÚRO laboratory, Prague.

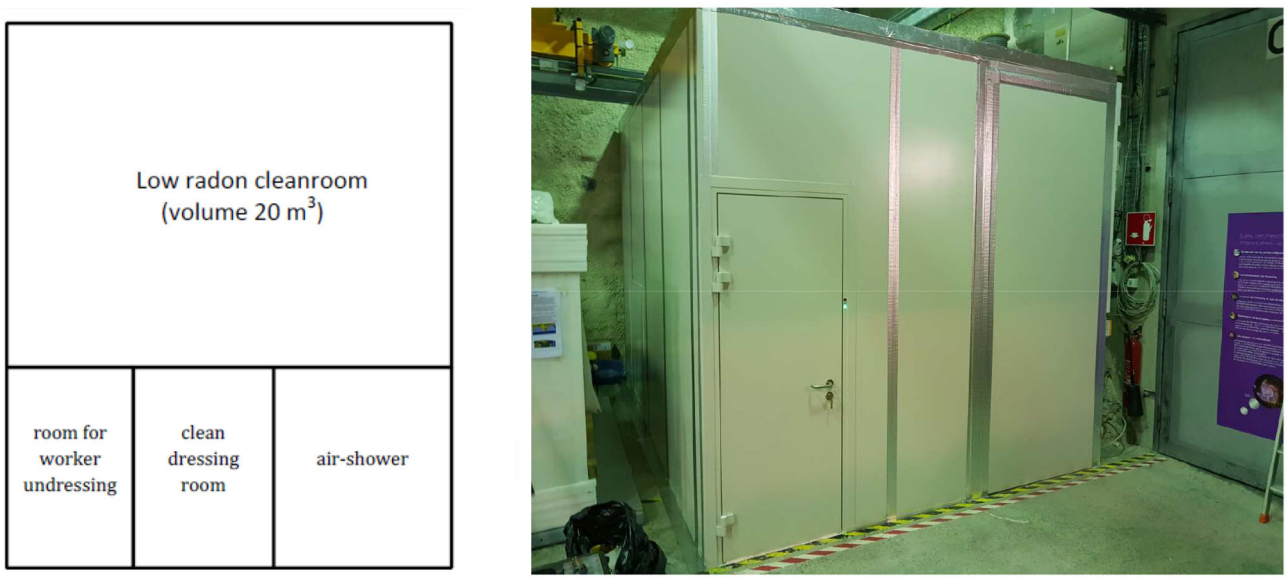

FIGURE 2 | Radon Cleanroom at underground laboratory LSM Modane (2).

we have used metal plate directly placed and fixed onto the laboratory floor. It means that all walls, ceiling, and floor are made of a metal with high diffusion resistance for radon. In order to minimize radon/thoron exhalation from the surfaces into the room all material used for construction (iron sheet, thermal insulation, sealant) was selected and controlled in terms of the content of the relevant radionuclides, particularly for ^{226}Ra and ^{228}Th. The same control concerns to all objects located in the cleanroom (tables, instruments etc.). The limit for radionuclide concentration and radon emanation is determined by the demand for minimum radon concentration in the cleanroom with the available air exchange rate in mind. While

air exchange rate is assumed to be above 1 h^{-1}, the total radon exhalation from all the surfaces (walls, ceilings, floor, and objects inside) should be as low as possible in any case no more than some $mBq{\cdot}h^{-1}$ in order to not increase the radon concentration significantly. To reduce transport of contaminated air from the air wash to the low radon cleanroom a tight door between these rooms is used and in addition the room is operated at overpressure. In fact, the key factor influencing magnitude and time variation of radon entry from ambient outdoor air into the cleanroom is radon penetration through filter-ventilation system which is installed on the top of the whole cleanroom envelope. Leakages in filter-ventilation system and pipes were fixed step by step by mastic sealant and covered also by anti-radon TROPAC® foil. Experiments lasting several months were performed of experiments were performed in SÚRO laboratory to optimize system performance, study of the system tightness and pressure differences. Their results showed however, that it is not manageable to seal this complex engineering system of pipes and fans with high volume filter-ventilation rate creating a high under-pressure into the cleanroom. Only if the filter-ventilation system was switched off, it was possible to reach suppression of outdoor radon air entry into cleanroom by means of the created overpressure radon free air supplied from the external radon trapping facility. From that reason more sophisticated solution of next prototype of the cleanroom designed in the LSM Modane (**Figure 2**) uses the filter-ventilation system which is completely deployed in the tight sealed metal box placed at the top of cleanroom.

The last factor which can cause radon elevation in the cleanroom could be radon exhalation from persons entering the low radon cleanroom. This will be analyzed in discussion.

Safety Elements and Equipment

Entire low radon cleanroom system is a closed system. The dried air from an anti-radon device guarantying an air exchange necessary for work (∼1.5 h^{-1} in our prototype) is a single air supply. In addition to the standard safety elements, the system has been supplemented also with CO_2 alarm sensor and camera for monitoring of the persons safety. Also humidifier with demineralized and radon-free water should be installed in case of long stay of persons inside.

RESULTS OF MEASUREMENTS

The first tests of the prototype of the low radon cleanroom built in SÚRO were focused on the

- tightness of the room
- radon gas measurement
- measurements of short-lived radon decay products and their unattached fraction
- measurements of deposition rate of radon decay products of and relevant surface contamination.

Results of Ventilation Rate Measurement

The ventilation rate is the crucial parameter affecting behavior of all types of aerosol and gaseous contaminants (radioactive, chemical, biological) including radon and its short-lived decay product in rooms and buildings and moreover mediates also their convective transport from the outdoor environment to interiors of rooms and building. The ventilation rate can be found as a measure of the tightness of the room. The following simple and well-known mass balance model describes the effect of ventilation on the radon behavior in the room (6):

$$\frac{da_i(t)}{dt} = Qr(t) - (K(t) + \lambda).(a_i(t) - a_0(t)) \quad (1)$$

$a_i(t)$, $a_o(t)$ is a time variation of indoor-outdoor radon gas activity concentration in ($Bq{\cdot}m^{-3}$)
$Qr\ (t)$ is time variation of a sum of radon entry rates coming into the room in ($Bq{\cdot}h^{-1}{\cdot}m^{-3}$)
λ is defined decay constant for radon 0.00755 (h^{-1})
$K\ (t)$ is time variation of ventilation (h^{-1})

To estimate ventilation of the room under a different operation conditions of the cleanroom (i.e., with the internal filtration system switched OFF and switched ON) we used so called tracer gas method based on both single injection and constant tracer gas entry into the room (7). In case of the use of the tracer gas method Equation (1) for radon gas can be modified as follows:

$$\frac{dc(t)}{dt} = G - (K(t))c(t) \quad (2)$$

$c(t)$ is continually measured tracer gas concentration in the room in ($kg{\cdot}m^{-3}$)
G is constant, and well-known tracer gas entry in the room in ($kg{\cdot}h^{-1}$)
$K(t)$ has the same meaning as in the previous Equation (1).

In case of the use of the single injection tracer gas method, the constant G is equal to zero in the Equation (2). For the constant gas method, time derivations $\frac{dc(t)}{dt} = 0$ in Equation (2) can be substituted with a numerical differences. Ventilation was also calculated when the tracer reached the steady state concentration and member $\frac{dc(t)}{dt} = 0$ in Equation (2).

As a tracer gas we used nitrous oxide(N_2O) with defined and well-known entry rate into the room and we used a current sensor Polytron IR N_2O (8) for continuous measurement of the tracer gas in the room (9). The results of multiple measurements indicated ventilation of the room ranged 0.015–0.02 h^{-1} for switched OFF filtration system and the same ventilation ranged 0.65–0.8 h^{-1} for switched ON filtration system with delivery of radon free air from the external radon trapping facility.

Results of Radon Measurements

During all radon tests radon gas activity concentration was simultaneously measured in the low radon room and outside the whole cleanroom in a SÚRO laboratory where is the whole cleanroom deployed. Radon concentration in this laboratory was measured continuously by TESLA Radon Probe TSR4 (10).

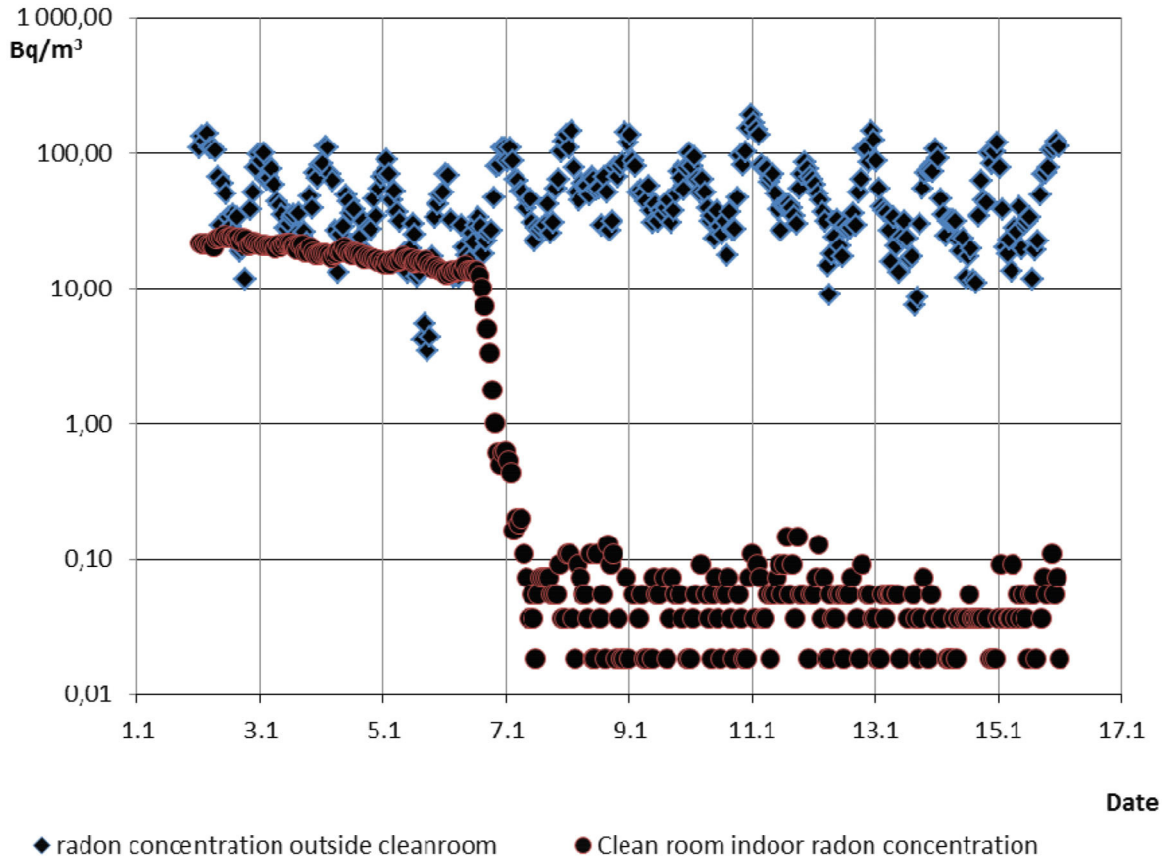

FIGURE 3 | Comparison of radon concentration in laboratory and in cleanroom before and after switching on anti-radon facility.

Radon concentration shown in **Figure 3** varied normally in the range of 10–200 Bq·m^{-3}. Measurements of low radon concentration in the low radon cleanroom were carried out by a special high sensitivity (up to 10 mBq·m^{-3}) continuous radon detector developed by IEAP CTU (11). After 2 years of experiments which included improvements in tightness and sealing of the system, proper overpressure in the low radon cleanroom and reasonable tightness between adjoining rooms (dressing room, air-shower, cleanroom) was achieved and radon concentration below 100 mBq·m^{-3} as is shown in (see **Figure 3**) was reached when the filter-ventilation system was switched off. The radon concentration mean value achieved in the low radon cleanroom was 52 mBq·m^{-3}, while in the laboratory the mean value was 55 Bq·m^{-3} in the same period, it means radon reduction factor is more than one thousand. Time for exponential decrease of radon concentration to low level value after starting of radon-free air supply was ∼6 h and is determined by air exchange rate 1.5 h^{-1}.

Results of Radon Decay Products Concentration and Equilibrium Factor

Investigation of the behavior of radon short-lived decay products was another goal of our tests. The key issue is concentration of short lived radon decay products ^{218}Po (half-life 3.1 min), ^{214}Pb (half-life 27 min), ^{214}Bi (half-life 20 min) in the air and their deposition on surfaces and subsequent irradiation of sensitive objects by alpha particles. Generally, radon decay products are not in equilibrium with radon concentration in the room due to filtration and their subsequent deposition on the room surfaces. After their creation some decay products are attached to aerosol particles with diameter higher than ∼10 nm (referred to as "attached" form). The rest is in the "unattached" fraction i.e., attached to clusters with a mobility diameter < ∼10 nm (12). Radon equilibrium equivalent concentration (EEC) defined as activity concentration of radon in equilibrium with its short-lived progeny that would have the same potential alpha energy concentration as the existing non-equilibrium mixture is a simple quantity often used in human dosimetry for describing mix of short-lived radon decay products concentration (13). The ratio of EEC to the activity of parent radon in air is called equilibrium factor F and characterizes the disequilibrium between the mixture of the short-lived progeny and radon. Equilibrium factor F for indoor buildings is usually in the range (0.3–0.6) (14), it means approximately half of radon decay products are in indoor air.

The cleanroom is equipped with a filtration system of high filtration rate 3,600 m^3·h^{-1}. It corresponds with the mean time for filtration of the room (volume 13 m^3) ∼13 s which is much

lower than the half-life of radon decay products. From that reason it could be expected that radon decay products will be very quickly removed from the air and equilibrium factor will be much lower than usual under normal conditions. In addition due to the use of a high efficiency HEPA filter in the room filtration unit a significant increase of a small clusters with only unattached ^{218}Po can be expected. The results of such experiments for attached and unattached fractions of radon decay products are not known for such high filtration rate.

Currently, it is not easy to measure continuously short lived radon decay products in the air in case of low radon concentration ranging below 0.1 Bq·m^{-3}. To estimate equilibrium factor and relationship between attached and unattached fractions of radon short-lived decay products all experiments had to be performed in an artificially high indoor radon concentration in the clean room during normal operation (huge filtration) so that radon and decay products are measurable with reasonable uncertainty. An artificial solid state ^{226}Ra/^{222}Rn flow-through source with ^{222}Rn production rate certified in the Czech Metrological Institute was used. Initial high radon activity accumulated in the source was injected directly in the low radon cleanroom in operation followed by constant and defined radon entry rate. To achieve a steady state of radon and its short-lived decay products concentrations, the experiment lasted always a several days. During each exposure the built–in HEPA filtration system was operating and the air from radon-free facility was supplied to the room for maximum simulation of the real situation. While the steady state radon gas activity concentration varied in the order of kBq·m^{-3}, the steady state activity concentration of measured unattached ^{218}Po varied in the order of tens Bq·m^{-3} and attached ^{218}Po varied in the order of units Bq·m^{-3}. The amount of artificially added radon atoms in clean room is so negligible that cannot affect indoor condition of aerosol particles. All measurements were carried out with the continuous radon monitor AlphaGUARD and a continuous monitor FRITRA4 enabling simultaneous measurement of unattached and attached activity concentration each short-lived radon decay product from the open-faced filter and from the screen and the filter placed behind the screen. Measurement is based on the theory Cheng and Yeh (15) and Nazarof (16). Unattached activity concentration of each radon progeny was measured from the screen with mesh 300 and cut-off diameter $d_{50} = 4$ nm and the attached activity concentration of each radon progeny from a Millipore filter type AA, 0.8 μm placed behind the screen Jílek et al. (17) and Jílek et al. (14). Both instruments were calibrated in the Czech Accredited Calibrated Laboratory at Kamenná near Příbram (Czech Republic) as well as in the SÚRO Radon chamber (18). All the results indicated extremely low average equilibrium factor F ranging from 0.0015 to 0.0022. Nearly all radon decay products ^{218}Po were in unattached fraction, average ratios of unattached ^{218}Po and unattached + attached ^{218}Po ranging from 95 to 98%. It could be deduced indirectly from this result that in case of a low radon cleanroom with reached indoor radon concentration of 50 mBq·m^{-3} the radon decay products concentration (EEC) of 1 mBq·m^{-3} will be approximately achieved with majority in the unattached fraction. This raises the question of what is the deposition on surfaces in such an unusual environment. Knowledge of this issue is important for research and technology fabrication in branches of nanoelectronic (to minimize "single event effect" by alpha particles), radiobiology (LNT hypothesis) etc.

Radon Decay Products Surface Deposition: Measurement and Results

Two other preliminary experiments with artificially high indoor radon concentrations (89 and 1.4 kBq·m^{-3}) in the cleanroom during operation of HEPA filtration system and ventilation by radon free air were performed to estimate deposition rate with reasonable uncertainty. An aluminum foil 1 m^2 was placed in horizontal position in that part of the cleanroom with laminar flow of air. Foil was exposed 10 min to reach steady state activity on surface for deposited short-lived ^{218}Po. The experiment was aimed at simulation of the manipulation with a metal surface, e.g., work with electronic circuits. The foils were measured by HPGe gamma spectrometry (deconvolution from ^{214}Pb and ^{214}Bi activity data set) at SÚRO laboratory. The deposition rate of ^{218}Po was estimated 0.05–0.1 Bq·m^{-2}·s^{-1} in case of indoor radon concentration 1.41 kBq·m^{-3} and 5–5.6 Bq·m^{-2}·s^{-1} in case of indoor radon concentration 89 kBq·m^{-3}. If related to unit indoor radon concentration of 1 Bq·m^{-3} estimated ^{218}Po deposition rates are 0.036–0.07 mBq·m^{-2}·s^{-1} per Bq·m^{-3} in first experiment and 0.056–0.06 mBq·m^{-2}·s^{-1} per Bq·m^{-3} in second experiment, which is in good agreement. It can be again indirectly deduced that in case of indoor radon concentration 50 mBq·m^{-3} (achievable in contemporary low radon cleanrooms) the ^{218}Po deposition rate will be ∼3 μBq·m^{-2}·s^{-1} and after the steady state is reached (as result of ^{218}Po deposition and its decay) the surface deposition can be estimated as 700 μBq·m^{-2} (so below 1 mBq·m^{-2}).

DISCUSSION

There should be mentioned another factor which may affect radon concentration in a low radon cleanroom. Persons exhale radon dissolved in their bodies by breathing mostly and become a source of an undesirable radon activity. The balance and time course of the exhalation from body is therefore of interest when persons are about to enter such premises. Before entering clean room the person must completely dress up into clean (radon free) clothes. Total radon activity in the human body depends on the radon concentration in the environment and time spent in it during last hours. Radon body content can range from units to some hundreds of Bq per body (19). Rapid radon exhalation from the body by breathing could cause increase of radon concentration in low radon cleanroom. The dynamics of the exhalation has been studied in the past by inhalation and ingestion experiments with ^{222}Rn or with noble gases generally. Study of the ^{222}Rn elimination from the human body subsequent to a relatively long-term inhalation was conducted (19). Recently, a biokinetic model for radon has been published (20, 21) based on theoretical approach and empirical data. The kinetics of radon exhalation decrease could be described by several exponentials,

the first shows rapid decrease in exhalation by approximately a factor of 10 during 5 min and by a factor 100 during 2 h, etc. (19). The importance of the radon exhalation phenomena was also analyzed at SÚRO by experiments confirming Harley kinetic data. As example it can be estimated from these models that a person who spent some hours in concentration 1,000 $Bq{\cdot}m^{-3}$ exhales by breathing some 5 $Bq{\cdot}min^{-1}$ just after leaving this concentration what could influence significantly radon concentration in low radon cleanroom. Therefore, it is advisable to monitor the radon concentration in areas where persons reside before their entering to the cleanroom. If the concentration of radon is elevated, it is necessary to let the person in a low-radon environment for some time before entering the cleanroom. If the person in the cleanroom should not exhale more than some tens of mBq per hour (comparable to achievable radon concentration in low radon cleanroom today), for person who resides before at 100 $Bq{\cdot}m^{-3}$ it is necessary to spent ∼2 h at low radon concentration only some $Bq{\cdot}m^{-3}$.There is also unavoidable radon exhalation from the body caused by natural ^{226}Ra content in the body [below 1 Bq in skeleton, (22)]. In this case only a fraction of radon is able to emanate from the body and radon activity emanation attributable to ^{226}Ra is approximately below $mBq{\cdot}h^{-1}$. The time needed to suppress the body radon exhalation up to levels that correspond with the inevitable radon exhalation due to natural ^{226}Ra content in the body ranges a few days.

SUMMARY

A prototype of a complex technology able to achieve minimum aerosol concentrations in the air in terms of ISO standard (ISO 1999) and low radon concentration levels of 10–100 $mBq{\cdot}m^{-3}$ is available. From the measurements of attached and unattached fractions of radon decay products and from low equilibrium factor of $F = 0.002$ we can deduce indirectly that radon decay products equilibrium equivalent concentration (EEC) can be reached in the range some $mBq{\cdot}m^{-3}$, while majority of activity occurs in unattached (nanoparticle) fraction of ^{218}Po. Preliminary results lead to an indirectly estimate that the deposition rate of ^{218}Po is approximately some $\mu Bq{\cdot}m^{-2}{\cdot}s^{-1}$ and deposition in steady state below 1 $mBq{\cdot}m^{-2}$ in the low radon cleanroom. A second improved prototype of a low radon cleanroom with improved tightness and delivery of 150 $m^3{\cdot}s^{-1}$ radon free air was placed in the underground laboratory LSM Modane and is prepared for research and development. In case of further shielding against gamma and neutrons it is prepared to provide cleanroom or at lease space with nearly zero dose environment for fundamental experiments in biology, nanotechnologies etc. The zero dose environment does not mean a completely zero radiation background, but reduction of all radiation background components by several orders of magnitude (23). Specifically—reducing the radon concentration from typical values in the atmosphere or laboratories (in the range of 10–100 $Bq.m^{-3}$) to tens of mBq. m^{-3} represents a reduction in the corresponding doses by a factor of 10^3-10^4. The muon flux (and dose) is reduced by a factor of 10^6 The strategy to protect experiments in clean room against the neutron and gamma ray fluxes is standard: multilayer shields made of iron or clean Pb (20–30 cm), polythylene (16 cm) to thermalize fast neutrons followed by borated polyethylene (8 cm) to capture thermal neutrons. Such shields will surround the detectors or devices installed in clean room to reduce photon and neutron fluxes coming from the rocks of the laboratory. The gamma background can be reduced by a factor of 10^3-10^4, the neutron flux by a factor of 10^3. It can be estimated that in LSM Modane the dose can be reduced by a factor of at least 10^3, i e., significantly lower than 1 μGy per year.

The technology could be useful also for radiobiology e.g., validation of LNT hypothesis for very low doses, study of dosimetry models of radon risk. It is well-known from theory that the risk from radon exposure is much more affected by unattached radon decay particles rather than by attached particles and up to now there was no technology available for such experiments, as well as for the dark matter in CCDs experiment (24).

DATA AVAILABILITY STATEMENT

The raw data supporting the conclusions of this article will be made available by the authors, without undue reservation.

AUTHOR CONTRIBUTIONS

IŠ, JH, and EČ performed the substantial contributions to work conception and design low radon cleanroom. FM and RH were responsible for low radon concentration monitoring, detector development, and improvement and research of room tightness. IŠ, JH, PF, and KJ performed the substantial contributions to drafted and revised the manuscript critically for important intellectual content and provided the approval for publication of content. PF performed key contribution to radon exhalation from human body. FM, KJ, and MH were responsible for the acquisition, analysis, and interpretation of data. MH for spectrometry analysis of surface deposition of radon decay products. All authors contributed to the article and approved the submitted version.

FUNDING

This work was funded by the Research Infrastructure Underground laboratory LSM – Czech participation to European-level research infrastructure, LM2018107.

REFERENCES

1. Grant D, Hallin A, Hanchurak S, Krauss C, Liu S, Soluk R. Low radon cleanroom at the University of Alberta. In: *AIP Conference Proceedings 1338, 161*. Sudbury, ON (2011) doi: 10.1063/1.3579575
2. Hodak R, Perrot F, Brudanin V, Busto J, Havelcová M, Hulka J, et al. Characterization and long-term performance of the radon trapping facility operating at the Modane Underground Laboratory. *J Phys G*. (2019) 46:115105. doi: 10.1088/1361-6471/ab368e
3. Fajt L, Kouba P, Mamedov F, Smolek K, Štekl I, Fojtík P, et al. Compact anti-radon facility. In: *AIP Conference Proceedings 1672, 120002*. Seattle, WA (2015). doi: 10.1063/1.4928008
4. Pahlka RB, the NEMO-3 Collaboration. The NEMO-3 experiment. *Nuclear Phys B - Proc Suppls*. (2012) 229–232:491. doi: 10.1016/j.nuclphysbps.2012.09.128
5. ISO 14644-1. *Standards: Cleanrooms and Associated Controlled Environments* (1999).
6. Mowris RJ. *Analytical and numerical models for estimation the efferct of exhaust ventilation on radon entry in houses with basement or crawl spaces*. Master thesis, Lawrence Berkeley Laboratory, United States (1986). doi: 10.2172/5100673
7. Lagus P, Persily AK. A Review of tracer gas techniques for measurement airflows in buildings. *ASHRAE Trans*. (1985) 91:1075–87.
8. Dräger. Available online at: www.draeger.com
9. Fronka A, Jílek K. Radon entry rate analyses using *in situ* tracer gas method application. *Radiat Prot Dosim*. (2018) 164:143–8. doi: 10.1093/rpd/ncu074
10. TESLA (2020). Available online at: https://www.tesla.cz/en/tsr4-3/ (accessed July 28, 2020).
11. Mamedov F, Štekl I, Smolek K, Cermák P. High sensitivity detectors for measurement of diffusion, emanation and low activity of radon. In: *AIP Conference Proceedings 1549, 120*. Assergi (2013). doi: 10.1063/1.4818090
12. Porstendörfer J, Reineking A. Indoor behaviour and characteristics of radon progeny. *Radiat Prot Dosim*. (1992) 45:303–11. doi: 10.1093/oxfordjournals.rpd.a081550
13. ICRP. Protection against Radon-222 at home and at work. *Ann ICRP*. (1993) 23:1–45.
14. Jílek K, Thomas J, Tomášek L. First results of measurement of equilibrium factors F and unattached fractions fp of radon progeny in Czech dwellings. *Nukleonika*. (2010) 55:439–44. Available online at: http://www.ichtj.waw.pl/nukleonikaa/?p=782
15. Cheng W, Yeh HC. Theory of a screen–type diffusion battery. *J Aerosol Sci*. (1980) 11:313. doi: 10.1016/0021-8502(80)90105-6
16. Nazaroff WW. Optimizing the total-alpha three-count technique for measuring concentration of radon progeny in residences. *Health Phys*. (1984) 46:395–405. doi: 10.1097/00004032-198402000-00015
17. JílekK, Thomas J, Tomášek L. QA programme for radon and its short-lived progeny measuring instruments in NRPI Prague. *Radiat Prot Dosim*. (2008) 130:43–7. doi: 10.1093/rpd/ncn113
18. Jílek K, Timková J. ICHLNRRA intercomparison of radon/thoron gas and radon short-lived decay products measuring instruments in the NRPI Prague. *Radiat Prot Dosim*. (2015) 164:556–62. doi: 10.1093/rpd/ncv311
19. Harley JH, Jetter ES, Nelson N. Elimination of radon from the body. *Environ Int*. (1994) 20:573–84. doi: 10.1016/0160-4120(94)90004-3
20. Leggett R, Marsh J, Gregoratto D, Blanchardon E. A generic biokinetic model for noble gases with application to radon. *J Radiol Prot*. (2013) 33:413–32. doi: 10.1088/0952-4746/33/2/413
21. ICRP. Occupational intakes of radionuclides: part 3. *Ann ICRP*. (2017) 46:1–486. doi: 10.1177/0146645317734963
22. Fisenne IM, Keller HW, Harley NH. Worldwide measurements of Ra 226 in human bone: estimated of skeltal alpha dose. *Health Phys*. (1981) 40:163–71. doi: 10.1097/00004032-198102000-00001
23. Loaiza P. Low radioactivity at the Modane Underground Laboratory. In: *AIP Conference Proceedings 785, 100*. Sudbury, ON (2005). doi: 10.1063/1.2060459
24. DAMIC-M. Available online at: https://damic.uchicago.edu/

Conflict of Interest: The authors declare that the research was conducted in the absence of any commercial or financial relationships that could be construed as a potential conflict of interest.

frontiers in Microbiology

ORIGINAL RESEARCH
published: 26 November 2020
doi: 10.3389/fmicb.2020.572104

Visualizing Microorganism-Mineral Interaction in the Iberian Pyrite Belt Subsurface: The *Acidovorax* Case

Cristina Escudero[1,2], Adolfo del Campo[3], Jose R. Ares[4], Carlos Sánchez[4], Jose M. Martínez[1], Felipe Gómez[2] and Ricardo Amils[1,2]*

[1] Centro de Biología Molecular Severo Ochoa (CBMSO, CSIC-UAM), Universidad Autónoma de Madrid, Madrid, Spain, [2] Departamento de Planetología y Habitabilidad, Centro de Astrobiología (CAB, INTA-CSIC), Madrid, Spain, [3] Departamento de Electrocerámica, Instituto de Cerámica y Vidrio, CSIC, Madrid, Spain, [4] Departamento de Física de Materiales, Universidad Autónoma de Madrid, Cantoblanco, Madrid, Spain

OPEN ACCESS

Edited by:
Carlos Peña Garay, Laboratorio Subterráneo de Canfranc, Spain

Reviewed by:
Aude Picard, University of Nevada, Las Vegas, United States
Sergey N. Gavrilov, Federal Research Centre Biotechnology (RAS), Russia

***Correspondence:**
Cristina Escudero
cescudero@cab.inta-csic.es

Specialty section:
This article was submitted to Extreme Microbiology, a section of the journal Frontiers in Microbiology

Received: *12 June 2020*
Accepted: *20 October 2020*
Published: *26 November 2020*

Citation:
Escudero C, del Campo A, Ares JR, Sánchez C, Martínez JM, Gómez F and Amils R (2020) Visualizing Microorganism-Mineral Interaction in the Iberian Pyrite Belt Subsurface: The Acidovorax Case. Front. Microbiol. 11:572104. doi: 10.3389/fmicb.2020.572104

Despite being considered an extreme environment, several studies have shown that life in the deep subsurface is abundant and diverse. Microorganisms inhabiting these systems live within the rock pores and, therefore, the geochemical and geohydrological characteristics of this matrix may influence the distribution of underground biodiversity. In this study, correlative fluorescence and Raman microscopy (Raman-FISH) was used to analyze the mineralogy associated with the presence of members of the genus *Acidovorax*, an iron oxidizing microorganisms, in native rock samples of the Iberian Pyrite Belt subsurface. Our results suggest a strong correlation between the presence of *Acidovorax* genus and pyrite, suggesting that the mineral might greatly influence its subsurface distribution.

Keywords: fluorescence *in situ* hybridization, confocal Raman microscopy, Raman-FISH, subsurface, *Acidovorax*, pyrite, geomicrobiology

INTRODUCTION

Interest in deep continental subsurface geomicrobiology has grown in the last decades and led to an increase in the amount of information on these environments. Today, we know that life in deep continental subterranean environments is widespread, diverse and active (Kieft, 2016; Escudero et al., 2018a; Magnabosco et al., 2018). However, more in-depth analyses are still needed to better understand the functioning of subsurface ecosystems.

One of the great unknowns that needs to be studied in depth is how mineralogy affects the distribution of the microbial populations, and conversely, how a specific microbial population affects the mineralogy of the system. Some investigations have shown that deep subsurface biodiversity depends directly on the mineralogical composition of the subsurface (Jones and Bennett, 2014, 2017; Rempfert et al., 2017; Casar et al., 2020). Minerals, one of the main sources of electron donors and acceptors in these oligotrophic ecosystems, could determine which metabolisms are carried out and, therefore, which microorganisms can inhabit a certain subsurface micro niche (Jones and Bennett, 2014). Actually, hydrogen produced by water-rock interaction (among others processes) is believed to be one of the principal drivers of subsurface

environments (Pedersen, 1997; Stevens and McKinley, 2000; Chapelle et al., 2002; Mayhew et al., 2013; Schrenk et al., 2013). Nonetheless, only a very limited number of studies have addressed the possible existence of a correlation between the presence of a given microorganism and hence its metabolism with the presence of a specific mineral (Jones and Bennett, 2014, 2017; Casar et al., 2020) and, to the best of our knowledge, we are unaware of any research analyzing how the microorganism-mineral interaction can affect the ecosystem.

Iberian Pyrite Belt Subsurface Life Detection (IPBSL) is a drilling project designed to characterize the Iberian Pyrite Belt (IPB) subsurface biosphere (Amils et al., 2013), whose activity is likely the origin of the peculiar characteristics of the Río Tinto basin (Fernández-Remolar et al., 2008a,b). Río Tinto is an acidic river with a high concentration of heavy metals in solution, mainly ferric iron, which is responsible for its characteristic red water and the constant pH of around 2.3 of the river (Amils et al., 2002). Operating as a natural bioreactor, the microbial community of the IPB subsurface makes use of the high concentration of metal sulfides, primarily pyrite, generating a high concentration of ferric iron in anaerobic conditions. Thus, the analysis of the microorganism-mineral interaction in IPB subsurface samples is essential to understand how this ecosystem operates.

Throughout the IPBSL project, a multimethodological approach was used to determine the biodiversity and its distribution along the column as well as to analyze the main energy sources available for life in the IPB (Amils et al., 2013). One of the most abundant microorganisms detected in the IPB subsurface was *Acidovorax* (Amils et al., under review), a circumneutral nitrate-dependent Fe^{2+} oxidizing bacteria (Straub et al., 2004; Kappler et al., 2005; Chakraborty and Picardal, 2013), which suggests that it may play an important role in the ecosystem. Hence, it would be interesting to know the *Acidovorax* distribution within the IBP subsurface and the minerals with which could be interacting.

Fluorescence *In Situ* Hybridization (FISH) techniques allow the visualization and identification of microorganisms in their natural environment (Moter and Göbel, 2000), which can be especially useful when analyzing microbial distribution in heterogeneous environments such as hard rock subsurface (Escudero et al., 2018b). However, the geochemical characterization of the sample is not possible using fluorescence microscopy. There are, nevertheless, other microscopy techniques that allow chemical analysis of the sample such as Confocal Raman Microscopy (CRM) (Dieing et al., 2011), although their usefulness is limited when identifying microorganisms. The combination of both techniques has been described previously, leading to the term Raman-FISH (Huang et al., 2007). Thanks to Raman-FISH, the metabolic characterization of microorganisms of interest was possible using isotopically labeled substrates and specific FISH probes (Huang et al., 2007). However, until now, Raman-FISH had never been applied to native rock subsurface samples.

In this study, fluorescence microscopy and Raman-FISH techniques were employed on natural rock samples from the IPB subsurface to analyze *in situ* whether mineralogy influences the distribution of members of the genus *Acidovorax* inhabiting the ecosystem.

MATERIALS AND METHODS

Drilling and Sampling

Drilling of borehole 10 (BH10) and sampling was previously described in detail by Amils et al. (2013) and Puente-Sánchez et al. (2018). Briefly, cores were transported to the field laboratory in anaerobic conditions using plastic bags in which oxygen was displaced with N_2. Cores were placed in an anaerobic chamber (N_2 95%, H_2 5%) decontaminated with Virkon S (Antec International Limited), ethanol and a 50:50 bleach:water solution before the introduction of each core. Then, central and untouched portions of the core were obtained using hydraulic core splitter and a rotary hammer with sterile bits, controlling the temperature (40°C maximum) with an infrared thermometer. Potential contamination of cores was monitored routinely by Ion Chromatography, used to detect sodium bromide, which was added to the drilling fluid as a contamination tracer. Additional controls carried out by DNA massive sequencing showed that no microbial contamination was introduced during sampling.

Rock samples for FISH analyses, consisting of small fragments and rock powder, were obtained from the central portion of the core with a sterile chisel. Rock samples were fixed in the field laboratory with 4% formaldehyde in Mackintosh minimal media [$(NH_4)_2SO_4$ 132 mg/l, KH_2PO_4 27 mg/l, $MgCl_2{*}6H_2O$ 53 mg/l, $CaCl_2{*}2H_2O$ 147 mg/l, pH 1.8] for 2 h at 4°C. After fixation, rock samples were washed with Mackintosh minimal media to remove the fixation agent, PBS (NaCl 8 g/l, KCl_2 0.2 g/l, Na_2HPO_4 1.44 g/l, KH_2PO_4 0.24 g/l) to neutralize the pH and, finally, stored in ethanol:PBS (1:1) at −20°C until further processing.

Fluorescence Microscopy

Samples were sonicated (20 s, 3 cycles, one pulse per second at 20% intensity) to detach microorganisms from rock and 100 μl of supernatant was filtered in 0.22 μm black membranes (Millipore, Germany) in aseptic conditions. Filters were washed with PBS and absolute ethanol and then air dried. Catalyzed Reported Deposition-FISH (CARD-FISH) experiments and their respective controls were performed in membrane filters as previously described in Escudero et al. (2018b). ACI145 and ACI208 probes (Amann et al., 1996; Schulze et al., 1999) (Biomers, Germany) were used to target the maximum number of microorganisms of the *Acidovorax* genus since both probes complement each other. Samples from the first 300 m of BH10 were analyzed.

Biofilm detection was performed directly on fixed rock samples. Rocks were ground gently in a sterile mortar and pestle under sterile conditions to the size of grains of sand. Double labeling of oligonucleotide probes-FISH (DOPE-FISH) was carried out as described previously in Escudero et al. (2018b) with double CY3-labeled ACI145 and ACI 208 probes. Polysaccharides were visualized by Fluorescence Lectin Binding Assay (FLBA), using Concanavalin A lectin conjugated with fluorescein isothiocyanate (FITC) fluorophore

(Vector Laboratories, United States). Fe^{3+} was stained with 2 μM Ferrum 430™ (Ursa BioScience, United States) diluted in ethanol/H_2O 90/10 (%Vol/Vol) for 10 min. Samples were washed with ethanol/H_2O 90/10 (%Vol/Vol) and let air dry in darkness.

Filters and powdered rock samples were counterstained with Syto9 (Thermo Fisher Scientific, United States) as manufacturer recommended and covered with a mix of 1:4 Vectashield (Vector Laboratories, United States): Citifluor (Citifluor, United Kingdom). Filters were mounted onto glass slides and rock samples were mounted onto μ-slides 8-well glass bottom (Ibidi, Germany).

Samples were imaged with a confocal laser scanning microscope LSM710 coupled with an inverted microscope AxioObserver (Carl Zeiss, Jena, Germany) and equipped with diode (405 nm), argon (458/488/514 nm) and helium and neon (543 and 633 nm) lasers. Images were collected with 63×/1.4 oil immersion lens. Fiji software was used to project the stacks to 2D images (Schindelin et al., 2012).

Raman-FISH

CARD-FISH was performed in powdered rocks as described above for biofilm detection. However, samples were not immobilized in agarose or covered with antifade mounting medium to avoid any interference of either agarose and Vectashield:Citifluor mixture with Raman spectroscopy. Samples were mounted onto a glass Micro-Slide Field Finder, on which a rectangular-coordinate grid pattern was drawn (EMS, United Kingdom).

Rock samples were imaged using a confocal laser scanning microscope LSM710 as described above but coupled with a vertical microscope AxioObserver (Carl Zeiss, Jena, Germany). Images were collected with a 50×/1.4 air lens.

Once the cells were located in the coordinate system by CLSM, samples were analyzed by confocal Raman microscopy after bleaching the fluorophore as described in Huang et al. (2007). Raman analyses were performed by using a confocal Raman microscope Witec alpha-300RA (Witec, Germany). Raman spectra were obtained using a 532 nm excitation laser and a 100X/0.95 air objective lens. The incident laser power was 2 mW and the acquisition time for a single Raman spectrum was 3 s (1 pixel, 1 μm^2). A total of 23 Raman mappings were carried out in the different samples examined. Collected spectra were analyzed by using Witec Control Plus software (Witec, Germany). Comparison of Raman band intensities and Raman shifts between different Raman spectra were analyzed using Lorentzian peak curves to fit the Raman bands and the results represented by derived Raman image. In each Raman mapping, spectra were divided in two groups: *Acidovorax*+, which includes those spectra that present *Acidovorax* signal; and *Acidovorax*-, which includes those spectra that do not present *Acidovorax* signal. From each group, the average of the Ag/Eg values of the pyrite Raman bands as well as the average of the Ag and Eg Raman peaks shift values were calculated. As a result, paired data from each Raman mapping were obtained and represented in box plots. Additionally, Pearson's correlation coefficient (PCC) was calculated from Raman images by using the ImageJ software plugins JACoP (Just Another Colocalization Plugin) (Bolte and Cordeliers, 2006) and EzColocalization (Stauffer et al., 2018). ImageJ was also used to generate the 2D images (z-projections) from Raman image stacks.

RESULTS

Acidovorax Distribution Along BH10

CARD-FISH analysis was performed to determine the depths at which *Acidovorax* genus is present throughout the first 300 meters below surface (mbl) of the IPB column (**Figure 1**). These initial CARD-FISH experiments were performed on membrane filters in which the supernatant of the sonicated rock samples was filtered to detect the detached microorganisms from the rock samples. Members of the *Acidovorax* genus were detected at 10 of 14 depths analyzed (**Figure 1A**).

Raman-FISH on IPB Subsurface Samples

To analyze the *Acidovorax*-minerals interaction, CARD-FISH experiments were repeated, but directly on the powdered rock samples, at those depths where the microorganisms were detected in the initial screening (**Figure 2**). Attached *Acidovorax* were only found at 6 of the 10 depths where these microorganisms were previously observed (**Figure 1A**). Once the *Acidovorax* colonies were located in the rock samples by fluorescence microscopy, the same area could be analyzed by CRM using the slide coordinate system (**Figure 3**). Raman analyses were carried out by mapping different focal planes (z-stack) of each studied area, in which a single spectrum/μm^2 was acquired. As a result, for each analyzed area thousands of spectra were obtained that provided information on the structure and chemical composition of the sample in three dimensions with high spatial resolution.

All the spectra could be classified into three representative groups, named spectra 1, 2, and 3 (**Figures 4A,B**). Both spectra 1 and 2 (**Figure 4A**) showed the characteristic bands of the CH stretching bond of organic matter in the range 2,800–3,020 cm^{-1} (Lin-Vien et al., 1991; Maquelin et al., 2002; Czamara et al., 2015). However, unlike spectrum 2, spectrum 1 presented Raman bands representative of different organic compounds such as proteins at 1,014 cm^{-1} and 1,672 cm^{-1}, assigned to the presence of phenylalanine and to the amide I bond respectively (Ivleva et al., 2009; Rygula et al., 2013); and DNA and phospholipids at 1,092 cm^{-1}, assigned to the phosphate ester bonds (Ivleva et al., 2009; Dieing et al., 2011). On the contrary, spectrum 2 is characterized by the presence of bands in the range of 530–540 cm^{-1} as well as 1,160 cm^{-1}, which are representative of carbohydrates (Schuster et al., 2000; Ivleva et al., 2009; Wagner et al., 2009). Thus, we assigned spectrum 1 to the presence of microorganisms, in this case to members of the genus *Acidovorax* (previously identified by CARD-FISH) and spectrum 2 to polysaccharides. **Figure 5A** is a two-dimensional representation of the organic matter distribution in the analyzed area of a sample taken at 228.6 mbs, showing the presence of exopolysaccharides surrounding the cells.

On the other hand, spectrum 3 (**Figure 4B**) corresponds to the spectra of the mineral substrate to which the microorganisms

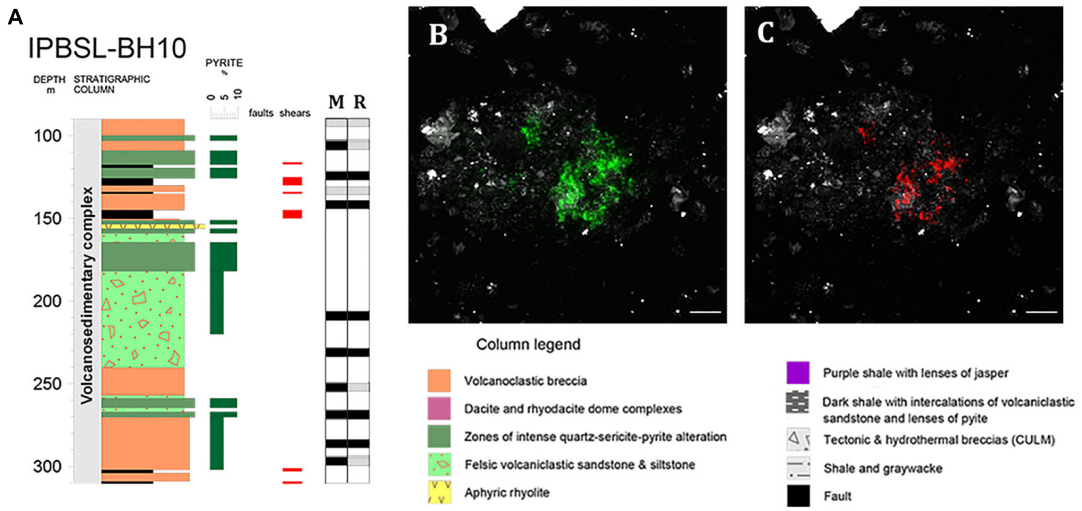

FIGURE 1 | *Acidovorax* genus in the IPB subsurface analyzed by CARD-FISH. **(A)** *Acidovorax* distribution along BH10 column. Black and gray squares indicate presence or absence of microorganisms at a determined depth respectively in membrane filters (M) and rocks (R). **(B,C)** *Acidovorax* sp. at 206.6 mbs. In green, Syto9 stain. In red, CARD-FISH signal. In gray, reflection. Scale bars, 5 μm.

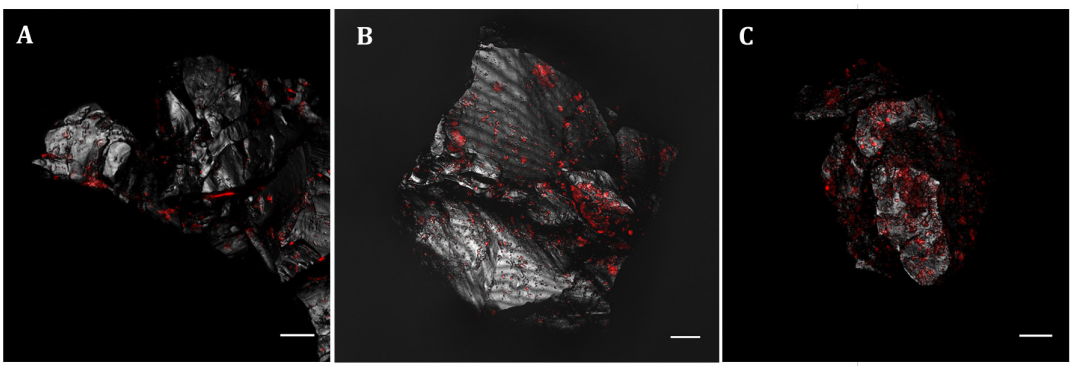

FIGURE 2 | *Acidovorax* genus members detected by CARD-FISH in IPB subsurface rock samples at –139.4 m **(A)**, –206.6 m **(B)** and –284 m **(C)**. In red, CARD-FISH signal. In gray, reflection. Scale bars, 10 μm.

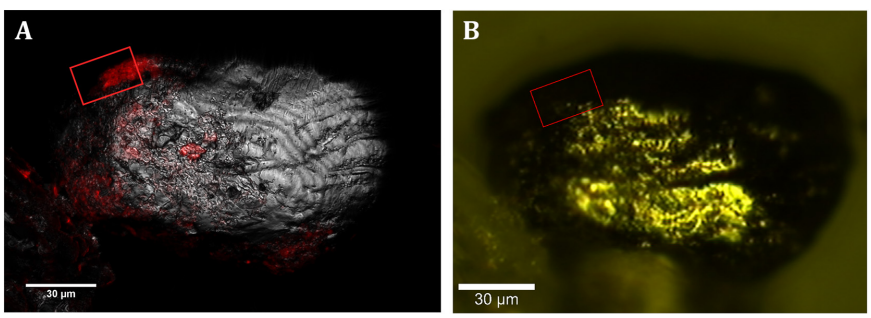

FIGURE 3 | CLSM and CRM correlation. **(A)** Localization of members of *Acidovorax* spp. (red) attached to a mineral particle (in gray, reflection) at –228.6 m by CARD-FISH/CLSM. **(B)** Same mineral particle located in the CRM. Area analyzed by CRM is indicated by a red square. Scale bars, 30 μm.

were found attached. Spectrum 3 shows two bands of high intensity at 347 and 384 cm^{-1} and a less intense band at 435 cm^{-1}, which are characteristic of the Raman-active modes of pyrite (Ushioda, 1972; Vogt et al., 1983; Bryant et al., 2018). The first corresponds to the S2 dumbbell libration (Eg), the second to the symmetric stretching of the S-S link in phase (Ag) and the

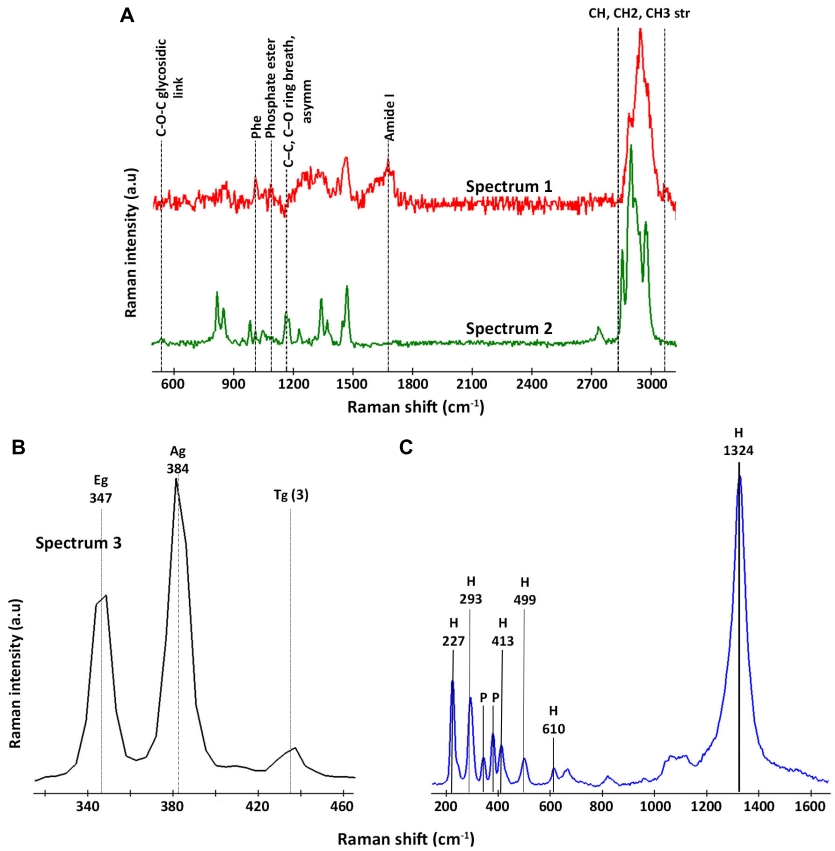

FIGURE 4 | Representative Raman spectra detected by CRM in areas where members of the genus *Acidovorax* were located by CARD-FISH. **(A)** Raman spectra assigned to organic matter: in red, spectrum 1/*Acidovorax*; in green, spectrum 2/polysaccharides. **(B)** Raman spectrum assigned to pyrite (spectrum 3); and **(C)** Raman spectrum assigned to hematite. The characteristic bands of each spectrum are indicated.

third to the coupling of the libration and stretch modes [Tg (3)] (Blanchard et al., 2005). 95% of the examined *Acidovorax* colonies were found attached to pyrite. Of the 20 analyzed areas, only one exception to pyrite was observed at 139.4 mbs, in which an *Acidovorax* colony was attached to a mineral that could not be identified by its Raman spectrum (**Supplementary Material 1**).

In some cases, in addition to pyrite, traces of hematite were detected in the analyzed area of the sample. The hematite Raman spectrum (**Figure 4C**) is easily recognizable due to the presence of bands at 227, 246, 293, 412, 498, 610 cm^{-1} and, above all, the strong band at 1,322 cm^{-1}, whose intensity varies with the intensity of the incident laser applied (De Faria et al., 1997; De Faria and Lopes, 2007).

Pyrite Spectra Variability

Pyrite Raman spectra vary from one sample to another and, interestingly, even within the same analyzed area its spectrum is not homogeneous. Variations at micrometer scale at the relative intensity of the Eg and Ag bands in the range of 0.8 ± 0.1–2.4 ± 0.2 (**Figures 5B,C**, **6B,E**) were observed in individual pyrite grains, showing a mean value of 1.5 ± 0.2. In addition, changes in the pyrite bands positions up to 9 cm^{-1} (**Figures 5D,E**) were detected in the analyzed area of the pyrite grains, with mean values of 347.8 ± 0.8 and 383.9 ± 0.6 for Eg and Ag bands respectively.

To determine if there is any relationship between the occurrence of *Acidovorax* and the relative intensity of the pyrite Eg and Ag Raman bands or their position displacement, the variations of both parameters were analyzed in the presence or absence of the microorganism in each of the mappings performed.

As shown in **Figures 6**, **7A**, it is clearly observed that there is an association between the location of *Acidovorax* and the low values of the relative intensities Ag/Eg of the pyrite spectra. In the presence of *Acidovorax*, the average of Ag/Eg ratio is 1.3 ± 0.1, while in the absence of *Acidovorax*, this value amounts to 1.6 ± 0.3. Statistics analysis corroborates the inverse correlation between *Acidovorax* Raman signal and the ratio Ag/Eg values of pyrite Raman spectra (PCC = −0.384 ± 0.111).

Regarding the Raman displacement of the Ag and Eg bands, the minimum difference in the average position of both bands in the presence and absence of the microorganism indicates that there is no correlation between the location of *Acidovorax* and this displacement (**Figures 7B,C**). Both in the presence and in the absence of *Acidovorax*, the positions of the Ag and Eg bands were 347.8 ± 0.8 and 383.9 ± 0.6 respectively.

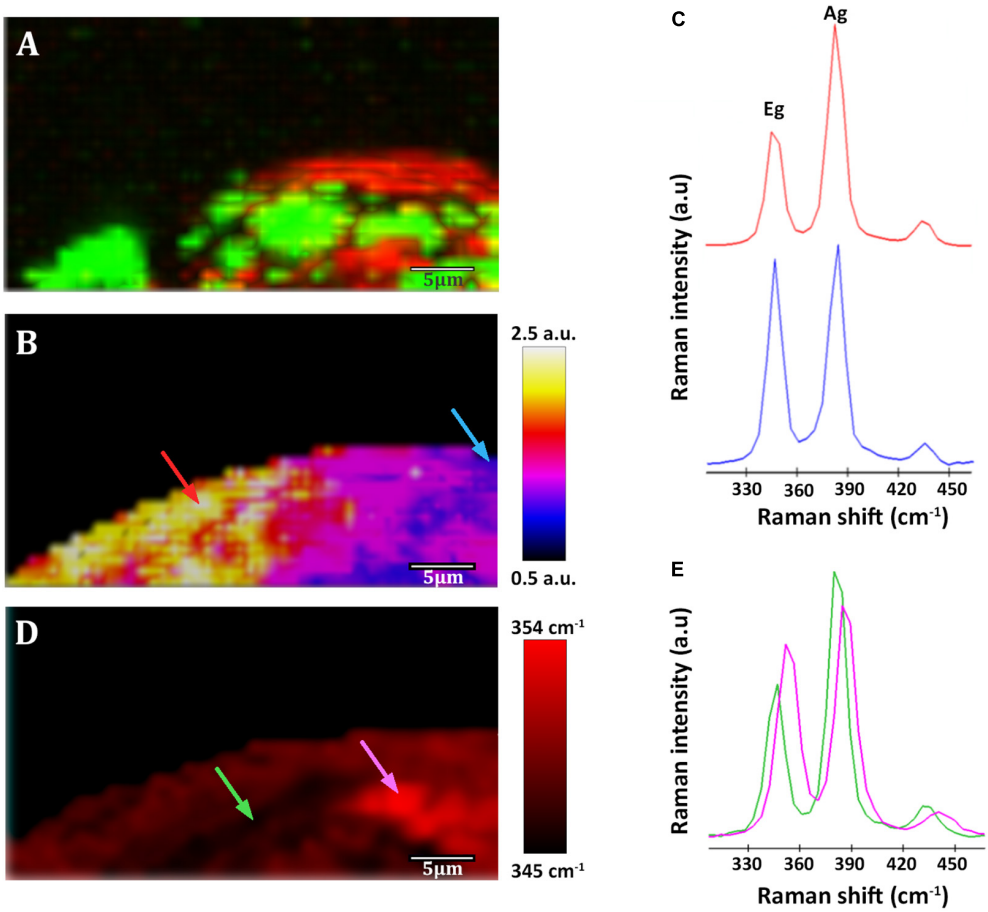

FIGURE 5 | Raman images of a native sample from –228.6 m of the IPB subsurface (see **Figure 3**). **(A)** Raman map of organic matter. In red, distribution of *Acidovorax*. In green, distribution of polysaccharides. **(B)** Raman map colored according to the Ag/Eg ratio intensity of pyrite spectra. **(C)** Pyrite Raman spectra corresponding to the arrows marked with blue and red color in the image shown in panel **(B)**. **(D)** Map showing the Raman shift corresponding to the pyrite Eg band in a color code. **(E)** Pyrite Raman spectra corresponding to the arrows marked with green and pink in the image shown in panel **(D)**. Scale bar, 5 µm.

Acidovorax Biofilms Detection

Fluorescence Lectin Binding Assay (FLBA) was carried out to determine if *Acidovorax* colonies are included in biofilms as CRM suggest. FLBA confirmed that most *Acidovorax* colonies attached to the rock samples are surrounded by exopolysaccharides (**Figure 8**), which explain their detection by CRM in some analyzed areas (in **Figures 5A**, **6D**). This observation corroborates the data presented in Escudero et al. (2018b), which indicated that biofilm formation is a common lifestyle of the rock attached microorganisms inhabiting the IPB subsurface. In addition, the use of a fluorescent iron sensor revealed that *Acidovorax* cells are surrounded by ferric iron (**Figure 8**).

DISCUSSION

Both the distribution and the microorganism-mineral relationship of *Acidovorax* genus in the IPB subsurface, a geological formation considered one of the largest massive sulfide deposits in the world (Tornos, 2006), have been analyzed in this work. *Acidovorax* was chosen for being one of the most abundant iron oxidizer microorganisms detected in the IPBSL (Amils et al., under review), a drilling project devoted to the study of the underground bioreactor responsible for the peculiarities of Río Tinto (Amils et al., 2013). Our CARD-FISH results indicated that, indeed, *Acidovorax* is a genus with a high distribution along the BH10 column (**Figure 1A**). This data together with the observation of a high distribution of *Acidovorax* in the MARTE project (Puente-Sánchez et al., 2014), performed also in the IPB subsurface, strongly suggest that this genus must play an important role in the iron and nitrogen cycles of this ecosystem.

To determine if there is any relation between the distribution of *Acidovorax* and the IPB subsurface mineralogy throughout BH10, we used Raman-FISH technique. Fluorescence microscopy allows a specific microorganism to be identified by using specific probes (Amann et al., 1995) while confocal Raman microscopy analyses the composition and molecular structure of the mineral substrate (Smith and Dent, 2013). Thus, while FISH provided the specific location of *Acidovorax* genus

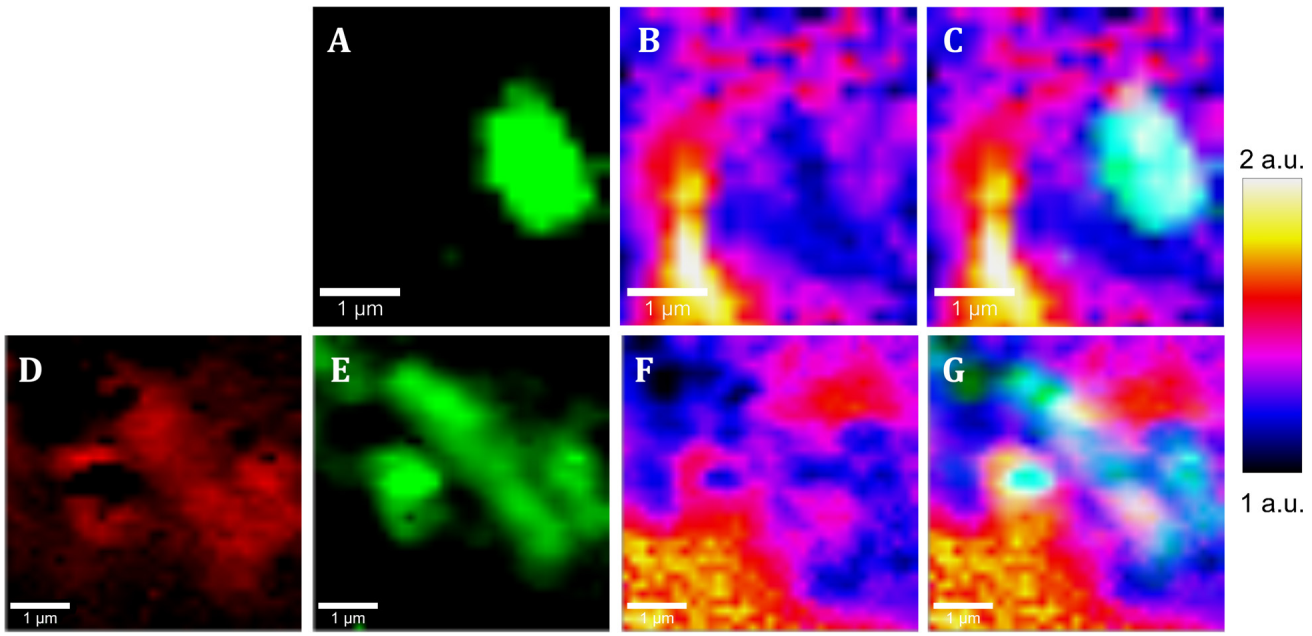

FIGURE 6 | Raman images of native samples from the IPB subsurface at –139.4 m **(A–C)** and –206.6 m **(D–G)** showing the co-localization of cells and pyrite areas with low intensity ratio of Ag band relative to Eg band. **(A,E)** Raman map of *Acidovorax* (green). **(E)** Raman map of exopolysaccharides (red), **(B,E)** Raman map colored according to the Ag/Eg ratio intensity of pyrite spectra. **(C,G)** merge. Scale bar, 1 µm.

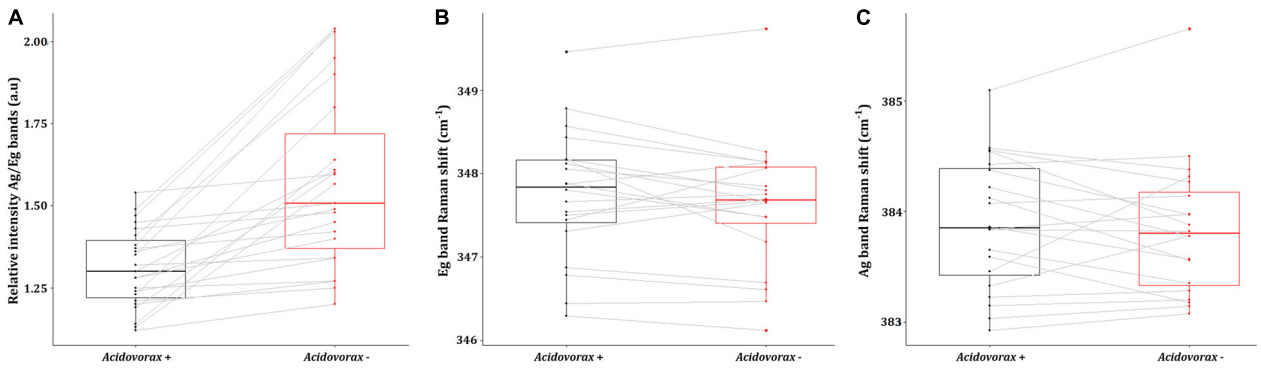

FIGURE 7 | Average values of the intensity ratio of the Ag band relative to Eg band **(A)**, the Eg band Raman shift **(B)** and the Ag band Raman shift **(C)** of pyrite Raman spectra in presence (red) or absence (black) of *Acidovorax* resulting from Raman analysis of the IPB subsurface native samples.

members, the mineral to which it is attached was identified by means of Raman spectroscopy. To perform Raman-FISH assay, CARD-FISH was carried out directly on the powdered rock samples (**Figures 2**, **3**). However, unlike the CARD-FISH performed on filter membranes, *Acidovorax* was only observed at 6 depths. This decrease may be due either to the heterogeneity of the sample, thus we could never analyze exactly the same sample even if it came from the same depth; or to the different protocol that has been applied to the sample depending on whether CARD-FISH is carried out on the membrane or directly on the solid substrate. In the first case, the microorganisms observed are those that have been detached from the rock by sonication while in the second case the microorganisms detected are those that remain attached after rock grinding. In addition, because the agarose interference is to be avoided in the Raman analyses, the rock samples were not immobilized. Thus, the microorganisms could have been detached from the rock surface during the different washes and treatments carried out throughout the CARD-FISH protocol. Consequently, the number of microorganisms remaining attached could be lower in agarose-free than in immobilized rocks, as well as the probability of detecting *Acidovorax* in a given depth when Raman-FISH protocol was applied.

All the detected *Acidovorax* colonies, but one at 139, 4 mbs, were attached to pyrite in each of the analyzed samples despite the array of different minerals detected along the column (**Figure 1A** and **Supplementary Material 2**). This data strongly suggests that the distribution of members of this genus in the system is

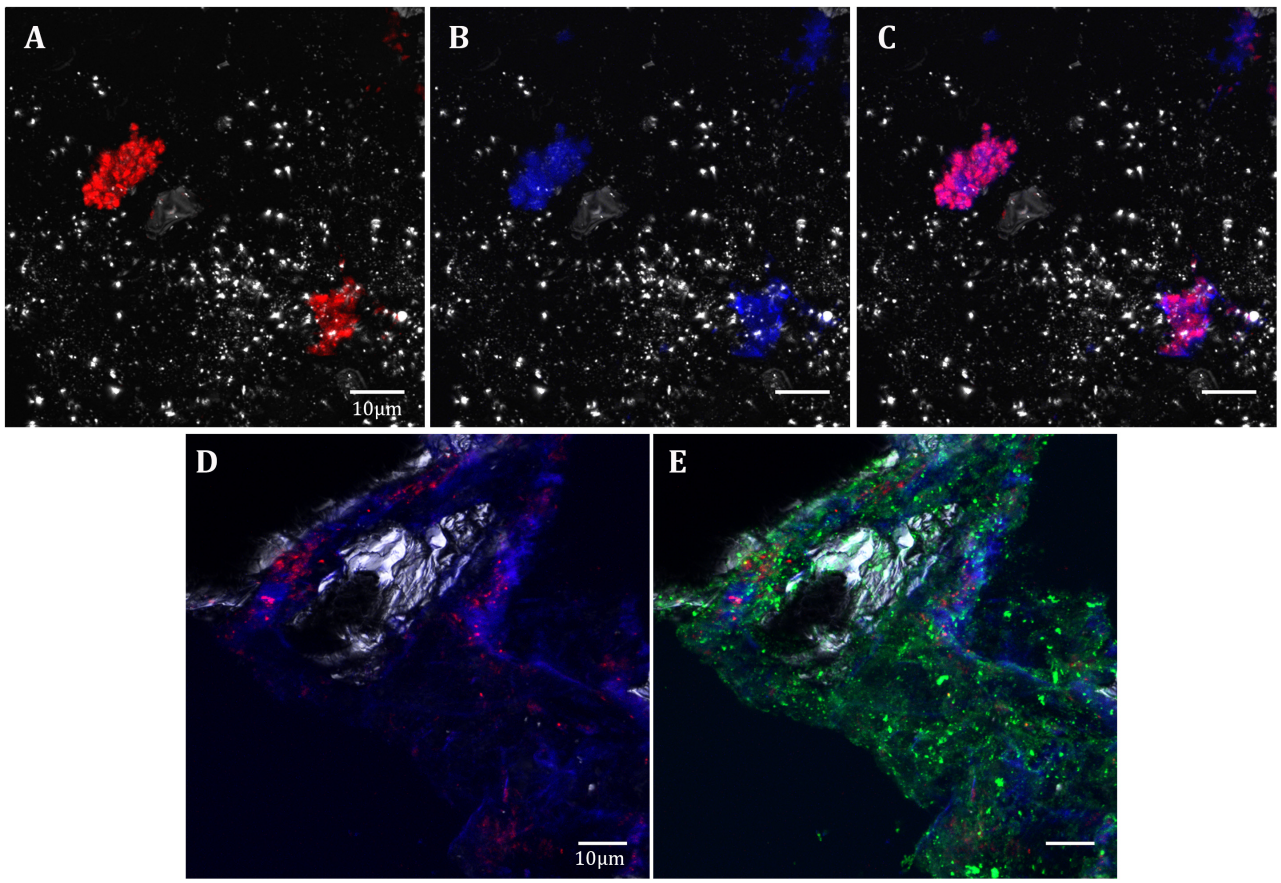

FIGURE 8 | *Acidovorax*-Fe^{3+}-EPS co-localization in the IPB subsurface. DOPE-FISH with *Acidovorax* probe (red) at 414.8 mbs **(A–C)** and at 139.4 mbs **(D,E)**; In blue, Fe^{3+} signal. In green, ConA lectin signal. In gray, reflection. Scale bars 10 μm.

related to the presence of this iron sulfide along the column. Members of the genus *Acidovorax* are nitrate reducers which are able to oxidize iron. These microorganisms were originally described as mixotrophs, capable of using iron as electron donor and acetate as carbon source (Straub et al., 2004; Kappler et al., 2005). However, the presence of iron is not essential for microorganism growth (Muehe et al., 2009; Chakraborty et al., 2011) and no proteins related with iron oxidation were detected in *Acidovorax* (Carlson et al., 2013). Thus, it was proposed that Fe^{2+} is most likely indirectly oxidized by these microorganisms through the reactive nitrogen species produced during the denitrification process (Picardal, 2012; Klueglein and Kappler, 2013; Klueglein et al., 2015). Even so, enzymatic oxidation of iron has not been ruled out and both processes, biotic and abiotic, are accepted today (Carlson et al., 2013; Schaedler et al., 2018). *Acidovorax* colonies in the IPB subsurface can be found surrounded by ferric iron (**Figure 8**), indicating that it was oxidized by the microorganism. Due to the ability of *Acidovorax* to indirectly oxidize iron, the possibility that the ferric iron produced could oxidize pyrite (Vera et al., 2013) even at neutral pH (Moses et al., 1987; Moses and Herman, 1991) cannot be discarded. Actually, detected Fe^{3+} by fluorescence microscopy was mostly co-localized with exopolysaccharides (**Figure 8B**), which are commonly responsible for metal ions binding and are essential to enhance the biooxidation of metallic sulfides (Sand and Gehrke, 2006). Such a reaction could result in the dissolution of the mineral and the liberation of sulfur compounds and ferrous iron, which may be seized by the microorganism as an electron donor, a nutrient or a detoxifying agent as suggested by Klueglein and Kappler (2013) and Carlson et al. (2013) respectively. Indeed, it has been shown that *Acidovorax* growth is improved by the presence of ferrous iron (Chakraborty et al., 2011). Therefore, the attachment of *Acidovorax* to pyrite and its subsequent dissolution could be an advantage for the microorganism in this oligotrophic environment. The detection of hematite, a ferric iron oxide whose appearance was observed after the dissolution of pyrite as a secondary mineral (Caldeira et al., 2003), in some of the analyzed samples, would support this hypothesis.

Pyrite dissolution by denitrifying microorganisms has been of interest for the past few decades due to its environmental interest (Postma et al., 1991; Schwientek et al., 2008; Zhang et al., 2009) and several studies support that pyrite can be used as electron donor by denitrifying chemolithotropic microorganisms (Jørgensen et al., 2009; Torrentó et al., 2010, 2011; Bosch et al., 2012; Vaclavkova et al., 2015). Nevertheless, preliminary studies

showed that *Acidovorax* BoFeN1 is not capable of dissolving pyrite or, at least, does not produce sulfate increment into the medium when it grows in the presence of this mineral (Yan et al., 2019). It should be noted, however, that other sulfur species such as thiosulfate or tetrathionate, which are more stable at neutral pH, may have been released into the medium instead of sulfate (Moses et al., 1987; Moses and Herman, 1991). Thus, more in depth analysis would be needed to unequivocally demonstrate whether *Acidovorax* is able to biooxidize pyrite.

In our Raman analysis, variations related with the displacement and the relative intensity of the Eg and Ag bands in the Raman spectrum of native subsurface pyrite were observed at micrometer scale (**Figures 5B–E**, **6B,E**). Actually, despite the absence of relation between the location of *Acidovorax* and the displacement of Raman pyrite bands (**Figures 7B,C**), our data indicate that there is a correlation between the location of *Acidovorax* and the low values of the relative intensity Ag/Eg of the pyrite spectra (**Figures 6**, **7A**).

Unfortunately, as far as we know, there is no data available about spatially resolved surface characterization of pyrite by CRM with which to contrast our results. All measurements made up to now were carried out with macroscopic techniques which provide only averaged pyrite spectra of a relatively large area (Bryant et al., 2018 and references therein). Still, the causes that may explain the differences in the pyrite Raman spectra observed between different studies has been analyzed in depth by Bryant et al. (2018). On the one hand, the displacement of the position of the pyrite bands toward lower wavelengths has been attributed either to an effect of laser heating or to the presence of trace elements such as copper, zinc or lead among others (Bryant et al., 2018). While in the latter case the variation of the position of the bands is minimal (up to $\sim$ 1 cm^{-1}), downshifting of the pyrite bands up to 12.7 cm^{-1} due to the laser heating has been reported (Bryant et al., 2018). However, these extreme variations in bands position have only been detected by modifying the laser power in the analysis of pyrite of a grain size below 10 μm. In our analysis, in which a constant low laser power was used, variations up to 9 cm^{-1} in the position of the pyrite were detected (**Figures 5D,E**). Hence, the observed Raman shifts in the pyrite grains analyzed in this work cannot be attributed to laser heating and further analysis are necessary to understand this phenomenon.

On the other hand, changes in the relative intensity of the Eg and Ag bands have been attributed to the crystalline orientation of pyrite with respect to the polarization plane of the incident laser, which, in addition, may be affected by the laser power. Bryant and collaborators showed variations in the range of 0.22–1.3 in centimeter scale cubic pyrite while in pyritohedral pyrite (12 faces) they varied from 0.81 to 2.01 due to the differential excitation of the bands of the diverse analyzed pyrite faces. In fact, the mean value of the intensity ratio Eg/Ag band varies from 0.9 to 3.5 in studies in which pyrite of varied sizes and morphologies were analyzed using a range of laser powers (Bryant et al., 2018 and references therein). Accordingly, the microscale variations of the intensity ratio Ag/Eg observed in our study (**Figures 5B,C**, **6B,E**) could be due to the fact that the analyzed pyrite particles present a polycrystalline structure. Thus, different faces could have been mapped in the same Raman analysis. Accordingly, the low value Eg/Ag preference by the microorganism could indicate that *Acidovorax* is attached preferentially to those faces of pyrite in which the band Eg, which represents the S2 dumbbell vibration of the pyrite structure, shows a greater intensity (**Figure 6**). However, the possibility that *Acidovorax*, in some way, could affect the pyrite structure should not be ruled out and we would like to clarify this interesting point in the future.

CONCLUSION

Since rocks are the matrix in which microorganisms live in subsurface, it is feasible to assume that their composition might influence the microbial distribution in this environment. Our Raman-FISH results suggest a strong relationship between the distribution of *Acidovorax* and pyrite, which may be explained by the microorganism's metabolic preference for pyrite. In addition, heterogeneity in uncolonized vs. *Acidovorax*-associated pyrite Raman spectra was observed. One possible explanation for this observation is the modification of the pyrite by *Acidovorax*. However, the lack of information about a possible biological alteration in pyrite Raman spectrum at the micrometer scale makes the interpretation of these results difficult. Thus additional experiments are needed to analyze any advantages to *Acidovorax* growing in the presence of pyrite or dissolution of the mineral carried out by the microorganism with the possible fingerprints resulting from their interaction. Nevertheless, correlative fluorescence and confocal Raman microscopy has been shown to be a useful method with which to analyze, *in situ*, the mineral dependent distribution of the subsurface biodiversity.

DATA AVAILABILITY STATEMENT

The raw data supporting the conclusions of this article will be made available by the authors, without undue reservation.

AUTHOR CONTRIBUTIONS

CE wrote the manuscript. CE and RA designed the study and interpreted the results. CE and JM carried out the fluorescence *in situ* hybridizations and fluorescence microscopy observations. AC performed confocal Raman microscopy analyses. CE, AC, CS, JA, and RA interpreted the Raman part of the study. RA, AC, CS, JA, JM, and FG corrected the manuscript. All authors contributed to the article and approved the submitted version.

FUNDING

The authors acknowledge financial support from the Spanish AEI, Project MDM-2017-0737 Unidad de Excelencia "María de Maeztu"- Centro de Astrobiología (INTA-CSIC), the Spanish MINECO, Project

MAT2017-86450-C4-1-R and the Spanish MICINN, Projects PID2019-104812GB-I00 and RTI2018-099794-B-I00.

ACKNOWLEDGMENTS

We thank the support of the Servicio de Microscopía Óptica Confocal (SMOC) at Centro de Biología Molecular Severo Ochoa and R.S.A's help reviewing the English language of the manuscript. The content of this manuscript has been published as part of the thesis of Escudero (2018).

SUPPLEMENTARY MATERIAL

The Supplementary Material for this article can be found online at: https://www.frontiersin.org/articles/10.3389/fmicb.2020.572104/full#supplementary-material

REFERENCES

Amann, R., Ludwig, W., Schulze, R., Spring, S., Moore, E., and Schleifer, K.-H. (1996). rRNA-targeted oligonucleotide probes for the identification of genuine and former pseudomonads. *Syst. Appl. Microbiol.* 19, 501–509. doi: 10.1016/S0723-2020(96)80023-3

Amann, R. I., Ludwig, W., and Schleifer, K.-H. (1995). Phylogenetic identification and in situ detection of individual microbial cells without cultivation. *Microbiol. Rev.* 59, 143–169. doi: 10.1128/mmbr.59.1.143-169.1995

Amils, R., Fernández-Remolar, D., Parro, V., Rodríguez-Manfredi, J. A., Timmis, K., Oggerin, M., et al. (2013). Iberian Pyrite Belt Subsurface Life (IPBSL), a drilling project of biohydrometallurgical interest. *Adv. Mater. Res.* 825, 15–18. doi: 10.4028/www.scientific.net/amr.825.15

Amils, R., González-Toril, E., Fernández-Remolar, D., Gómez, F., Rodríguez, N., and Durán, C. (2002). Interaction of the sulfur and iron cycles in the Tinto River ecosystem. *Rev. Environ. Sci. Biotechnol.* 1, 299–309. doi: 10.1023/A:1023232002312

Blanchard, M., Alfredsson, M., Brodholt, J., Price, G. D., Wright, K., and Catlow, C. R. A. (2005). Electronic structure study of the high-pressure vibrational spectrum of FeS2 pyrite. *J. Phys. Chem. B* 109, 22067–22073.

Bolte, S., and Cordeliers, F. (2006). A guided tour into subcellular colocalization analysis in light miocrscopy. *J. Micros.* 224, 213–232. doi: 10.1111/j.1365-2818.2006.01706.x

Bosch, J., Lee, K.-Y., Jordan, G., Kim, K.-W., and Meckenstock, R. U. (2012). Anaerobic, nitrate-dependent oxidation of pyrite nanoparticles by Thiobacillus denitrificans. *Environ. Sci. Technol.* 46, 2095–2101. doi: 10.1021/es2022329

Bryant, R. N., Pasteris, J. D., and Fike, D. A. (2018). Variability in the raman spectrum of unpolished growth and fracture surfaces of pyrite due to laser heating and crystal orientation. *Appl. Spectros.* 72, 37–47. doi: 10.1177/0003702817736516

Caldeira, C., Ciminelli, V., Dias, A., and Osseo-Asare, K. (2003). Pyrite oxidation in alkaline solutions: nature of the product layer. *Int. J. Min. Process.* 72, 373–386. doi: 10.1016/S0301-7516(03)00112-1

Carlson, H. K., Clark, I. C., Blazewicz, S. J., Iavarone, A. T., and Coates, J. D. (2013). Fe (II) oxidation is an innate capability of nitrate-reducing bacteria that involves abiotic and biotic reactions. *J.Bacteriol.* 195, 3260–3268. doi: 10.1128/JB.00058-13

Casar, C. P., Kruger, B. R., Flynn, T. M., Masterson, A. L., Momper, L. M., and Osburn, M. R. (2020). Mineral-hosted biofilm communities in the continental deep subsurface, Deep Mine Microbial Observatory, SD, USA. *Geobiology* 18, 508-522. doi: 10.1111/gbi.12391

Chakraborty, A., and Picardal, F. (2013). Induction of nitrate-dependent Fe (II) oxidation by Fe (II) in Dechloromonas sp. *strain UWNR*4 and Acidovorax sp. strain 2AN. *Appl. Environ. Microbiol.* 79, 748–752. doi: 10.1128/AEM.02709-12

Chakraborty, A., Roden, E. E., Schieber, J., and Picardal, F. (2011). Enhanced growth of Acidovorax sp. *strain* 2AN during nitrate-dependent Fe (II) oxidation in batch and continuous-flow systems. *Appl. Environ. Microbiol.* 77, 8548–8556. doi: 10.1128/AEM.06214-11

Chapelle, F. H., O'neill, K., Bradley, P. M., Methé, B. A., Ciufo, S. A., Knobel, L. L., et al. (2002). A hydrogen-based subsurface microbial community dominated by methanogens. *Nature* 415, 312–315. doi: 10.1038/415312a

Czamara, K., Majzner, K., Pacia, M. Z., Kochan, K., Kaczor, A., and Baranska, M. (2015). Raman spectroscopy of lipids: a review. *J. Raman Spectros.* 46, 4–20. doi: 10.1002/jrs.4607

De Faria, D., and Lopes, F. (2007). Heated goethite and natural hematite: can Raman spectroscopy be used to differentiate them? *Vib. Spectros.* 45, 117–121. doi: 10.1016/j.vibspec.2007.07.003

De Faria, D., Venâncio Silva, S., and De Oliveira, M. (1997). Raman microspectroscopy of some iron oxides and oxyhydroxides. *J. Raman Spectros.* 28, 873–878. doi: 10.1002/(sici)1097-4555(199711)28:11<873::aid-jrs177>3.0.co;2-b

Dieing, T., Hollricher, O., and Toporski, J. (2011). *Confocal Raman Microscopy*. Berlin: Springer-Verlag.

Escudero, C., Oggerin, M., and Amils, R. (2018a). The deep continental subsurface: the dark biosphere. *Int. Microbiol.* 21, 3–14. doi: 10.1007/s10123-018-0009-y

Escudero, C., Vera, M., Oggerin, M., and Amils, R. (2018b). Active microbial biofilms in deep poor porous continental subsurface rocks. *Sci. Rep.* 8:1538. doi: 10.1038/s41598-018-19903-z

Fernández-Remolar, D. C., Gómez, F., Prieto-Ballesteros, O., Schelble, R. T., Rodríguez, N., and Amils, R. (2008a). Some ecological mechanisms to generate habitability in planetary subsurface areas by chemolithotrophic communities: the Río Tinto subsurface ecosystem as a model system. *Astrobiology* 8, 157–173. doi: 10.1089/ast.2006.0022

Fernández-Remolar, D. C., Prieto-Ballesteros, O., Rodríguez, N., Gómez, F., Amils, R., Gómez-Elvira, J., et al. (2008b). Underground habitats in the Río Tinto basin: a model for subsurface life habitats on Mars. *Astrobiology* 8, 1023–1047. doi: 10.1089/ast.2006.0104

Huang, W. E., Stoecker, K., Griffiths, R., Newbold, L., Daims, H., Whiteley, A. S., et al. (2007). Raman-FISH: combining stable-isotope Raman spectroscopy and fluorescence in situ hybridization for the single cell analysis of identity and function. *Environ. Microbiol.* 9, 1878–1889. doi: 10.1111/j.1462-2920.2007.01352.x

Ivleva, N. P., Wagner, M., Horn, H., Niessner, R., and Haisch, C. (2009). Towards a nondestructive chemical characterization of biofilm matrix by Raman microscopy. *Anal. Bioanal. Chem.* 393, 197–206. doi: 10.1007/s00216-008-2470-5

Jones, A. A., and Bennett, P. C. (2014). Mineral microniches control the diversity of subsurface microbial populations. *Geomicrobiol. J.* 31, 246–261. doi: 10.1080/01490451.2013.809174

Jones, A. A., and Bennett, P. C. (2017). Mineral Ecology: surface specific colonization and geochemical drivers of biofilm accumulation, composition, and phylogeny. *Front. Microbiol.* 8:491. doi: 10.3389/fmicb.2017.00491

Jørgensen, C., Jacobsen, O. S., Elberling, B., and Aamand, J. (2009). Microbial oxidation of pyrite coupled to nitrate reduction in anoxic groundwater sediment. *Environ. Sci. Technol.* 43, 4851–4857. doi: 10.1021/es803417s

Kappler, A., Schink, B., and Newman, D. K. (2005). Fe (III) mineral formation and cell encrustation by the nitrate-dependent Fe (II)-oxidizer strain BoFeN1. *Geobiology* 3, 235–245. doi: 10.1111/j.1472-4669.2006.00056.x

Kieft, T. L. (2016). *"Microbiology of the Deep Continental Biosphere," in Their World: A Diversity of Microbial Environments*. Berlin: Springer, 225–249.

Klueglein, N., and Kappler, A. (2013). Abiotic oxidation of Fe (II) by reactive nitrogen species in cultures of the nitrate-reducing Fe (II) oxidizer Acidovorax sp. BoFeN1–questioning the existence of enzymatic Fe (II) oxidation. *Geobiology* 11, 180–190. doi: 10.1111/gbi.12019

Klueglein, N., Picardal, F., Zedda, M., Zwiener, C., and Kappler, A. (2015). Oxidation of Fe (II)-EDTA by nitrite and by two nitrate-reducing Fe (II)-oxidizing Acidovorax strains. *Geobiology* 13, 198–207. doi: 10.1111/gbi.12125

Lin-Vien, D., Colthup, N. B., Fateley, W. G., and Grasselli, J. G. (1991). *The Handbook of Infrared and Raman Characteristic Frequencies of Organic Molecules*. Amsterdam: Elsevier.

Magnabosco, C., Lin, L. H., Dong, H., Bomberg, M., Ghiorse, W., Stan-Lotter, H., et al. (2018). The biomass and biodiversity of the continental subsurface. *Nat. Geosci.* 11, 707–717. doi: 10.1038/s41561-018-0221-6

Maquelin, K., Kirschner, C., Choo-Smith, L.-P., van den Braak, N., Endtz, H. P., Naumann, D., et al. (2002). Identification of medically relevant microorganisms by vibrational spectroscopy. *J. Microbiol. Methods* 51, 255–271. doi: 10.1016/S0167-7012(02)00127-6

Mayhew, L., Ellison, E., McCollom, T., Trainor, T., and Templeton, A. (2013). Hydrogen generation from low-temperature water–rock reactions. *Nat. Geosci.* 6, 478–484. doi: 10.1038/ngeo1825

Moses, C. O., and Herman, J. S. (1991). Pyrite oxidation at circumneutral pH. *Geochim. Cosmochim. Acta* 55, 471–482. doi: 10.1016/0016-7037(91)90005-P

Moses, C. O., Nordstrom, D. K., Herman, J. S., and Mills, A. L. (1987). Aqueous pyrite oxidation by dissolved oxygen and by ferric iron. *Geochim. Cosmochim. Acta* 51, 1561–1571. doi: 10.1016/0016-7037(87)90337-1

Moter, A., and Göbel, U. B. (2000). Fluorescence in situ hybridization (FISH) for direct visualization of microorganisms. *J. Microbiol. Methods* 41, 85–112. doi: 10.1016/S0167-7012(00)00152-4

Muehe, E. M., Gerhardt, S., Schink, B., and Kappler, A. (2009). Ecophysiology and the energetic benefit of mixotrophic Fe (II) oxidation by various strains of nitratereducing bacteria. *FEMS Microbiol. Ecol.* 70, 335–343. doi: 10.1111/j.1574-6941.2009.00755.x

Pedersen, K. (1997). Microbial life in deep granitic rock. *FEMS Microbiol. Rev.* 20, 399–414. doi: 10.1111/j.1574-6976.1997.tb00325.x

Picardal, F. (2012). Abiotic and microbial interactions during anaerobic transformations of Fe (II) and NOx. *Front. Microbiol.* 3:112. doi: 10.3389/fmicb.2012.00112

Postma, D., Boesen, C., Kristiansen, H., and Larsen, F. (1991). Nitrate reduction in an unconfined sandy aquifer: water chemistry, reduction processes, and geochemical modeling. *Water Resour. Res.* 27, 2027–2045. doi: 10.1029/91WR00989

Puente-Sánchez, F., Arce-Rodríguez, A., Oggerin, M., García-Villadangos, M., Moreno-Paz, M., Blanco, Y., et al. (2018). Viable cyanobacteria in the deep continental subsurface. *Proc. Natl. Acad. Sci. U.S.A.* 115, 10702–10707. doi: 10.1073/pnas.1808176115

Puente-Sánchez, F., Moreno-Paz, M., Rivas, L., Cruz-Gil, P., García-Villadangos, M., Gómez, M., et al. (2014). Deep subsurface sulfate reduction and methanogenesis in the Iberian Pyrite Belt revealed through geochemistry and molecular biomarkers. *Geobiology* 12, 34–47. doi: 10.1111/gbi.12065

Rempfert, K. R., Miller, H. M., Bompard, N., Nothaft, D., Matter, J. M., Kelemen, P., et al. (2017). Geological and geochemical controls on subsurface microbial life in the Samail Ophiolite, Oman. *Front. Microbiol.* 8:56. doi: 10.3389/fmicb.2017.00056

Rygula, A., Majzner, K., Marzec, K. M., Kaczor, A., Pilarczyk, M., and Baranska, M. (2013). Raman spectroscopy of proteins: a review. *J. Raman Spectros.* 44, 1061–1076. doi: 10.1002/jrs.4335

Sand, W., and Gehrke, T. (2006). Extracellular polymeric substances mediate bioleaching/biocorrosion via interfacial processes involving iron (III) ions and acidophilic bacteria. *Res. Microbiol.* 157, 49–56. doi: 10.1016/j.resmic.2005.07.012

Schaedler, F., Lockwood, C., Lueder, U., Glombitza, C., Kappler, A., and Schmidt, C. (2018). Microbially mediated coupling of Fe and N cycles by nitrate-reducing Fe (II)-oxidizing bacteria in littoral freshwater sediments. *Appl. Environ. Microbiol.* 84, e02013–e02017.

Schindelin, J., Arganda-Carreras, I., Frise, E., Kaynig, V., Longair, M., Pietzsch, T., et al. (2012). Fiji: an open-source platform for biological-image analysis. *Nat. Methods* 9, 676–682. doi: 10.1038/nmeth.2019

Schrenk, M. O., Brazelton, W. J., and Lang, S. Q. (2013). Serpentinization, carbon, and deep life. *Rev. Mineral. Geochem.* 75, 575–606. doi: 10.1515/9781501508318-020

Schulze, R., Spring, S., Amann, R., Huber, I., Ludwig, W., Schleifer, K.-H., et al. (1999). Genotypic diversity of Acidovorax strains isolated from activated sludge and description of Acidovorax defluvii sp. *nov. Syst. Appl. Microbiol.* 22, 205–214. doi: 10.1016/S0723-2020(99)80067-8

Schuster, K. C., Reese, I., Urlaub, E., Gapes, J. R., and Lendl, B. (2000). Multidimensional information on the chemical composition of single bacterial cells by confocal Raman microspectroscopy. *Anal. Chem.* 72, 5529–5534. doi: 10.1021/ac000718x

Schwientek, M., Einsiedl, F., Stichler, W., Stögbauer, A., Strauss, H., and Maloszewski, P. (2008). Evidence for denitrification regulated by pyrite oxidation in a heterogeneous porous groundwater system. *Chem. Geol.* 255, 60–67. doi: 10.1016/j.chemgeo.2008.06.005

Smith, E., and Dent, G. (2013). *Modern Raman Spectroscopy: A Practical Approach*. Hoboken, NJ: John Wiley & Sons.

Stauffer, W., Sheng, H., and Lim, H. (2018). EzColocalization: an ImageJ plugin for visualizing and measuring colocalization in cells and organisms. *Sci. Rep.* 8:15764. doi: 10.1038/s41598-018-33592-8

Stevens, T. O., and McKinley, J. P. (2000). Abiotic controls on H2 production from basalt-water reactions and implications for Aquifer Biogeochemistry. *Environ. Sci. Technol.* 34, 826–831. doi: 10.1021/es990583g

Straub, K. L., Schönhuber, W. A., Buchholz-Cleven, B. E., and Schink, B. (2004). Diversity of ferrous iron-oxidizing, nitrate-reducing bacteria and their involvement in oxygen-independent iron cycling. *Geomicrobiol. J.* 21, 371–378. doi: 10.1080/01490450490485854

Tornos, F. (2006). Environment of formation and styles of volcanogenic massive sulfides: the Iberian Pyrite belt. *Ore Geol. Rev.* 28, 259–307. doi: 10.1016/j.oregeorev.2004.12.005

Torrentó, C., Cama, J., Urmeneta, J., Otero, N., and Soler, A. (2010). Denitrification of groundwater with pyrite and Thiobacillus denitrificans. *Chem. Geol.* 278, 80–91. doi: 10.1016/j.chemgeo.2010.09.003

Torrentó, C., Urmeneta, J., Otero, N., Soler, A., Viñas, M., and Cama, J. (2011). Enhanced denitrification in groundwater and sediments from a nitrate-contaminated aquifer after addition of pyrite. *Chem. Geol.* 287, 90–101. doi: 10.1016/j.chemgeo.2011.06.002

Ushioda, S. (1972). Raman scattering from phonons in iron pyrite (FeS2). *Solid State Commun.* 10, 307–310. doi: 10.1016/0038-1098(72)90013-0

Vaclavkova, S., Schultz-Jensen, N., Jacobsen, O. S., Elberling, B., and Aamand, J. (2015). Nitrate-controlled anaerobic oxidation of pyrite by Thiobacillus cultures. *Geomicrobiol. J.* 32, 412–419. doi: 10.1080/01490451.2014.940633

Vera, M., Schippers, A., and Sand, W. (2013). Progress in bioleaching: fundamentals and mechanisms of bacterial metal sulfide oxidation—part A. *Appl. Microbiol. Biotechnol.* 97, 7529–7541. doi: 10.1007/s00253-013-4954-2

Vogt, H., Chattopadhyay, T., and Stolz, H. (1983). Complete first-order Raman spectra of the pyrite structure compounds FeS2. MnS2 and SiP2. *J. Phys. Chem. Solids* 44, 869–873. doi: 10.1016/0022-3697(83)90124-5

Wagner, M., Ivleva, N. P., Haisch, C., Niessner, R., and Horn, H. (2009). Combined use of confocal laser scanning microscopy (CLSM) and Raman microscopy (RM): investigations on EPS–matrix. *Water Res.* 43, 63–76. doi: 10.1016/j.watres.2008.10.034

Yan, R., Kappler, A., Muehe, E. M., Knorr, K.-H., Horn, M. A., Poser, A., et al. (2019). Effect of reduced sulfur species on chemolithoautotrophic pyrite oxidation with nitrate. *Geomicrobiol. J.* 36, 19–29. doi: 10.1080/01490451.2018.1489915

Zhang, Y.-C., Slomp, C. P., Broers, H. P., Passier, H. F., and Van Cappellen, P. (2009). Denitrification coupled to pyrite oxidation and changes in groundwater quality in a shallow sandy aquifer. *Geochim. Cosmochim. Acta* 73, 6716–6726. doi: 10.1016/j.gca.2009.08.026

Conflict of Interest: The authors declare that the research was conducted in the absence of any commercial or financial relationships that could be construed as a potential conflict of interest.

frontiers in Microbiology

ORIGINAL RESEARCH
published: 01 December 2020
doi: 10.3389/fmicb.2020.580363

Compositions and Co-occurrence Patterns of Bacterial Communities Associated With Polymer- and ASP-Flooded Petroleum Reservoir Blocks

Guoling Ren[1,2†], Jinlong Wang[1,2†], Lina Qu[1,2], Wei Li[3], Min Hu[1,2], Lihong Bian[1,2], Yiting Zhang[1,2], Jianjun Le[3], Xumou Dou[3], Xinhong Chen[3], Lulu Bai[3] and Yue Li[2]*

[1] Heilongjiang Provincial Key Laboratory of Oilfield Applied Chemistry and Technology, Daqing, China, [2] College of Bioengineering, Daqing Normal University, Daqing, China, [3] Exploration and Development Research Institute, Daqing Oil Field Company, Ltd., Daqing, China

OPEN ACCESS

Edited by:
Geoffrey Battle Smith, New Mexico State University, United States

Reviewed by:
Peike Gao, Nankai University, China
Tamara N. Nazina, Winogradsky Institute of Microbiology (RAS), Russia

***Correspondence:**
Lina Qu
quln123@163.com

† These authors have contributed equally to this work

Specialty section:
This article was submitted to Extreme Microbiology, a section of the journal Frontiers in Microbiology

Received: 05 July 2020
Accepted: 05 November 2020
Published: 01 December 2020

Citation:
Ren G, Wang J, Qu L, Li W, Hu M, Bian L, Zhang Y, Le J, Dou X, Chen X, Bai L and Li Y (2020) Compositions and Co-occurrence Patterns of Bacterial Communities Associated With Polymer- and ASP-Flooded Petroleum Reservoir Blocks. Front. Microbiol. 11:580363. doi: 10.3389/fmicb.2020.580363

Polymer flooding technology and alkaline-surfactant-polymer (ASP) flooding technology have been widely used in some oil reservoirs. About 50% of remaining oil is trapped, however, in polymer-flooded and ASP-flooded reservoirs. How to further improve oil recovery of these reservoirs after chemical flooding is technically challenging. Microbial enhanced oil recovery (MEOR) technology is a promising alternative technology. However, the bacterial communities in the polymer-flooded and ASP-flooded reservoirs have rarely been investigated. We investigated the distribution and co-occurrence patterns of bacterial communities in ASP-flooded and polymer-flooded oil production wells. We found that *Arcobacter* and *Pseudomonas* were dominant both in the polymer-flooded and ASP-flooded production wells. *Halomonas* accounted for a large amount of the bacterial communities inhabiting in the ASP-flooded blocks, whereas they were hardly detected in the polymer-flooded blocks, and the trends for *Acetomicrobium* were the opposite. RDA analysis indicated that bacterial communities in ASP-flooded and polymer-flooded oil production wells are closely related to the physical and chemical properties, such as high salinity and strong alkaline, which together accounted for 56.91% of total variance. Co-occurrence network analysis revealed non-random combination patterns of bacterial composition from production wells of ASP-flooded and polymer-flooded blocks, and the ASP-flooded treatment decreased bacterial network complexity, suggesting that the application of ASP flooding technology reduced the tightness of bacterial interactions.

Keywords: bacterial community composition, network analysis, Illumina MiSeq sequencing, polymer-flooding, ASP-flooding

INTRODUCTION

Several large oilfields in China, including Daqing Oil Field, have entered the late stage of high water cut production in recent years. The oil recovery of these oil reservoirs has been faced with different degrees of decline year by year. The average recovery ratio of crude oil is less than 30% by using the conventional oil recovery technology (Yang et al., 2004; Kang et al., 2011). Chemical enhanced oil recovery (EOR) technologies, including polymers flooding and alkaline/surfactant/polymer (ASP) flooding which were considered as the tertiary oil recovery have been widely used in many oil reservoirs (Chang et al., 2006). The mechanism of polymer flooding technology is to use hydrolyzed polyacrylamide to block the large channel in formation and improve the viscosity of displacement phase so as to improve the remaining oil recovery (Nasr-El-Din et al., 1991; Gao, 2013). ASP flooding technology could improve oil recovery by producing ultra-low interfacial tension at oil/water, improving oil fluidity, blocking large pore channels, and effectively improving the sweep efficiency of displacement phase (Wang et al., 2019). However, some polymers were adsorbed and trapped in the pores and surfaces of reservoir rocks, which made oil recovery more difficult. Improving oil recovery of the reservoirs after chemical flooding is a very important and arduous work. MEOR technology is a tertiary oil recovery method based on the activity of a microbial community producing oil-releasing metabolites (including biogas, biosurfactant, biomass, and acid) to enhance oil recovery (Van Hamme et al., 2003; Li et al., 2007; She et al., 2019; Nazina et al., 2020). Indigenous microorganisms have the advantages of strong adaptability to oil reservoir environment (Gao et al., 2018). Bacteria such as *Pseudomonas* sp., *Acinetobacter* sp., *Bacillus* sp., and *Rhodococcus* sp., etc., often occurring in oilfields, have the characteristics of degrading and/or emulsifying crude oil and reducing oil-water surface tension (Desai and Banat, 1997). It is very important to study the microbial community compositions and stimulation strategy in the process of MEOR with endogenous microbials (Xiao et al., 2013). However, the effects of polymer flooding and ASP flooding on indigenous bacterial communities are not understood in detail. Considering the critical roles of bacterial communities in MEOR process, revealing the influence of polymer flooding and ASP flooding on activity of bacteria could facilitate the implementation of MEOR technology in the future.

Due to the complexity of reservoir system (Pannekens et al., 2019) and the diversity of injection production technology, the ecosystem of the oil reservoirs appears to be more physiologically and phylogenetically complex and diverse than previously thought (Amend and Teske, 2005). In recent years, culture dependent and culture independent methods have been used to study microbial communities to reveal microbial diversity and genetic relationships inhabiting the oil reservoirs (Li et al., 2006). It has been reported that some microorganisms could metabolize polymers and low molecular weight polymer products (Gu et al., 1998). *Acinetobacter* sp., *Bacillus* sp., etc., isolated from oil reservoir environment were directly involved in the biodegradation of hydrolyzed polyacrylamide to reduce HPAM viscosity (Matsuoka et al., 2002; Youssef et al., 2009). However, to our knowledge, bacterial diversity and community compositions have rarely been reported in polymer-flooded and ASP-flooded reservoirs. *Pseudomonas* and *Acinetobacter* related with hydrocarbon biodegradation and surfactant production accounted for 17.79 and 6.02% in four produced wells of the reservoir after polymer flooding in Daqing Oil Field, respectively. However, these reports represented only a limited number of water samples from production wells in a separate block. Co-occurrence network analysis provides a deep understanding of the structure of microbial communities and the interactions between different microbes (Barberán et al., 2012). However, we have not found any reports about bacterial co-occurrence network patterns in the ASP-flooded and polymer-flooded reservoirs.

This study focused on comparison of the diversity and composition of bacterial communities and bacterial co-occurrence patterns in production waters from polymer-flooded and ASP-flooded blocks at the Daqing Oil Field. The injected alkali, surfactants, and hydrolyzed polyacrylamide that influenced the microbial communities in the ASP-flooded block have been detected. We hypothesize that (I) the community compositions of bacteria would be varied among polymer-flooded and ASP-flooded reservoirs. Alkali-tolerating populations in ASP-flooded blocks would be higher than those in polymer-flooded blocks, (II) the co-occurrence patterns of bacteria will differ from each other after the two EOR treatment. In conclusion, this study will enhance our understanding of bacterial community structure, interrelationships, and symbiotic networks in deep oil reservoir environment.

MATERIALS AND METHODS

Samples Collection

The polymer-flooded blocks and ASP-flooded blocks are located in Daqing Oil Field in Northeast China. Both blocks had been developed by water flooding for several decades, and the average water content of the produced liquid is above 90%. Polymer flooding technology and ASP flooding technology were first applied in 1995 and 2014 in the Daqing Oil Field, respectively. The pH of the production water samples obtained from polymer-flooded blocks and ASP-flooded blocks were approximate 11.5 and 8.5, respectively, and the salinities were about 13,196 and 8,678 mg/L, respectively.

Water samples from 45 and 76 production wells at the polymer-flooded and ASP-flooded blocks, respectively, were collected into 10 L plastic containers. The containers were filled with oil-water production fluid to maintain an anoxic condition. All containers were autoclaved and rinsed with distilled water before sampling. About 1 L of water samples were centrifuged repeatedly under 12,000 g for 30 min to collect microbial cells (Pham et al., 2009; Tully et al., 2012). Genomic DNA was extracted from microbial cells using bacterial genomic extraction kit (TianGen, China). Quality of DNA was examined on agarose gel, and then used in the analysis described below or stored at −20°C.

PCR Amplification and 16S rRNA Gene Sequencing

PCR Amplification

The V3-V4 hypervariable regions of the bacterial 16S rRNA gene were amplified with primers 338F (5′-ACTCCTACGGGAGGCAGCAG-3′) and 806R (5′-GGACTACHVGGGTWTCTAAT-3′) by thermocycler PCR instrument (Barberán et al., 2012). PCR reactions were performed in triplicate 20 μL mixture containing 12.5 μL of dNTP and Taq enzyme premix, 0.8 μL of each primer (5 μM) and 10 ng of template DNA. The PCR reactions were conducted by referring to the previous reference (Gloor et al., 2010). The PCR products were detected from a 2% agarose gel and further purified using the DNA Gel Extraction Kit (BoRi, China).

Illumina MiSeq Sequencing

The sequencing was performed on the Illumina MiSeq platform according to the standard protocols in Majorbiogroup, Shanghai, China.

Processing of Sequencing Data

Raw fastq files were demultiplexed using QIIME2, merged by FLASH and quality filtered by Trimmomatic to meet the following criteria: (I) The filtering of sequences with a tail quality score below 20 using a 50 bp sliding window; (II) barcodes and primers at both ends of the sequence were used to distinguish the samples, and the sequences with the maximum primer mismatch of two were removed; and (III) sequences whose minimum overlap length of 10 bp were merged according to the overlap relation between PE reads.

Operational taxonomic units (OTUs) were employed with 97% similarity using UPARSE. The representative sequence sets were aligned, and the taxonomy was analyzed by RDP Classifier algorithm[1] against the Silva132 16S rRNA database at an 70% confidence level.

Statistical Analysis

The relative OTU abundance was calculated as the percentage of sequences grouped into that OTU within a sample. The species richness of bacteria was counted by the numbers of OTUs in a sample. Whether the sequencing data volume was adequate or not was determined according to whether the species rarefaction curve reached a flat level. One-way ANOVA was performed to examine the alpha diversity among precipitation treatments, and the significant differences were determined with Duncan's multiple comparison tests at the 95% confidence level. To explicitly test whether bacterial communities differed between two different EOR treatments, we first performed non-metric multidimensional scaling (NMDS) analysis for studying microorganisms of the oilfields. Next, we used PERMANOVA (1,000 permutations) using the adonis function of the VEGAN package in R on the OTU data matrix (Anderson, 2001; Jari Oksanen et al., 2016). Redundancy analysis (RDA) was performed in R to determine which environmental variables best explained the assemblage's variability.

[1]http://rdp.cme.msu.edu/

In order to analyze the effects of EOR on bacterial co-occurrence pattern, the underlying co-occurrences among bacterial taxa was depicted through network analysis. These OTUs with more than 20 sequences were retained for the construction of networks in order to reduce the complexity. Only robust ($r > 0.6$ or $r < -0.6$) and Significant Spearman correlations ($p < 0.01$) calculated within the "picante" R package (Xue et al., 2018) were incorporated into the network analyses (Hu et al., 2017). Network visualization and modular analysis were made with Gephi version 0.9.2. Node-level topological properties (i.e., degree, betweenness, closeness, and eigenector) were further calculated in the "igraph" R package. Statistical differences in measured node-level attributes across different taxa were determined using non-parametric Mann–Whitney *U*-test. Nodes with high degree (in top 1%) are recognized as keystone species in co-occurrence networks (Marasco et al., 2018).

RESULTS

Overall Pyrosequencing Information

Using Illumina MiSeq sequencing, 4460334 16S rRNA sequences ranging in length from 200 to 592 bp (most of the sequences were 435 bp) from 76 production water samples at ASP-flooded blocks and 2181316 16S rRNA sequences ranging from 167 to 592 bp (most of the sequences were 434 bp) from 45 production water samples at polymer-flooded blocks were obtained. A total of 1,451 OTUs were detected in 16S rRNA libraries constructed from production water samples obtained at polymer-flooded and ASP-flooded blocks based on 97% similarity (**Supplementary Table S1**). These OTUs belonged to 48 phyla, 76 classes, 302 families, 603 genera, and 935 species. The species rarefaction curve reached saturation with increasing sample numbers, indicating that the sequencing data volume had reached the requirements of sequencing (**Supplementary Figure S1**). The diversity (Simpson and Shannon) and richness (ACE and Chao 1) indices for the OTUs from bacterial communities were determined for all samples (**Supplementary Table S2**). The results showed that there was no significant difference in the diversity and richness of bacterial communities between polymer-flooded blocks and ASP-flooded blocks. Our results indicated that the two EOR technologies did not cause significant differences in the diversity and richness of the bacterial communities in the production wells.

Bacterial Community Compositions in Polymer-Flooded and ASP-Flooded Blocks

Four phyla including *Proteobacteria*, *Epsilonbacteraeota*, *Firmicutes*, and *Synergistetes* were dominant (relative abundance > 5%), accounting for 84.33% of the total bacteria in the libraries from production wells at polymer-flooded blocks. In contrast, three phyla including *Proteobacteria*, *Epsilonbacteraeota,* and *Firmicutes* were dominant (relative abundance > 5%), accounting for 85.52% of the total bacteria in production wells at polymer-flooded blocks (**Supplementary Figure S2**). At the genus level, *Arcobacter*,

Pseudomonas, *Acetomicrobium*, *Thauera,* and *Sulfuricurvum* were dominant (relative abundance > 5%), accounting for 56.47% of the total bacteria in polymer-flooded production wells. Bacteria of the genera *Pseudomonas*, *Halomonas*, *Arcobacter,* and *Nitrincola* were dominant, accounting for 45.68% in ASP-flooded production wells (**Figure 1**). At the phylum level, a Wilcoxon rank-sum test indicated that *Proteobacteria*, *Synergistetes*, *Bacteroidetes*, *Atribacteria, Coprothermobacteraeota*, *Thermotogae,* and *Caldiserica* were the dominant populations, the relative abundances difference was significant between production wells at polymer-flooded and ASP-flooded blocks (**Supplementary Figure S3**). *Proteobacteria* was the predominant group in production wells at polymer-flooded and ASP-flooded blocks. Relative abundance of *Proteobacteria* was higher in production water samples from polymer-flooded blocks than from ASP-flooded blocks. At the genus level, a Wilcoxon rank-sum test indicated that *Pseudomonas*, *Thauera*, *Acinetobacter,* and *Halomonas* were the dominant populations with significantly different relative abundances between the polymer-flooded block and ASP-flooded block (**Figure 2**). The relative abundance of *Acinetobacter* was higher in production wells at polymer-flooded blocks than in production wells at ASP-flooded blocks. NMDS analysis based on relative abundance of OTUs showed differences in bacterial community compositions between polymer-flooded blocks and ASP-flooded blocks (**Figure 3**). This observation was confirmed by multivariate analysis PERMANOVA ($R^2 = 0.058$, $P = 0.001$).

Bacterial Co-occurrence Network Analysis

In order to determine the general effects of Enhanced oil recovery (EOR) treatments on bacterial associations, two networks were constructed for two enhanced oil recovery practices by combining all bacteria originating from polymer-flooded and ASP-flooded blocks (**Figure 4**). The modularity index (MD) was 0.655 and 0.483 in network of polymer-flooded and ASP-flooded blocks, respectively, where $MD > 0.4$ suggests that the network has a modular structure, indicating that the network structure was non-random (Xue et al., 2017). The polymer-flooded blocks' network consisted of 1,242 nodes linked by 39,614 edges, and the ASP-flooded blocks' network consisted of only 1,200 nodes with 10,073 edges. Compared to polymer flooding treatment, the clustering coefficient of the network of ASP-flooded blocks was decreased by 0.040, and the network density of microbiome networks in polymer-flooded blocks was decreased by 0.037, indicating that oil reservoir bacterial associations were more tightened in responding to the application of polymer flooding technology.

In the co-occurrence network, *Proteobacteria*, *Acidobacteria,* and *Firmicutes* (Genus-level classifications are presented in **Supplementary Materials**) appeared most frequently, indicating that these generalists had adapted to these environments. Keystone taxa were defined as taxa interacting with many other members (i.e., top 1% of interactions), which were thought to play crucial roles in the overall community (Berry and Widder, 2014). A total of 12 OTUs were defined as keystone species in polymer-flooded blocks' network, including *Proteobacteria* (2 OTUs), *Firmicutes* (2 OTUs), *Chloroflexi* (2 OTUs), *Caldiserica* (1 OTU), *Bacteroidetes* (1 OTU), *Actinobacteria* (1 OTU), *Synergistetes* (1 OTU), and unclassified Bacteria (2 OTUs). There also 12 keystone species were defined in ASP-flooded blocks' network, including *Firmicutes* (5 OTUs), *Patescibacteria* (2 OTUs), *Actinobacteria* (1 OTU), Chloroflexi (1 OTU), *Verrucomicrobia* (1 OTU), and unclassified bacteria (2 OTUs).

Factors Related to Variation of the Bacterial Community

Physicochemical parameters of production water samples, such as CO_3^{2-}, pH, HCO_3^{2-}, Mg^{2+}, Ca^{2+}, Na^{+}, and temperature were all significantly different among polymer flooded and ASP-flooded blocks (**Supplementary Table S3**). In order to explore the relationship between environmental factors and the microbial community in different water-flooded oil reservoirs, Redundancy Analyses (RDA) were conducted. Based on the results of the RDA (**Figure 5**), there were large variations between polymer-flooded and ASP-flooded blocks, the first two RDA axes explained a total of 56.91% of the variance in the composition of bacterial communities among the two EOR treatments. pH ($R^2 = 0.12$, $p = 0.002$), temperature ($R^2 = 0.06$, $p = 0.037$), SO_4^{2-} ($R^2 = 0.17$, $p = 0.007$), HCO_3^{-} ($R^2 = 0.11$, $p = 0.002$), and Ca^{2+} ($R^2 = 0.09$, $p = 0.007$) showed strongly significant correlation to the species of distribution of bacterial communities.

DISCUSSION

In this study, we examined the bacterial community assembly in oil reservoir after application of different EOR technologies. Our results showed that *Proteobacteria*, *Epsilonbacteraeota*, *Firmicutes,* and *Synergistetes* were predominant in the total sequences in both studied sites. *Arcobacter*, *Pseudomonas*, *Acetomicrobium*, *Thauera,* and *Sulfuricurvum* were dominant (relative abundance > 5%) in polymer-flooded production wells. *Pseudomonas*, *Halomonas*, *Arcobacter,* and *Nitrincola* were dominant in ASP-flooded production wells. These results suggested that the bacterial community structure was significantly different among polymer-flooded and ASP-flooded blocks, whereas bacterial diversity was not affected by different EORs. This is in accordance with the previous investigation on microbial communities in oil reservoirs, which showed that bacterial community was significantly influenced by reservoir environments (Gao et al., 2016, 2019). The injected alkali, surfactants, and hydrolyzed polyacrylamide have greatly affected the microbial communities in ASP-flooded blocks. We found that the environmental changes that occur with changes in EOR process contribute differently to bacterial community. In particular, in our research, the injected alkali could result in the pH increase of formation water up to 10.76 in ASP-flooded blocks, which is much higher than those of polymer flooded blocks with pH 8.2 (**Supplementary Table S3**). The results showed the alkaline environment may have served as a major selective force in ASP-flooded

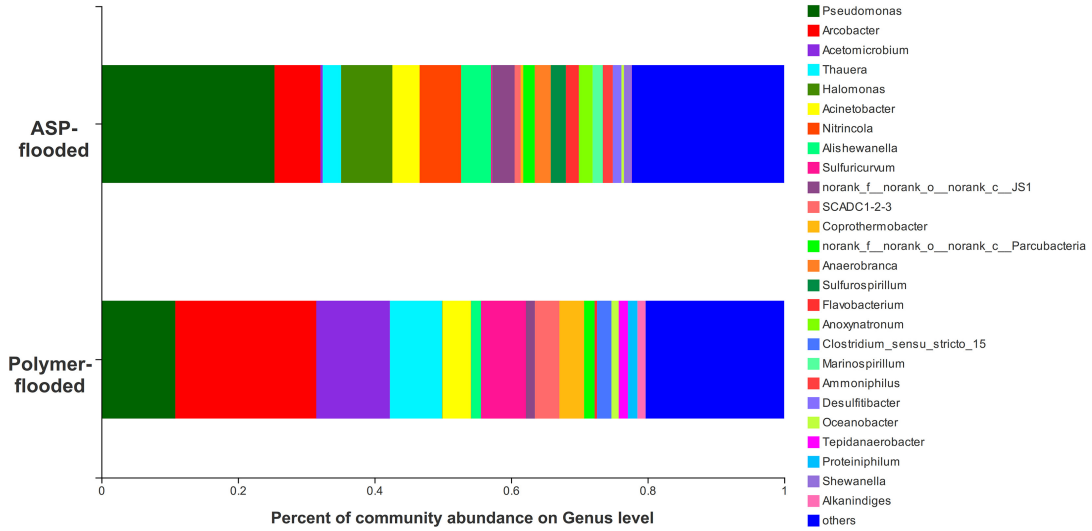

FIGURE 1 | Bacterial community compositions at the genus level from production wells at ASP-flooded and polymer-flooded blocks.

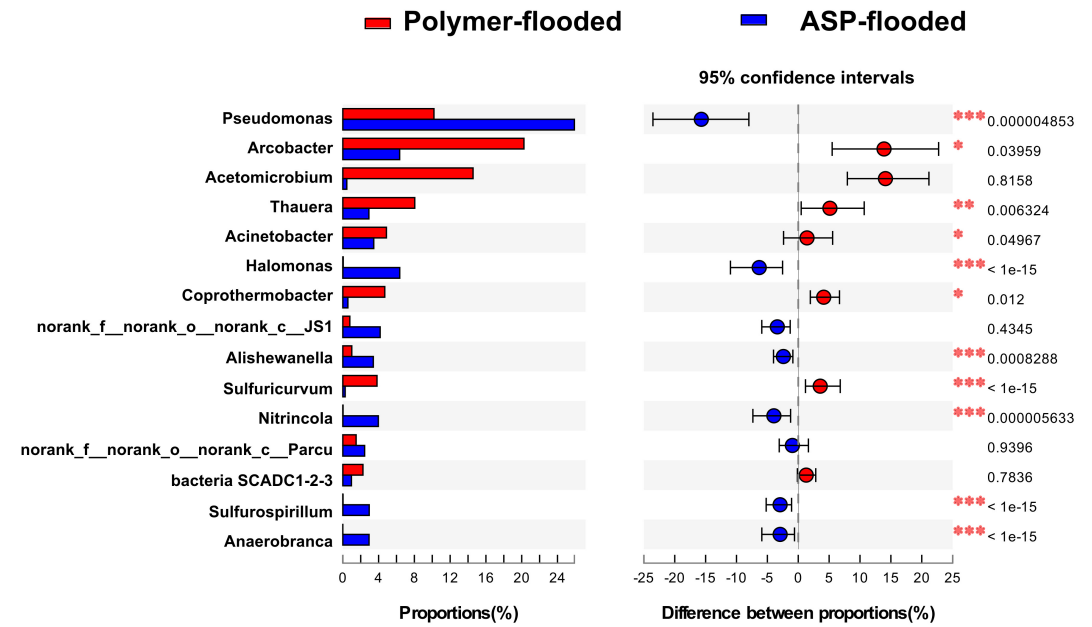

FIGURE 2 | Wilcoxon rank-sum test revealed the bacterial populations with significant differences in the relative abundance between ASP-flooded blocks and polymer-flooded blocks. *$P < 0.05$, **$P < 0.01$, ***$P < 0.001$.

blocks. The high pH inhibited the survival of most microbial populations. Recent studies have also demonstrated that bacterial communities were strongly correlated with environmental pH (Fierer and Jackson, 2006; Rousk et al., 2010). Alkali-tolerating populations *Pseudomonas*, *Halomonas*, *Alishewanella*, *Sulfurospirillum*, *Nitrincola,* and *Anaerobranca* in ASP-flooded blocks were higher than those in polymer-flooded blocks. Besides pH, CO_3^{2-}, HCO_3^-, Ca^{2+}, and Na^+ could also be important driving factors for shaping bacterial communities in the oil reservoirs.

In the study, we found that some functional microbes which could enhance oil production are dominant in polymer-flooded and ASP-flooded reservoirs. Proteobacteria dominated in both polymer-flooded and ASP-flooded blocks. Relative abundance was higher in ASP-flooded blocks than in polymer-flooded blocks. *Pseudomonas* sp., which belongs to *Proteobacteria,* has been widely used in tertiary oil recovery and pollution remediation due to its capability to degrade petroleum hydrocarbons, produce surfactants, and degrade polyacrylamide (Banat, 1995). In addition, the rhamnolipid produced by

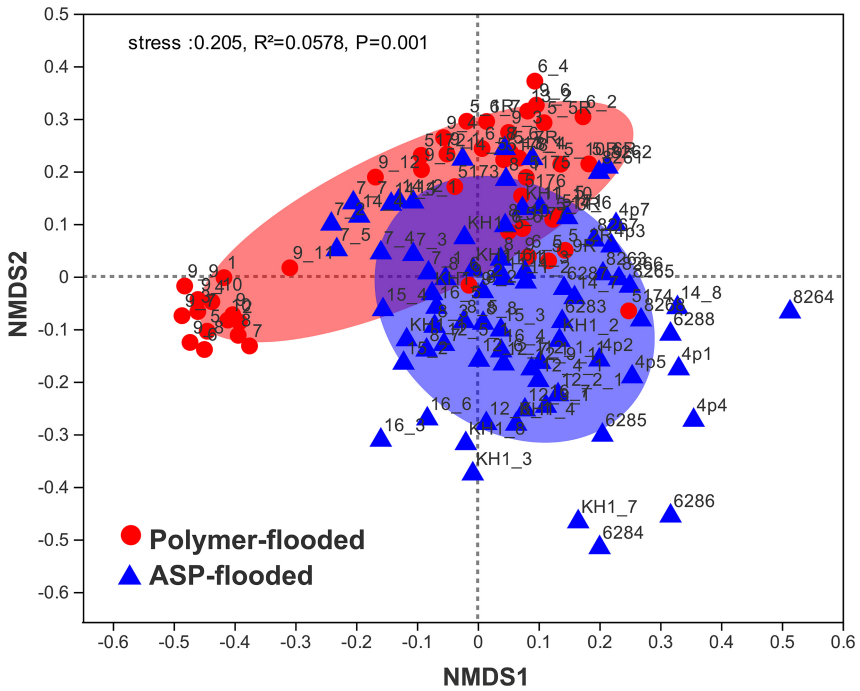

FIGURE 3 | Non-metric multidimensional scaling (NMDS) ordination plot of bacterial communities from production wells at ASP-flooded and polymer-flooded blocks. PERMANOVA analysis showed significant differences in bacterial communities between ASP-flooded blocks and polymer-flooded blocks.

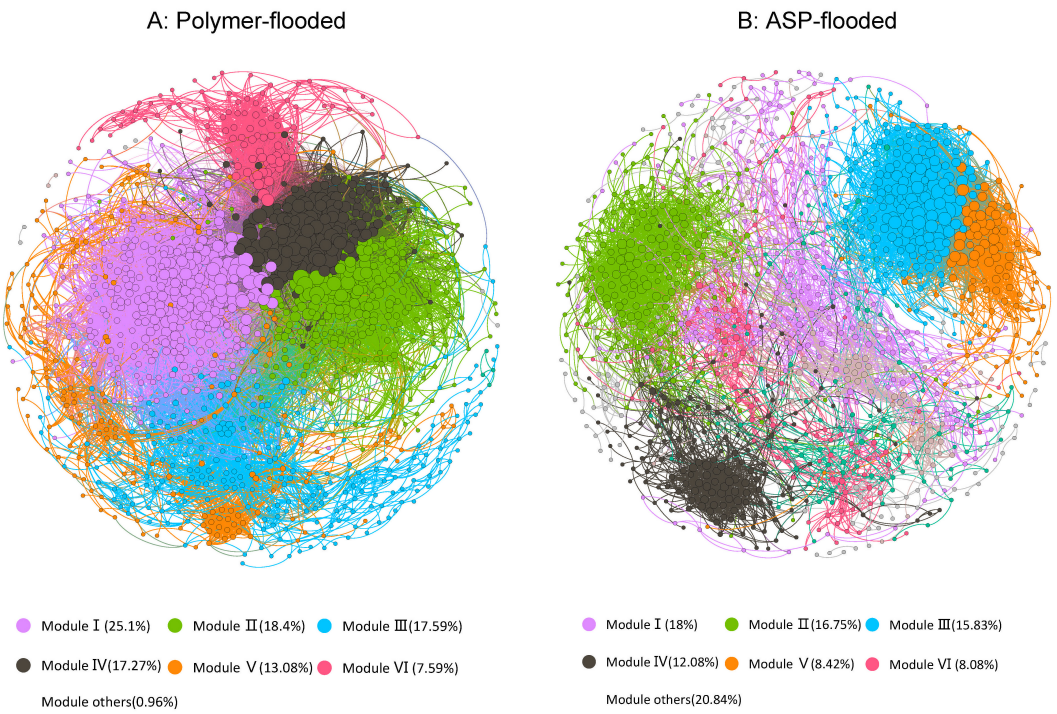

FIGURE 4 | The co-occurrence patterns among OTUs revealed by network analysis. The nodes were colored according to different types of modularity classes **(A)** and supergroups **(B)**, respectively. A connection stands for a strong (Spearman's $r > 0.6$ or $r < -0.6$) and significant (P-value < 0.01) correlation.

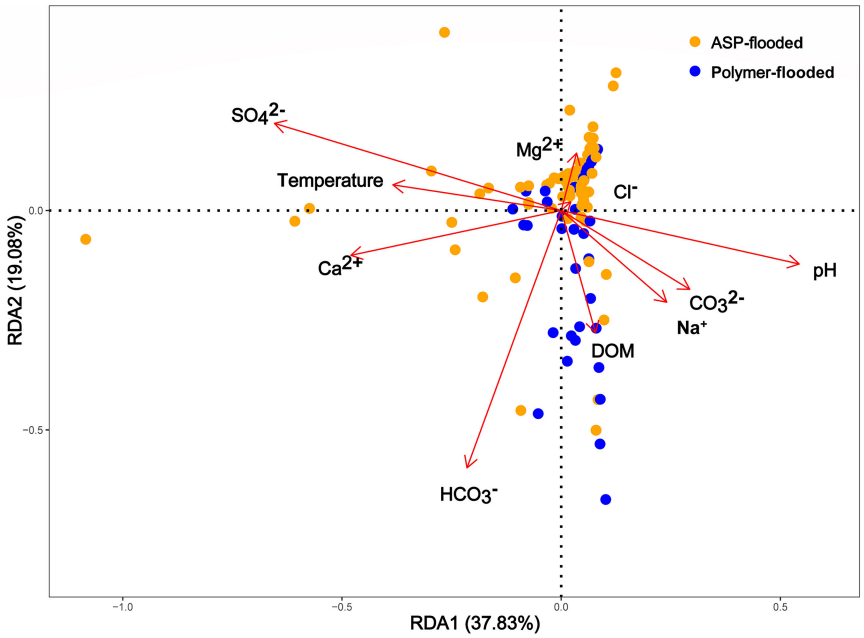

FIGURE 5 | Spatially constrained, distance-based redundancy analysis of plot based quantitative bacterial community composition. The ASP-flooded and polymer-flooded samples (different color) are shown. Arrows indicate the direction of the maximum change in variables. DOM, Degree of mineralization (total salinity of water).

Pseudomonas sp. could reduce the interfacial tension of oil-water phase (Bognolo, 1999) to EOR (Chrzanowski et al., 2012). *Acinetobacter* sp. were also found in both polymer-flooded and ASP-flooded blocks, and the relative abundance was higher in polymer-flooded blocks than in ASP-flooded blocks. *Acinetobacter* sp. has the ability to degrade saturated and aromatic hydrocarbons (Sugiura et al., 1996). These results indicate that both the polymer-flooded and ASP-flooded reservoirs have the basis of implementing microbial oil recovery technologies.

Networks analysis could perform richness and composition analysis and could also provide in-depth research on microbial interaction and ecological assembly rules (Ziegler et al., 2018). In the study, for the first time we applied correlation-based network analysis to explore the co-occurrence models of bacterial communities across polymer-flooded and ASP-flooded blocks. Previous studies have shown that microbial interactions can maintain ecosystem function and stability (Ziegler et al., 2018). Our results showed that network complexity was higher in polymer-flooded blocks than in ASP-flooded blocks. Increased network connectivity and complexity are previously undescribed properties of bacterial community assemblages and represent fundamental differences microhabitat among polymer-flooded and ASP-flooded blocks. Our results also showed that fewer connections and lower clustering coefficient and network density were observed in co-occurrence network of ASP-flooded blocks when compared with those of polymer-flooded blocks. The increase of pH of formation water resulted in the reduction of the most connections (Nearly 3/4) in the ASP-flooded blocks' network. This may also indicate that the alkaline environment served as a major selective force in ASP-flooded blocks. Keystone players were thought to play crucial roles in the overall microbiome and could maintain the network stability and structure (Berry and Widder, 2014). *Firmicutes* and *Patescibacteria* were more important in ASP-flooded blocks than in polymer-flooded blocks, this suggested that they may play an irreplaceable role in maintaining the structure of bacterial communities in high pH environments. Previous studies have shown that microbial interactions can maintain ecosystem function and stability (Ziegler et al., 2018).

CONCLUSION

In this paper, the characteristics of bacterial communities in ASP-flooded blocks were revealed by comparison with those of polymer-flooded blocks. We found that application of different EOR technologies significantly altered bacterial community compositions but had no remarkable effects on species diversity and richness. Bacteria of the genera *Arcobacter*, *Pseudomonas*, *Acetomicrobium*, *Thauera,* and *Sulfuricurvum* were dominant in formation water samples from polymer-flooded blocks. The extreme environment of the ASP-flooded reservoirs led to the predominance of alkali-tolerating *Pseudomonas*, *Halomonas*, and *Nitrincola*. The network of bacterial communities at the ASP-flooded blocks was less complex and tighter than that of polymer-flooded blocks. Indigenous microbes are better adapted to the oil reservoir environment, and how to stimulate these bacteria to enhance oil recovery would be the basis for meaningful future work.

DATA AVAILABILITY STATEMENT

The original contributions presented in the study are publicly available. This data can be found here: https://www.ncbi.nlm.nih.gov/sra/PRJNA673922.

AUTHOR CONTRIBUTIONS

JLW, and GLR proposed and organized the overall project. MH, WL, LHB, and LNQ performed the majority of the experiments. MH and LNQ gave assistance in lab work and laboratory analyses. JLW and GLR wrote the main manuscript text. YTZ, JJL, XMD, YL, LLB, XHC and contributed insightful discussions. All authors reviewed the manuscript.

FUNDING

Financial supports from the Heilongjiang Natural Science Foundation Joint Guiding Project (JJ2020LH2327), Scientific research project of Daqing Oil Field Co., Ltd. "Research on functional bacteria and activator system of chemical flooding microbial oil recovery (dq-2016-sc-ky-001), and Daqing Oil Field Co., Ltd. Scientific Research Project "Using RNA High-throughput Sequencing Technology to Optimize Functional Genes for Oil Recovery (dq-2018-sc-ky-001) are acknowledged.

SUPPLEMENTARY MATERIAL

The Supplementary Material for this article can be found online at: https://www.frontiersin.org/articles/10.3389/fmicb.2020.580363/full#supplementary-material

REFERENCES

Amend, J. P., and Teske, A. (2005). Expanding frontiers in deep subsurface microbiology. *Palaeogeogr. Palaeoclimatol. Palaeoecol.* 219, 131–155. doi: 10.1016/b978-0-444-52019-7.50012-7

Anderson, M. J. (2001). A new method for non-parametric multivariate analysis of variance. *Austral. Ecol.* 26, 32–46. doi: 10.1111/j.1442-9993.2001.01070.pp.x

Banat, I. M. (1995). Biosurfactants production and possible uses in microbial enhanced oil recovery and oil pollution remediation: a review. *Bioresour. Technol.* 51, 1–12. doi: 10.1016/0960-8524(94)00101-6

Barberán, A., Bates, S. T., Casamayor, E. O., and Fierer, N. (2012). Using network analysis to explore co-occurrence patterns in soil microbial communities. *ISME J.* 6, 343–351. doi: 10.1038/ismej.2011.119

Berry, D., and Widder, S. (2014). Deciphering microbial interactions and detecting keystone species with co-occurrence networks. *Front. Microbiol.* 5:219. doi: 10.3389/fmicb.2014.00219

Bognolo, G. (1999). Biosurfactants as emulsifying agents for hydrocarbons. *Colloids Surf. Physicochem. Eng. Aspects* 152, 41–52. doi: 10.1016/s0927-7757(98)00684-0

Chang, H., Zhang, Z., Wang, Q., Xu, Z., Guo, Z., Sun, H., et al. (2006). Advances in polymer flooding and alkaline/surfactant/polymer processes as developed and applied in the People's Republic of China. *J. Petrol. Technol.* 58, 84–89. doi: 10.2118/89175-jpt

Chrzanowski, Ł, Dziadas, M., Ławniczak, Ł, Cyplik, P., Białas, W., Szulc, A., et al. (2012). Biodegradation of rhamnolipids in liquid cultures: effect of biosurfactant dissipation on diesel fuel/B20 blend biodegradation efficiency and bacterial community composition. *Bioresour. Technol.* 111, 328–335. doi: 10.1016/j.biortech.2012.01.181

Desai, J. D., and Banat, I. M. (1997). Microbial production of surfactants and their commercial potential. *Microbiol. Mol. Biol. Rev.* 61, 47–64. doi: 10.1128/.61.1.47-64.1997

Fierer, N., and Jackson, R. B. (2006). The diversity and biogeography of soil bacterial communities. *Proc. Natl. Acad. Sci.* 103, 626–631. doi: 10.1073/pnas.0507535103

Gao, C. (2013). Viscosity of partially hydrolyzed polyacrylamide under shearing and heat. *J. Petrol. Explorat. Product. Technol.* 3, 203–206. doi: 10.1007/s13202-013-0051-4

Gao, P., Tan, L., Li, Y., Guo, F., and Ma, T. (2019). Composition of bacterial and archaeal communities in an alkali-surfactant-polyacrylamide-flooded oil reservoir and the responses of microcosms to nutrients. *Front. Microbiol.* 10:2197. doi: 10.3389/fmicb.2019.02197

Gao, P., Li, G., Le, J., Liu, X., Liu, F., and Ma, T. (2018). Succession of microbial communities and changes of incremental oil in a post-polymer flooded reservoir with nutrient stimulation. *Appl. Microbiol. Biotechnol.* 102, 2007–2017. doi: 10.1007/s00253-018-8766-2

Gao, P., Tian, H., Wang, Y., Li, Y., Li, Y., Xie, J., et al. (2016). Spatial isolation and environmental factors drive distinct bacterial and archaeal communities in different types of petroleum reservoirs in China. *Sci. Rep.* 6:20174.

Gloor, G. B., Hummelen, R., Macklaim, J. M., Dickson, R. J., Fernandes, A. D., MacPhee, R., et al. (2010). Microbiome profiling by illumina sequencing of combinatorial sequence-tagged PCR products. *PLoS One* 5:e15406. doi: 10.1371/journal.pone.0015406

Gu, J.-D., Roman, M., Esselman, T., and Mitchell, R. (1998). The role of microbial biofilms in deterioration of space station candidate materials. *Int. Biodeterior. Biodegradation* 41, 25–33. doi: 10.1016/S0964-8305(98)80005-X

Hu, A., Ju, F., Hou, L., Li, J., Yang, X., Wang, H., et al. (2017). Strong impact of anthropogenic contamination on the co-occurrence patterns of a riverine microbial community. *Environ. Microbiol.* 19, 4993–5009. doi: 10.1111/1462-2920.13942

Jari Oksanen, F., Friendly, M., Kindt, R., Legendre, P., McGlinn, D., Minchin, P. R., et al. (2016). *vegan: Community ecology package. R package version 2.4-1*. Vienna: The R Project for Statistical Computing.

Kang, X., Zhang, J., Sun, F., Zhang, F., Feng, G., Yang, J., et al. (2011). "A review of polymer EOR on offshore heavy oil field in Bohai Bay, China," in *SPE enhanced oil recovery conference*, (Texas: Society of Petroleum Engineers).

Li, H., Yang, S.-Z., Mu, B.-Z., Rong, Z.-F., and Zhang, J. (2006). Molecular analysis of the bacterial community in a continental high-temperature and water-flooded petroleum reservoir. *FEMS Microbiol. Lett.* 257, 92–98. doi: 10.1111/j.1574-6968.2006.00149.x

Li, H., Yang, S., Mu, B., Rong, Z., and Zhang, J. (2007). Molecular phylogenetic diversity of the microbial community associated with a high-temperature petroleum reservoir at an offshore oilfield. *FEMS Microbiol. Ecol.* 60, 74–84. doi: 10.1111/j.1574-6941.2006.00266.x

Marasco, R., Mosqueira, M. J., Fusi, M., Ramond, J.-B., Merlino, G., Booth, J. M., et al. (2018). Rhizosheath microbial community assembly of sympatric desert speargrasses is independent of the plant host. *Microbiome* 6:215.

Matsuoka, H., Ishimura, F., Takeda, T., and Hikuma, M. (2002). Isolation of polyacrylamide-degrading microorganisms from soil. *Biotechnol. Bioproc. Engin.* 7, 327–330. doi: 10.1007/bf02932844

Nasr-El-Din, H., Hawkins, B., and Green, K. (1991). "Viscosity behavior of alkaline, surfactant, polyacrylamide solutions used for enhanced oil recovery," in *SPE International Symposium on Oilfield Chemistry*, (Texas: Society of Petroleum Engineers).

Nazina, T., Sokolova, D., Grouzdev, D., Semenova, E., Babich, T., Bidzhieva, S., et al. (2020). The Potential Application of Microorganisms for Sustainable Petroleum Recovery from Heavy Oil Reservoirs. *Sustainability* 12:15. doi: 10.3390/su12010015

Pannekens, M., Kroll, L., Müller, H., Mbow, F. T., and Meckenstock, R. U. (2019). Oil reservoirs, an exceptional habitat for microorganisms. *N. Biotechnol.* 49, 1–9. doi: 10.1016/j.nbt.2018.11.006

Pham, V. D., Hnatow, L. L., Zhang, S., Fallon, R. D., Jackson, S. C., Tomb, J. F., et al. (2009). Characterizing microbial diversity in production water from an Alaskan mesothermic petroleum reservoir with two independent molecular methods. *Environ. Microbiol.* 11, 176–187. doi: 10.1111/j.1462-2920.2008.01751.x

Rousk, J., Bååth, E., Brookes, P. C., Lauber, C. L., Lozupone, C., Caporaso, J. G., et al. (2010). Soil bacterial and fungal communities across a pH gradient in an arable soil. *ISME J.* 4, 1340–1351. doi: 10.1038/ismej.2010.58

She, H., Kong, D., Li, Y., Hu, Z., and Guo, H. (2019). Recent advance of microbial enhanced oil recovery (MEOR) in China. *Geofluids* 2019:187 1392

Sugiura, K., Ishihara, M., Shimauchi, T., and Harayama, S. (1996). Physicochemical properties and biodegradability of crude oil. *Environ. Sci. Technol.* 31, 45–51. doi: 10.1021/es950961r

Tully, B. J., Nelson, W. C., and Heidelberg, J. F. (2012). Metagenomic analysis of a complex marine planktonic thaumarchaeal community from the Gulf of Maine. *Environ. Microbiol.* 14, 254–267. doi: 10.1111/j.1462-2920.2011.02628.x

Van Hamme, J. D., Singh, A., and Ward, O. P. (2003). Recent advances in petroleum microbiology. *Microbiol. Mol. Biol. Rev.* 67, 503–549. doi: 10.1128/mmbr.67.4.503-549.2003

Wang, X., Li, X., Yu, L., Xiu, J., Li, Y., Cui, Q., et al. (2019). Evaluation of a new alkaline/microbe/polymer flooding system for enhancing heavy oil recovery. *Pet. Sci. Technol.* 37, 163–170. doi: 10.1080/10916466.2018.1522341

Xiao, M., Zhang, Z.-Z., Wang, J.-X., Zhang, G.-Q., Luo, Y.-J., Song, Z.-Z., et al. (2013). Bacterial community diversity in a low-permeability oil reservoir and its potential for enhancing oil recovery. *Bioresour. Technol.* 147, 110–116. doi: 10.1016/j.biortech.2013.08.031

Xue, L., Ren, H., Li, S., Leng, X., and Yao, X. (2017). Soil Bacterial Community Structure and Co-occurrence Pattern during Vegetation Restoration in Karst Rocky Desertification Area. *Front Microbiol* 8:2377. doi: 10.3389/fmicb.2017.02377

Xue, Y., Chen, H., Yang, J. R., Liu, M., Huang, B., and Yang, J. (2018). Distinct patterns and processes of abundant and rare eukaryotic plankton communities following a reservoir cyanobacterial bloom. *ISME J.* 12, 2263–2277. doi: 10.1038/s41396-018-0159-0

Yang, F., Wang, D., Yang, X., Sui, X., Chen, Q., and Zhang, L. (2004). "High concentration polymer flooding is successful," in *SPE Asia Pacific Oil and Gas Conference and Exhibition*, (Texas: Society of Petroleum Engineers).

Youssef, N., Elshahed, M. S., and McInerney, M. J. (2009). Microbial processes in oil fields: culprits, problems, and opportunities. *Adv. Appl. Microbiol.* 66, 141–251. doi: 10.1016/s0065-2164(08)00806-x

Ziegler, M., Eguíluz, V. M., Duarte, C. M., and Voolstra, C. R. (2018). Rare symbionts may contribute to the resilience of coral–algal assemblages. *ISME J.* 12, 161–172. doi: 10.1038/ismej.2017.151

Conflict of Interest: WL, JJL, XMD, and XHC were employed by company Daqing Oil Field Company, Ltd.

The remaining authors declare that the research was conducted in the absence of any commercial or financial relationships that could be construed as a potential conflict of interest.

frontiers in Earth Science

BRIEF RESEARCH REPORT
published: 05 March 2021
doi: 10.3389/feart.2021.590257

Exploring Microbial Biosignatures in Mn-Deposits of Deep Biosphere: A Preliminary Cross-Disciplinary Approach to Investigate Geomicrobiological Interactions in a Cave in Central Italy

Ilaria Vaccarelli[1,2], *Federica Matteucci*[1], *Marika Pellegrini*[1]*, *Fabio Bellatreccia*[3] and *Maddalena Del Gallo*[1]

[1]Dept. of Life, Health and Environmental Sciences, University of L'Aquila, L'Aquila, Italy, [2]Instituto de Recursos Naturales y Agrobiologia de Sevilla (IRNAS-CSIC), Sevilla, Spain, [3]Dept. of Sciences, Roma Tre University, Rome, Italy

OPEN ACCESS

Edited by:
Geoffrey Battle Smith,
New Mexico State University,
United States

Reviewed by:
Huan Cui,
Université de Paris, France
Diana Eleanor Northup,
University of New Mexico,
United States

***Correspondence:**
Marika Pellegrini
marika.pellegrini@univaq.it

Specialty section:
This article was submitted to Biogeoscience, a section of the journal Frontiers in Earth Science

Received: 31 July 2020
Accepted: 11 January 2021
Published: 05 March 2021

Citation:
Vaccarelli I, Matteucci F, Pellegrini M, Bellatreccia F and Del Gallo M (2021) Exploring Microbial Biosignatures in Mn-Deposits of Deep Biosphere: A Preliminary Cross-Disciplinary Approach to Investigate Geomicrobiological Interactions in a Cave in Central Italy. Front. Earth Sci. 9:590257. doi: 10.3389/feart.2021.590257

The terrestrial subsurface offers privileged sites both to search for microbial life and to observe still mostly unknown characteristic lithologies. In particular, caves represent natural laboratories to investigate unique minerogenetic processes and biotic interactions, connected to these phenomena. Manganese mineralization in cave environments provides a window to understand the complex Mn cycle and the development of microbial communities in special conditions, such as low constant temperature, absence of light and, in particular, low-energy environments. In the current study, we isolated and characterized Mn-samples taken from the cave "Grotta Grande dei Cervi," L'Aquila, Central Italy, and we used a multidisciplinary approach to characterize them, with the purpose of understanding the biogeochemical processes in extreme environments. A chemical characterization of the samples was done by EDS; further investigations are underway with other multidisciplinary methodologies to understand whether the Mn laminae are related to biological processes. SEM investigations revealed microbial imprints, showing cell-like structures and suggesting that the cell-like shapes occur within internal laminae. A culture-independent approach was used to assess the possibility that biotic factors may be involved in the production of these mineralizations and to investigate the nature of the microbial community in these materials. A molecular approach was the first step to investigate the role of microorganisms in forming manganese oxides associated with water bearing rocks. DNA from the black deposits was extracted and sequence analyses of specimens were performed. Our data support the hypothesis that microorganisms may contribute to the mineralizations of manganese in this environment, providing new encouraging insight into the role of microorganisms in the Mn cycle and the processes of energy acquisition in unfavorable conditions, with relevant implications for astrobiology.

Keywords: black deposits, Grotta Grande dei Cervi cave, Mn-bacteria, deep biosphere biosignatures, SEM-EDS analysis, 3D modeling, Next Generation Sequencing

INTRODUCTION

Caves are still understudied habitats from both exploration and scientific perspectives. These limitations constitute a real knowledge gap, recently proposed by Ficetola et al. (2019) under the name of Racovitzan impediment. Subsurface hosts a real interdisciplinary laboratory in which it is possible to investigate chemical, physical, geological, ecological and biological processes (Barton and Northup, 2007; Miller et al., 2015; Tisato et al., 2015). Subterranean environments provide many redox interfaces and stable physical-chemical environments, which in turn may promote secondary mineral precipitation and microbial growth near starvation conditions. Microbes can trigger different reactions with the rock matrix which may enhance mineral formation and dissolution through different biochemical reactions, including redox transformations (Northup and Lavoie, 2001). These peculiar microbial reactions are involved in the formation of cave manganese deposits (Boston, 2000; Northup and Lavoie, 2001; Carmichael and Bräuer, 2015). Specifically, when electron transfer reactions take place at the microbe-mineral interface, these geomicrobiological interactions might leave residues of life throughout the geological records (Naylor, 2005; Noffke, 2009; Miot et al., 2014; Corenblit et al., 2019). Typically, manganese oxides can be found in the caves, as fine-grained, poorly crystalline black/dark brown coatings and crusts, manganese flowstones, manganese stromatolites or as biofilms on rock surfaces (Carmichael and Bräuer, 2015; Kimble et al., 2018).

The subsurface offers one of the best environment to search for extant, recently alive, and long-dead microbial lifeforms and their characteristic lithologies due to its sheltering from a large part of atmospheric events (Boston et al., 2001). Subsurface fabrics, fossil bacteria preserved in minerals, mineralized nano-sized structures and biologically generated textures represent some of the "biosignature suites" which have been proposed for exobiological research (Boston et al., 2001; Naylor, 2005; Northup et al., 2011). Biomineralization studies are therefore useful for the investigation of biogenic secondary mineral deposits, which can represent useful biosignatures for the search of early life on Earth and on other planets (Boston et al., 2001; Naylor, 2005; Miller et al., 2015; Tisato et al., 2015; Corenblit et al., 2019). The interest in these environments has also reached several space agencies, enough to develop research and training projects right inside the caves (e.g. PANGEA-X project, coordinated by ESA) (Miller et al., 2018; Miller et al., 2020). If these subsurface minerals are firmly recognized as biogenic activity indicators on Earth, then exobiological research is today focused on the millimeter-sized spherules revealed by NASA's Opportunity rover in Meridiani Planum, a Martian region once covered by iron-rich waters.

As suggested by Boston et al. (2001), "biosignature suites" should be detectable at both macroscopic and microscopic level. This combination of features could be essential in the design of instrumentation and strategies for robotic, artificially intelligent and human-crewed extra-terrestrial missions (Boston, 2000; Boston et al., 2001). Thanks to recent developments of rover, orbiter and other technologies, now it is possible to observe, detect and quantify Martian landform characteristics at all scales (from mm to km) and in 2D/3D dimensions. The Perseverance rover (from NASA) launched in July 2020 and the ExoMars rover (from ESA/Roscosmos) scheduled to be launched in 2022, are equipped with devices capable of ascertaining surface and subsurface putative biogeomorphological signatures of life. With these instruments, it will be possible to investigate outcrops, rocks, and substrate debris and their macroscopic texture, structure, and layering (Coates et al., 2017; Vago et al., 2017; Corenblit et al., 2019).

Recently, the explorations on Mars with robotic tools increased the attention in Mn-rich rock varnishes of Earth, interesting for their involvement in the terrestrial and extra-terrestrial Mn biogeochemical cycling (Northup et al., 2010). One of the keys to establishing the biological origin for black rock deposits is to obtain more data from the laminae, containing a major concentration of manganese oxides. Currently, no detailed and systematic geomicrobiological explorations of most known caves have been carried out. This fragmentation of knowledge is primarily due to the difficulties of accessing a cave as well as to the lack of communication between different disciplines (Miot et al., 2014). In this context, highlytechnical sampling could represent a challenge to providing this information since the deepest areas are less sampled due to access difficulties. Thus, more complete and comprehensive knowledge of the geomicrobiology and biogeochemistry of caves, as well as biosignature identification, are needed. In this perspective, we applied an integrative and multi-scaled approach, applied to samples collected in a far, deep zone of a cave "Grotta Grande dei Cervi," located in L'Aquila province in Central Italy. A series of tools from geology, mineralogy, geochemistry, microscopy, informatics and molecular microbiology was used: 1) to characterize particular black deposits on the wall of the cave; 2) to identify and characterize the microbial communities within black deposits using new powerful molecular tools; 3) to recognize microbial fabrics or fossil bacteria as valuable biosignatures for astrobiology by using innovative and experimental approaches.

METHODS

Description of Cave

The "Grotta Grande dei Cervi" is located in the middle portion of the Monti Carseolani ridge, 60 km NE of Rome, in Central Apennines (Italy). A well-structured cave system is found within the carbonatic ridge, known as Pietrasecca karst system (whose "Grotta Grande dei Cervi" and the Ovito di Pietrasecca represent the most important caves). This system evolved in a ridge formed by Upper Cretaceous-Miocene limestones and younger flysch deposits, bounded by a set of faults trending NE-SE Agostini and Piccini, 1994. The caves proceed along with these fractures, which occur transversely to the ridge. Part of both caves shows an evident vadose morphology. These features suggest a fast development under a high hydraulic gradient with significant erosion activity. The sampling of manganese deposits was conducted within "Grotta Grande dei Cervi". The cave entrance opens at an altitude of

858 m a.s.l. (42°8′9.136″ N 13°7′43.558″ E), has an overall height difference of 107 m (+6/−113 m) and a linear extent of 1875 m. "Grotta Grande dei Cervi" cave also represents the paleoponor of the karst system, which is now active with the poor of the Ovito di Pietrasecca.

Sampling of Cave Secondary Deposits

In this study, the geomicrobiology of the ferromanganese deposits was investigated within a poorly studied epigenetic cave system, located in the cave-rich Central Apennine karst region. Manganese oxides within "Grotta Grande dei Cervi" occur as black crusts on walls and floors and can be observed in the inner part of the cave (highlighted with a circle in **Supplementary Figure S1**). Five different samples replications were collected in the areas above a flow of water where was a Mn patina on the wall (**Supplementary Figures S2, S3**) during the fall season in 2019. The sampling area is located in the unsaturated zone, at 50 m of depth and 1 km from the entrance. Speleological techniques were used to reach the sampling site, with the scientific team backed by a group of expert speleologists. The portion of the cave holds a nearly constant air temperature, which is 8°C throughout the year and relative humidity close to saturation (97.7%). After the collection by sterile tools, all microbial samples were stored in Eppendorf tubes. The same specimens were replicated and filled with a solution of RNAlater (Ambion, Austin, TX, United States), according to the instructions of the manufacturer. A portable fridge was used for the carriage of the samples from the cave to the laboratory. All specimens were stored at −20°C until analyzed.

Morphological and Geo-Chemical Characterization of Microbial Deposits From Speleothems by SEM and SEM-EDS

Black crusts samples from "Grotta Grande dei Cervi" were analyzed by scanning electron microscopy (SEM) combined with energy dispersive X-ray spectroscopy (EDS). Air-dried samples were directly mounted on sample stubs and prepared with a chromium sputter-coating to avoid surface charging, and at high vacuum, 7.00 kV. Samples were observed by a Gemini500 scanning electron microscope (SEM) (Zeiss, Germany) and EDS microanalysis were performed using a INCA X-ACT PELTIER COOLED detector (Aztec Energy, Oxford). For any sample, with GeminiSEM there is the possibility of work at variable pressure. Thanks to the Inlens detection signal at high performances, this system carries more signals and details, particularly at very low voltages. These features allow the fast acquisition of crisp images with minimum sample damage and the resolution of nanoscale details. The sample analyzed by SEM-EDS was cut, the surface polished and observed for microanalysis at low pressure. The microanalysis acquisitions were carried out at 12.00 kV.

2D and 3D Modeling of SEM Images by Origin-Pro Software

A small portion from a SEM image, which presented microbial traces, was selected to produce 3D and 2D models. The small portion was processed in GIS environment to simplify each pixel value to a more general surface (x, y and z values represented simplified pixel values). These values were subsequently processed through Origin-pro software (Origin Lab Corporation, Northampton, MA). 3D Colormap and Contour tools were used to obtain both a planar 2D vision and a 3D graph, highlighting peaks and valleys occurring on the surface of the black crusts' specimens.

DNA Extraction and Analysis

Homogeneous samples were taken from the black deposits, stored in Eppendorf and fixed by a DNA fixer. Genomic DNA was extracted from about 0.5 g of solid phase with a bead beating technique using a "NucleoSpin® Soil kit" (Macherey Nagel, Germany), according to the manufacturer's protocol. This kit is designed for the isolation of high molecular weight genomic DNA from microorganisms like Gram-positive and Gram-negative bacteria, archaea, fungi, and algae in soil, sludge, and sediment samples. The DNA was then filtered to remove humic acids that could inhibit the subsequent stages of amplification and sequencing. A specific 16S rRNA protocol has designed to amplify prokaryotes (bacteria and archaea) using paired-end 16S rRNA community sequencing on the Mi-Seq Illumina platform (Bio-Fab Research, Italy). The primers used in this protocol target the 16S rRNA V3 and V4 region (Mizrahi-Man et al., 2013; Choi et al., 2020). Illumina adapter overhang nucleotide sequences were added to the gene-specific sequences. The full-length primer sequences, using standard IUPAC nucleotide nomenclature, to follow the protocol targeting this region are: 16S Amplicon PCR Forward Primer = 5′ TCGTCG GCAGCGTCAGATGTGTATAAGAGACAGCCTACGGGNG GCWGCAG, 16S Amplicon PCR Reverse Primer = 5′ GTCTCGTGGGCTCG GAGATGTGTATAAGAGACAGGA CTACHVGGGTATCTAATCC. These primers were used to amplify template out of the DNA samples by PCR. MiSeq system provides on-instrument secondary analysis using the MiSeq Reporter software (MSR). The Metagenomics workflow obtained, classifies organisms from V3 and V4 amplicon using a database of 16S rRNA data. The classification was based on the SILVA 132 database (https://www.arb-silva.de/). The taxonomic assignments were then checked with LPSN service (https://lpsn.dsmz.de). The data were analyzed by QIIME2 (Bolyen et al., 2019). We analyzed the DNA of both samples separately, but since they were very similar, we then considered them as a single sample for the further elaborations.

RESULTS

Morphological and Geo-Chemical Characterization of Microbial Deposits From Speleothems by SEM and SEM-EDS

To assess microbe-mineral interactions, biogenicity and to describe microbial features and unusual mineral formations, samples were investigated by SEM. **Supplementary Figure S4** shows the optical microscope enlargements of the "Grotta Grande dei Cervi" sample analyzed by SEM and SEM-EDS. **Figure 1** shows the SEM

micrographs obtained from a broken Mn layer. The observations revealed microbial imprints, showing cell-like structures (**Figures 1A,D**) and suggesting that the cell-like shapes occur within internal laminae. Tubular empty sheaths, mineralized cells and pits or holes in the surface produced by bacterial cells also occurred on minerals (**Figure 1C**). Small micro borings, identified as putative paths carved by microorganisms, were observed (**Figure 1B**). Microscopically, the Mn patina shows a layered texture (**Supplementary Figure S4**) where layers of black Mn oxides, about 0.5 mm thick, alternates irregularly with interstices filled with silico-clastic materials. Furthermore, the Mn oxide layers also show an internal structure consisting of an alternation of thin laminae. SEM-EDS chemical map in **Figure 2A** shows that Mn is concentrated almost exclusively in the black laminated layers, but also Ca and, to a lesser extent, C seem to be enriched in these areas of the sample. This could be due to the coprecipitation of calcium carbonate (possibly in the calcite form) during the Mn oxides deposition. On the other hand, Al and Si are concentrated essentially in the interstices between the layers of Mn. This shows that the materials that fill the interstices are insoluble clastic aluminosilicates minerals (quartz, feldspars, clay minerals). Finally, Fe shows a fairly homogeneous distribution, at least in this EDS map. The SEM-EDS map in **Figure 2B**, is a detail of a single layer of Mn and shows that also the fine structure of these layers is an alternation of laminae of Mn oxides with small levels of clastic minerals. The deposition of Mn compounds in the cave could be a reaction to the changes in the hydrogeochemical conditions of the karst aquifer, caused by the formation of the cave and its drying. Based on chemical composition and considering the apparent correlation between Mn and Ca observed in EDS maps (**Figures 2A,B**), it could be inferred that the sample is composed by Mn minerals. Birnessite, todorokite or ranciéite could be the composing phases, as they are the most common minerals in this geological context.

2D and 3D Modeling of SEM Images by Origin-Pro Software

Figure 3 shows the SEM image (**Figure 3A**) processed by Origin-pro software to obtain 2D (**Figure 3B**) and 3D models (**Figure 3C**). In the SEM images is underlined the area which presented microbial traces and that was selected for the construction of the models. The planar 2D model allows areas and perimeters measurements. These parameters can be useful for the evaluation of the potential microbial colonization area. The 3D model represents peaks and valleys. These microzones allow the calculation of 3D volumes. Thus, this 3D elaboration allowed us to simplify the SEM observations and the selection of the zones where microbial biosignatures were more probable found.

DNA Extraction and Analysis

Sequencing and data processing revealed a rather large microbial community in which bacteria predominate. Bacteria accounted

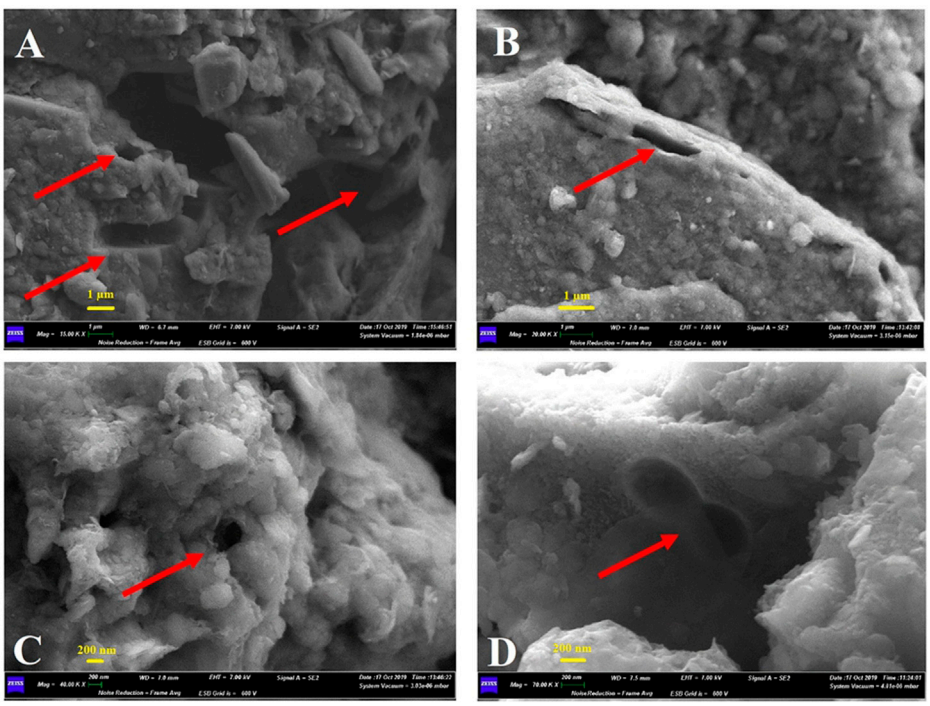

FIGURE 1 | Micrographs of rock sections under scanning electron microscope; **(A)** 15 K magnification that shows clear microbial imprints and pits (scale bar 1 µm); **(B)** 20 K magnification that shows micro borings, identified as putative paths carved by microorganisms (scale bar 1 µm); **(C)** 40 K magnification that shows a clear hole on the surface, probably produced by bacterial cells (scale bar 200 nm); **(D)** 70 K magnification that shows a microbial imprint on the surface, identified as a putative predivisional cell stage typical of staked bacteria (scale bar 200 nm).

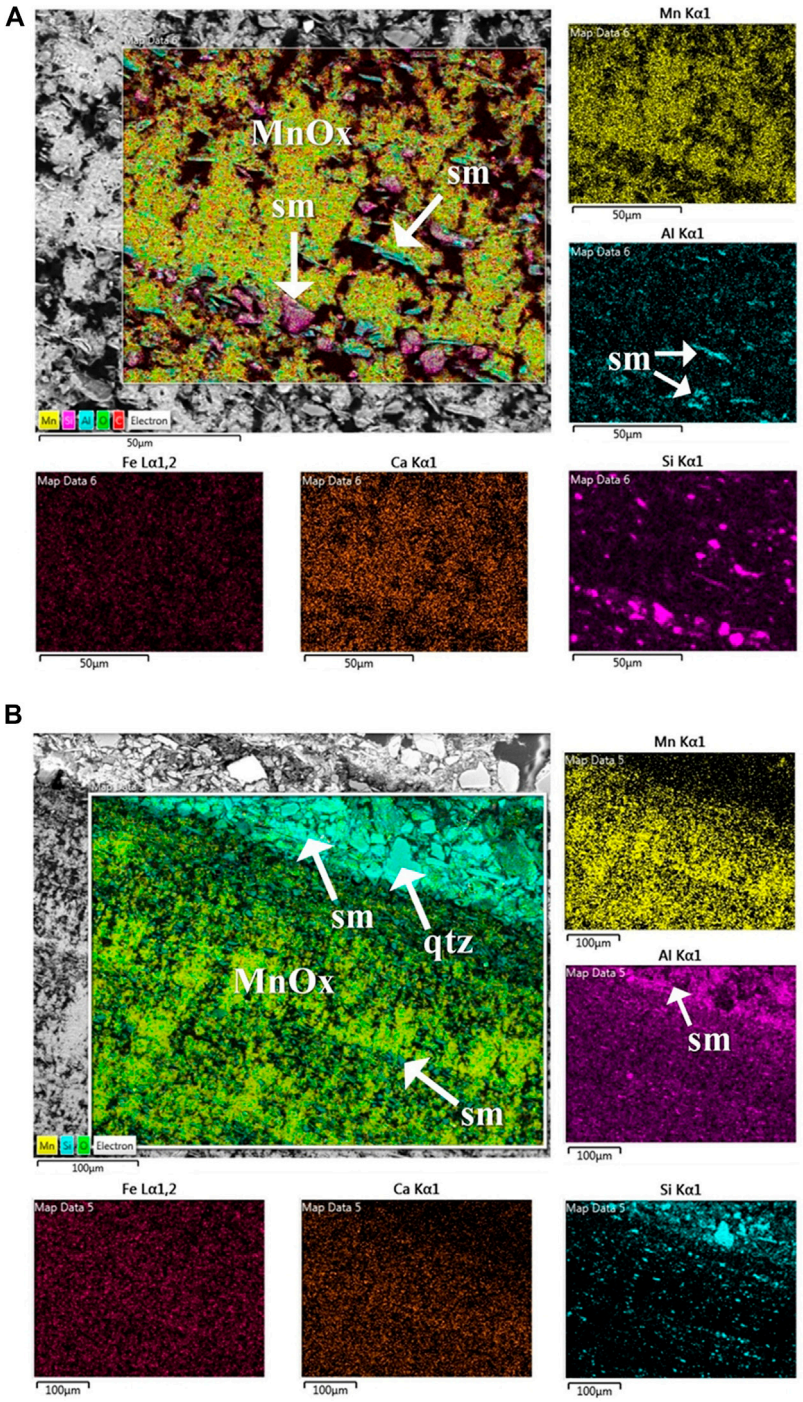

FIGURE 2 | Energy dispersive spectroscopy (EDS) elemental mapping images of a layer deposited on the rock wall, showing the distribution of chemical elements. **(A)** The area of the map is occupied essentially of Ca-bearing Mn oxides (MnOx on the combined map, Mn and Ca maps) intermixed with Fe-oxides and minor silicoclastic minerals (sm in the combined map and in Al map). **(B)** The combined map shows the layered structure of the sample where layers of quite pure Ca-bearing Mn oxides (MnOx on the combined map, Mn and Ca maps) intermixed with very minor siliciclastic minerals (sm in the combined map and in Al map). The grain qtz in the combined map is a grain of quartz, which is the most abundant minerals in the silicoclastic component. Notably, Fe appears homogeneously distributed on all the mapped area (Fe map).

for 99% of the total abundance, while archaea were present to a very limited extent, less than 1%. **Figure 4** shows the bar plot of genera found in the Mn-layer sample. The most common genus (31%) was represented by *Bacillus*, followed by *Flavobacterium* (5%), *Massilia* (3%), *Nitrospira* (3%), *Paenisporosarcina* (2%), *Polaromonas* (2%), *Pseudomonas* (2%), *Lysinibacillus* (2%) and

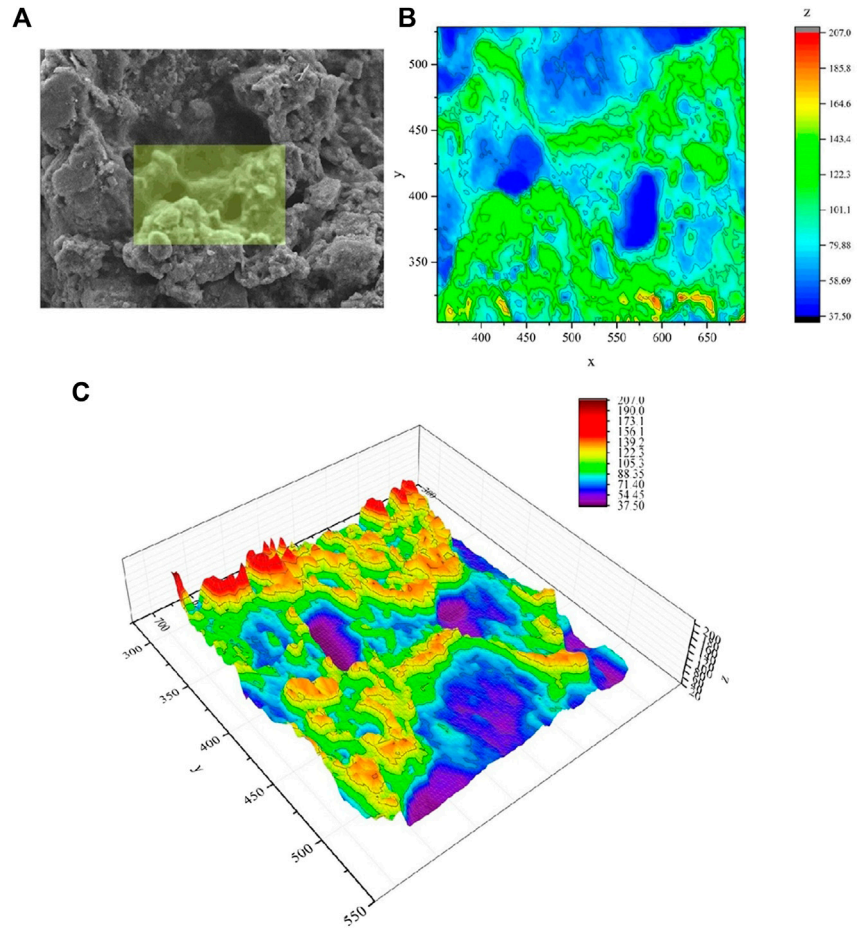

FIGURE 3 | (A) micrograph of the inner section of the crust acquired by scanning electron microscopy (SEM). In the micrograph is highlighted the area processed through Origin-pro software. **(B)** The 2D model obtained from Origin-pro software that allowed to measure areas and perimeters (the units of measure of the axis are in pixels); **(C)** The 3D model obtained from Origin-pro software that allowed to represents microzones (peaks and valleys) useful for the calculation of the volumes and were useful for the detection of potential microbial colonization area (the bar colors and axes units are in pixels).

Candidatus Methylomirabilis (1%). 19% was represented by unknown genera and 6% by uncultured bacteria. The remaining percentage of the community was represented by genera with an abundance of less than 1%. Among them, there was the presence of Mn-oxidazing bacteria genera, such as *Caulobacter* (0.4%), *Pedomicrobium* (0.2%), *Rhodococcus* (0.1%), and *Hyphomicrobium* (0.1%).

DISCUSSION

Caves offer the possibility to characterize and observe conversion from life to biosignature (Uckert et al., 2017). Indeed, microbes often leave detectable traces of their presence long after death (Boston et al., 2001). In addition to microfossils, microbial mats and biofilms can form biofabrics in rocks and bigger assemblies (e.g., microbialites). However, the interpretation of other life by-products (e.g., anomalous concentrations of elements, biologically fractionated isotopic signatures, and biominerals) is more difficult (Westall et al., 2015). Moreover, the detection of life traces could be further complicated by different degree of preservation and processes of post-fossilization alteration.

The implications related to the deposition of cave Mn compounds, in response to hydrogeochemical conditions' changes, have been reported by several authors (Kotula et al., 2019 and references therein). The manganese in the cave might come from chemically reduced water infiltrated within the cave containing chemically reduced and dissolved manganese and soluble complex organic molecules. Mixing of this surface water with cave-stream water-oxygenated, neutral-to-slightly alkaline and bicarbonate-rich - may cause the water to become supersaturated with manganese. Manganese therefore may precipitate under the influence of microorganisms and under anaerobic conditions. Indeed, changes of the hydrogeochemical condition may produce an alkalinity increase and gradual conversion from reducing into oxidizing conditions. This conversion leads to Mn compounds precipitation, generally in the hydroxides form. Manganese bacteria can participate in the

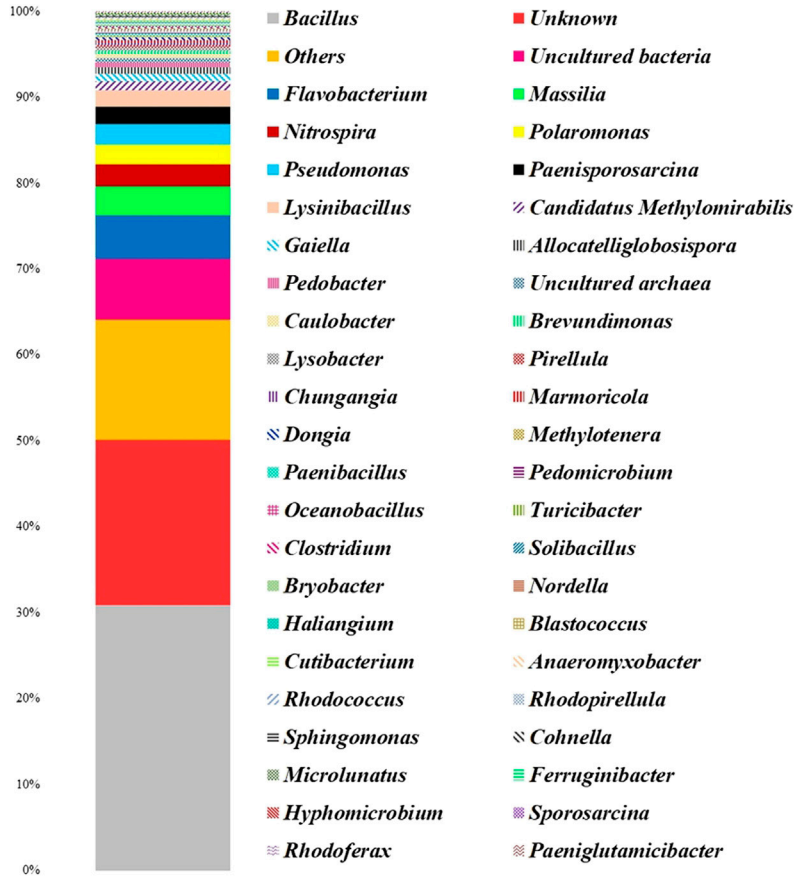

FIGURE 4 | Taxonomy bar chart at the genus level. The genera relative percentages were calculated on the sequencing results obtained from both sequenced samples.

oxidation of Mn, exploiting the energy released from Mn(II) oxidation to Mn(III) and Mn(IV) (Kotula et al., 2019). In these environments, chemolithotrophic microorganisms may perform metal oxidation, such as manganese-oxidation, as a source of energy (Konhauser, 2007). As reported by Spilde et al. (2005), the Al-rich composition confirms that ferromanganese deposits are not speleogenesis left residues. The pH can have a role in the control of the presence of minerals inside the black deposits. Indeed, with a decrease of pH, there is an increased solubility of aluminum (higher solubility of Al^{3+}). However, at neutrality and basic conditions, the control of pH is mainly due to Al(OH)-species. Near neutrality, Al hydroxides are almost insoluble; while, with an increase of pH there is an increase of Al hydroxides solubility. Thus, within a pH range of 6-8, Al is less soluble and hydroxy-aluminium forms are the main compounds present. With pH values lower than 6, the Al is mobilized by aluminosilicate minerals breakdown (e.g., feldspar), with a release of residues rich of Si. Furthermore, there is a pH buffer action by $CaCO_3$-mineralized layer physical-chemically precipitated by CO_2 degassing (Sjöberg et al., 2018). In summary, the abiotic Mn(III/IV) oxidation is not promoted by the acid/neutral pH that characterizes the majority of the surface environments (Spilde et al., 2005). Therefore, in the alkaline environments, there is the dominance of microbial Mn(III/IV) oxide production (Cloutier et al., 2017).

In the Mn deposit analyzed from "Grotta Grande dei Cervi," an abundant and active microbial community was present with several genera already known to be implicated in Mn-oxidation. The most abundant genus in our sample was *Bacillus*, one of the most reported Mn-oxidizer genera (Spiro et al., 2010; Carmichael and Bräuer, 2015 and references therein). Among the other genera with an abundance less than 5%, those reported to be Mn-oxidizers are *Flavobacterium* (Sjöberg et al., 2018), *Pseudomonas* (Carmichael and Bräuer, 2015), *Lysinibacillus* (Johnson et al., 2012), *Polaromonas* (Northup et al., 2003), *Rhodococcus* (Ahmad et al., 2011), *Caulobacter* (Gregory and Staley, 1982), *Pedomicrobium* and *Hyphomicrobium* (Poindexter, 2006; Carmichael et al., 2013). Within this community, is interesting the presence of *Caulobacter*, *Pedomicrobium* and *Hyphomicrobium* genera. The imprint of a putative predivisional cell detected in the Mn layers analyzed by SEM (**Figure 1D**) could correspond to these dimorphic prosthecate bacteria. *Pedomicrobium* and *Hyphomicrobium* genera are both chemoheterotrophic aerobes. Moreover, *Pedomicrobium* Mn-oxidizers deposit manganese on their extracellular acidic polysaccharides (Spilde et al., 2006) and were found within

manganese concretions and in the Lechuguilla Cave punk rock and ferromanganese deposits (Northup et al., 2003). The contribution of Archaea to the microbial communities from the manganese patinas was insignificant (0.6%). However, a few authors related their presence with manganese (Carmichael and Bräuer, 2015).

In this study, SEM-EDS investigations revealed microbial imprints, with characteristic features that showed interactions between microorganisms and minerals. These interactions can represent mineralogical signatures of life. Microbial communities *in situ* preservation via mineralization can be observed in cave environments, even when microorganisms are still alive (i.e., *in vivo* biomineralization) (Boston et al., 2001). The term biomineralization in this context refers to the intern and extern mineralization/lithification of microorganism cells and of the extracellular components of them (e.g., biofilm). Criteria for the identification of fossilized bacteria have been established by several studies (Boston et al., 2001; Iniesto et al., 2015; McMahon et al., 2018). The bacteria preservation in rocks is a valid tool for the exploration of the eldest sign of life on Earth, but also life beyond Earth. McKay et al. (1996) suggested that in Martian meteorites there is the presence of fossil bacteria. However, preparation for SEM analysis can cause microbial biomass loss, extracellular polymeric structures removal and/or dehydration, and mineral alteration. Furthermore, there is the oxidation of living cells organic compounds by manganese, many non-living elements with cell-like structures might create artefacts and microorganisms may leave only a few traces. For these reasons the determination of now alive, once alive, or never alive natural objects' status can be ambiguous. Furthermore, SEM observations can be challenging due to artefacts created by sample preparation or operating conditions. The combination of SEM observations with a modeling program could represent a valid approach to ascertains microbial "macro-imprints" (i.e., putative paths carved by microorganisms and areas occupied by microbial clusters). Thus, the elaboration of SEM micrographs—or areas of them—with 3D models could be useful for the confirmation of biogenic imprints.

After microbe's death, the manganese oxides-rich bacterial capsules seem to disintegrate into granules and be incorporated into the clay structures. The black deposits tubular forms look like Mn- and Fe-encrusted capsules fragments, probably produced by Mn- and Fe-oxidizing bacteria. Thus, the occurrence of Mn-rich black coatings is probably due to the activity of these bacteria (Šebela et al., 2015). For caves of North America, comparable features have been described by White et al. (2009).

A great research effort is needed in order to ascertain either the affiliation of these sheath-forming microorganisms and their metabolic capabilities, most likely related to the oxidation of mineral compounds, for tracing biological processes on early Earth. Nevertheless, the more frequently instances of dubious-fossils and pseudo-biosignatures will be documented and published by the astrobiology community, the more valued will be the speculation about biological biosignatures. Indeed, it is equally important to publish both valuable biosignature and biosignature imposters (Boston et al., 2001).

The study of primitive microbe-mineral interactions and biomineralization processes can be carried out in subsurface, an interesting environment from both a microbiological and mineralogical perspective. Several hypotheses argue that primordial life arisen in the dark early Earth and on other planets' surfaces, thanks to protection from the UV radiation (Tisato et al., 2015). Recent results indicate traces of an early wet Mars and a volcanic activity relatively recent suggesting that organic molecules or traces of microbial life can be present on the subsurface of Mars (Miller et al., 2015). Recently, possible varnish coatings on Martian surface rocks have been discovered. These varnish coatings might protect from UV radiation and other conditions of hostile surface. This stimulates the understanding of the microorganisms' role in the varnish formation (Northup et al., 2010). Moreover, rock varnish layers show microscopic cracks that over time would allow the percolation of any liquid water from fogs or dew over them. This aspect is of utmost interest for astrobiologists because it could allow the migration of any adventitious rock surface microorganisms into the cracks; these microorganisms might colonize the inner and underneath part of the porous rock varnish layers (DiGregorio, 2002). This migration can represent a very important mechanism of survival in hot or cold deserts and probably even on Mars. Thus, micro-borings, holes, tubes and other features related to black deposits can probably host microbial biofilms. Mats and biofilms formation tendency offers same valid benefits (e.g., cohesive community formation, environmental particles trap, immediate chemical, redox, and ionic environment change, needed materials sequester) to organisms that may be expected to live on other planets, under different biological conditions, and perhaps with other chemistries.

The literature on biogenically mediated mineral structures from caves is rather limited. Within Italy, as well as worldwide, new caves continue to be discovered, which may provide potentially unique geochemical environments to be investigated. In any case, the direct investigation of these low-accessible environments is essential, and add value to a research field that is usually more theoretical. Moreover, investigations in pristine environments, protected by law, entails low-impact methodologies similar to Planetary Protection Protocols for extraterrestrial missions. A holistic vision of the subterranean microbiome, assisted by the contribution of other disciplines, could thus clarify many elusive geomicrobiological phenomena and may represent concrete support for exobiological research. In our case, this multidisciplinary approach afforded us aclear evidence of the presence of Mn-oxidizers within the Mn-layer. More in deep studies, with a wider sampling campaign and petrographic and geochemical analyses, need be carried out. However, our preliminary findings demonstrate that the combination of SEM-EDS characterization, 16S rRNA gene sequencing and 3D modeling could represent a valid approach to evaluate the involvement of microbial component in the formation of Mn-secondary deposits.

DATA AVAILABILITY STATEMENT

The Sequencing results and dataset processed by QIIME2 can be found in the Figshare repository (https://doi.org/10.6084/m9.figshare.12771002.v1) as Samples "Grotte4" and "Grotte5."

AUTHOR CONTRIBUTIONS

IV took the lead in data acquisition, processing, analyses and interpretation, and writing the manuscript. FM contributed to laboratory work and data acquisition. MP contributed to data acquisition, processing, manuscript writing and responding to reviews. FB collected samples and analyzed EDS data. MD coordinated and supervised the experimental work and contributed to the writing of the manuscript.

FUNDING

The Scientific committee of the "Club Alpino Italiano" supported the participation to the DULIA-bio Workshop 2019.

ACKNOWLEDGMENTS

The authors wish to thank Maria Giammatteo and Lorenzo Arrizza for SEM-EDS analysis, the Group "Grotte e Forre Francesco de Marchi" for sampling support, the township of Carsoli (L'Aquila) and "Aliena Srl" for sampling authorization, the "uPIX—uNDER PIXel Fotografia Ipogea" for the cave pictures, Simone Bernardini (Roma Tre University) for the useful suggestions, and Cesareo Saiz-Jimenez and Valme Jurado (IRNAS-CSIC) for hosting and supporting IV.

SUPPLEMENTARY MATERIAL

The Supplementary Material for this article can be found online at: https://www.frontiersin.org/articles/10.3389/feart.2021.590257/full#supplementary-material.

REFERENCES

Agostini, S., and Piccini, L. (1994). Aspetti geomorfologici ed evolutivi del sistema carsico di Pietrasecca (M. Carseolani - Appennino Centrale, Italia). *Ist. Ital. di Speleol. Mem.* 5, 61–70.

Ahmad, M., Roberts, J. N., Hardiman, E. M., Singh, R., Eltis, L. D., and Bugg, T. D. H. (2011). Identification of DypB from *Rhodococcus jostii* RHA1 as a lignin peroxidase. *Biochemistry* 50, 5096–5107. doi:10.1021/bi101892z

Barton, H. A., and Northup, D. E. (2007). Geomicrobiology in cave environments: past, current and future perspectives. *J. Cave Karst Stud.* 69, 163–178.

Bolyen, E., Rideout, J. R., Dillon, M. R., Bokulich, N. A., Abnet, C. C., Al-Ghalith, G. A., et al. (2019). Reproducible, interactive, scalable and extensible microbiome data science using QIIME 2. *Nat. Biotechnol.* 37, 852–857. doi:10.1038/s41587-019-0209-9

Boston, P. J. (2000). "Bubbles in the rocks: natural and artificial caves and cavities as life support structures," in *Mars greenhouses: concepts and challenges: proceedings from a 1999 Workshop*. Editors R. M. Wheeler and C. Martin-Brennan (Cape Canaveral, Florida, USA: NASA Technical Memorandum), 9–17.

Boston, P. J., Spilde, M. N., Northup, D. E., Melim, L. A., Soroka, D. S., Kleina, L. G., et al. (2001). Cave biosignature suites: microbes, minerals, and Mars. *Astrobiology* 1, 25–55. doi:10.1089/153110701750137413

Carmichael, M. J., Carmichael, S. K., Santelli, C. M., Strom, A., and Bräuer, S. L. (2013). Mn(II)-oxidizing bacteria are abundant and environmentally relevant members of ferromanganese deposits in caves of the upper Tennessee river basin. *Geomicrobiol. J.* 30, 779–800. doi:10.1080/01490451.2013.769651

Carmichael, S. K., and Bräuer, S. L. (2015). "7. Microbial diversity and manganese cycling: a review of manganese-oxidizing microbial cave communities," in *In microbial life of cave systems*. Editor A. S. Engel (Berlin, München, Boston: De Gruyter), 137–160. doi:10.1515/9783110339888-009

Choi, K., Choi, J., Lee, P. A., Roy, N., Khan, R., Lee, H. J., et al. (2020). Alteration of bacterial wilt resistance in tomato plant by microbiota transplant. *Front. Plant Sci.* 11, 1186. doi:10.3389/fpls.2020.01186

Cloutier, M. L. C., Carmichael, S. K., Carson, M. A., Madritch, M. D., and Bräuer, S. L. (2017). Carbon quantity and quality drives variation in cave microbial communities and regulates Mn(II) oxidation. *Biogeochemistry* 134, 77–94. doi:10.1007/s10533-017-0343-8

Coates, A. J., Jaumann, R., Griffiths, A. D., Leff, C. E., Schmitz, N., Josset, J.-L., et al. (2017). The PanCam instrument for the ExoMars rover. *Astrobiology* 17, 511–541. doi:10.1089/ast.2016.1548

Corenblit, D., Darrozes, J., Julien, F., Otto, T., Roussel, E., Steiger, J., et al. (2019). The search for a signature of life on Mars: a biogeomorphological approach. *Astrobiology* 19, 1279–1291. doi:10.1089/ast.2018.1969

DiGregorio, B. E. (2002). "Rock varnish as a habitat for extant life on Mars," in *Proc. SPIE 4495, instruments, methods, and missions for astrobiology IV*. Editors R. B. Hoover, G. V. Levin, R. R. Paepe, and A. Y. Rozanov, 120–130. doi:10.1117/12.454750

Ficetola, G. F., Canedoli, C., and Stoch, F. (2019). The Racovitzan impediment and the hidden biodiversity of unexplored environments. *Conserv. Biol.* 33, 214–216. doi:10.1111/cobi.13179

Gregory, E., and Staley, J. T. (1982). Widespread distribution of ability to oxidize manganese among freshwater bacteria. *Appl. Environ. Microbiol.* 44, 509–551.

Iniesto, M., Zeyen, N., López-Archilla, A. I., Bernard, S., Buscalioni, Á. D., Guerrero, M. C., et al. (2015). Preservation in microbial mats: mineralization by a talc-like phase of a fish embedded in a microbial sarcophagus. *Front. Earth Sci.* 3. doi:10.3389/feart.2015.00051

Johnson, K. W., Carmichael, M. J., McDonald, W., Rose, N., Pitchford, J., Windelspecht, M., et al. (2012). Increased abundance of *gallionella* spp., *leptothrix* spp. and total bacteria in response to enhanced Mn and Fe concentrations in a disturbed southern appalachian high elevation wetland. *Geomicrobiol. J.* 29, 124–138. doi:10.1080/01490451.2011.558557

Kimble, J. C., Winter, A. S., Spilde, M. N., Sinsabaugh, R. L., and Northup, D. E. (2018). A potential central role of Thaumarchaeota in N-Cycling in a semi-arid environment, Fort Stanton Cave, Snowy River passage, New Mexico, United States. *FEMS Microbiol. Ecol.* 94, fiy173. doi:10.1093/femsec/fiy173

Konhauser, K. (2007). *Introduction to geomicrobiology, microbial weathering*. Oxford, Great Britain: Blackwell Publishing Ltd.

Kotula, P., Andreychouk, V., Pawlyta, J., Marynowski, L., and Jendrzejewska, I. (2019). Genesis of iron and manganese sediments in Zoloushka Cave (Ukraine/Moldova) as revealed by δ13C organic carbon. *Int. J. Speleol.* 48, 221–235. doi:10.5038/1827-806X.48.3.2255

McKay, D. S., Gibson, E. K., Thomas-Keprta, K. L., Vali, H., Romanek, C. S., Clemett, S. J., et al. (1996). Search for past life on Mars: possible relic biogenic activity in martian meteorite ALH84001. *Science* 273, 924–930. doi:10.1126/science.273.5277.924

McMahon, S., Bosak, T., Grotzinger, J. P., Milliken, R. E., Summons, R. E., Daye, M., et al. (2018). A field guide to finding fossils on Mars. *J. Geophys. Res. Planets* 123, 1012–1040. doi:10.1029/2017JE005478

Miller, A., Gonzalez Pimentel, J., Maurer, M., Stahl, S., Castro-Wallace, S., Bessone, L., et al. (2020). "Geomicrobiological field researching a subsurface analogue environment for future planetary caves mission," in 3rd international planetary caves conference, San Antonio, Texas, February 18–21, 2020.

Miller, A., Gonzalez Pimentel, J., Stahl, S., Castro-Wallace, S., Sauro, F., Pozzobon, R., et al. (2018). "Exploring possible Mars-like microbial life in a lava tube from Lanzarote: preliminary results of *in-situ* DNA-based analysis as part of the PANGAEA-X test campaign," in *General assemblies of the European geosciences union (EGU)* (Vienna, Austria: European Geosciences Union (Geophysical Research Abstracts).

Miller, A. Z., Jurado, V., Pereira, M. F. C., Fernández, O., Calaforra, J. M., Dionísio, A., et al. (2015). Cave speleothems as repositories of microbial biosignatures.

EGU General Assembly Conference Abstracts. (AA(IRNAS-CSIC, Seville, Spain), AB(IRNAS-CSIC, Seville, Spain), AC(CERENA, Instituto Superior Técnico, Universidade de Lisboa, Lisbon, Portugal), AD(Grupo de Espeleología Tebexcorade-La Palma, La Palma, Spain). AE(Department of Biology and Geology, Univer), 14276, 2015. Available at: https://ui.adsabs.harvard.edu/abs/2015EGUGA.1714276M.

Miot, J., Benzerara, K., and Kappler, A. (2014). Investigating microbe-mineral interactions: recent advances in X-ray and electron microscopy and redox-sensitive methods. *Annu. Rev. Earth Planet Sci.* 42, 271–289. doi:10.1146/annurev-earth-050212-124110

Mizrahi-Man, O., Davenport, E. R., and Gilad, Y. (2013). Taxonomic classification of bacterial 16S rRNA genes using short sequencing reads: evaluation of effective study designs. *PloS One* 8, e53608. doi:10.1371/journal.pone.0053608

Naylor, L. A. (2005). "The contributions of biogeomorphology to the emerging field of geobiology," in *Geobiology: objectives, concepts, perspectives* (Amsterdam, Netherlands: Elsevier), 35–51. doi:10.1016/B978-0-444-52019-7.50006-1

Noffke, N. (2009). The criteria for the biogeneicity of microbial induced sedimentary structures (MISS) in Archean and younger, sandy deposits. *Earth Sci. Rev.* 96, 173–180. doi:10.1016/j.earscirev.2008.08.002

Northup, D. E., Barns, S. M., Yu, L. E., Spilde, M. N., Schelble, R. T., Dano, K. E., et al. (2003). Diverse microbial communities inhabiting ferromanganese deposits in Lechuguilla and Spider caves. *Environ. Microbiol.* 5, 1071–1086. doi:10.1046/j.1462-2920.2003.00500.x

Northup, D. E., and Lavoie, K. H. (2001). Geomicrobiology of caves: a review. *Geomicrobiol. J.* 18, 199–222. doi:10.1080/01490450152467750

Northup, D. E., Melim, L. A., Spilde, M. N., Hathaway, J. J., Garcia, M. G., Moya, M., et al. (2011). Lava cave microbial communities within mats and secondary mineral deposits: implications for life detection on other planets. *Astrobiology* 11, 601–618. doi:10.1089/ast.2010.0562

Northup, D. E., Snider, J. R., Spilde, M. N., Porter, M. L., van de Kamp, J. L., Boston, P. J., et al. (2010). Diversity of rock varnish bacterial communities from Black Canyon, New Mexico. *J. Geophys. Res. Biogeosciences* 115. doi:10.1029/2009JG001107

Poindexter, J. S. (2006). "Dimorphic prosthecate bacteria: the genera Caulobacter, asticcacaulis, Hyphomicrobium, Pedomicrobium, hyphomonas and thiodendron," in *The prokaryotes*. New York, NY: Springer, 72–90. doi:10.1007/0-387-30745-1_4

Šebela, S., Miler, M., Skobe, S., Torkar, S., and Zupančič, N. (2015). Characterization of black deposits in karst caves, examples from Slovenia. *Facies* 61, 6. doi:10.1007/s10347-015-0430-z

Sjöberg, S., Callac, N., Allard, B., Smittenberg, R. H., and Dupraz, C. (2018). Microbial communities inhabiting a rare Earth element enriched birnessite-type manganese deposit in the Ytterby mine, Sweden. *Geomicrobiol. J.* 35, 657–674. doi:10.1080/01490451.2018.1444690

Spilde, M. N., Northup, D. E., and Boston, P. J. (2006). "Ferromanganese deposits in the caves of the guadalupe mountains," in *Caves and karst of southeastern New Mexico*. Editors L. Land, V. W. Lueth, W. Raatz, P. Boston, and D. L. Love (Socorro, New Mexico: New Mexico Geological Society), 161–166.

Spilde, M. N., Northup, D. E., Boston, P. J., Schelble, R. T., Dano, K. E., Crossey, L. J., et al. (2005). Geomicrobiology of cave ferromanganese deposits: a field and laboratory investigation. *Geomicrobiol. J.* 22, 99–116. doi:10.1080/01490450590945889

Spiro, T. G., Bargar, J. R., Sposito, G., and Tebo, B. M. (2010). Bacteriogenic manganese oxides. *Acc. Chem. Res.* 43, 2–9. doi:10.1021/ar800232a

Tisato, N., Torriani, S. F. F., Monteux, S., Sauro, F., De Waele, J., Tavagna, M. L., et al. (2015). Microbial mediation of complex subterranean mineral structures. *Sci. Rep.* 5, 15525. doi:10.1038/srep15525

Uckert, K., Chanover, N. J., Getty, S., Voelz, D. G., Brinckerhoff, W. B., McMillan, N., et al. (2017). The characterization of biosignatures in caves using an instrument suite. *Astrobiology* 17, 1203–1218. doi:10.1089/ast.2016.1568

Vago, J. L., Westall, F., L. S. Coates, A. J., Jaumann, R., Korablev, O., et al.Pasteur Instrument Teams (2017). Habitability on early Mars and the search for biosignatures with the ExoMars rover. *Astrobiology* 17, 471–510. doi:10.1089/ast.2016.1533

Westall, F., Foucher, F., Bost, N., Bertrand, M., Loizeau, D., Vago, J. L., et al. (2015). Biosignatures on Mars: what, where, and how? Implications for the search for martian life. *Astrobiology* 15, 998–1029. doi:10.1089/ast.2015.1374

White, W., Vito, C., and Scheetz, B. (2009). The mineralogy and trace element chemistry of black manganese oxide deposits from caves. *J. Cave Karst Stud.* 71, 136–143.

Conflict of Interest: The authors declare that the research was conducted in the absence of any commercial or financial relationships that could be construed as a conflict of interest.

frontiers in Astronomy and Space Sciences

ORIGINAL RESEARCH
published: 14 August 2020
doi: 10.3389/fspas.2020.00050

There's Plenty of Room at the Bottom: Low Radiation as a Biological Extreme

Jennifer Wadsworth[1]*, *Charles S. Cockell*[1], *Alexander StJ Murphy*[1], *Athoy Nilima*[1], *Sean Paling*[2], *Emma Meehan*[2], *Christopher Toth*[2], *Paul Scovell*[2] and *Leander Cascorbi*[3]

[1] School of Physics and Astronomy, University of Edinburgh, Edinburgh, United Kingdom, [2] Boulby Underground Laboratory, Saltburn-by-the-Sea, United Kingdom, [3] Trinity College, Oxford University, Oxford, United Kingdom

The effects of high radiation as a biological extreme have historically been, and continue to be, extensively researched in the fields of radiation biology and astrobiology. However, the absence of radiation as an extreme has received relatively limited attention from the scientific community, with its effects on life remaining unclear. The currently accepted model of the radiation dose-damage relationship for organisms is the linear no-threshold (LNT) model, which predicts a positive linear correlation between dose and damage that intercepts at zero dose corresponding to zero damage. Despite its wide-spread implementation, the LNT model is continuously being challenged by various new models, with the hormesis model as one of its main competitors. This model also postulates damage at high doses but, in contrast to the LNT model, it predicts beneficial stimulation of growth at low doses. Experiments to date have not yet been able to conclusively validate or dismiss either of these models. The aim of the collaborative Subsurface Experiment of Life in Low Radiation (SELLR) project was to test these competing models on prokaryotes in a well-characterised environment and provide a robust experimental set up to investigate low radiation in terrestrial and non-terrestrial environments. Bacterial growth assays using *Bacillus subtilis* and *Escherichia coli* were performed under ultra low ionising radiation in the Boulby International Subsurface Astrobiology Laboratory (BISAL) facilities of the Boulby Underground Laboratory at Boulby mine (Redcar & Cleveland, UK) and were used to investigate effects on viability and signs of preconditioning. No significant effect on bacterial growth was observed from exposure to radiation doses ranging from 0.01 times the levels of background radiation typically found in terrestrial surface environments to 100 times that background. Additionally, no preconditioned susceptibility to stress was observed in the bacterial strains grown in sustained low radiation. These data suggest that the extremes of low radiation do not alter growth parameters of these two organisms and that an improved model should be considered for prokaryotes, consisting of a dose-damage response with a threshold at ultra low radiation. We discuss the implications of these data for low radiation as a novel microbiological "extreme."

Keywords: subsurface microbiology, low radiation, extreme habitat, dose response, threshold model

OPEN ACCESS

Edited by:
Geoffrey Battle Smith, New Mexico State University, United States

Reviewed by:
Evgenios Agathokleous, Nanjing University of Information Science and Technology, China
Oliver Strbak, Comenius University, Slovakia

***Correspondence:**
Jennifer Wadsworth
jenn@wadsworth.ch

Specialty section:
This article was submitted to Astrobiology, a section of the journal Frontiers in Astronomy and Space Sciences

Received: *05 May 2020*
Accepted: *06 July 2020*
Published: *14 August 2020*

Citation:
Wadsworth J, Cockell CS, Murphy AS, Nilima A, Paling S, Meehan E, Toth C, Scovell P and Cascorbi L (2020) There's Plenty of Room at the Bottom: Low Radiation as a Biological Extreme. Front. Astron. Space Sci. 7:50. doi: 10.3389/fspas.2020.00050

INTRODUCTION

Radiation biology research is mostly conducted in the context of effects of, and protection from, high radiation exposure such as from radioactive fallout and medical treatments (e.g., de González and Darby, 2004; Preston et al., 2004; Finch, 2007). In this regard, the field of Astrobiology is no exception with a seemingly exclusive focus on the effects of the high radiation conditions of low Earth orbit, interplanetary space, and other planetary environments on organisms (e.g., Horneck, 1992; Moeller et al., 2017; de Vera et al., 2019). The historical and continuing scientific focus on high radiation is by no means unfounded, as the connection between irradiation from an ionising or an energetic radiation source and biological damage, resulting in mutations or cell death, is well-established (Lorenz, 1944; Wanebo et al., 1968; Chang et al., 1985; Ward, 1988). However, extreme opposites of physical variables exist and, to use the title of Richard Feynman's (1959) address to the annual American Physical Society meeting at Caltech (Feynman, 1960), there's "plenty of room at the bottom" of the radiation dose range to explore as a physical extreme. In order to build a holistic understanding of how environmental parameters shape the viability potential of life on Earth and, by extension, on other planetary bodies, all parameter extremes should be examined.

All life on Earth is constantly being subjected to a low dose of naturally occurring radiation in various forms. For example, non-ionising ultraviolet (UV) light (UVA = 315–400 nm, UVB = 280–315 nm) from the sun can pass through the Earth's atmosphere and reach us, sometimes causing skin melanomas (International Agency for Research on Cancer, 1992). Of the naturally occurring radiation, ionising radiation is of particular significance due to its increased potential for causing biological damage (e.g., Prise et al., 2001). Rock radionuclides from various long-lived radioisotopes, such as uranium, thorium and potassium, and cosmic rays are sources of natural ionising radiation (Hamilton, 1989; Shahbazi-Gahrouei et al., 2013). Moreover, airborne radon and its decay radionuclides contribute to more than half the total average worldwide dose rate of naturally occurring radiation of ∼2.8 mGy/y. With additional man-made radiation, the mean global surface radiation dose rate is estimated to be ∼3.01 mGy/y (United Nations, 2008), although this can vary locally e.g., 0.6 mGy/y measured at the Boulby mine surface to 260 mGy/y in Ramsar, Iran (Ghiassi-Nejad et al., 2002). Usually, doses/dose rates below the global or local background dose average are referred to as "low" or "ultra low" doses in low radiation studies.

There are currently three main ideas on how a low radiation environment might influence an organism's viability: (1) Any amount of radiation, however small, will negatively impact viability and continue to do so in a linear manner ("linear no-threshold" model), (2) A hyperbolic dose-damage response to low radiation in the form of either hypersensitivity or positive stimulation (the latter being the "hormesis" model), which would be a unique property among extreme conditions. In the hormesis model, low levels of ionising radiation are therefore beneficial for life, and (3) At some low level of radiation there is no effect on life, with a threshold below which there is no discernible effect on cellular physiology or growth parameters. However, above the determined threshold the radiation dose-damage continues in a linear manner. This is known as the "threshold" model (e.g., Mancuso et al., 2012; Siasou et al., 2017; **Figure 1**). Since the mid-twentieth century, the generally accepted model for describing an organism's radiation dose-response relationship has been the linear no-threshold (LNT) model (Muller, 1946; **Figure 1**), which was further supported by the National Research Council (NRC) (2006). The LNT model is largely based on studies in above-background radiation conditions, i.e., high radiation exposure. Radiation-induced mutations in rats in the early twentieth century (Olson and Lewis, 1928), and subsequent research on fruit fly exposure to high radiation doses (10^3 times background dose) served as the basis for development of the LNT model (Muller, 1954). However, subsequent studies have indicated that when dealing with lower doses, the LNT model may not be applicable (e.g., Calabrese and Baldwin, 2003; Feinendegen et al., 2007; Smith et al., 2011; Shamoun, 2016; Shibamoto and Nakamura, 2018; Costantini and Borremans, 2019).

Despite the long-standing application of the LNT model, it is strongly contested in the literature by proponents of the hormesis (hormetic) model (**Figure 1**), who argue that the LNT model is not representative of the cellular response to lower radiation doses and dose rates (e.g., Feinendegen et al., 2007). The principle of hormesis is based on a low dose stimulatory effect of a physical or chemical component that, at high doses, has an inhibitory effect (Lorenz, 1950; Stebbing, 1982; Mine et al., 1990). Additional, less prevalent hypotheses include the "threshold" and "sensitization/hypersensitivity" models, with the former proposing a lack of impact below a certain dose range and the latter serving as an opposite to hormesis, implying an increased negative effect on viability at low dose exposure (**Figure 1**). Although it is reasonable to presume the LNT model is also applicable to prokaryotes at higher doses of radiation, there is still no definitive consensus within the scientific community on the effects of low radiation exposure on microbes (**Figure 1**).

Here we present data from the Subsurface Experiment of Life in Low Radiation (SELLR) project on the effects of below background radiation on the growth of *Bacillus subtilis* and *Escherichia coli*. We also describe a robust experimental set-up that allows for the study of prokaryotic biology at below background levels of radiation using an underground astrobiology laboratory. The aim of the Subsurface Experiment of Life in Low Radiation (SELLR) project, described in this work, is to provide a well-controlled and characterised experimental set up with minimal variables in which comparable bacterial growth experiments can be carried out. The robust set up establishes a baseline study for future work simulating low radiation (planetary) environments.

MATERIALS AND METHODS

Previous low radiation experiments (i.e., below the local terrestrial surface radiation doses) have been carried out in various facilities by research groups examining a variety of cells and with different experimental set-ups. Furthermore, when

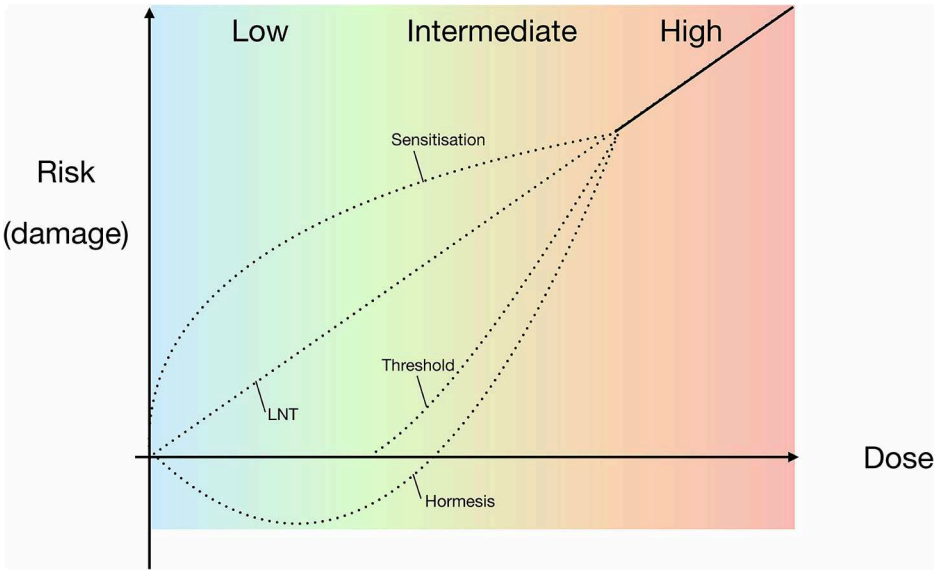

FIGURE 1 | Proposed models for experimental and theoretical correlations of radiation dose and the risk of damage to organisms, including the widely accepted LNT model. Models are based on high-dose data, extrapolating responses for lower dose ranges. High doses are defined as those causing observable, serious or irreparable damage to an organism. The dotted lines indicate the potential models that may be applicable to prokaryotes in the intermediate and low radiation does ranges, i.e., either side of background radiation up until high doses. LNT = linear relationship between dose and risk of damage to an organism; sensitivity = a heightened risk of damage at lower doses; hormesis = high dose inhibition with low dose stimulation; threshold = no/negligible risk of damage below a specific dose.

establishing and working in a low radiation experimental set up there are additional factors to those of standard experiments to consider. This and the lack of a universal, gold-standard low radiation set up has continued to impede the comparability of data in low radiation literature. **Table 1** illustrates some of the potential experimental difficulties in a low radiation set up and the experimental design adjustments that were adopted for the SELLR project to avoid the outlined issues.

Experimental Overview

Two prokaryotic model organisms were grown in the low radiation, underground experimental set-up that consisted of two identical plate readers housed in a lead "castle" to further reduce radiation exposure. Within the castle, the plate readers were separated by a lead brick wall, such that one half of the castle provided the ultra low radiation environment whilst the other half provided an artificially created background radiation environment mimicking that of the local surface, established using a ^{137}Cs source (**Figure 2**). The model organisms were then grown in the plate readers for varying lengths of time in the low radiation environment and the artificial background radiation environment, which served as the control. After growth in either radiation condition, the organisms were briefly exposed to UVC to test potential differences in stress response.

Location and Radiation Set-Up

Unless specifically stated, all experiments were carried out in the Boulby Underground Laboratory at the Boulby Mine, Redcar & Cleveland UK. At 1.1 km depth, the rock accounts for a cosmic ray attenuation by a factor of 10^6 (Reichhart et al., 2013). Any changes caused by the attenuation to the cosmic ray energy spectrum are assumed to be irrelevant as the cosmic rays are of high enough energies to be minimally ionising, such that energy deposition by muons and secondary neutron spallation rates will scale linearly with absolute cosmic ray flux.

With the cosmic ray flux minimised, the Boulby Laboratory is particularly well-suited to provide radiation protection as the local salt has low natural background radiation, with low levels of γ-ray and neutron emission. Moreover, the salt and general geographical area of Boulby have a low rate of radon production, resulting in an airborne background level of 2.4 Bq/m^3 (Araújo et al., 2012). To establish an ultra low radiation environment, the experiments were additionally encased in a radon-free lead-lined container (castle). This resulted in a 100-fold reduction of the average local ionising surface radiation dose rate (see the following method sections for details on the radiation environment). To reduce systematic uncertainties, measurements were performed in two experimental stations, formed by partitioning the lead-lined container in to two equal halves, separated by a 10 cm-thick wall formed of low-radioactivity lead bricks. Identical SPECTROstar Nano plate readers (BMG Labtech) were then positioned in each half of the lead-lined box (**Figure 2**).

To achieve elevated (above low background radiation doses), a ^{137}Cs source was placed above one of the plate readers to artificially generate surface radiation doses, and up to 100 times higher, while with no such source, the samples in the other plate reader provided well-defined controls. The ^{137}Cs source was used to approximate ionising radiation biological damage on the surface, recognizing that it is difficult to artificially reconstruct

TABLE 1 | Potential problems facing low radiation experiments and the respective adjustments made for the SELLR experimental set up.

Potential issues for low radiation experimental set ups	SELLR Set Up adjustments
Lack of controls in identical conditions. In the case of underground experiments and ground controls, differences such as air pressure and humidity between surface and sub-surface environments can skew bacterial growth results.	Controls were situated underground with the low radiation samples. An artificial radiation source was used to provide surface and above surface radiation dose exposure; all other parameters were identical.
Model organisms used were known to be radio-resistant and would not show representative effects of low radiation exposure of the majority of microbes.	Well-characterised environmental model organisms were used to represent Gram positive and negative microbes without specific radio-resistance.
Use of end-point analysis of growth curves, which limit analysis of the full growth curve and the possible effects of below background radiation on different parts of the growth curve.	Analysis of radiation impact on the whole growth curve so that the linear exponential growth phase (growth rate) could be determined as well as final growth parameters.
Lack of replicates and sufficient time points to examine growth data.	Continuous measurement of growth curves to determine bacterial growth rate, large number of replicates, and experiment repetition.
Only two doses tested (background radiation and low radiation); insufficient to plot or rule out different models.	Low, artificial background radiation, 10× and 100× artificial background radiation doses were used in identical experimental set-ups for multiple dose data points.
Reliant on simulation of low radiation environment dose, with no *in situ* confirmation of real dose environment.	Simulation and *in situ* measurement of low and artificial background radiation environment.

the complete spectrum of natural radiation of the surface in a confined subsurface laboratory environment. The temperature of both plate readers was internally controlled, the outside temperature was constant at 22°C (±1°C) and 82% relative humidity (± 2%).

Artificial Background and Low Radiation Environments

Theoretical Dose Rates

Both the low dose and control samples were located in the same sub-surface experimental set up (described in section Location and Radiation Set-Up) to avoid differences in environmental conditions.

Control samples were exposed to a 15.5 MBq (± 0.1 MBq) ^{137}Cs γ-source to approximate a natural surface background radiation dose rate. The collimated but unattenuated source provided a dose rate of $D = 27.8$ mGy/y (± 0.506 mGy/y) at a 59 cm height from the top of the 96-well plate, which was lowered to 1 mGy/y by placing lead sheets between the source and samples. It was calculated that 11 lead sheets (3.3 cm total thickness) would be required to attenuate radiation from the ^{137}Cs γ-source to obtain a final dose rate comparable to that measured at the local surface (∼0.18–0.6 mGy/y).

To generate higher dose rates $D(r)$ of 10 × and 100 × background, the inverse square rule is applied.

$$D(r) = \left(\frac{59\ cm}{r}\right)^2 \times D(59\ cm)$$

As the distance r between source and sample is decreased, the difference in local dose rates across the plate becomes more significant, i.e., as the source is moved closer to the samples there is a larger discrepancy between the dose rate of the centre of the plate compared to that of the periphery. It was calculated that for our maximum dose rate used (100 mGy/y) the maximum difference in dose rate across the plate would be 3.3 mGy/y.

Measured Dose Rates

A series of measurements were taken to establish the *in situ* dose rates of the artificial background radiation and low radiation environments. The measurements were taken with a NaI detector (InSpector 1000 with an IRPOS-2: Stabilised 2" × 2" probe), which gives real time values with a minimum dose rate equivalent of 10 nSv/h (0.088 mSv/y). Measurements of the unattenuated source yielded an absorbed dose rate of $D(0) = 29.9$ mGy/y ± 0.5 mGy/y and the 11-lead sheet-shielded dose rate of D (3.3 cm lead) = 1.067 mGy/y ± 0.2 mGy/y. The higher measured value than the theoretical value for the unattenuated source dose rate is consistent with measurement errors and backscattering of γ-rays from the walls of the lead castle. The measured dose rate within the castle with the lid closed and without the source was 0.0044 mGy/y, a reduction to ∼1% natural background radiation. The measured local surface dose rates at Boulby ranged from 0.18 to 0.6 mGy/y. These were measured once at the beginning of the SELLR project with the same detector as stated above.

Intrinsic Radiation From Experimental Apparatus

Due to the need to ensure an ultra low radiation environment, the internal intrinsic radiation of both the equipment and the samples had to be established to quantify the contribution to the final radiation dose. The radioactivity of the components used in this experiment was determined using γ-ray spectroscopy at the Boulby Underground Germanium Suite (BUGS). BUGS operates several low-background high purity germanium detectors in the Boulby Underground Laboratory (Scovell et al., 2018). This technique measures γ-ray emission associated with the decay of radioisotopes (usually U/Th/K along with anthropogenic radioisotopes) found in all materials and uses the detected flux to calculate a specific activity for each (Gilmore, 2011). This technique is widely used in material radio-assay for low-background particle physics experiments (Araújo et al., 2012; Abgrall et al., 2016; Aprile et al., 2017) where even small contaminations can severely impact detector sensitivity to rare event searches. For SELLR, the plate readers, plates and 500 mL of bacterial growth media (with and without bacteria) were assayed. Each sample was placed on a germanium detector for ∼1 week.

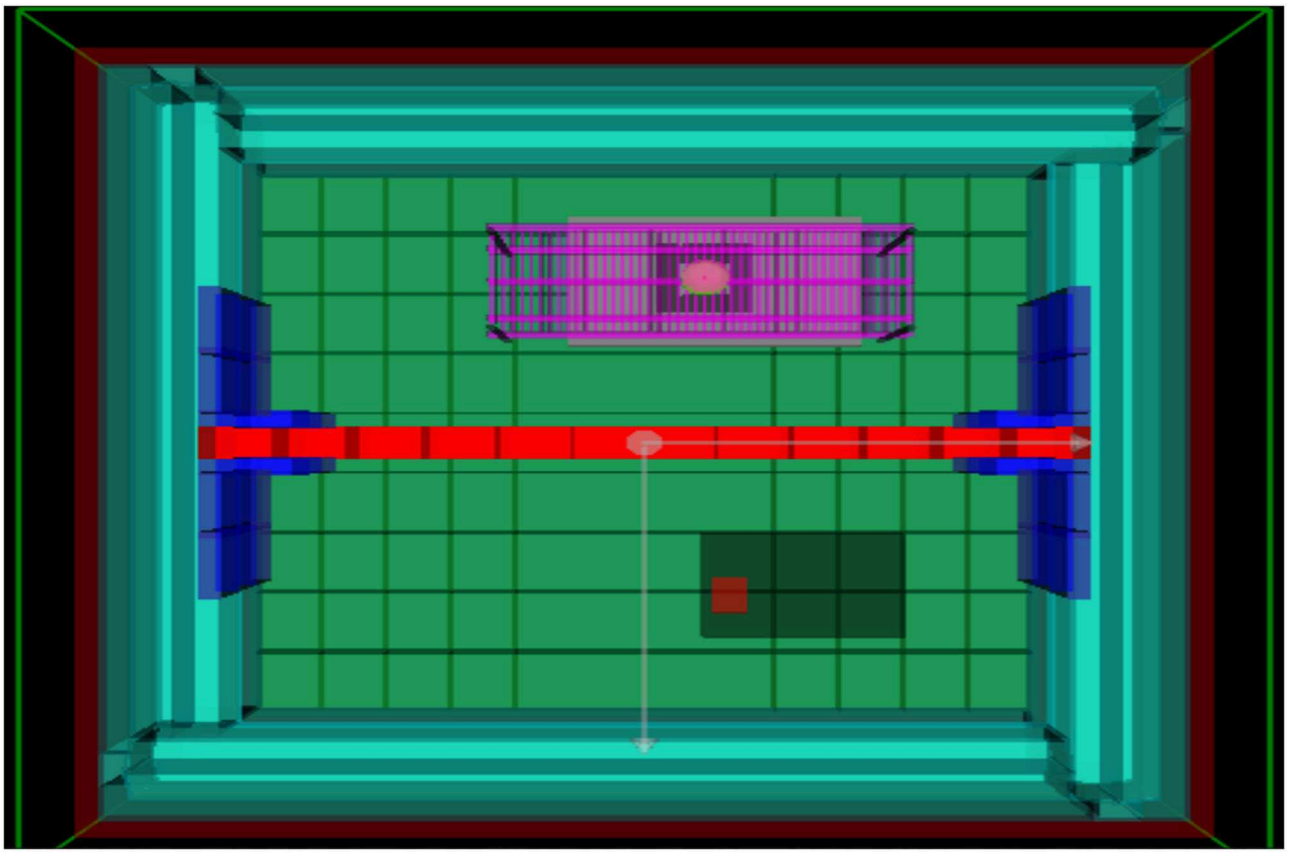

FIGURE 2 | Geometry of lead-lined chamber in GEANT4, view from above. The lead wall is marked in red, separating the container into a low and artificial background radiation environment. The ^{137}Cs γ-source is located on the purple platform above the one plate reader, providing the artificial background radiation.

From this, it was possible to determine that the potassium activity of all the constituent parts was substantially sub-dominant to the potassium activity of the bacteria. **Table 2** shows the bacterial radiation contribution.

The highest internal nuclide activity from the bacterial sample was potassium (^{40}K), which undergoes β-decay (1,311 keV end point energy with an 89% branching ratio) and electron capture (10.7% branching ratio, almost always followed by a 1,461 keV γ-ray emitted from the ^{40}Ar daughter). Values of other nuclides are upper limits as they are below the sensitivity of the detector. The expected dose rate due to potassium is:

$$D_{K-40} = 0.0273\ mGy/y \pm 0.00352 mGy/y$$

and the expected maximum absorbed dose rate due to other nuclides is given by:

$$D_{other} < 0.17104\ mGy/y$$

Although the expected dose rate of nuclides (excluding potassium) would exceed the levels necessary for the low radiation experiments, these values are the expected maximum calculated at 90% confidence level. The true values—and, by extension the true dose rate—are therefore highly likely to be below the maxima shown in **Table 2** and below the expected dose rate. To further constrain the actual experimental radiation environment, additional simulations, and *in situ* measurements were also carried out (see sections Artificial Background and Low Radiation Environments and Radiation Simulation).

TABLE 2 | Dose contribution of nuclide series in the bacterial sample (growth media + *B. subtilis* inoculate).

Nuclide series	Activity in [Bq/kg]
^{238}U(e)	–
^{238}U(l)	<0.4
^{232}Th(e)	<0.6
^{232}Th(l)	<0.4
^{40}K	11.5 ± 1.5
^{60}Co	<0.1
^{235}U	<0.8

Radiation Simulation

To understand the radiation environment in the lead-lined castle, the entire experimental set up was constructed in GEANT4, and

TABLE 3 | SELLR experiment nomenclature for *B. subtilis* replicate experiments and *E. coli* experiments indicating growth time, radiation exposure, and the week of experimental execution; art., artificial.

Sample name	Growth time	Radiation exposure	Organism
B1	48 h	Low and artificial background	*B. subtilis*
B2	24 and 48 h	Low and artificial background	*B. subtilis*
B3	24 and 48 h	Low and artificial background	*B. subtilis*
10 ×	24 h	Low and 10 × background	*B. subtilis*
100 ×	24 h	Low and 100 × background	*B. subtilis*
E. coli	24 and 48 h	Low and artificial background	*E. coli*

known radiation sources were added to simulate the resulting radiation. GEANT4 is a toolkit using Monte Carlo methods for simulating the passage of particles through matter (Agostinelli et al., 2003). This simulation was performed to provide insight into possible daughter particle radiation that must be taken into consideration when establishing the artificial background and low radiation environments. Radiation from a variety of sources was simulated, including the ^{137}Cs source, radon from the air, activities in the surrounding bedrock, and lead in the castle. Uranium and thorium decay chains were assumed to be in secular equilibrium. It was concluded that γ-rays from the decay chains of uranium-thorium-potassium contamination in lead and the decay products of airborne radon could result in a $\sim$0.1 mGy/y contribution to the radiation background in both halves of the castle. However, due to the higher dose contribution of the growth medium (see section Intrinsic Radiation From Experimental Apparatus) the contribution of the airborne radon was discounted. Additionally, the simulation showed the ^{137}Cs source used to produce the artificial radiation environment resulted in an additional dose rate of 314 nGy/year in the shielded, low radiation part of the castle. This value is however low enough to not significantly contribute to the low radiation environment.

Model Organism Selection

Bacillus subtilis (strain 168, DM 402) and *Escherichia coli* (MG 1655) were chosen as model organisms to test the effect of low radiation doses on microbial growth. Both microbes are well-characterised environmental bacteria that can be cultured in the laboratory and were chosen to represent Gram positive and negative bacteria, respectively. Both have approximately the same, short doubling time of $\sim$20 min, which allows for an efficient collection of multiple growth curves. Neither is classed as radio-resistant. We deliberately chose these characteristics to maximise the likelihood of detecting a response to the low radiation doses.

Cell Growth Set-Up

Bacillus subtilis and *E. coli* were grown in the artificial background and low radiation environments for 24 and 48 h. In some experiments, the dose rate was increased to 10 × and 100 × artificial surface background radiation by adjusting the distance of the ^{137}Cs source to the samples. The gradient of the bacterial exponential growth phase (growth rate) was determined, to establish whether either radiation environment had an effect on the bacterial growth. In addition to affecting growth rate, previous research (Satta et al., 1995) has claimed that prolonged exposure to a low radiation environment leaves cells more sensitive to stress factors, such as toxins or exposure to brief increases in radiation. To investigate this hypothesis, *B. subtilis* and *E. coli* were subjected to brief UVC radiation exposure after growth in the different radiation environments (see section UV Radiation Exposure).

Bacterial Growth Experiments

Because of the limited access to the mine, the growth experiments were performed in blocks of 5–6 days at a time. The terminology of "week 1, 2.." refers to the week in which the set of experiments was carried out, for ease of comparison (see **Table 3** for experimental nomenclature). To obtain aliquots of bacteria for the experiments, monocultures of *B. subtilis and E. coli* were grown at 37°C before being frozen into 25% glycerol 1 mL-aliquots and stored at −80°C at the University of Edinburgh. To obtain overnight cultures for experiments, 40 mL of nutrient broth was inoculated with 10 μL of thawed aliquots and cultured overnight at 37°C before use in the experiments. This was done at the overground laboratory at Boulby. The culture was then brought down to the underground laboratory at the beginning of each experimental run. At the beginning of each growth experiment, 5 μL of culture was added to 84 wells of a 96-well plate containing 200 μL of fresh nutrient broth. The last row of the plate contained only nutrient broth to serve as a blank for the plate reader. *B. subtilis* was grown at 30°C and *E. coli* at 37°C, respectively, for 24 h, with optical density (OD_{600}) measurements being taken every 20 min to coincide with both bacterial doubling times. For the 48 h experiments, 5 μL of the 24 h culture was added to 84 wells of a 96-well plate containing 200 μL of fresh nutrient broth and grown for 24 h under the same conditions as it was in the previous 24 h. The reason for having both 24 and 48 h growth data was to determine whether an extended period of exposure to the low radiation environment accentuated any observed responses in bacterial growth. This also gave us information on an increased number of generations, with 48 h resulting in $\sim$144 generations for both *B. subtilis* and *E. coli*.

UV Radiation Exposure

In order to assess whether the microbes' ability to cope with stress was influenced by growth in the various radiation environments, cells were exposed to a short pulse of UVC and their viability was assessed by plating on Oxoid (LP0011) nutrient agar. Immediately after being grown for the specified amount of time in the respective radiation environments, the plates were irradiated with a monochromatic UVC lamp ($\lambda = 254$ nm; I = 11.2 W/m^2; formally UVP Company now Analytik Jena AG) at distance of 5 cm for 30 s. Triplicates were selected from random wells of each condition and serially diluted by a factor of 10^6. One hundred microliters of each triplicate was plated in triplicate on nutrient agar and cultured overnight at 37°C. All steps of the UVC exposure and cultivation were conducted underground.

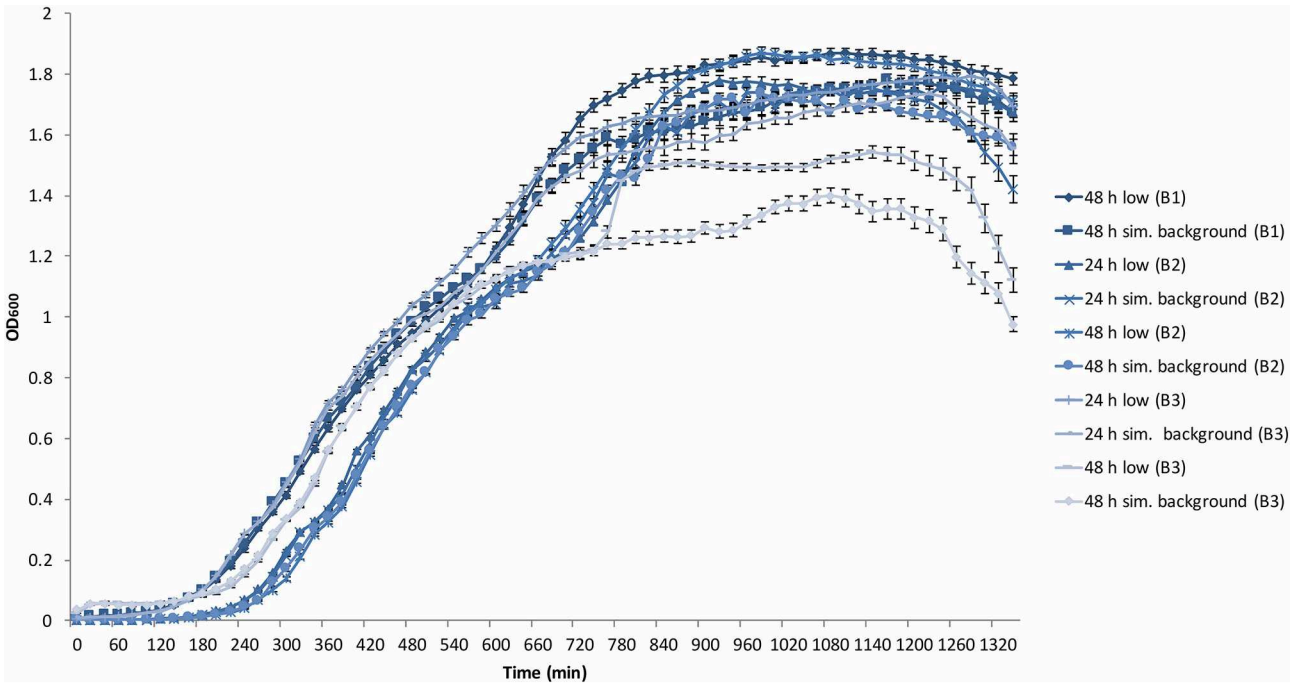

FIGURE 3 | Average ($n = 84$) of *B. subtilis* growth curves at the determined low radiation (low) and artificial background radiation ("sim. background") dose rate: 24 and 48 h denote time in hours that bacteria batch has spent in respective conditions; B1-3 = experiment run number. Error bars show ± standard error ($n = 84$).

Experimental Nomenclature

Three replicate low and artificial background radiation experiments were run with *B. subtilis*. For clarity when presenting these results, each set of experiments will be referred to with the nomenclature in **Table 3** to differentiate between experimental runs. Whether the data is from the low or artificial background environment, and whether it is from the 24 or 48 h growth curves, will be stated in the text and figures. Henceforth, the one half of the experimental set up with 1% background radiation environment will be referred to as the "low" condition. The experimental set up involving enhanced radiation (background, 10 × and 100 × background radiation) containing the ^{137}Cs source will henceforth be referred to as the "artificial background" condition.

Analysis

All plate reader experiments were performed using 84 replicates; UV experiments were performed in triplicate with each triplicate plated on three agar plates. Numbers in figures show averages of replicates, error bars show standard error (s.e.) among replicates. Gradients of the exponential growth phases were established by an automated, linearly-fit trendline in excel. Error of gradients was calculated using the LINEST function in excel. Growth rates were calculated with the equation:

$$\mu = \frac{lnOD_2 - lnOD_1}{t_2 - t_1}$$

which when converted to the decadic logarithm becomes:

$$\mu = \frac{2.303(logOD_2 - logOD_1)}{t_2 - t_1}$$

OD_1 and OD_2 as well as respective t_1 and t_2 were determined in each growth curve as the beginning of the exponential growth phase. Statistical analysis was performed using one-way ANOVA and two-tailed unpaired equal variance Student's *t*-tests, where $p < 0.05$ was considered significant. Analysis of the bacterial growth curves focused on the linear exponential growth phases, which were most comparable and were used as a proxy for the relative fitness of each sample. When a non-linear "shoulder" in the exponential growth phase was observed, only data from the primary linear phase was used to calculate gradients.

RESULTS

Overview of Bacterial Growth in Low and Artificial Background Radiation

Variations in growth were observed between experimental runs, but not between the differing radiation conditions.

All *B. subtilis* samples progressed through the lag, exponential and stationary growth phases. The upper cluster of final yield data in **Figure 3** contained data points from the 48 h B1 data, 24 and 48 h B2 data, as well as the B3 24 h data, whilst the lower cluster contained all B3 48 h data points. Each growth curve showed the presence of a "shoulder" in the exponential growth phase

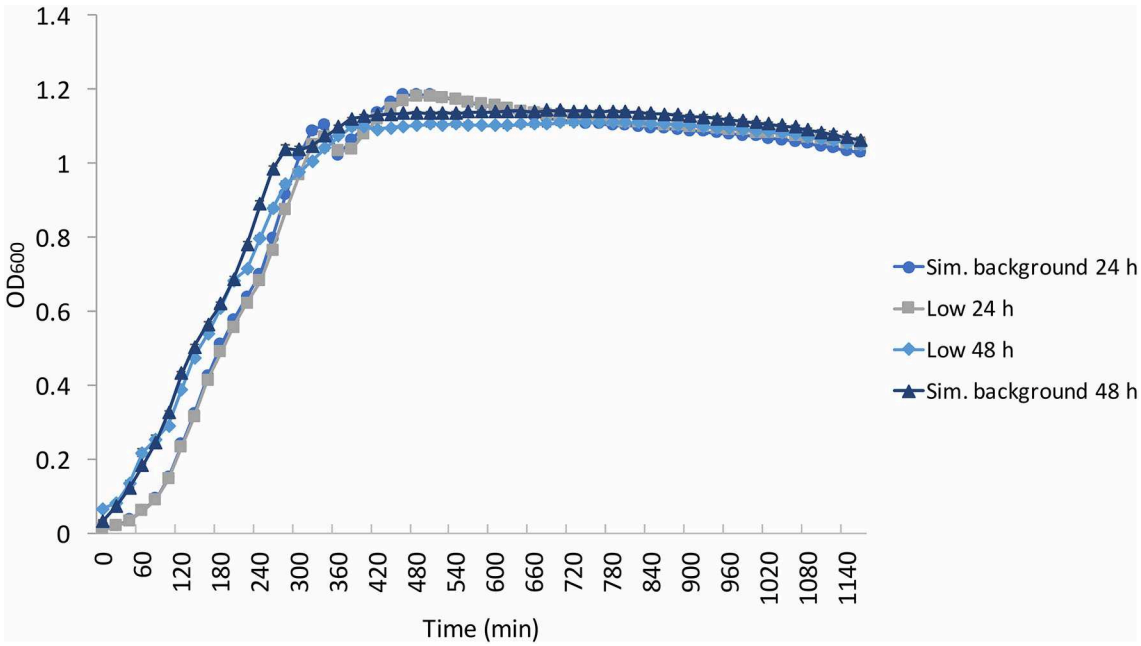

FIGURE 4 | Average ($n = 84$) of *E. coli* growth curves at the determined low radiation ("low") and artificial background radiation ("sim. background") dose rate: 24 and 48 h denote time in hours that bacteria batch has spent in respective conditions. Error bars show ± standard error ($n = 84$).

approximately between 480 and 600 min into growth after which all experimental runs, except the B3 48 h artificial background, progressed to a secondary exponential phase.

The stationary phase was reached with varying ODs from 1.5 to 1.8 with the exceptions of both B3 low and artificial background samples that reached between 1.2 and 1.5.

The last 2 h of the plate reader data showed the onset of the death phase in all samples. However, in B3 48 h low and artificial background samples, the OD dropped more rapidly to below 1 and 1.2, respectively. These variations between samples is addressed in the discussion.

To verify whether this lack of effect of the different radiation environments on the exponential growth phase could be extended to other bacteria, experiments were replicated using *E. coli* (**Figure 4**). Once again, there was grouping according to experimental run (24 and 48 h), not according to radiation environment, with the 24 h run having a shorter lag phase than that of the 48 h run. Similar to *B. subtilis*, "shoulders" appeared in the growth curves at ∼200 min and at 300–400 min. However, unlike the wide variation of OD in the stationary and death phase of *B. subtilis*, the *E. coli* stationary phase OD values remained between 1 and 1.2. Additionally, there was no obvious grouping in the final yield between the low and artificial background samples, in contrast to the *B. subtilis* samples. The *E. coli* death phase was not captured during the aliquoted time of the experimental run.

Effects of Radiation on Growth Gradients and Rates

Figures 5A,B show the growth gradients and growth rates, respectively, of each experimental condition during the linear exponential growth phase. There was no significant ($p > 0.05$) difference between the low and artificial background radiation growth gradient at either time condition in the *B. subtilis* samples. However, the *E. coli* growth gradient showed a significant ($p < 0.05$) difference between the two time conditions in the artificial background radiation. The *E. coli* growth gradients for 24 and 48 h in artificial background radiation were 0.0866 ($\pm 4.33 \times 10^{-3}$) and 0.0693 ($\pm 3.92 \times 10^{-3}$), respectively. The growth rates in **Figure 5B** were calculated for the average of all 84 samples in each condition and reflect the general trends shown by the growth gradients in **Figure 5A**.

B. subtilis Exposure to 10 × and 100 × Background Radiation

The *B. subtilis* growth curves displayed the same characteristics as the previous experiments, exhibiting a grouping in the exponential phase according to time condition, not radiation environment, in addition to a "shoulder" in the growth curve, and variation in OD during the stationary and death phases (**Figure 6**). Despite a non-significant ($p = 0.13$) difference in growth gradient (**Figure 5A**) and difference growth rate (**Figure 5B**) between the 10 × and 100 × artificial background radiation values, neither the 10 × or 100 × values were significantly ($p > 0.05$) different from the corresponding low radiation values in experiments run simultaneously as controls (**Figure 5A**). This implies that the difference in radiation dose rate was not the variable affecting growth.

Response to Stress

The final preconditioning experiment was carried out to determine whether cells grown in a low radiation environment

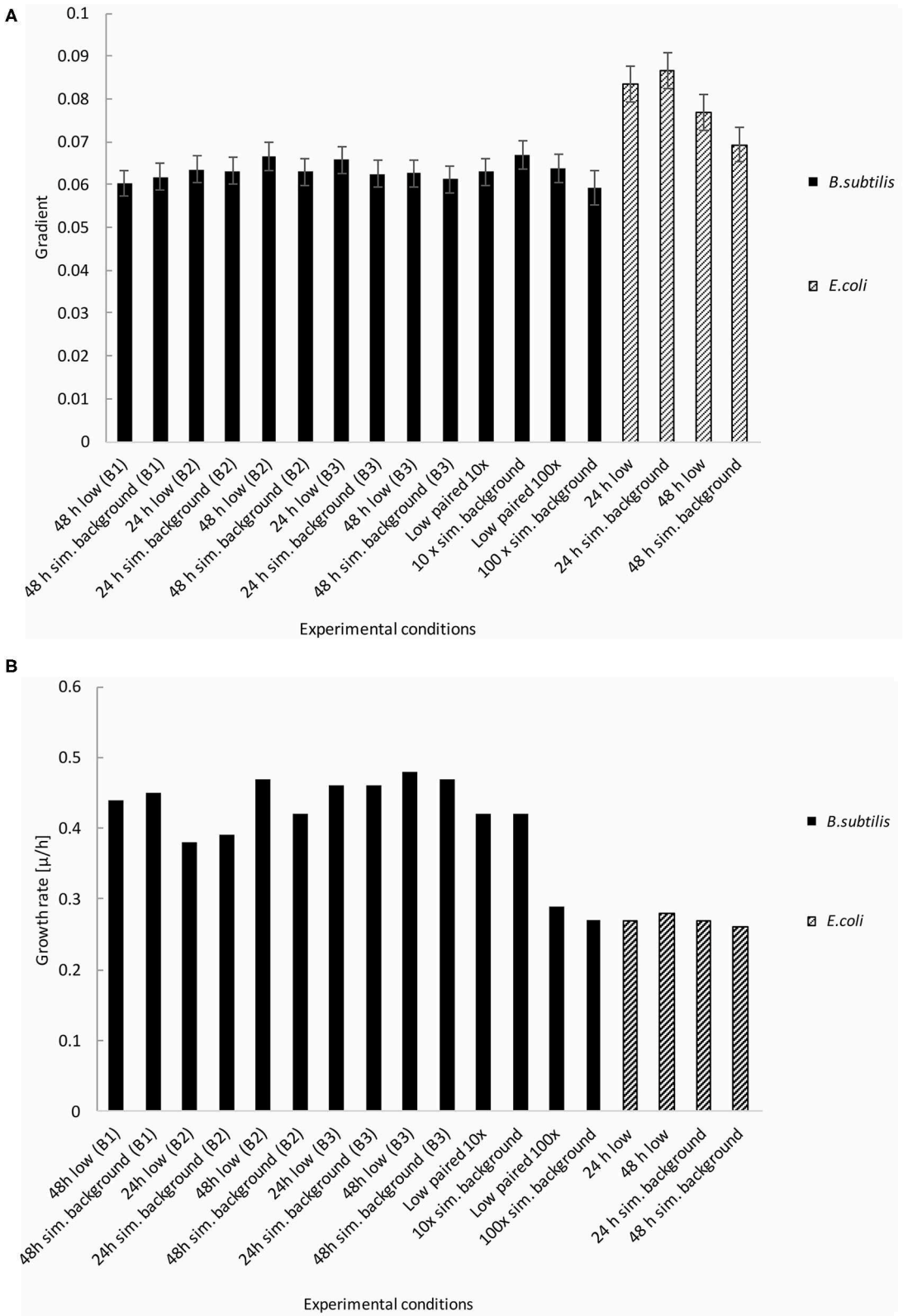

FIGURE 5 | Growth gradients and rates of *B. subtilis* and *E. coli* linear exponential growth phases at the determined low radiation ("low") and artificial background radiation ("sim. background") dose rate: 24 and 48 h denote time in hours that bacteria batch has spent in respective conditions; B1-3 denote week number when the multiple *B. subtilis* samples were run; 10 × = 10 × the artificial background dose rate; 100 × = 100 × the artificial background dose rate; Low paired = low dose rate samples run parallel to 10 × and 100 × dose rates. Error bars show ± error of gradient. "B.s" and "E.c." stand for *B. subtilis* and *E. coli*, respectively. **(A)** Growth gradients of *B. subtilis* and *E. coli* from the linear exponential growth phase. **(B)** Growth rates of *B. subtilis* and *E. coli* from the linear exponential growth phase.

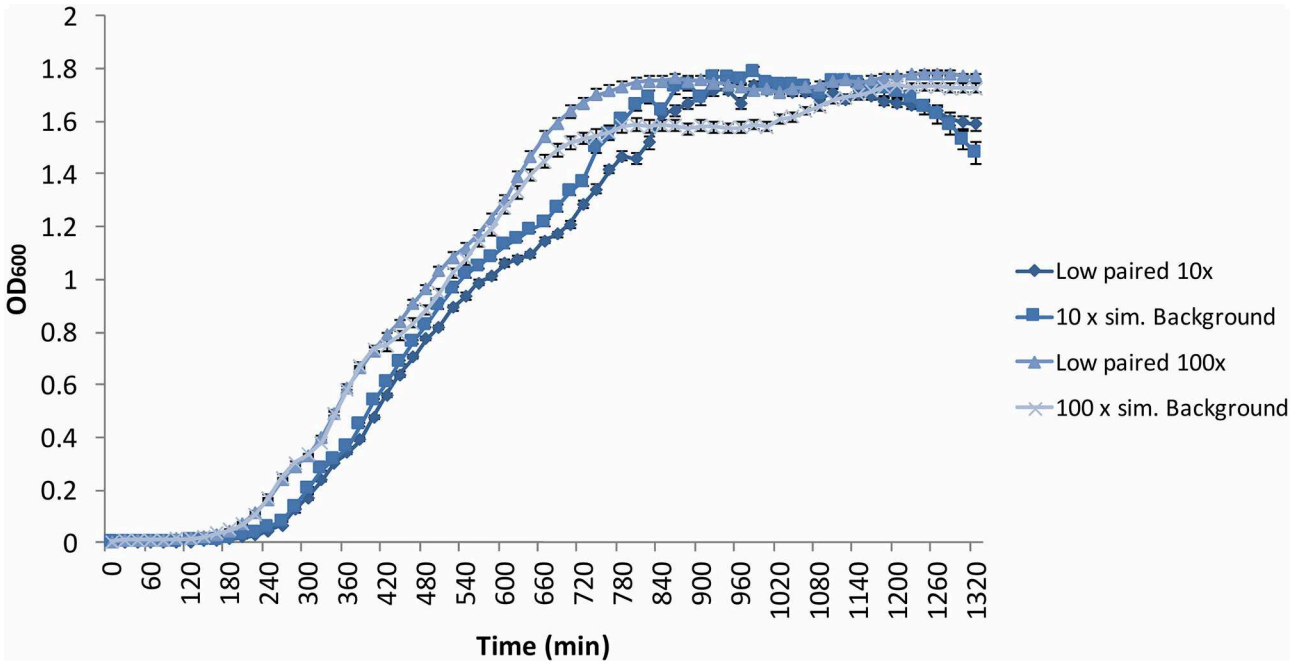

FIGURE 6 | Average ($n = 84$) of *B. subtilis* growth curves at increased radiation dose rates: 10× = 10× the artificial background dose rate; 100 × = 100 × the artificial background dose rate; Low paired = samples run parallel at the low dose rate. Error bars show ± standard error ($n = 84$).

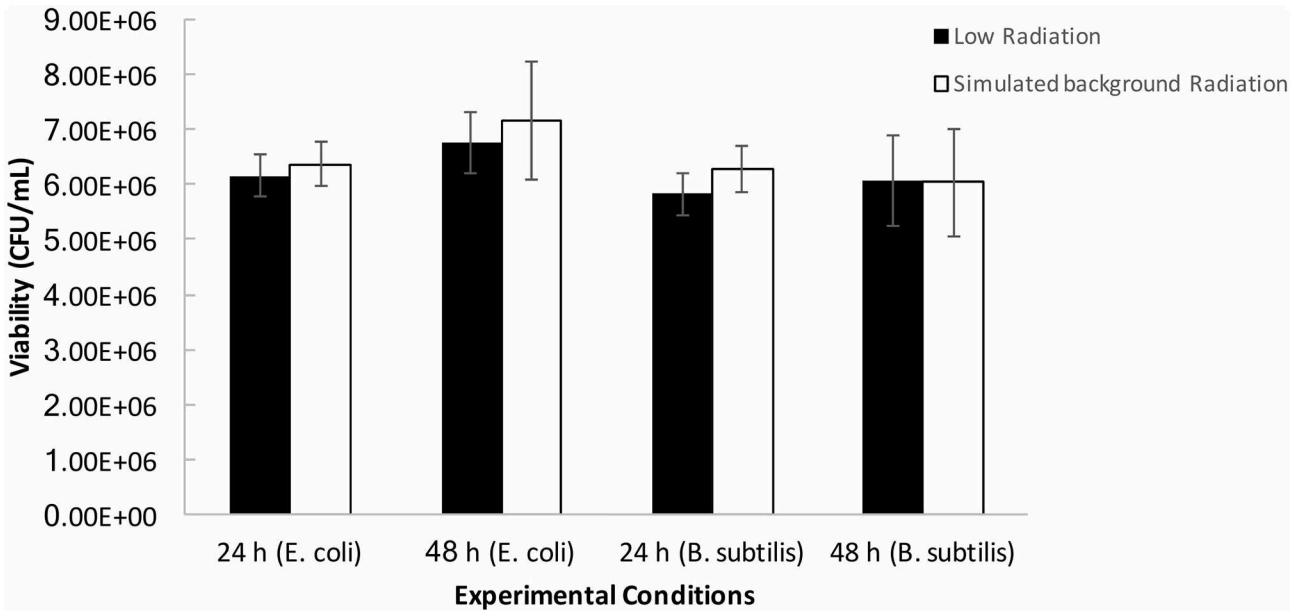

FIGURE 7 | Averages ($n = 9$ per condition) of post-UV irradiation cell counts of *B. subtilis* and *E. coli* grown under the determined low radiation ("low") and artificial background radiation ("sim. background") dose rate: 24 and 48 h denote time in hours that bacteria batch has spent in respective conditions. Error bars show ± standard error ($n = 9$ per condition).

are more susceptible to short-term imposed stress compared to cells grown with the artificial background radiation exposure. *B. subtilis* and *E. coli* cultures that had been growing in low and artificial background radiation environments for 24 and 48 h, respectively, were exposed to a short burst of UVC radiation ($\lambda = 254$ nm) for 30 s and plated to assess their post-irradiation viability (**Figure 7**). There was no significant ($p > 0.05$) difference in viability observed after stress exposure between the cells

grown in low or artificial background radiation, or between the two organisms.

DISCUSSION

Scientific investigation of the lethal consequences caused by high radiation exposure for both prokaryotic and eukaryotic organisms continues to shape the understanding of habitability and the limits of life. Although there is an abundance of off-planet, high-radiation environments of interest (e.g., Cockell et al., 2000; Marion et al., 2003), naturally occurring low radiation environments represent equally important extreme conditions of potential habitability to examine. These might include subsurface environments with low abundances of radioactive minerals, older planets with decayed radioactive minerals, solar systems containing stars with a lower ionising radiation output and regions of the galaxy with a quieter cosmic ray background, compared to the Earth.

Effects of Radiation on Bacterial Growth

We did not observe significant effects of low, artificial background, or heightened radiation environments (10 and 100 × surface background levels) on the linear exponential growth phase gradients of *B. subtilis* and *E. coli* when compared to the respective controls. This contradicts the LNT model which predicts increasing levels of radiation would have an increasing effect on growth rate from a zero dose upwards. These data also contradict the hormesis model, that predicts a beneficial effect on growth rate at low levels of radiation. Instead, the data point to a threshold model for bacterial growth, whereby at low levels of radiation below background and up to 100 times background no effect is observable on growth. It should be noted that although the SELLR experimental set up was designed to observe the bacterial responses without bias toward any particular model, the set up may unintentionally favour certain models. We cannot rule out that hormesis takes place between any of the tested dose rates of 1 ×, 10 ×, and 100 × background radiation. Future studies may wish to investigate a further narrowing of dose rates to more accurately rule out hormesis below our chosen radiation threshold.

We did observe variations in our experiments. The variation of lag phase is observed in all experiments performed. However, the variation in samples is grouped by experimental run and not by radiation environment, making the difference in radiation dose rate unlikely to be the cause. The variation in lag phase length is most likely due to small discrepancies in starting concentration of the samples. This experimental problem is not applicable to the exponential growth phase as it will be comparable regardless of small variations in starting inoculum.

An additional artefact in the *B. subtilis* and *E. coli* growth curves is the presence of a "shoulder" in the exponential growth phase. This may be a result of the bacteria exhausting the primary nutrient source and switching to a secondary one, which is probable in the nutrient-rich media used. We did not use this secondary growth in our calculations.

The final growth yield data also show a wide diversity of OD values for *B. subtilis*. Factors that explain this may include, for example, cell lysis resulting in the release of various organics, which would influence cell growth and thus the final optical density measurement. Previous research has used final yield OD data as a measure of microbial responses to low radiation conditions (e.g., Castillo et al., 2015). However, the different contributions of cell growth, stationary phase, and cell death will determine final OD readings and can therefore make the final OD interpretation potentially unreliable. As the exponential phase provides a measure of the rate of cell division and thus the effects of the radiation environment on cell reproduction, we consider this to be a good way to measure the effects of radiation.

Although the Boulby data challenges the LNT and hormesis models for low radiation doses, the indication that low dose rates do not impede bacterial growth is not unexpected. The empirical lethal dose necessary to sterilise 90% ("lethal dose" LD_{90}) of *E. coli* MG 1655 is 700 Gy (2.59×10^8 higher than the 24 h total dose received by Boulby control cells) (Daly et al., 2004). Although no LD_{90} data could be found for vegetative *B. subtilis* cells, the majority of life is not radio-resistant and can be killed by <500 Gy (Moeller et al., 2010; Slade and Radman, 2011). The cells subjected to 24 h of artificial background radiation in our experiment are exposed to a total dose of 2.7 μGy (or 5.4 μGy for 48 h experiments), whereas the cells' total dose after 24 h in the low radiation environment amounts to 0.012 μGy (0.024 μGy for 48 h experiments). Therefore, the total dose experienced by cells would have to be up to 8 orders of magnitude higher than the artificial background total dose to reach LD_{90} (Daly, 2012). This also explains why, when the artificial background dose rate is increased by 10 × and 100 ×, it is unsurprising that no effect on bacterial growth was observed.

To further understand the scale at which radiation dose can influence cell viability, the likelihood of radiation-cell interaction must be considered. This likelihood was calculated by Lampe et al. (2016) for evolutionary research in the Modane Underground Laboratory (LSM) at 1.7 km below the Fréjus Peak [4.8 km water equivalent (Piquemal, 2012), Boulby is 3 km water equivalent Robinson et al., 2003]. Using 7.4×10^{-4} mutations per generation as the spontaneous point mutation occurrence in *E. coli* (Barrick et al., 2009), they calculate that such natural mutation occurrences would happen at a 1.04×10^2 higher frequency than what they calculate for radiation-cell interactions. They compute that a dose rate of >20 μGy/h (=175 mGy/y) is required for the radiation-cell interactions to have a detectable impact above the natural mutation "noise." These calculations further explain the lack of observable difference between the Boulby low, artificial background, and 100 × artificial background (100 mGy/y) radiation dose rates on bacterial exponential growth. These data suggest that the radiation levels studied here are much lower than those required for significant cellular damage and reduction in growth.

Although the growth data may not rule out sublethal biochemistry and genetic responses caused by low radiation, as suggested by Castillo et al. (2015, 2018), growth (i.e., reproduction) is the ultimate metric of whether an organism is able to expand into a habitat. If sublethal effects are present, they remain insufficient to ramify through metabolic pathways to impede growth rates. Based on our study, we can assume that

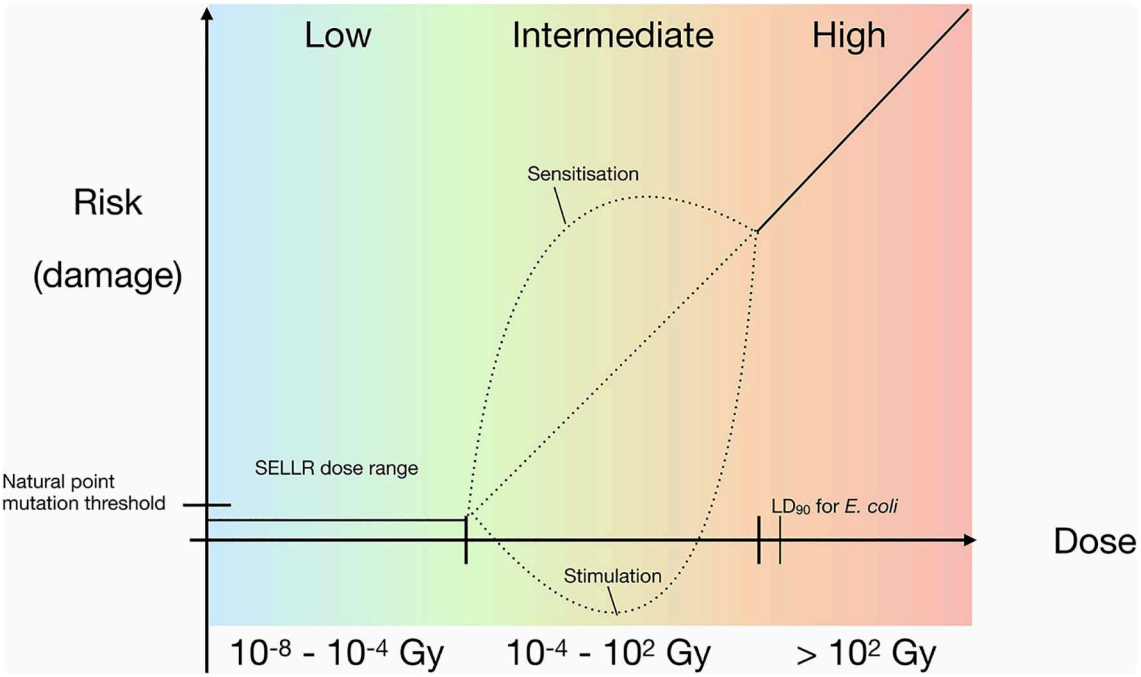

FIGURE 8 | Updated prokaryotic dose-response model with a linear relationship for higher doses and added SELLR (Subsurface Experiment of Life in Low Radiation) observations from sub-background to 100 × background, representing the "low" dose range where we observe no difference in growth. Black dotted lines indicate hypothetical risk of damage at intermediate radiation exposure, which requires further research.

exposure to an extremely low radiation environment would not negatively impact life.

Response to Stress

Previous research has put forward the hypothesis that growth in a low radiation environment causes heightened sensitivity to stress factors. Satta et al. (1995) demonstrated that *Saccharomyces cerevisiae* had increased sensitivity to the carcinogen methyl methanesulfonate after growth in a low radiation environment (0.6 μGy/d, compared to Boulby's 0.012 μGy/d). Additionally, it has been suggested (Castillo et al., 2015) that cultures grown in low radiation for 24 h are less able to respond to reactive oxygen species (ROS) attacking the cell. ROS can be produced by radiation interacting with water (Ward, 1988), with higher dose rates causing higher ROS production. It was proposed that the lack of radiation, and by extension lower ROS production, fails to "prime" cells' response pathways for internal ROS removal, resulting in ROS accumulation and consequent stress.

This prompted our own experiment using UVC radiation exposure as a stress factor to determine whether there was any difference in cell sensitivity to stress after growth at low radiation vs. growth under artificial surface radiation. The cellular response was measured in terms of cell viability after UV exposure. The results show no significant difference in either *B. subtilis* or *E. coli* viability grown at low or artificial background radiation dose rates.

These results suggest that even if there are biochemical effects in cells at below background radiation levels that are not manifested in growth, they also do not affect a cell's short-term response to oxidative and radiation stress imposed by UV radiation.

Threshold Model

Figure 8 synthesises the results obtained in this work. Between the total dose range of 10^{-8} to 10^{-4} Gy our data suggests a threshold model where there is no effect on bacterial growth at this dose and lower. The lowest total dose received by the Boulby samples was that of the 24 h exposure at the artificial background dose rate of 0.01 mGy/y resulting in a total dose of 2.74×10^{-8} Gy; the highest total dose received was the 100 × the artificial background sample resulting in 2.74×10^{-4} Gy. Above this threshold but below doses that lead to loss of viability (10^{-4} to 10^{2} Gy), we cannot rule out hypersensitivity or hermetic effects. There may be many additional "saddle points" in the model depending on factors such as dose-rate and organism-specific effects. Thus, the possibility of hypersensitivity or hormetic effect models may still be valid. Our results also focus on the exponential growth phase. However, if sublethal biochemical effects occur at below background radiation levels, as has been suggested for other cells (e.g., Kawanishi et al., 2012; Castillo et al., 2018), then it could suggest that different models apply depending on the scale or process considered and that no universal model for low radiation effects exists.

The data presented here indicate that there are no significant effects at either ultra low, artificial terrestrial surface, or heightened radiation dose rates on bacterial growth, and

no difference in bacterial sensitivity to stress in the form of shortwave UV exposure after growth in low radiation environments. Thus, the preliminary data indicate that the extreme condition of low radiation in an environment would not restrict microbial expansion in a potential habitat. Additionally, the lack of a measurable linear effect or beneficial effects of low-level radiation suggest that both the LNT and hormesis models are inapplicable at these doses. Instead, a threshold model is suggested with no observable effect on viability below the terrestrial surface radiation dose up to a critical level exceeding the surface dose. The "critical threshold model" that emerges from our data might be applicable to a wide range of physiological processes in prokaryotes and be a useful model to consider in future low radiation environment studies. However, the further questions raised by our data show that further research on life in low radiation environments is merited.

DATA AVAILABILITY STATEMENT

The raw data supporting the conclusions of this article will be made available by the authors, without undue reservation, to any qualified researcher.

AUTHOR CONTRIBUTIONS

Internal dose measurements were performed by PS. Internal and external dose calculations were carried out by LC. External dose measurements were carried out by SP and LC. GEANT4 simulations were performed by AN under the supervision of AM. Growth measurements were performed by JW with the help of CT and EM. The manuscript was written by JW with help from CC, AM, and PS. All authors contributed to the article and approved the submitted version.

FUNDING

JW was funded by the UK Space Agency Aurora Studentship grant (STFC ST/M003612/1); CC was funded by the Science and Technology Facilities Council grant (ST/R000875/1); AN was funded by the Commonwealth Scholarship Commission grant (BDCS-2016-49); AM was funded by the Science and Technology Facilities Council grant (ST/N000269/1); LC was funded though the Trinity College M.Sc Physics programme; Boulby Underground Laboratory staff were funded by core Science and Technology Facilities Council facility funding.

ACKNOWLEDGMENTS

We would like to acknowledge the technical assistance provided by Scott McLaughlin and general assistance provided by Barbara Suckling and Louise Yeoman.

REFERENCES

Abgrall, N., Arnquist, I. J., Avignone, F. T. III., Barabash, A. S., Bertrand, F. E., Boswell, M., et al. (2016). The majorana demonstrator radioassay program. *Nucl. Instrum. Meth. A* 828, 22–36. doi: 10.1016/j.nima.2017.08.005

Agostinelli, S., Allison, J., Amako, K., Apostolakis, J., Araujo, H., Arce, P., et al. (2003). GEANT4—a simulation toolkit. *Nucl. Instrum. Meth. A* 506, 250–303. doi: 10.1016/S0168-9002(03)01368-8

Aprile, E., Aalbers, J., Agostini, F., Alfonsi, M., Amaro, F. D., Anthony, M., et al. (2017). The XENON1T dark matter experiment. *Eur. Phys. J. C* 77:881. doi: 10.1140/epjc/s10052-017-5326-3

Araújo, H. M., Akimov, D. Y., Barnes, E. J., Belov, V. A., Bewick, A., Burenkov, A. A., et al. (2012). Radioactivity backgrounds in, ZEPLIN–III. *Astropart. Phys.* 35, 495–502. doi: 10.1016/j.astropartphys.2011.11.001

Barrick, J. E., Yu, D. S., Yoon, S. H., Jeong, H., Oh, T. K., Schneider, D., et al. (2009). Genome evolution and adaptation in a long-term experiment with *Escherichia coli*. *Nature* 461,1243–1247. doi: 10.1038/nature08480

Calabrese, E. J., and Baldwin, L. A. (2003). Hormesis: the dose-response revolution. *Ann. Rev. Pharmacol. Toxicol.* 43, 175–197. doi: 10.1146/annurev.pharmtox.43.100901.140223

Castillo, H., Li, X., Schilkey, F., and Smith, G. B. (2018). Transcriptome analysis reveals a stress response of *Shewanella oneidensis* deprived of background levels of ionising radiation. *PLoS ONE* 13:e0196472. doi: 10.1371/journal.pone.0196472

Castillo, H., Schoderbek, D., Dulal, S., Escobar, G., Wood, J., Nelson, R., et al. (2015). Stress induction in the bacteria *Shewanella oneidensis* and *Deinococcus radiodurans* in response to below-background ionising radiation. *Int. J. Radiat. Biol.* 91, 749–756. doi: 10.3109/09553002.2015.1062571

Chang, J. C., Ossoff, S. F., Lobe, D. C., Dorfman, M. H., Dumais, C. M., Qualls, R. G., et al. (1985). UV inactivation of pathogenic and indicator microorganisms. *Appl. Environ. Microbiol.* 49, 1361–1365. doi: 10.1128/AEM.49.6.1361-1365.1985

Cockell, C. S., Catling, D. C., Davis, W. L., Snook, K., Kepner, R. L., Lee, P., et al. (2000). The ultraviolet environment of mars: biological implications past, present, and future. *Icarus* 146, 343–359. doi: 10.1006/icar.2000.6393

Costantini, D., and Borremans, B. (2019). The linear no-threshold model is less realistic than threshold or hormesis-based models: an evolutionary perspective. *Chem. Biol. Interac.* 301, 26–33. doi: 10.1016/j.cbi.2018.10.007

Daly, M. J. (2012). Death by protein damage in irradiated cells. *DNA Repair* 11, 12–21. doi: 10.1016/j.dnarep.2011.10.024

Daly, M. J., Gaidamakova, E. K., Matrosova, V. Y., Vasilenko, A., Zhai, M., Venkateswaran, A., et al. (2004). Accumulation of Mn (II) in deinococcus radiodurans facilitates gamma-radiation resistance. *Science* 306, 1025–1028. doi: 10.1126/science.1103185

de González, A. B., and Darby, S. (2004). Risk of cancer from diagnostic X-rays: estimates for the UK and 14 other countries. *Lancet* 363 345–351. doi: 10.1016/S0140-6736(04)15433-0

de Vera, J. P., Alawi, M., Backhaus, T., Baqué M., Billi, D., Böttger, U., et al. (2019). Limits of life and the habitability of mars: the ESA space experiment BIOMEX on the ISS. *Astrobiology* 19, 145–157. doi: 10.1089/ast.2018.1897

Feinendegen, L. E., Pollycove, M., and Neumann, R. D. (2007). Whole-body responses to low-level radiation exposure: new concepts in mammalian radiobiology. *Exp. Hematol.* 35, 37–46. doi: 10.1016/j.exphem.2007.01.011

Feynman, R. P. (1960). *There's Plenty of Room at the Bottom.* Boca Raton, FL: California Institute of Technology, Engineering and Science Magazine.

Finch, S. C. (2007). Radiation-induced leukemia: lessons from history. *Best Prac. Res. Clin. Haematol.* 20, 109–118. doi: 10.1016/j.beha.2006.10.009

Ghiassi-Nejad, M., Mortazavi, S. M. J., Cameron, J. R., Niroomand-Rad, A., and Karam, P. A. (2002). Very high background radiation areas of ramsar, Iran: preliminary biological studies. *Health Phys.* 82, 87–93. doi: 10.1097/00004032-200201000-00011

Gilmore, G. (2011). *Practical Gamma-Ray Spectroscopy*. Warrington, UK: John Wiley and Sons.

Hamilton, E. I. (1989). Terrestrial radiation—an overview. *Int. J. Radiat. Appl. Instrument. Part C* 34, 195–212. doi: 10.1016/1359-0197(89)90230-0

Horneck, G. (1992). Radiobiological experiments in space: a review. *Int. J. Radiat. Appl. Instrument. Part D* 20, 185–205. doi: 10.1016/1359-0189(92)90099-H

International Agency for Research on Cancer (1992). *Monograph on the Evaluation of Carcinogenic Risks to Humans: Solar and Ultraviolet Radiation, Vol. 55.* World Health Organization, 113–122.

Kawanishi, M., Okuyama, K., Shiraishi, K., Matsuda, Y., Taniguchi, R., Shiomi, N., et al. (2012). Growth retardation of *paramecium* and mouse cells by shielding them from background radiation. *J. Radiat. Res.* 53, 404–410. doi: 10.1269/jrr.11145

Lampe, N., Biron, D. G., Brown, J. M. C., Incerti, S., Marin, P., Maigne, L., et al. (2016). Simulating the impact of the natural radiation background on bacterial systems: implications for very low radiation biological experiments. *PLoS ONE* 11:e016364. doi: 10.1371/journal.pone.0166364

Lorenz, E. (1944). Radioactivity and lung cancer; a critical review of lung cancer in the miners of schneeberg and joachimsthal. *J. Natl. Cancer Inst.* 5, 1–15.

Lorenz, E. (1950). Some biologic effects of long continued irradiation. *Am. J. Roentgenol. Radium Ther.* 63, 176–185.

Mancuso, M., Pasquali, E., Giardullo, P., Leonardi, S., Tanori, M., Di Majo, V., et al. (2012). The radiation bystander effect and its potential implications for human health. *Curr. Mol. Med.* 12, 613–624. doi: 10.2174/156652412800620011

Marion, G. M., Fritsen, C. H., Eicken, H., and Payne, M. C. (2003). The search for life on Europa: limiting environmental factors, potential habitats, and Earth analogues. *Astrobiology* 3, 785–811. doi: 10.1089/153110703322736105

Mine, M., Okumura, Y., Ichimaru, M., Nakamura, T., and Kondo, S. (1990). Apparently beneficial effect of low to intermediate doses of A-bomb radiation on human lifespan. *Int. J. Radiat. Biol.* 58, 1035–1043. doi: 10.1080/09553009014552341

Moeller, R., Douki, T., Rettberg, P., Reitz, G., Cadet, J., Nicholson, W. L., et al. (2010). Genomic bipyrimidine nucleotide frequency and microbial reactions to germicidal UV radiation. *Arch. Microbiol.* 192, 521–529. doi: 10.1007/s00203-010-0579-3

Moeller, R., Raguse, M., Leuko, S., Berger, T., Hellweg, C. E., Fujimori, A., et al. (2017). STARLIFE—An international campaign to study the role of galactic cosmic radiation in astrobiological model systems. *Astrobiology* 17101–109. doi: 10.1089/ast.2016.1571

Muller, H. J. (1946). *Nobel Prize Lecture. Sweden: Stockholm*, 12.

Muller, H. J. (1954). Damage to posterity caused by irradiation of the gonads. *Am. J. Obstetr. Gynecol.* 67, 467–483. doi: 10.1016/0002-9378(54)90039-3

National Research Council (NRC) (2006). *Health Risks from Exposure to Low Levels of Ionizing Radiation: BEIR VII Phase 2, Vol. 7.* Washington, DC: National Academies Press.

Olson, A. R., and Lewis,. G. N. (1928). Natural reactivity and the origin of species. *Nature* 121673–674. doi: 10.1038/121673a0

Piquemal, F. (2012). Modane underground laboratory: Status and project. *Eur. Phys. J. Plus* 127:110. doi: 10.1140/epjp/i2012-12110-3

Preston, D. L., Pierce, D. A., Shimizu, Y., Cullings, H. M., Fujita, S., Funamoto, S., et al. (2004). Effect of recent changes in atomic bomb survivor dosimetry on cancer mortality risk estimates. *Radiat. Res.* 162, 377–389. doi: 10.1667/RR3232

Prise, K. M., Pinto, M., Newman, H. C., and Michael, B. D. (2001). A review of studies of ionising radiation-induced double-strand break clustering. *Radiat Res.* 156, 572–576. doi: 10.1667/0033-7587(2001)1560572:AROSOI2.0.CO;2

Reichhart, L., Lindote, A., Akimov, D. Y., Araújo, H. M., Barnes, E. J., Belov, V. A., et al. (2013). Measurement and simulation of the muon-induced neutron yield in lead. *Astroparticle Phys.* 47, 67–76. doi: 10.1016/j.astropartphys.2013.06.002

Robinson, M., Kudryavtsev, V. A., Lüscher, R., McMillan, J. E., Lightfoot, P. K., Spooner, N. J. C., et al. (2003). Measurements of muon flux at 1070m vertical depth in the Boulby underground laboratory. *Nucl. Inst. Methods Phys. Res. Section A* 511, 347–353. doi: 10.1016/S0168-9002(03)01973-9

Satta, L., Augusti-Tocco, G., Ceccarelli, R., Esposito, A., Fiore, M., Paggi, P., et al. (1995). Low environmental radiation background impairs biological defence of the yeast *Saccharomyces cerevisiae* to chemical radiomimetic agents. *Mutat. Res. Lett.* 347, 129–133. doi: 10.1016/0165-7992(95)00031-3

Scovell, P. R., Meehan, E., Araújo, H. M., Dobson, J., Ghag, C., Kraus, H., et al. (2018). Low-background gamma spectroscopy at the Boulby Underground Laboratory. *Astropart. Phys.* 97, 160–173. doi: 10.1016/j.astropartphys.2017.11.006

Shahbazi-Gahrouei, D., Gholami, M., and Setayandeh, S. (2013). A review on natural background radiation. *Adv. Biomed. Res.* 2:65 doi: 10.4103/2277-9175.115821

Shamoun, D. Y. (2016). Linear No-Threshold model and standards for protection against radiation. *Reg. Toxicol. Pharmacol.* 77, 49–53. doi: 10.1016/j.yrtph.2016.02.011

Shibamoto, Y., and Nakamura, H. (2018). Overview of biological, epidemiological, and clinical evidence of radiation hormesis. *Int. J. Mol. Sci.* 19:2387. doi: 10.3390/ijms19082387

Siasou, E., Johnson, D., and Willey, N. J. (2017). An extended dose–response model for microbial responses to ionising radiation. *Front. Environ. Sci.* 5:6. doi: 10.3389/fenvs.2017.00006

Slade, D., and Radman, M. (2011). Oxidative stress resistance in *Deinococcus radiodurans*. *Microbiol. Mol. Biol. Rev.* 75, 133–191. doi: 10.1128/MMBR.00015-10

Smith, G. B., Grof, Y., Navarrette, A., and Guilmette, R. A. (2011). Exploring biological effects of low level radiation from the other side of background. *Health Phys.* 100, 263–265. doi: 10.1097/HP.0b013e318208cd44

Stebbing, A. R. D. (1982). Hormesis—the stimulation of growth by low levels of inhibitors. *Sci. Total Environ.* 22, 213–234. doi: 10.1016/0048-9697(82)90066-3

United Nations (2008). *Scientific Committee on the Effects of Atomic Radiation.* Report of the United Nations Scientific Committee on the Effects of Atomic Radiation: Fifty-Sixth Session (10-18 July 2008). No. 46. United Nations Publications.

Wanebo, C. K., Johnson, K. G., Sato, K., and Thorslund, T. W. (1968). Breast cancer after exposure to the atomic bombings of hiroshima and nagasaki. *N Engl J Med.* 279, 667–671. doi: 10.1056/NEJM196809262791301

Ward, J. F. (1988). DNA damage produced by ionising radiation in mammalian cells: identities, mechanisms of formation, and reparability. *Prog. Nucl. Acid Res. Mol. Biol.* 35, 95–125. doi: 10.1016/S0079-6603(08)60611-X

Conflict of Interest: The authors declare that the research was conducted in the absence of any commercial or financial relationships that could be construed as a potential conflict of interest.

frontiers in Earth Science

ORIGINAL RESEARCH
published: 31 July 2020
doi: 10.3389/feart.2020.00327

A Research Environment 2 km Deep-Underground Impacts Embryonic Development in Lake Whitefish (*Coregonus clupeaformis*)

*Jake Pirkkanen[1], Andrew M. Zarnke[2], Taylor Laframboise[1], Simon J. Lees[3,4], T. C. Tai[1,2,5], Douglas R. Boreham[1,2,5,6] and Christopher Thome[1,2,5]**

[1] Department of Biology, Laurentian University, Sudbury, ON, Canada, [2] Biomolecular Sciences Program, Laurentian University, Sudbury, ON, Canada, [3] Department of Biology, Lakehead University, Thunder Bay, ON, Canada, [4] Medical Sciences Division, Northern Ontario School of Medicine, Thunder Bay, ON, Canada, [5] Medical Sciences Division, Northern Ontario School of Medicine, Sudbury, ON, Canada, [6] Bruce Power, Tiverton, ON, Canada

Biological research conducted in deep-underground environments is limited due to the lack of scientific infrastructure to accommodate the investigations, and only a few studies have utilized complex whole organism models. In this study, lake whitefish (*Coregonus clupeaformis*) embryogenesis was examined in two different unique laboratory environments; at the Earth's surface and 2 km deep underground shielded from cosmic radiation. Established developmental endpoints and morphometric analysis were utilized to investigate differences between lake whitefish embryos reared in these two laboratories. No significant differences were observed between the surface and underground laboratories with respect to the timing of hatch or percent survival. However, a significant increase in body length and body weight of up to 10% was observed in embryos reared underground. These findings have been interpreted and discussed in the context of the novel research challenges faced in an inherently difficult to control deep-underground environment. This study represents one of the few investigations with an established whole organism model deep-underground and provides an opportunity to discuss the highly unique technical and logistical challenges of conducting biological experiments in this novel field of scientific research.

Keywords: deep-underground environment, *Coregonus clupeaformis*, lake whitefish, embryonic development, morphometric analysis, SNOLAB

OPEN ACCESS

Edited by:
Maria Antonella Tabocchini, Istituto Superiore di Sanità (ISS), Italy

Reviewed by:
Deborah Oughton, Norwegian University of Life Sciences, Norway
Geoffrey Battle Smith, New Mexico State University, United States

****Correspondence:***
Christopher Thome
cthome@nosm.ca

Specialty section:
This article was submitted to Biogeoscience, a section of the journal Frontiers in Earth Science

Received: *01 April 2020*
Accepted: *14 July 2020*
Published: *31 July 2020*

Citation:
Pirkkanen J, Zarnke AM, Laframboise T, Lees SJ, Tai TC, Boreham DR and Thome C (2020) A Research Environment 2 km Deep-Underground Impacts Embryonic Development in Lake Whitefish (Coregonus clupeaformis). Front. Earth Sci. 8:327. doi: 10.3389/feart.2020.00327

INTRODUCTION

There is a scarcity of empirical biological research in deep-underground environments, due to the lack of access to infrastructure available to facilitate these endeavors. There are only a small number of underground research laboratories located across the world, which vary in depth as well as type of space, including active mines, caves, tunnels, and a nuclear waste repository (Liu et al., 2018). The majority of these current facilities were established to conduct astroparticle physics experiments, predominantly based in dark matter and neutrino detection (Smith, 2012). These types of explorations necessitate a deep-underground research facility with a significant rock overburden in order to shield out background noise caused by cosmic radiation. Even further limited has been the use of subterranean laboratory facilities to conduct biological experiments, though studies to this end have been gaining traction, with notable work performed at the Waste

Isolation Pilot Plant (WIPP) in New Mexico, United States and Gran Sasso National Laboratory (LNGS) in Abruzzo, Italy (Castillo et al., 2015, 2018; Fratini et al., 2015; Castillo and Smith, 2017; Morciano et al., 2018).

The majority of these biological studies have investigated the effects of sub-natural background radiation (NBR) exposures, relying on underground laboratories to provide a sub-background radiation environment. Previous experiments have shown in a variety of model organisms, including paramecium, blue-green algae, and mammalian cells, that protracted incubation in an environment shielded from NBR can induce negative biological effects including attenuation of growth rates (Planel et al., 1976; Conter et al., 1983; Kawanishi et al., 2012). Interestingly, this attenuation could be rescued by the exogenous re-introduction of a radiation source at levels comparable to natural background (Conter et al., 1983; Kawanishi et al., 2012). Additionally, in biological systems cultured underground an increase in background and induced damage, mutation rates, and apoptotic sensitivity were observed as well as greater micronuclei formation and reduced free radical scavenging capacity (Satta et al., 2002; Carbone et al., 2009, 2010; Smith et al., 2011). However, most of this previous research has been conducted using simple cell culture or single-celled organisms.

One of the most important scientific gaps in the current deep-underground biology research is experimentation with complex multicellular whole organisms. However, logistical challenges with working in underground environments make numerous classic research species, for example murine models, non-viable options to fill these needs. It is therefore critical that research models require minimal maintenance in terms of both space and resources. Researching the Effects of the Presence and Absence of Ionizing Radiation (REPAIR) is a recently established research project within SNOLAB. The goal of this project is to study the effects of exposure to a deep underground environment shielded from naturally occurring background radiation on biological systems, including whole organism models (Pirkkanen et al., 2017; Thome et al., 2017c). One of the whole organism models that REPAIR is utilizing is the embryonic development of lake whitefish (*Coregonus clupeaformis*).

Significant work has been done characterizing developmental staging in lake whitefish as well as their response to a variety of stressors, including chemicals, thermal stress, and ionizing radiation (Sreetharan et al., 2015; Thome et al., 2017a,b). Based on this robust previous characterization, the minimal requirements needed for rearing embryos, and their prolonged embryonic developmental period of several months, lake whitefish represent a unique whole organism for investigating the effects of a deep-underground environment. Lake whitefish embryos can be raised in significantly large numbers in commercially available refrigerator units within basic laboratory petri dishes filled with lake water or dechlorinated municipal tap water (Mitz et al., 2014). Additionally, lake whitefish embryos have a protracted developmental period of up to 200 days depending on temperature (Sreetharan et al., 2015), providing an excellent whole organism model for examining potentially subtle effects over an extended period in a deep-underground environment.

The REPAIR project is located within SNOLAB, a research facility located 2 km underground within an active mine in Sudbury, ON, Canada. The technical details of the research facility and the scientific goals of the REPAIR project have been previously discussed (Boger et al., 2000; Smith, 2012; Thome et al., 2017c). The overall long-term goals of the REPAIR project are to explore the effects of a below natural background radiation environment in a variety of biological models. This article reports on an initial pilot project, where lake whitefish embryos were raised in the REPAIR project's research space within SNOLAB, as well as at an above ground control laboratory at Laurentian University. These data represent one of the only whole organism model experiments conducted deep-underground, and an excellent opportunity to review the technical, logistical, and scientific challenges of conducting these types of niche investigations.

MATERIALS AND METHODS

Embryo Collection

Lake whitefish embryos were produced through *in vitro* fertilization. Milt and eggs were collected from spawning adult fish that were gillnetted in Eastern Lake Huron (44.995, −81.386) on December 1, 2016. Eggs were wet fertilized for 10 min and then disinfected with 5 mL L^{-1} Ovadine (Syndel Laboratories, BC, Canada) for 30 min. Fertilized eggs were transported on ice to Laurentian University in 1 L plastic bottles filled with water from Lake Huron. Following transportation, and for the remainder of embryonic development, embryos were incubated in water taken from Ramsey Lake adjacent to Laurentian University (46.472, −80.973).

Embryo Rearing

Embryos were raised in two different experimental environments. The "surface" laboratory was located at Laurentian University in the Vale Living with Lakes Centre. The "underground" laboratory was located 2 km underground within SNOLAB in the REPAIR project's research space (Thome et al., 2017c). The SNOLAB facility is located approximately 27 km from Laurentian University and the Vale Living with Lakes Centre. The SNOLAB surface facility and the Vale Living with Lakes Centre are located at similar altitudes of 305 and 288 m above sea level, respectively.

On the day of fertilization (day 0) embryos were stored overnight in a 3°C refrigeration unit in the surface laboratory. The following morning (day 1) half of the embryos were transported underground to SNOLAB in 1 L plastic bottles on ice. As a transportation sham, the embryos remaining on the surface were also temporarily transferred to 1 L plastic bottles on ice. The total transportation time was approximately 2 h. It is unlikely that there were any significant changes to water quality during transportation since newly fertilization lake whitefish embryos have a very low metabolic activity and minimal oxygen consumption (Mueller et al., 2015).

In both the surface and underground laboratories, embryos were reared in refrigeration units (**Figure 1A**) using methods described previously (Mitz et al., 2014). Culturing conditions

within the units were kept as similar as possible, i.e., controlled respective incubation temperature and all ambient room light was blocked from entering the inside of the unit. Embryos were incubated in 10 cm petri dishes (0875711Z, Thermo Fisher Scientific) with 50 embryos per dish (**Figure 1B**). Petri dishes were filled with chilled water collected from Ramsey Lake. Natural water sources were used for embryonic rearing as they are free from additives such as chlorine found in municipal water sources. Water was transported underground throughout the experiment in 1 L plastic bottles.

Each of the laboratory environments contained two refrigeration units (GDM-10PT, True Manufacturing Company, O'Fallon, MO, United States). The refrigeration units were retrofitted with a digital temperature controller (JC-104, Juchuang Electronic Science and Technology Co., Ltd.) for more precise temperature regulation. The units in each experimental location were set to an approximate temperature of either 3 or 5°C. There were slight variations in temperature depending on the specific location of petri dishes within the units as well as the frequency at which the compressor turned on and off. Actual temperatures were continuously monitored using HOBO pendant data loggers (UA-002, Onset, Bourne, MA, United States). Temperature readings were collected from three different spatial location within each unit and analyzed using HOBOware software (Onset, Bourne, MA, United States). The mean temperature within the 3 and 5°C units in each laboratory were within 0.1°C of each other (**Table 1**). Between 38 and 43 petri dishes were housed in each refrigeration unit, resulting in between 1,900 and 2,150 embryos being raised in each environmental condition (**Table 1**). Water was changed on all petri dishes twice per week for the duration of embryonic development, approximately 100 mL per petri dish. At the time of water change, dead or hatched embryos were removed from the petri dish and were numerically recorded.

Morphometric Analysis

Embryos were preserved for analysis at three different time points, corresponding to approximately 40, 60, and 80% development (**Table 1**). The number of days post fertilization (dpf) to reach each of these development stages was estimated based on the lake whitefish temperature model developed previously (Mitz et al., 2017b). Embryos raised at the warmer 5°C temperature develop faster and were therefore preserved at earlier time points (38, 58, and 79 dpf) compared to 3°C (50, 73, and 101 dpf). Embryos were fixed in 10% neutral buffered formalin (5701, Richard-Allan Scientific) for 7 days and were then transferred to 50% ethanol (A995-4, Thermo Fisher Scientific) for long term storage. Size and mass measurements were taken according to the methods previously established (Sreetharan et al., 2015). Briefly, the preserved embryo and yolk sac were removed from the chorion and separated under an Axio Zoom V16 stereomicroscope (ZEISS) with a Canon EOS Rebel T1i camera mounted (Canon Inc.). A dorsal image was taken of the embryo from which a body length was measured

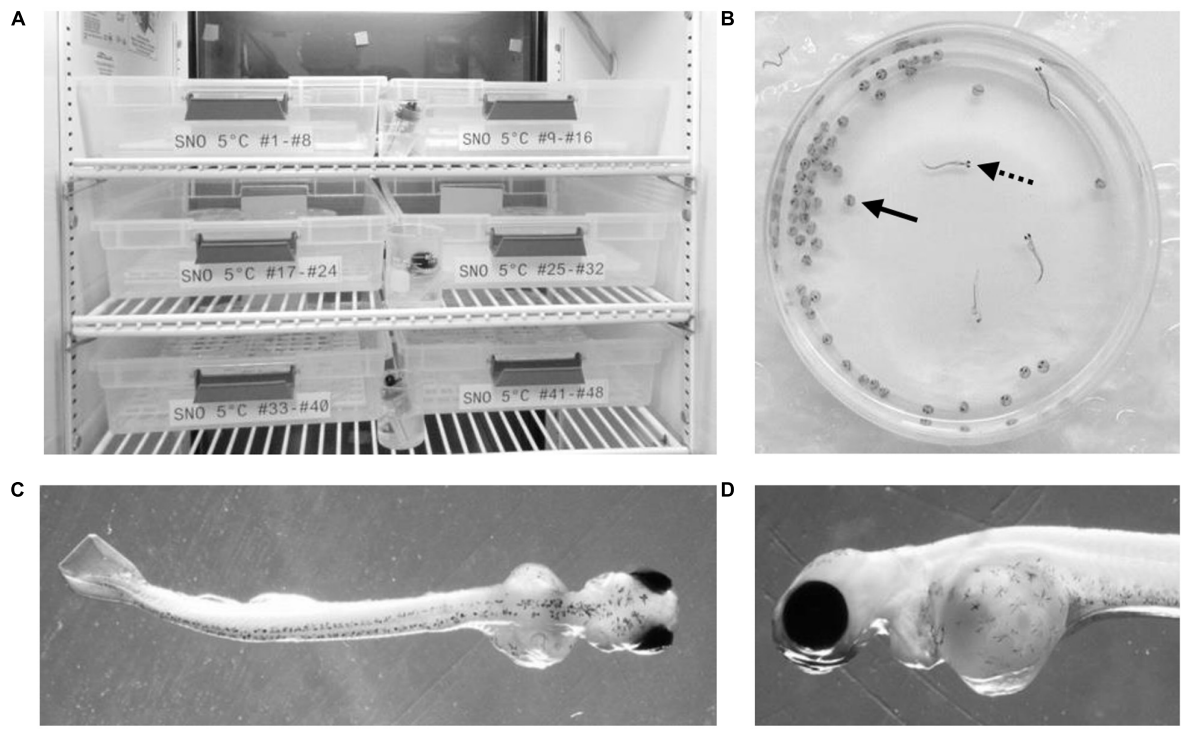

FIGURE 1 | Embryonic development experimental setup. Embryos were raised in temperature controlled refrigeration units at the surface and underground **(A)**. Embryonic development took place within petri dishes **(B)** where chorionated embryos (solid arrow) were raised until hatch (dotted arrow). A dorsal image of each hatched embryo **(C)** was used for body length measurements while a lateral image **(D)** was taken of the yolk sac in order to calculate the yolk area.

TABLE 1 | Experimental setup.

	Temperature (°C ± SD)	Petri dishes (#)	Embryos (#)	Sampling timepoint (dpf*)		
				40%	60%	80%
Surface 5°C	4.7 ± 0.2	39	1,950	38	58	79
Underground 5°C	4.6 ± 0.3	43	2,150	38	58	79
Surface 3°C	3.3 ± 0.4	38	1,900	50	73	101
Underground 3°C	3.4 ± 0.2	42	2,100	50	73	101

*Embryos were raised underground in SNOLAB and in the surface laboratory at Laurentian University at a temperature of approximately 5 or 3°C. Each petri dish was loaded with 50 embryos. Five petri dishes of embryos from each environmental condition were preserved for analysis at three different timepoints (40, 60, and 80% development). *Days post fertilization.*

(**Figure 1C**). A lateral image was taken of the yolk sac from which two perpendicular diameters were measured and used to calculate the yolk area (**Figure 1D**). Post imaging, the embryo and yolk were dried overnight at 70°C in an oven (1500EM, VWR) and weighed on an analytical balance (XA105DU, ±0.01 mg, Mettler Toledo). All size and mass measurements were taken with the researcher blinded to the rearing location. A subset of 10 embryos were fixed on day 1 post fertilization and weighed. At each of the three development stages, a yolk conversion efficiency (YCE) was calculated according to the equation:

$$\text{YCE } (\%) = \frac{\text{yolk free body dry mass}}{(\text{1 dpf yolk dry mass } - \text{yolk dry mass})} \times 100$$

Statistical Analysis

Statistical analysis was conducted using JMP V13.0 (SAS Institute Inc., Cary, NC, United States). Cumulative percent mortality at hatch and the time to 50% hatch were compared between the petri dishes that were not fixed for morphometric analysis (n = 24 for surface 5°C, n = 28 for underground 5°C, n = 23 for surface 3°C, n = 27 for underground 3°C). Mortality was compared using a two-way ANOVA followed by Tukey's HSD test with location (surface, underground) and temperature (5, 3°C) as the independent variables. Due to a temperature spike in the underground 3°C incubator prior to 50% hatch, a time to 50% hatch could only be calculated for the underground 5°C embryos and it was compared to the surface 5°C embryos using a t-test. Morphometric measurements and YCE were compared between embryos (n = 46–106) using a three-way ANOVA followed by Tukey's HSD test with location (surface, underground), temperature (5, 3°C) and percent development (40, 60, 80%) as the independent variables.

RESULTS

Embryonic Survival and Hatching

Across all incubation conditions the majority of embryonic mortality occurred during the first month of development (**Figure 2A**). Mortality then remained minimal from approximately day 30 until hatch. The cumulative percent survival at hatch ranged from 33–37% (**Figure 2C**) but was not significantly impacted by temperature (p = 0.91) or by the laboratory location (p = 0.30). Similarly, the laboratory location did not impact the timing of hatch. Embryos incubated at 5°C began to hatch earlier compared to those at 3°C (**Figure 2B**). The hatch window lasted approximately 60 days in embryos incubated at 5°C but the average time to 50% hatch was not significantly different underground (128 ± 11 days) or on the surface (128 ± 10 days, p = 0.98, **Figure 2D**). Embryos incubated at 3°C in both laboratories started hatching at approximately the same time and the hatching rate followed the same trend for the first 4 weeks (**Figure 2B**). However, on April 25, 2016 (145 dpf) the compressor failed on the refrigeration unit underground resulting in a temperature spike. At that point, only approximately 30% of the embryos in each petri dish had hatched. The temperature spike resulted in a premature hatching of all the remaining embryos. Therefore, a time to 50% hatch could not be accurately calculated for 3°C embryos.

Morphometric Analysis

Morphometric measurements were taken at three stages of development from both laboratories at each temperature. The temperature spike in the underground 3°C refrigeration unit did not impact these measurements as it occurred during the hatching stage, after the 80% development time point. As was expected, morphometric measurements correlated with the stage of development ($p < 0.05$). Body length, body mass and YCE were progressively larger (**Figures 3**, **5**) while yolk mass and yolk size were progressively smaller (**Figure 4**) as development progressed. The incubation temperature had a significant impact on body length, body mass, and yolk mass ($p < 0.05$). In general, embryos raised at the colder temperature had a larger body mass and body length (**Figure 3**) and a smaller yolk mass (**Figure 4A**). However, temperature did not significantly impact yolk area (p = 0.18) or YCE (p = 0.80). The laboratory location (surface vs underground) significantly impacted body and yolk morphometric measurements ($p < 0.05$) but not YCE (p = 0.80). Specifically, body size was greater in embryos incubated underground compared to the surface. This was evident in the 3°C embryos at 40 and 60% development, as well as the 5°C embryos at 80% development. The opposite trend was observed in yolk measurements which were smaller in embryos incubated underground compared to the surface. This was observed in the 3°C embryos at 40% development and the 5°C embryos at 80% development.

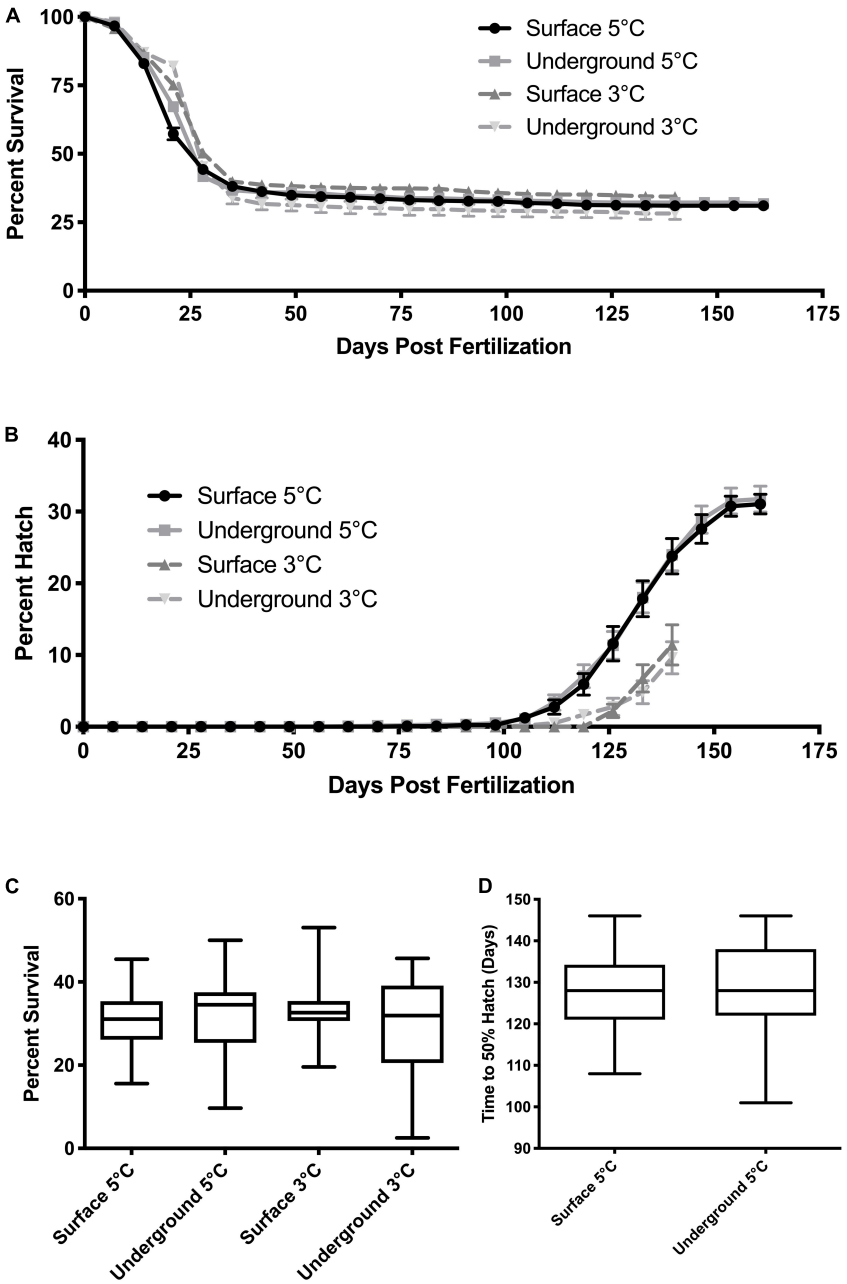

FIGURE 2 | Embryo survival and hatch timing. The cumulative percent survival **(A)** and percent hatch **(B)** was recorded each week starting at fertilization. Data points represent the mean ± SE across the replicate petri dishes (n = 38–43). Quartiles and range for the cumulative survival at hatch **(C)** and the time to 50% hatch **(D)** were calculated across the replicate petri dishes. Due to equipment failure, data from the 3°C conditions were only collected until day 140 post hatch and a time to 50% hatch could not be calculated. Mortality was compared using a two-way ANOVA followed by Tukey's HSD test with location (surface, underground) and temperature (5, 3°C) as the independent variables. Time to 50% was compared using a t-test.

DISCUSSION

There is a significant lack of published scientific studies with whole organism biological models in deep-underground environments. The data from this pilot study represent one of the first experiments to successfully raise a complex, multicellular, whole organism model in an underground laboratory. However, this study also highlights some of the unique challenges that are associated with this type of research.

In this study, we investigated growth and development during embryogenesis in lake whitefish (*C. clupeaformis*) within SNOLAB and in our surface control laboratory. Approximately 4,000 fertilized embryos were reared in each environment (**Table 1**). Embryonic mortality was highest in the first month

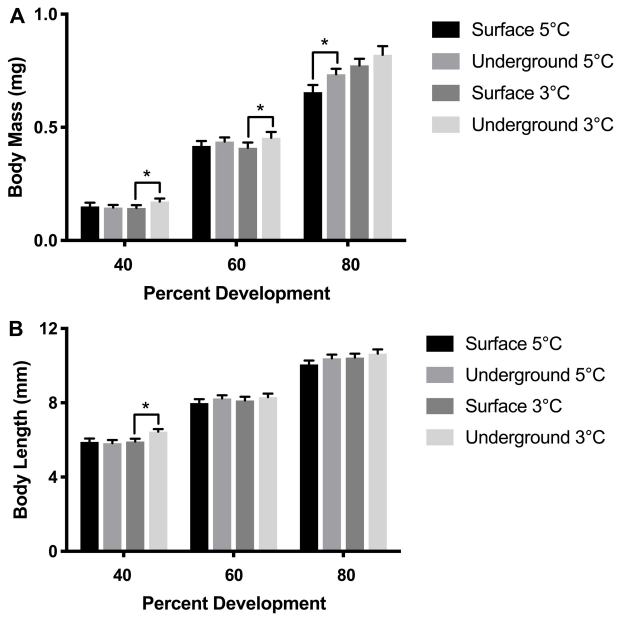

FIGURE 3 | Embryo size measurements. Body mass **(A)** and body length **(B)** were compared between embryos using a three-way ANOVA followed by Tukey's HSD test with location (surface, underground), temperature (5, 3°C) and percent development (40, 60, 80%) as the independent variables. Asterisk denote statistical differences ($p < 0.05$). Bars represent means ± 95% confidence intervals (n = 46–106).

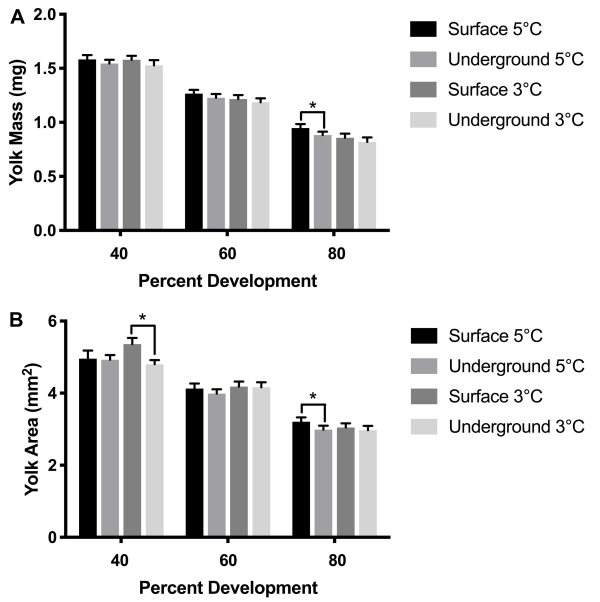

FIGURE 4 | Yolk size measurements. Yolk mass **(A)** and yolk area **(B)** were compared between embryos using a three-way ANOVA followed by Tukey's HSD test with location (surface, underground), temperature (5, 3°C) and percent development (40, 60, 80%) as the independent variables. Asterisk denotes statistical difference ($p < 0.05$). Bars represent means ± 95% confidence intervals (n = 57–105).

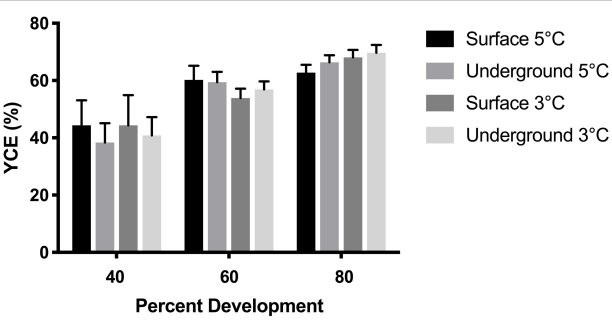

FIGURE 5 | Yolk conversion efficiency (YCE) was compared between embryos using a three-way ANOVA followed by Tukey's HSD test with location (surface, underground), temperature (5, 3°C) and percent development (40, 60, 80%) as the independent variables. Bars represent means ± 95% confidence intervals (n = 53–105).

post fertilization and then remained minimal for the remainder of development, which is common during lake whitefish laboratory rearing (Brooke, 1975; Mitz et al., 2014). The initial spike in mortality was therefore expected and was observed under all experimental conditions (**Figure 2A**). Rearing temperature did not significantly impact embryonic survival, but it did have an effect on time of hatch, with embryos incubated at the warmer 5°C temperature hatching earlier than at 3°C. Both of these effects were also expected and have been previously observed in lake whitefish (Brooke, 1975; Mitz et al., 2019). Both 3 and 5°C are within the optimal range for lake whitefish development, so mortality should be similar across the two temperatures (Brooke, 1975). At the same time, however, warmer temperatures are known to increase embryonic development rate, explaining why 5°C embryos hatched earlier (Mitz et al., 2019). The laboratory location (surface vs underground) did not significantly impact the cumulative percent survival, percent hatch or the timing of hatch (**Figures 2A,B**). This was expected as lake whitefish embryos are more robust to changes in rearing conditions with respect to survival and hatching, and changes in these two parameters would represent a more significant environmental stress.

Morphometric measurements are a sensitive endpoint that can be used to detect more subtle physiological changes. Morphometric analysis was performed in embryos raised in all experimental conditions at three stages of development based on previously established methods (Sreetharan et al., 2015). These morphometric endpoints: body and yolk mass, body length, and YCE, are ideal to evaluate the biological effects of different rearing environments. Body mass, length, and YCE increased with developmental advancement (**Figures 3**, **5**) whereas yolk size and mass decreased (**Figure 4**) as expected. Interestingly, the laboratory location (surface or underground) was also found to significantly affect body mass and length. The body size at several development points was greater when reared underground (**Figure 3**), which was paralleled by a reduction in yolk mass and area (**Figure 4**). Taken together, these data suggest that incubating embryos within SNOLAB can have a subtle yet significant effect on embryonic growth and development.

Changes in embryonic size have previously been shown in lake whitefish following different environmental stressors. In the current study, embryos incubated underground were up to 10% larger in size compared to the surface (**Figure 3**). A similar magnitude of size change has been shown following a temperature shift, where embryos incubated at 3°C were significantly larger compared to 5°C (Lim et al., 2017). Similarly, chronic chemical exposure to morpholine (1,000 mg/L) resulted in a reduction in embryo size of approximately 10% (Thome et al., 2017b). Of note, low dose radiation has been previously shown to stimulate growth in developing lake whitefish embryos when it was delivered as a chronic or fractionated exposure (Mitz et al., 2017a; Thome et al., 2017a).

The exact cause of the growth changes in the current experiment is not known. Deep-underground research is subject to unique experimental challenges, in terms of controlling variables compared to surface laboratories. In previous studies, challenges have included temperature, humidity, type of rock environment, radiation, and air pressure (Liu et al., 2018). The SNOLAB facility, where the REPAIR project is located is a Class 2000 cleanroom with highly regulated and monitored temperature, air quality, and humidity (Boger et al., 2000). Within SNOLAB, the rock overburden provides significant shielding from cosmic radiation. However radon, a radioactive gas that emanates from the decay of natural uranium found in the surrounding rock, is significantly higher in the air underground (Boger et al., 2000; Smith, 2012). Radon concentrations in SNOLAB vary depending on the time of day and the time of year, ranging from 100–150 Bq/m^3 (Hall, 2020). Conversely, ambient surface air radon levels in Sudbury are approximately 10 times lower ranging from 11–14 Bq/m^3 (Grasty, 1994). Future experiments planned by REPAIR will incorporate technologies to reduce radon levels in the underground laboratory. However, during this initial pilot project, radon was not controlled for. Radon gas comprises more than half of the natural background radiation dose (NCRP, 2009). Therefore, even though cosmic radiation levels are reduced underground, the elevated radon levels likely resulted in a greater total background dose to embryos. Our previous studies have shown that exposure to low dose gamma radiation stimulated growth in lake whitefish (Thome et al., 2017a). The higher radon levels underground may be one explanation for why embryos reared in SNOLAB were significant larger in body size. Another variable that was not controlled was air pressure, which is up to 25% higher underground (Duncan et al., 2010). This represents a variable that could potentially effect biological results as previously reviewed and discussed (Lampe et al., 2017; Liu et al., 2018; Xie et al., 2018). Future studies conducted by REPAIR will also add in experimental controls for the pressure differences underground.

One of the most challenging technical and logistical considerations with performing deep-underground research in the active mine where SNOLAB and the REPAIR project are located, is access to the facility. To access the underground laboratory facility, researchers assemble dressed in full personal protective equipment (PPE) mining gear and travel underground on an access cage to a depth of 2 km. Travel on foot is approximately 1.5 km through a mine drift to reach the facility. Once at SNOLAB, mine gear is removed, and a decontamination shower is required to eliminate remaining mine dust on the skin or in hair before re-dressing in Class 2000 cleanroom attire and PPE. Travel from the surface to the underground laboratory is limited by cage (elevator) runs, which are not available on every day of the week and can be variable dependent on the status of active mine work. This can be problematic for many biological experiments that require daily maintenance. Low maintenance models, such as lake whitefish, are ideal in this respect since they can survive multiple days between water changes. The restricted access to the laboratory also means that unexpected equipment issues become a challenge. For example, in the current experiment, at 145 dpf the 3°C underground refrigeration unit's compressor unexpectedly failed, resulting in a considerable temperature spike that led to a premature hatching of all remaining embryos. Although this did not influence morphometric analysis as 80% development had already been reached, this is an example of the types of novel challenges faced with this field of experimentation. Under normal surface laboratory conditions, researchers are usually available to mitigate unexpected situations. Limited access to the underground facility makes these types of events more probable and difficult to remediate. Finally, unexpected or planned power outages are another factor that needs to be considered when planning experiments in an underground facility. All of the REPAIR equipment is connected to uninterrupted power supply units that can provide battery backup power for several hours. Taken together, this emphasizes the highly unique nature of conducting experimental investigations within such a facility, and highlights the atypical logistical and technical challenges that researchers face in these environments.

The long-term research goals of the REPAIR project are focused on understanding the effects of a deep-underground environment in a variety of biological model systems (Pirkkanen et al., 2017; Thome et al., 2017c). Lake whitefish embryogenesis was chosen as a model system in this pilot project in order to evaluate the viability of performing biological experiments deep-underground within SNOLAB, where REPAIR is located. We have successfully demonstrated that a whole organism investigation is feasible. We have gained important insight into the unique technical and scientific challenges of this type of research. Based on this experience, projects currently underway by REPAIR were designed to control these special variables (e.g., underground radiological conditions). Moving forward, this will allow improved more precise investigations of effects of deep-underground environments on biological systems.

DATA AVAILABILITY STATEMENT

The raw data supporting the conclusions of this article will be made available by the authors, without undue reservation.

ETHICS STATEMENT

Ethical review and approval was not required for the animal study as per Canadian Council on Animal Care guidelines

section 4.1.2.2: "Work not requiring protocols or inclusion in animal use inventories: fish eggs, embryos or larvae that have not developed beyond exclusive reliance on their own yolk nutrients." All embryos in this study were preserved for analysis prior to consumption of yolk nutrients.

AUTHOR CONTRIBUTIONS

JP, AZ, TL, and CT performed embryonic rearing experiments underground and at the surface. JP performed morphometric analysis. CT performed statistical analysis and prepared figures. DB and CT designed and supervised experiments. JP and CT wrote sections of the first draft of the manuscript. SL and TT were collaborators and hold the NSERC CRD grants supporting this work. All authors contributed to manuscript editing, revision, and approved the submitted version.

FUNDING

The REPAIR project was supported through a Natural Sciences and Engineering Research Council (NSERC) Collaborative Research and Development (CRD), and MITACS grants in partnership with Bruce Power Inc.

ACKNOWLEDGMENTS

The authors would like to thank SNOLAB and its staff for support through underground space, logistical, and technical services. SNOLAB operations are supported by the Canada Foundation for Innovation and the Province of Ontario Ministry of Research and Innovation, with underground access provided by Vale at the Creighton mine site. The authors would like to additionally thank E. Hulley, S. Sreetharan, and C. West for technical assistance with morphometric analysis.

REFERENCES

Boger, J., Hahn, R. L., Rowley, J. K., Carter, A. L., Hollebone, B., Kessler, D., et al. (2000). The sudbury neutrino observatory. *Nucl. Instrum. Methods Phys.* 449, 172–207.

Brooke, L. T. (1975). Effect of different constant incubation temperatures on egg survival and embryonic-development in lake whitefish (*Coregonus-clupeaformis*). *Trans. Am. Fish. Soc.* 104, 555–559. doi: 10.1577/1548-86591975104<555:Eodcit<2.0.Co;2

Carbone, M. C., Pinto, M., Antonelli, F., Amicarelli, F., Balata, M., Belli, M., et al. (2009). The cosmic silence experiment: on the putative adaptive role of environmental ionizing radiation. *Radiat. Environ. Biophys.* 48, 189–196. doi: 10.1007/s00411-008-0208-6

Carbone, M. C., Pinto, M., Antonelli, F., Balata, M., Belli, M., Devirgiliis, L. C., et al. (2010). Effects of deprivation of background environmental radiation on cultured human cells. *Nuovo Cim. Della Soc. Ital. Fisica B Basic Top. Phys.* 125, 469–477. doi: 10.1393/ncb/i2010-10889-y

Castillo, H., Li, X., Schilkey, F., and Smith, G. B. (2018). Transcriptome analysis reveals a stress response of *Shewanella oneidensis* deprived of background levels of ionizing radiation. *PLoS One* 13:e0196472. doi: 10.1371/journal.pone.0196472

Castillo, H., Schoderbek, D., Dulal, S., Escobar, G., Wood, J., Nelson, R., et al. (2015). Stress induction in the bacteria *Shewanella oneidensis* and *Deinococcus radiodurans* in response to below-background ionizing radiation. *Int. J. Radiat. Biol.* 91, 749–756. doi: 10.3109/09553002.2015.1062571

Castillo, H., and Smith, G. B. (2017). Below-background ionizing radiation as an environmental cue for bacteria. *Front. Microbiol.* 8:177. doi: 10.3389/fmicb.2017.00177

Conter, A., Dupouy, D., and Planel, H. (1983). Demonstration of a biological effect of natural ionizing radiations. *Int. J. Radiat. Biol. Relat. Stud. Phys. Chem. Med.* 43, 421–432. doi: 10.1080/09553008314550481

Duncan, F., Noble, A. J., and Sinclair, D. (2010). The construction and anticipated science of SNOLAB. *Annu. Rev. Nucl. Part Sci.* 60, 163–180. doi: 10.1146/annurev.nucl.012809.104513

Fratini, E., Carbone, C., Capece, D., Esposito, G., Simone, G., Tabocchini, M. A., et al. (2015). Low-radiation environment affects the development of protection mechanisms in V79 cells. *Radiat. Environ. Biophys.* 54, 183–194. doi: 10.1007/s00411-015-0587-4

Grasty, R. L. (1994). Summer outdoor radon variations in Canada and their relation to soil moisture. *Health Phys.* 66, 185–193. doi: 10.1097/00004032-199402000-00009

Hall, J. (2020). The SNOLAB underground laboratory. *J. Phys. Conf. Ser.* 1468:012252. doi: 10.1088/1742-6596/1468/1/012252

Kawanishi, M., Okuyama, K., Shiraishi, K., Matsuda, Y., Taniguchi, R., Shiomi, N., et al. (2012). Growth retardation of *Paramecium* and mouse cells by shielding them from background radiation. *J. Radiat. Res.* 53, 404–410. doi: 10.1269/jrr.11145

Lampe, N., Breton, V., Sarramia, D., Sime-Ngando, T., and Biron, D. G. (2017). Understanding low radiation background biology through controlled evolution experiments. *Evol. Appl.* 10, 658–666. doi: 10.1111/eva.12491

Lim, M. Y., Manzon, R. G., Somers, C. M., Boreham, D. R., and Wilson, J. Y. (2017). The effects of fluctuating temperature regimes on the embryonic development of lake whitefish (*Coregonus clupeaformis*). *Comp. Biochem. Physiol. A Mol. Integr. Physiol.* 214, 19–29. doi: 10.1016/j.cbpa.2017.08.010

Liu, J., Ma, T., Liu, Y., Zou, J., Gao, M., Zhang, R., et al. (2018). History, advancements, and perspective of biological research in deep-underground laboratories: a brief review. *Environ. Int.* 120, 207–214. doi: 10.1016/j.envint.2018.07.031

Mitz, C., Thome, C., Cybulski, M. E., Laframboise, L., Somers, C. M., Manzon, R. G., et al. (2014). A self-contained, controlled hatchery system for rearing lake whitefish embryos for experimental aquaculture. *North Am. J. Aquac.* 76, 179–184. doi: 10.1080/15222055.2014.893472

Mitz, C., Thome, C., Cybulski, M. E., Somers, C. M., Manzon, R. G., Wilson, J. Y., et al. (2017a). Is there a trade-off between radiation-stimulated growth and metabolic efficiency? *Radiat. Res.* 188, 486–494. doi: 10.1667/RR14665.1

Mitz, C., Thome, C., Thompson, J., Manzon, R. G., Wilson, J. Y., and Boreham, D. R. (2017b). A method to transform a variable thermal regime to a physiologically equivalent effective temperature. *J. Therm. Biol.* 65, 21–25. doi: 10.1016/j.jtherbio.2016.12.011

Mitz, C., Thome, C., Cybulski, M. E., Somers, C. M., Manzon, R. G., Wilson, J. Y., et al. (2019). Thermal dependence of size-at-hatch in the lake whitefish (*Coregonus clupeaformis*). *Can. J. Fish. Aquat. Sci.* 76, 2069–2079. doi: 10.1139/cjfas-2018-0097

Morciano, P., Iorio, R., Iovino, D., Cipressa, F., Esposito, G., Porrazzo, A., et al. (2018). Effects of reduced natural background radiation on *Drosophila melanogaster* growth and development as revealed by the FLYINGLOW program. *J. Cell Physiol.* 233, 23–29. doi: 10.1002/jcp.25889

Mueller, C. A., Eme, J., Manzon, R. G., Somers, C. M., Boreham, D. R., and Wilson, J. Y. (2015). Embryonic critical windows: changes in incubation temperature alter survival, hatchling phenotype, and cost of development in lake whitefish (*Coregonus clupeaformis*). *J. Comp. Physiol. B* 185, 315–331. doi: 10.1007/s00360-015-0886-8

NCRP (2009). *Ionizing Radiation Exposure of the Population of the United States. Report No. 160*. Bethesda, MD: NCRP.

Pirkkanen, J. S., Boreham, D. R., and Mendonca, M. S. (2017). The CGL1 (HeLa x Normal Skin Fibroblast) human hybrid cell line: a history of ionizing radiation induced effects on neoplastic transformation and novel future directions in SNOLAB. *Radiat. Res.* 188, 512–524. doi: 10.1667/RR14911.1

Planel, G., Soleilhavoup, J. P., Tixador, R., Croute, F., and Richoilley, G. (1976). *Demonstration of a Stimulating Effect of Natural Ionizing Radiation and of Very Low Radiation Doses on Cell Multiplication*. IAEA: International Atomic Energy Agency (IAEA).

Satta, L., Antonelli, F., Belli, M., Sapora, O., Simone, G., Sorrentino, E., et al. (2002). Influence of a low background radiation environment on biochemical and biological responses in V79 cells. *Radiat. Environ. Biophys.* 41, 217–224. doi: 10.1007/s00411-002-0159-2

Smith, G. B., Grof, Y., Navarrette, A., and Guilmette, R. A. (2011). Exploring biological effects of low level radiation from the other side of background. *Health Phys.* 100, 263–265. doi: 10.1097/hp.0b013e318208cd44

Smith, N. J. T. (2012). The SNOLAB deep underground facility. *Eur. Phys. J. Plus* 127:108.

Sreetharan, S., Thome, C., Mitz, C., Eme, J., Mueller, C. A., Hulley, E. N., et al. (2015). Embryonic development of lake whitefish *Coregonus clupeaformis*: a staging series, analysis of growth and effects of fixation. *J. Fish Biol.* 87, 539–558. doi: 10.1111/jfb.12725

Thome, C., Mitz, C., Hulley, E. N., Somers, C. M., Manzon, R. G., Wilson, J. Y., et al. (2017a). Initial characterization of the growth stimulation and heat-shock-induced adaptive response in developing lake whitefish embryos after ionizing radiation exposure. *Radiat. Res.* 188, 475–485. doi: 10.1667/RR14574.1

Thome, C., Mitz, C., Sreetharan, S., Mitz, C., Somers, C. M., Manzon, R. G., et al. (2017b). Developmental effects of the industrial cooling water additives morpholine and sodium hypochlorite on lake whitefish (*Coregonus clupeaformis*). *Environ. Toxicol. Chem.* 36, 1955–1965. doi: 10.1002/etc.3727

Thome, C., Tharmalingam, S., Pirkkanen, J., Zarnke, A., Laframboise, T., and Boreham, D. R. (2017c). The REPAIR project: examining the biological impacts of sub-background radiation exposure within SNOLAB, a deep underground laboratory. *Radiat. Res.* 188, 470–474. doi: 10.1667/RR14654.1

Xie, H. P., Liu, J. F., Gao, M. Z., Wan, X. H., Liu, S. X., Zou, J., et al. (2018). [The Research Advancement and Conception of the Deep-underground Medicine]. *Sichuan Da Xue Xue Bao Yi Xue Ban* 49, 163–168.

Conflict of Interest: DB was employed by the company Bruce Power.

The remaining authors declare that the research was conducted in the absence of any commercial or financial relationships that could be construed as a potential conflict of interest.

frontiers in Public Health

ORIGINAL RESEARCH
published: 16 October 2020
doi: 10.3389/fpubh.2020.581796

The Phenotypic and Transcriptomic Response of the *Caenorhabditis elegans* Nematode to Background and Below-Background Radiation Levels

Wayne A. Van Voorhies[1]*, *Hugo A. Castillo*[2], *Cung N. Thawng*[1] and *Geoffrey B. Smith*[1]

[1] *Molecular Biology Program and Biology Department, New Mexico State University, Las Cruces, NM, United States,* [2] *Human Factors and Behavioral Neurobiology Department, Embry-Riddle Aeronautical University, Daytona Beach, FL, United States*

Studies of the biological effects of low-level and below-background radiation are important in understanding the potential effects of radiation exposure in humans. To study this issue we exposed the nematode *Caenorhabditis elegans* to average background and below-background radiation levels. Two experiments were carried-out in the underground radiation biology laboratory at the Waste Isolation Pilot Plant (WIPP) in New Mexico USA. The first experiment used naïve nematodes with data collected within 1 week of being placed underground. The second experiment used worms that were incubated for 8 months underground at below background radiation levels. Nematode eggs were placed in two incubators, one at low radiation (ca.15.6 nGy/hr) and one supplemented with 2 kg of natural KCl (ca. 67.4 nGy/hr). Phenotypic variables measured were: (1) egg hatching success (2) body size from larval development to adulthood, (3) developmental time from egg to egg laying adult, and (4) egg laying rate of young adult worms. Transcriptome analysis was performed on the first experiment on 72 h old adult worms. Within 72 h of being underground, there was a trend of increased egg-laying rate in the below-background radiation treatment. This trend became statistically significant in the group of worms exposed to below-background radiation for 8 months. Worms raised for 8 months in these shielded conditions also had significantly faster growth rates during larval development. Transcriptome analyses of 72-h old naïve nematode RNA showed significant differential expression of genes coding for sperm-related proteins and collagen production. In the below-background radiation group, the genes for major sperm protein (*msp*, 42% of total genes) and sperm-related proteins (7.5%) represented 49.5% of the total genes significantly up-regulated, while the majority of down-regulated genes were collagen (*col,* 37%) or cuticle-related (28%) genes. RT-qPCR analysis of target genes confirmed transcriptomic data. These results demonstrate that exposure to below-background radiation rapidly induces phenotypic and transcriptomic changes in *C. elegans* within 72 h of being brought underground.

Keywords: low radiation, biological response, *c. elegans*, deep biosphere, major sperm protein

OPEN ACCESS

Edited by:
Carmel Mothersill, McMaster University, Canada

Reviewed by:
Nguyen T. K. Vo, McMaster University, Canada
Jennifer Lemon, Northern Ontario School of Medicine, Canada

***Correspondence:**
Wayne A. Van Voorhies
wavanvoo@nmsu.edu

Specialty section:
This article was submitted to Radiation and Health, a section of the journal Frontiers in Public Health

Received: *09 July 2020*
Accepted: *31 August 2020*
Published: *16 October 2020*

Citation:
Van Voorhies WA, Castillo HA, Thawng CN and Smith GB (2020) The Phenotypic and Transcriptomic Response of the Caenorhabditis elegans Nematode to Background and Below-Background Radiation Levels. Front. Public Health 8:581796. doi: 10.3389/fpubh.2020.581796

INTRODUCTION

Life on earth has evolved with a constant exposure to ionizing radiation (1, 2). While all organisms are continuously exposed to ionizing radiation, natural rates of exposure can vary widely. Worldwide there is an ∼1,000-fold range in natural background radiation levels, with radiation exposure levels ranging from under 50 nGy hr^{-1}, to almost 30,000 nGy hr^{-1} (3, 4). No cytogenetic differences were documented in people living at elevated levels of radiation in Ramsar, Iran compared to control groups living at normal background (3). In a more thorough review of elevated radiation sites across the world (5), report little or no detrimental effects in residents of elevated radiation areas, but point out the need for more controlled studies. For the purposes of the discussion below, we follow (5) in defining normal background as levels ranging from 1 to 5 mSv/yr (114–570 nGy/hr).

Because of the known adverse effects of high levels of radiation exposure in biological systems, scientific and regulatory agencies have established occupational and public exposure limits. These are based on the "Linear No Threshold" (LNT) model. This model assumes that there is a linear increase in deleterious effects as radiation dose levels rise, and according to this model, no radiation level is considered safe (6). There are numerous animal model studies which contradict the LNT model and Skyes (7) has recently proposed that "Until those on one side of the debate can convince the other, it would be sensible to move forward toward a graded (risk-based) approach to regulation, where the stringency of control is commensurate with the risk, resulting hopefully in more sensible practical thresholds."

While the high-dose region of this model is well-supported by epidemiological and experimental data, its validity at low doses, particularly near background values, has been challenged (8–10). Experiments have shown that cells grown at below normal levels of radiation exhibit potentially deleterious responses compared to cell grown under normal background radiation levels (11, 12). The biologic effects of below-normal background radiation are relatively unstudied (13). One reason for the lack of information on the effects of low radiation are the difficulties associated with conducting such studies. In order to obtain the low radiation levels required for such studies, experiments must be carried out deep underground to provide shielding from cosmic radiation or in lead-shielded incubators aboveground. Low-level, underground radiation experiments studies require that the geologic formation is itself a low radiation emitter with minimal levels of radon present.

The few studies that have been done in such sites show interesting biological responses in organisms grown in below-normal background radiation levels. Pioneering experiments examining effects of below-normal background radiation levels demonstrated that cultures of *Paramecium tetraurelia* grown at 11.4 nGy hr^{-1} had a reduced grow rate and longer generation time, compared to control cultures grown at 199 nGy hr^{-1} (14). A similar result was reported for bacterial cultures of *Synechococcus lividus* grown at 30 nGy hr^{-1} and 172 nGy hr^{-1}. In both cases, normal growth was restored upon the addition of a radiation source equivalent to control levels (14).

In similar experiments Satta et al. reported that *Saccharomyces cerevisiae* cells grown at 4.5 nGy hr^{-1} exhibited a higher frequency of DNA damage when exposed to the genotoxin methyl-methane sulfonate compared to cultures grown at background levels (15). They also found numerous biological differences between the hamster tissue cell cultures grown at 4.5 nGy hr^{1} and normal background radiation levels. Specifically, they found that compared to cultures grown at normal background radiation levels, cells grown at low radiation levels had a lower cell density at confluence, increased accumulation of reactive oxygen species, an increased mutation rate when exposed to acute doses of gamma rays, and a higher rate of cellular apoptosis in the presence of cycloheximide (16). Castillo et al. (17–19) have documented a stress response in two bacterial species within 48 h of being brought underground and grown in the absence of normal radiation levels. Morciano et al. (20) were the first group to document these effects in a multi-cellular organism (*Drosophila),* with reduced radiation causing a 30% reduction in fertility in males and females, while also causing an increase in life span.

Understanding the biological effects of low level radiation exposure has become more urgent in the face of the widespread and increasing use of ionizing radiation in medical imaging and treatments (21). Knowledge of the effects of low level radiation are also critical in determining appropriate levels of radiation exposure for workers involved with nuclear clean-up or other activities involving nuclear material. To further document the effects of low level radiation on a multicellular organism we conducted experiments at the U.S. underground nuclear waste repository at the Waste Isolation Pilot Plant (WIPP) located near Carlsbad, NM. For this study we grew parallel populations of the nematode *Caenorhabditis elegans* underground in an incubator that was shielded from radiation and in an incubator supplemented with KCl to give background radiation levels. We then compared basic life-history and gene expression patterns between these two groups to document if these low radiation levels induced any biological response.

MATERIALS AND METHODS

Low Background Radiation Experiment, LBRE

All of the low level radiation experiments were carried out at a nuclear waste disposal site operated by the United States Department of Energy located 42 km east of Carlsbad, NM. This site, designated as the Waste Isolation Pilot Plant (WIPP), was designed to permanently store transuranic wastes generated from the U.S. military weapons program. The nuclear waste material is stored 650 m underground in a 610-m-thick Permian aged sea-salt deposit. The WIPP site began receiving nuclear waste in March 1999. An underground equipment fire and radiation release from a spontaneous fire in a waste storage drum in 2014 halted underground storage for ∼3 years, with the site resuming emplacement of nuclear waste in January 2017.

In addition to nuclear waste storage, the WIPP site also has hosted several scientific projects that take advantage of the

naturally occurring, extremely low background radiation levels found underground. These low background radiation levels are a consequence of the shielding from cosmic radiation provided by the underground depth of the site, and because the NaCl layer in which the site is located does not produce any natural radioactive decay particles. A low background radiation biology laboratory (the LBRE lab) was established in the North Experimental Area section of the mine in 2009 and is located ∼one km from any nuclear waste. To further reduce background radiation levels, the LBRE laboratory houses a multi-ton, 2.5 × 2 × 2 m by 15 cm-thick steel vault that provides additional radiation shielding. This vault was made from steel produced prior to World War II and is free of any radioactive contamination caused by fallout from aboveground nuclear bomb testing.

Two Sable System (Sable Systems, Las Vegas, NV, USA) incubators were placed adjacent to each other in this vault. Because of this close spacing both incubators would have essentially identical air pressures. The control group was exposed to a radiation level of ∼70 nGy hr^{-1}, a level matching typical average surface background radiation levels. To provide this radiation level 2 kg of KCl was placed in four hollow plexiglass panels that surrounded the rack containing the Petri dishes in which the *C. elegans* were grown. KCl emits radiation due to the decay of the naturally occurring ^{40}K isotope. By carefully regulating the amount and location of the KCl a radiation field approximating normal surface radiation can be created (17, 18). While a single radiation source will not fully represent the radiation spectrum of natural sources, as discussed previously (17), K is the dominant terrestrial radiation source and the majority of the photons from the ^{40}K 1460 KeV emission undergo Compton scattering, which then produces a cascade of lower-energy electrons and deflected gamma rays. This results in a broad range of secondary ionization events with a wide spectrum of ionizing energies (22). Ion Chamber detector measurements were taken inside the KCl-supplemented incubator. The dose rate was measured to be 52 (+/- 8.7) nGy $hr^{-1}$and, in combination with the dose received from the media (15.4 nGy/hr, see below), the KCl-supplemented cells were exposed to ∼67.4 nGy/hr. Radon was measured to be 15.6 Bq/m^3 in the underground (19) and is close to outdoor levels in the region, ∼14.8 Bq/m^3 (U.S. EPA map of radon zones) (23).

In order to shield radiation from the KCl control incubator, five water-filled 20-L carboys were placed around the outside of the incubator. The below background radiation *C. elegans* group was located in a separate incubator surrounded by an identical set of panels that were filled with 2 kg of NaCl. In previous work, radiation levels inside the vault were calculated to be ∼0.16 nGy hr^{-1} by Monte Carlo MCNP analyses (17). However, due to the 25 mM potassium buffer present in the nematode growth medium, the below background radiation levels were substantial but too diffuse to measure and so were calculated: 15.4 nGy hr^{-1} from the NGM medium and 0.16 nGy/hr by MCNP to give ∼15.6 nGy/hr for the dose rate for the shielded cells [the MCNP calculation was described by Castillo et al. (17)]. The incubators were set to 20.0°C, with temperatures monitored at 5-min increments with Hobo temperature data loggers (Pendant UA-002-64, Onset, Borne, MA, USA).

The phenotypic variables measured in these experiments were: (1) egg hatching success, (2) the body size of worms from larval development to adulthood, (3) developmental time from egg to egg laying adult, and (4) the egg laying rate of young adult worms. The advantage of measuring these four easy-to-quantify parameters is that they provide a very sensitive indicator of any factors influencing the physiological condition of the worm (24). Additionally, groups of worms were collected to determine patterns of gene expression at 24, 48, and 72-h time points by transcriptome analysis and RT-PCR verification.

A potential complication in measuring all of these variables, however, is that they are also very sensitive to the ambient temperature at which the worms are reared. For this reason, it is critical that the worms were maintained in incubators that are precisely able to regulate and maintain a constant temperature. To ensure that the temperature in the incubators remained within 0.1°C of the 20°C set-point we used Sable Systems incubators that employ Peltier-based heating and cooling units regulated by a proportional-integral-derivative temperature controller. Extensive testing of these incubators showed that all of the incubators were able to maintain the incubator temperature within 0.1°C of the set-point temperature over the course of the experiment. Additional details on this are provided in the **Supplemental Materials**.

C. elegans Cultures

All experiments were done using the wild-type N2 strain obtained from the *Caenorhabditis* Genetics Center (Minneapolis, MN, USA). The worm culture used was revived from laboratory storage in liquid nitrogen in May 2015 and maintained in 15–20°C incubators prior to the start of the experiments. Worms were grown on Petri dishes filled with NGM [Nematode Growth Medium, (25)] inoculated with bacterial lawns of *Escherichia coli* strain OP50.

A starter culture of worms was prepared 3 days prior to the start of the experiment. Groups of around 25 adult worms laid eggs for 3 h to produce an age-synchronized cohort of eggs. The adults that developed from this age-synchronized cohort were then used to produce the eggs used in the experiment. To control for potential effects of parental age (26), the eggs used in all the experiments were laid by hermaphrodites that were between 72 and 78 h of age and the age of the starter (Po) worms was matched for each set of experiments.

One belowground experiment was done in December 2016, and a second in August 2017. The first experiment was started using age-synchronized 76-h-old Po worms that had developed in a 20°C incubator located at New Mexico State University. A temperature of 20°C is close to the thermal optimum for *C. elegans*, with the worms having maximal fecundity, rapid egg laying, and rapid development at this temperature (27). These worms were transported to the WIPP site in a portable incubator kept at 20°C and taken to the underground lab to start the experiment. Adult worms from these starter plates were placed on each of 18 NGM 65 mm Petri dishes for 3 h, with ∼25 worms placed on each of the plates. At the end of this 3-h period the adult worms were removed from the plates and an individual egg was transferred onto a 35 mm NGM-filled Petri

dish spotted with OP50 using a fine platinum wire. A total of 50–60 such plates were obtained; half of the plates were placed in the below background incubator, and the other half were placed in the KCl- supplemented control incubator. Additionally, nine 65 mm NGM plates with eggs were placed in each of the respective incubators. These plates were used over the course of the experiment to collect worms for gene expression studies. A subset of 125 eggs from the 65 mm Petri dishes was monitored for egg hatching success by observing how many eggs remained unhatched after 24 h. These groups of worms were then placed in the incubators and surrounded with plexiglass panels filled with KCl (surrogate for normal background radiation) or NaCl (low radiation group).

Development of these eggs to egg-laying adults was monitored for the next 72 h at ∼24-h intervals. Each egg placed in the 35 mm Petri dish was individually measured for body based on an image of the worms recorded with a digital video camera (Scion, Fredrick, MD, USA) connected to a MS5 Lecia dissecting microscope and linked to an Apple MacBook Pro computer. These images were analyzed using ImageJ software to determine the length of the developing worms at 24, 48, and 72 h of age. Depending on the magnification, either a hemocytometer slide or a calibrated scale standard was used as a size standard and the worms were measured at magnifications between 40 and 80 X. The time of egg laying was ranked as age 0 h.

The rate of egg laying and age of first reproduction were determined by monitoring the developing worms at 2-h intervals once the worms were ∼64-h old. The age of first reproduction was based on when the first laid egg was observed on the Petri dish. The egg-laying rate was then calculated from the number of eggs laid by the worm in the proceeding 2-h interval. If eggs were already present on the plate by the first observation interval, the age of first reproduction was calculated based on the average egg-laying rate of the group of worms. Due to safety restrictions, WIPP personnel had to be on the surface by early evening. Because of this worms could not be monitored for egg laying past the 74 h time point and it was not possible to collect data for the total number of progeny produced by a worm. If the worm had not laid eggs by the end of the day-three sampling period, it was not included in the analysis. Three such worms were removed from each of the background and low level radiation groups for the first underground experiment and one from each group for the second experiment.

The second underground low radiation experiment was done in August 2017. The intent of the second underground experiment was to see if long-term, multigenerational exposure to below background radiation levels had any detectable effect on the worms. While conceptually identical to the first experiment, the major difference between this experiment and the first was that the starter worms for the low radiation group had been exposed to below background radiation since December 2016, ∼8 months. This worm culture was derived from the low radiation treatment group used in the December 2016 experiment and left in a 20°C incubator inside the steel vault. They were transferred to new plates four times prior to the start of second belowground experiment. When left on NGM plates for long periods *C. elegans* can complete approximately three generations before all the food on the plate is depleted. The remaining worms then reduce their metabolism and become relatively dormant, but quickly revive when placed on new NGM plates (28). Based on this, a conservative estimate is that the belowground worms would have been exposed to low level radiation conditions for a minimum of 10 generations. Other studies have shown that the effects of a biological perturbations to *C. elegans* can persist for many generations (29). The control group for the second underground experiment was derived from an identical population of *C. elegans* maintained and transferred in parallel in a 20°C surface incubator at New Mexico State University. To control for the potential effects of transporting the worms to the test site, the worms used to produce the eggs used in the experiment were reared for one full generation at the WIPP underground site while exposed to KCl radiation. This should minimize any residual effects of transport stress or acclimatization on the experimental results.

RNA Extraction, Library Preparation, and Sequencing

Worms were washed off plates using ∼2 ml of M9 buffer (25), and spun down at room temperature for 1 min at 2,000 rpm. The supernatant was removed and 400 ul of Trizol was added to lyse the worms, vortexed for 30 s and frozen at −80C. In both the initial short-term and the **second** long-term incubations, only the 72-h time-point yielded enough RNA for transcriptome analysis, and in the 2nd experiment this was further limited by only having **one** replicate control sample. Therefore, presentation of transcriptome data will be limited to only the **first** experiment.

One ug of RNA was used for cDNA library construction at Novogene (Sacramento, CA) using the NEBNext® Ultra 2 RNA Library Prep Kit for Illumina® (cat NEB **#E7775**, New England Biolabs, Ipswich, MA, USA) according to the manufacturer's protocol. After a series of terminal repair, poly-adenylation, and sequencing adaptor ligation, the double-stranded cDNA library was completed followed size selection and PCR enrichment. The resulting 250–350 bp insert libraries were quantified using a Qubit 2.0 fluorometer (Thermo Fisher Scientific, Waltham, MA, USA) and quantitative PCR. Size distribution was analyzed using an Agilent 2100 Bioanalyzer (Agilent Technologies, Santa Clara, CA, USA). Qualified libraries were sequenced on an Illumina Nova Seq 6000 Platform (Illumina, San Diego, CA, USA) using a paired-end 150 run (2 × 150 bases). ∼20 million raw reads were generated from each library. An average of 26.5 ± 3.5 million reads were generated from each library.

Experimental Design and Data Analysis

Two experiments were run in the WIPP underground, the first using naïve nematodes, the second using nematodes that were incubated for 8 months in sub-normal underground radiation conditions. For the phenotypic analyses of both experiments, there were between 15 and 30 biological replicates for each timepoint, represented by randomly chosen single nematodes on 15–30 NGM agar plates. It is standard practice in *C. elegans* studies to consider a single worm as an individual when analyzing data [e.g., (28, 30–33)]. Consistent with this, in our experiments a separate animal in an individual Petri dish was counted

as a single biological replicate for the analysis of phenotypic traits. For the transcriptome analyses, only the 72-h timepoint from the 1st experiment was analyzed. Two biological replicates (two independent NGM agar plates of ∼ 300 nematodes on each plate) of the control (amended with KCl to represent background radiation) and treatment (below background radiation) underwent transcriptome pipeline analyses.

Statistical analysis of the phenotypic trait data was done using StatPlus v5 (AnalystSoft Inc, Walnut, CA). For the transcriptome analyses, three programs were utilized ArrayStar (ArrayStar® and QSeq®. Version 16.0.0. DNASTAR, Inc., Madison, Wisconsin, USA), CLC Genomics Workbench 12.2 (Qiagen Bioinformatics, Germantown, MD, USA) and Partek Flow (Partek Inc., St. Louis, MO, USA). The raw reads of RNA Seq were mapped against reference genome assembly of *C. elegans* (strain Bristol N2) (GCF_000002985.6) using analysis pipeline of Partek Flow software (Partek Inc., St. Louis, MO, USA) with default parameter. Alignment was performed with Bowtie 2 and differential gene expression was identified by Partek GSA algorithm. All RNA Seq data were screened for False Discovery Rate (FDR), and were accepted if FDR $<$ 0.05 (34) with 2-fold change cut-off. Raw RNA sequences were trimmed, aligned and mapped against the reference genome of *C. elegans* (strain Bristol N2) (GCF_000002985.6). Expression of the genes was normalized by calculating RPKM (reads per kilobase of transcripts per million mapped reads]. The raw reads of RNA seq were also mapped against reference genome of *C. elegans* (strain Bristol N2) (NC_003279.8, NC_003280.10, NC_003281.10, NC_003282.8, NC_003283.11, NC_003284.9) using ArrayStar (ArrayStar® and QSeq®. Version 16.0.0. DNASTAR, Inc., Madison, Wisconsin, USA). The reads were normalized by RPKM method and gene expression were performed by using default parameter of ArrayStar. Raw RNA sequences were also analyzed by CLC genomics pipeline with default parameter. The raw RNA sequences obtained in this study were deposited at NCBI database (Accession number PRJNA631208). The significantly up and down regulated genes were analyzed for gene ontology (GO) term enrichment (FDR value $<$0.05) using g:Profiler (35) and REVIGO (36) for visualization. Functional analysis was also performed by WormCat: an online tool for an annotation and visualization of C. *elegans* Genome scale data (37).

RT-qPCR

The validity of differential expression was verified by using RT-qPCR for direct comparison with RNA Seq. The qPCR reactions (10 uL) were performed in triplicate using iTaq Universal One-Step RT-qPCR kit (BioRad, Hercules, CA, USA) with 0.5 μM of each primer (**Supplementary Table 1**), and 1 ng of total RNA as template. A first cDNA was synthesized by reverse transcription at 50°C for 10 min followed by RT inactivation at 95°C for 1 min. The reaction was directly followed by PCR amplification as follows: 40 cycles of denaturation: 30 s at 95°C; annealing: 30 s at 60°C; and extension: 30 s at 72°C. After amplification, the melt curve protocol followed with 30 s at 96°C and then 5 s each at 0.5°C increment between 60 and 95°C. The relative expression of the target genes *was* calculated using *act-1 and ubq-1* as reference genes and using the efficiency-corrected model (38). Ten genes from the transcriptome data were selected as potential reference gene for RT-PCR based on their downregulation (fold change $<$ +1 and $>$ −0.01). Primers were synthesized for 20 representative *msp* and *col* genes, and 10 reference genes using NCBI primer designing tool (https://www.ncbi.nlm.nih.gov/tools/primer-blast/index.cgi). From these 30 primer sets, properly calibrated standard RT-PCR curves were generated for 10 *msp*, 3 *col* and 8 reference genes. The act-1 and ubq-1 genes were chosen from a group of 10 potential reference genes (**Supplementary Table 1**) after being screened by NormFinder (39) and BestKeeper (40) method. For each comparison, 6 Ct values from two biological replicates were used for all calculations for relative expression of the target genes.

RESULTS

Phenotypic Response to Below Background Radiation Levels

Conducting underground experiments at the WIPP site presented unusual challenges. The primary difficulty encountered was gaining access to the underground laboratory in a timely manner. Underground access was limited due to factors such as nuclear waste transportation issues, personnel access limitations due to ventilation restrictions in place since the radiation contamination event, planned and unplanned power outages, mine equipment failures, and above- and belowground safety drills. All of these factors restricted when data could be collected during the underground experiments. One experiment had to be terminated due to an underground power failure which caused the incubator temperatures to rise to unacceptable levels. As a result, complete phenotypic and partial genotypic data sets were obtained from two separate underground experiments.

The four phenotypic traits assayed: egg hatching success, body size over time, age at first reproduction, and early egg laying rate, proved to be sensitive markers for differences in radiation exposure. This was particularly the case for the population of *C. elegans* that had a long-term, multi-generational exposure to extremely low radiation levels.

Egg Hatch Rate, Body Size, and Life Cycle Time

For the second underground experiment, egg hatching rates were determined for 125 eggs divided into five sets of eggs for both the normal radiation and low below background radiation groups. Hatch rate was 100% for both groups ($n = 125$ for both groups).

There were no apparent differences between any of the groups in feeding or egg laying behavior. These observation periods, however, were minimized as it was important to keep the worms in the temperature and radiation controlled incubators for as much of the experiment as possible.

Measurements of body size were based on comparisons of worm length. In nematodes there is a near perfect correlation with overall volume, i.e., size, and worm length. As seen in **Figure 1A**, in the first underground experiment the body size of the two groups was similar. The low level radiation group was slightly, but not statistically larger than the control level radiation group at 48 h of age. In the second experiment larvae

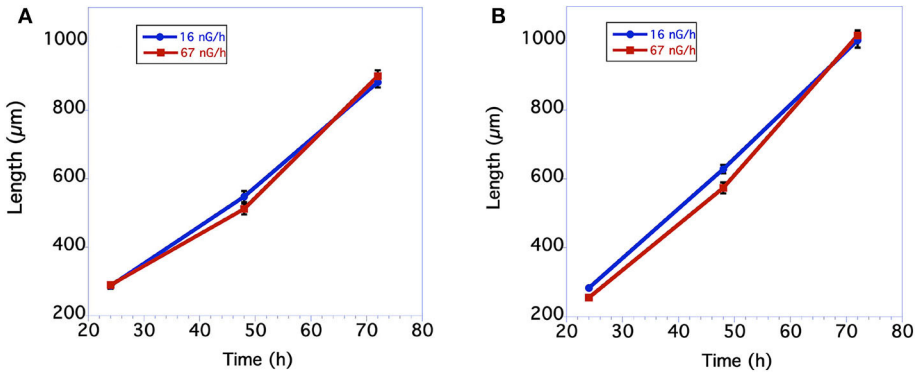

FIGURE 1 | Comparison in length of *C. elegans* grown at normal background or low radiation levels. **(A)** Data from first underground experiment on 12/2016. The means and SEM are plotted for each group. $N = 15–22$ for each time point. No significant differences in worm size between the 2 groups at any of the 3 time points. For 24 h size $p = 0.84$ $T = 0.21$, df = 30; For 48 h size $p = 0.12$ $T = 1.60$, df = 38; for 72 h size $p = 0.45$ $T = 0.76$, df = 39. All data were analyzed using a Student's *T*-test with a two-tailed distribution. **(B)** Data from second underground experiment on 8/2017. The means and SEM are plotted for each group. $N = 23–30$ for each time point. Low radiation worms are significantly bigger at the 24 and 48 h time points. For 24 h size $p = 0.00004$ $T = 4.55$ df = 48; For 48 h size $p = 0.008$ $T = 2.77$ df = 54; for 72 h size $p = 0.62$ $T = 0.50$, df = 51. All data were analyzed using a Student's *T*-test with a two-tailed distribution.

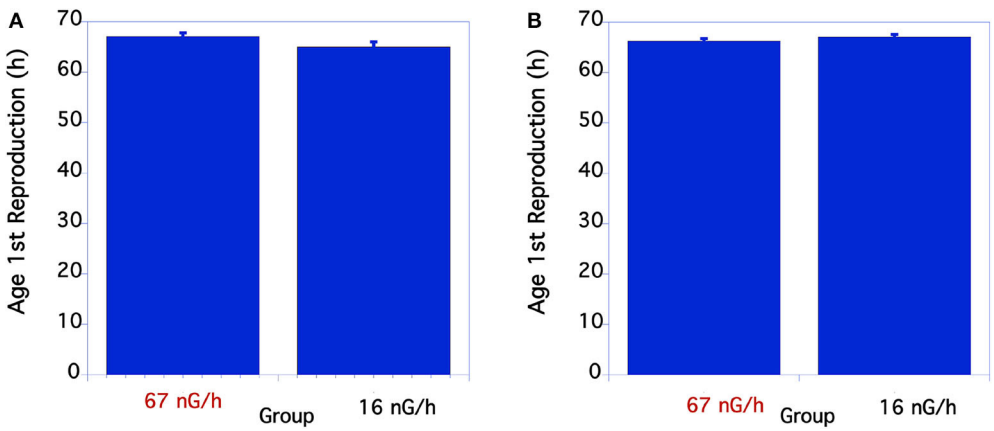

FIGURE 2 | Comparison of time to complete life cycle *in C. elegans* grown at normal or low radiation levels. **(A)** Lifecycle time comparison of *C. elegans* in 12/2016. $N = 18-22$. $p = 0.078$ $T = 1.8$, df = 29. In the second underground experiment on 8/2017 the developmental times of the two groups was almost identical **(B)** $p = 0.21$ $T = 1.26$, df = 50. **(B)** From 8/17 Experiment. The means and SEM are plotted for each group. $N = 23–30$ for each time point. There were no significant differences in developmental time between the two groups.

growing in low radiation conditions for ∼10 generations were significantly larger than larvae from the normal radiation level group through 48 h (**Figure 1B**). The adult body size of 72 h old worms from these two groups, however, was not significantly different. The time from when an egg was first laid until it developed into an egg-laying adult was compared between the normal and low level radiation groups. As seen in **Figure 2A**, in the first underground experiment the low radiation group developed slightly, but not significantly, faster than the Control radiation group. In the second experiment the developmental times of the two groups was almost identical (**Figure 2B**) and not significantly different. All data were analyzed using a Student's *T*-test with a two tailed distribution.

For the two aboveground experimental controls there were no significant differences between the life cycle time of the worms at any of the timepoints measured when compared within each experiment.

Egg Laying Rate

The initial egg laying rate of *C. elegans* was compared between the control and low level, below background radiation groups. As seen in **Figure 3A**, in the first underground experiment the low-radiation group had a slightly, but not significantly greater egg-laying rate than the normal background radiation group. In the second experiment the egg-laying rate of the low radiation group was significantly greater than the normal radiation control group (**Figure 3B**).

For the two aboveground experimental controls there were no significant differences between the size of the worms at any of the timepoints measured when compared within each experiment.

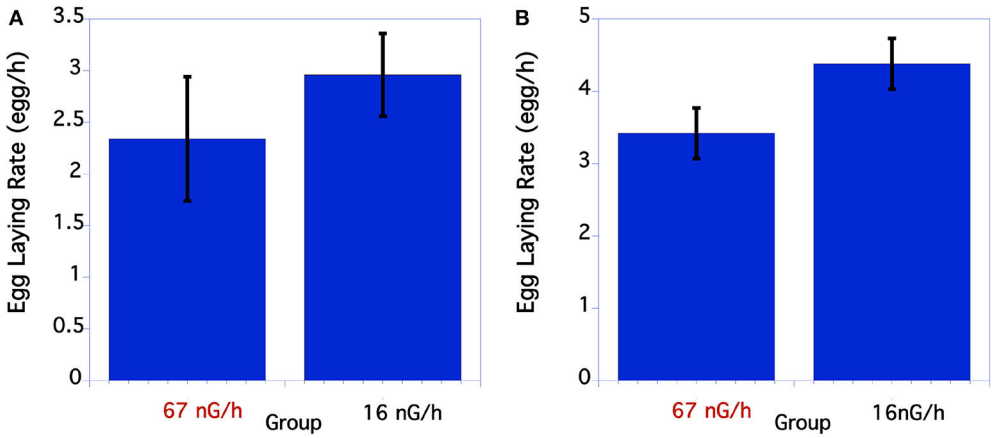

FIGURE 3 | Comparison of egg laying rate of *C. elegans* grown at normal or low radiation levels. **(A)** Egg laying rate of *C. elegans* grown at high or low radiation levels 12/2016. There were no significant differences in egg laying rate. $P = 0.39$ $T = 0.86$, df $= 29$. **(B)** Data from second underground experiment on 8/2017. The means and SEM are plotted for each group. The lay rate of low radiation worms is significantly higher than the normal radiation group. $p = 0.04$ $T = 2.10$, df $= 50$.

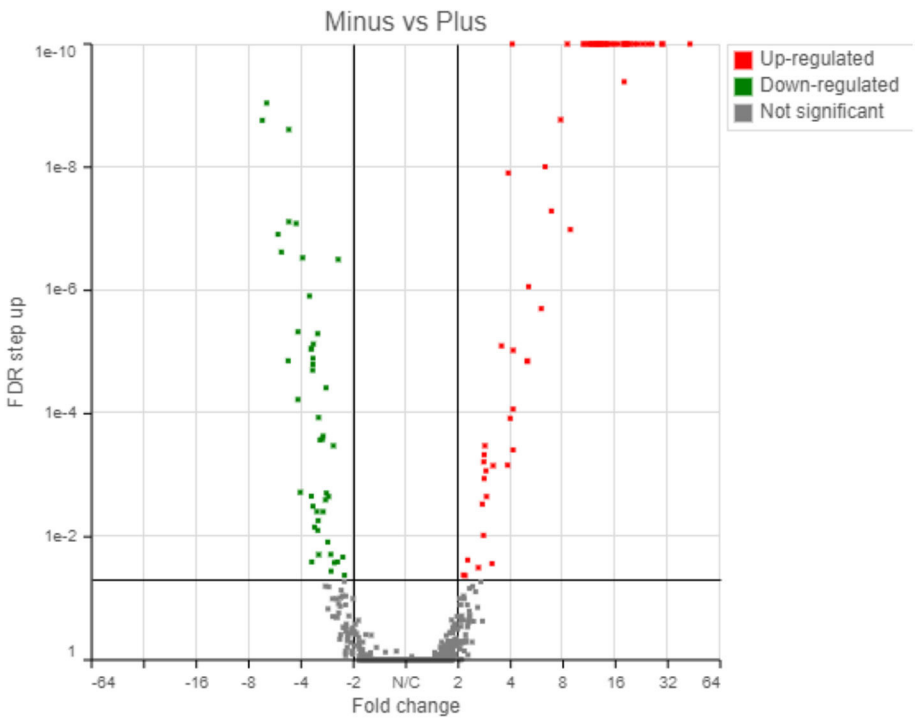

FIGURE 4 | Transcriptome results from Partek analyses showing 67 genes upregulated and 46 genes downregulated in response to the radiation treatment (False Discovery Rate, FDR < 0.05).

Incubator Temperatures

Incubator temperatures remained very close to each other for all of the experiments (**Supplementary Table 1**). For the underground experiments the incubator temperatures were within 0.1°C of each other. If any biases existed from differences in temperature it would be that the normal radiation group would grow, develop, and lay eggs at a higher rate than the low radiation group, opposite to what was observed.

Transcriptome Changes After Exposure to Below Background Radiation

The transcriptome analysis revealed a total of 5,053 genes detected using the Partek workflow software. Differential expression of control and treatment revealed that 67 and 46 genes were up- and down-regulated, respectively, based on a 2-fold change with a False Discovery Rate (FDR) < 0.05 (**Supplementary Tables 2**, **3**). Using the Partek transcriptome

analysis software (the other software packages will be compared below), volcano plot analysis of the 1st experiment indicated a statistically significant regulatory response to the radiation differences after only 72 h incubation in the two radiation treatments (**Figure 4**).

The up-regulated and down-regulated genes are shown in **Supplementary Tables 2**, **3**. Interestingly, about half (49.5%) of the significantly up-regulated genes were different groups of major sperm proteins (*msp,* 42%), sperm-related genes (6%) and 1.5% were related to the major sperm genes. The rest of the upregulated genes were clustered in gene families related to collagen and cuticle related genes (16.4%), non-coding RNA (15%), and hypothetical proteins (7%). The most common down-regulated genes were collagen (*col,* 37% of total), cuticle related genes (28% of total) and hypothetical proteins (17.4%).

Similar transcriptional responses were demonstrated when three different transcriptome pipeline programs were used. For example, **Table 1** shows the treatment to control ratios of all the up-regulated *msp* genes by Partek analysis and compares them to what was obtained by the two other RNA Seq analyses programs. All three programs gave similar results with only one exception (**Table 1**, marked in red) and, similarly, all the col genes identified as down-regulated by Partek were also identified as such by the other two programs (data not shown).

Real-Time (RT) PCR was used to verify transcriptome results from 72 h culture (**Figure 5**). As expected, results of the 8 potential reference genes (*act-1, ubq-1, act-2, pmp-3, eif-3.C, tba-1, ama-1, rbd-1*) showed no difference in Cq values between the treatment and control RNA samples in agreement with transcriptome analysis results. By using two reference genes (*act-1* and *ubq-1*), 10 of the *msp* (*msp-78, msp-65, msp-10, msp-31, msp-59, msp-79, msp-19, msp-113, msp-56, msp-81*) and 3 of the *col* (*col-90, col-169, col-107*) genes gave similarly significant ($p < 0.005$) up and down RT-PCR responses of the RNA samples (**Figure 5**).

TABLE 1 | Comparison of up-regulated fold-change values of the *msp* genes using three transcriptome pipelines.

Gene	Partek	CLC genomic	DNA star
msp-78	42.9	33.9	25.5
msp-65	29.5	39.6	40.9
msp-10	26.0	22.2	21.7
msp-31	24.5	ND	19.8
msp-19	22.9	16.2	22.6
msp-59	21.4	26.4	16.1
msp-79	20.5	18.7	13.9
msp-113	18.8	18.2	15.3
msp-56	18.2	29.1	19.4
msp-81	17.9	19.6	16.7
msp-77	17.8	30.1	24.3
msp-53	16.6	32.6	21.3
msp-40	15.8	25.4	20.1
msp-49	15.2	24.2	20.2
msp-152	14.0	20.2	23.9
msp-57	13.9	25.0	17.9
msp-36	13.1	23.8	17.4
msp-55	13.0	18.5	14.7
msp-51	12.8	14.7	12.9
msp-76	11.8	15.0	12.7
msp-45	11.7	−29.1	17.3
msp-3	11.4	20.2	17.3
msp-33	10.6	16.5	10.7
msp-142	10.5	28.4	22.0
msd-4	8.5	23.8	17.9
msp-50	6.9	19.7	16.7

Fold-change values are from the ratio of treatment vs. control. ND, not detected.

DISCUSSION

This study differs from most studies on the effects of low level radiation on organisms. Such studies typically expose a control group to normal background radiation levels and then compare this group to a group that is exposed to a group slightly higher radiation levels (41). In this study the effects of levels of a radiation exposure that was around 1/3 of normal background was compared to a group kept at normal background radiation levels. We hypothesized three outcomes this experiment. First, if any level of radiation has adverse biological effects, worms reared in below background radiation conditions should develop more quickly, lay eggs at a faster rate, and potentially grow faster than worms exposed to normal radiation levels. Conversely, if below background radiation levels have an adverse biologic effect, worms reared in these low radiation conditions should take longer to develop to adults, have a reduced rate of egg laying, and a slower growth rate compared to counterparts reared in normal background radiation levels. The null hypothesis is probably the most parsimonious, that is, the differences in radiation levels between the low level and normal background radiation are so minor that no physiological effect would be observed.

C. elegans is an ideal organism to use to investigate this question. It grows easily in culture, has a rapid life cycle and is one of the best-studied organisms in the world, with extensive knowledge available on its genetics and gene function, developmental biology, and physiology (42, 43). *C. elegans* has also become a useful model organism in toxicity assays. Studies in *C. elegans* have been validated as good predictors for the adverse effects of many chemicals in mammalian species (44).

In spite of the observations that *C. elegans* is both resistant to relatively high levels of radiation (45, 46) and also tolerant of oxidative stress (47), a significant phenotypic and transcriptomic response to these low levels of radiation was documented in this study. Worms in the below normal radiation environment had faster rates of larval growth, a faster rate of early egg laying, and more than 100 genes were differentially regulated, compared to normal background radiation levels.

From these results in *C. elegans*, there is no evidence of an obvious negative effect of depriving worms from normal levels of radiation. While an argument could be made that the observed increase in egg laying rate in the low radiation

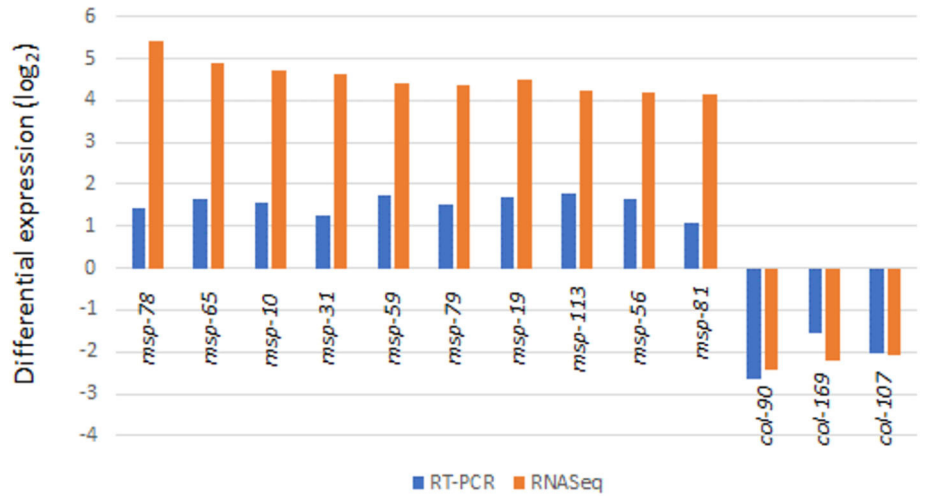

FIGURE 5 | Validation of transcriptome results by RT-PCR analysis (for all values shown, $p < 0.05$).

group is a stress response, such a response is the opposite to that usually seen when *C. elegans* is exposed to environmental stressors. When exposed to an array of environmental stresses such as reduced food levels, vibrations, temperature extremes, osmotically taxing environments, exposure to high radiation levels, moderate amounts of glucose, and hypoxia, *C elegans* typically both reduces its growth and egg laying rate (27, 28, 31–33, 48, 49). Early reproduction appears to be a critical factor in *C. elegans* ecology. Worms with a shorter generation time outcompete populations of mutant worms that produce more progeny but have a longer generation time (Hodgkins and Barnes (50). One factor which does increase the egg laying rate in a hermaphrodite *C. elegans* is when it mates with a male worm (51), an event which did not occur in these experiments.

In contrast, previous research has shown that bacteria and eukaryotic cell cultures exposed to below background levels of radiation exhibit a stress response compared to control groups exposed to normal surface levels of radiation (13, 14, 17, 19, 52, 53). These inhibitory effects on single-celled organisms may be considered a type of hormetic response in which background levels of radiation were needed for optimal growth (4, 54). Results here with the multicellular nematode did not show this response in that worms in reduced radiation had higher egg-laying rates than worms grown in the presence of KCl, a treatment designed to mimic background radiation levels.

Consistent with the *C. elegans* phenotypic response, there were more than 100 genes that were significantly regulated. This response was documented after only 72 h of the worms being brought underground with almost half of the significantly up-regulated genes in the low radiation treatment related to nematode sperm production. There are 85 distinct major sperm protein genes (MSP) located on all six of the nematode chromosomes (NCBI, https://www.ncbi.nlm.nih.gov/genome/?term=txid6239[orgn]), of which 28 were up-regulated in the below background radiation group. MSP was first identified as being involved in sperm motility and is required for the sperm's unusual amoeboid-like sperm "crawling" (55). More recent studies have found that MSP is also critical in other aspects of *C. elegans* reproduction including oocyte and egg development, ovulation, spermathecal valve dilation and parthenogenesis (51, 56–59). Recently, Maremonte et al. demonstrated that high radiation induced the down-regulation of 28 major sperm protein genes which was followed by a reduction in reproduction and the number of spermatids in *C. elegans* (60). Seeing how functionally multifaceted major sperm proteins are, it is likely that the upregulation of the *msp* genes is related to the increase in egg laying rate seen in the low radiation group.

Gene ontology analyses [REVIGO; (36)], listed oocyte development as one of the GO terms significantly upregulated and extracellular structure organization (i.e., cuticle development) as down regulated, and these terms are consistent with the most prevalent genes regulated. The fact that col genes were down regulated, but a smaller percentage was up regulated, is related to the fact that there are 186 distinct col genes in *C. elgans* (https://www.ncbi.nlm.nih.gov/genome/browse/#!/proteins/41/43998%7CCaenorhabditis%20elegans/col, NCBI) and they likely represent different functions. Using WormCat (37), the dominant upregulated genes were major sperm protein related to the reproductive system while the majority of downregulated genes are extracellular material related to cuticle development. Interestingly, three genes (*cpr-3*, *gst-22,* F17C11.11) which are known to be related to stress responses, were also downregulated.

In our previous work with two species of bacteria (*Shewanella oneidensis* and *Deinococcus radiodurans*), we have repeatedly documented within 48 h of bringing cells underground, a phenotypic and genotypic stress response to growing the cells in below background radiation (13, 17–19). Intriguingly, within 72 h of growth underground at WIPP, we have documented in *C. elegans* a similarly rapid biological response. The apparent inhibition in egg-laying rate of *C. elegans* in the presence of normal background levels of radiation (at least the gamma

radiation provided by our underground KCl source) contrasts with the growth stimulation we've seen in some species of bacteria in background radiation. Nevertheless, in both model organisms, it is apparent that fitness costs and benefits are related to extremely small differences in levels of ionizing radiation. This minuscule stimulus and genome-wide response in prokaryotes and eukaryotes challenges our understanding of the biological role of normal, background levels of radiation.

As Lampe et al. (61) have pointed out, based on the physics of the two radiation fields of background and below background radiation, it is challenging to propose that biological organisms could sense these miniscule differences in ionizing radiation. This point was initially and reasonably brought up by Washington University's Jonathan Katz (62), and, in our response to his critique in which we agreed with his calculations, we posited the idea that biological "sensors" rival our most sensitive radiation detection instruments [Castillo and Smith response to Professor Katz, Castillo et al. (63)]. And, in agreement with the Morciano et al. (20) work with *Drosophila* underground at Italy's Gran Sasso lab, we provide further evidence that multicellular organisms are also capable of responding to these vanishingly low differences in radiation fields. These results and those coming from other deep underground laboratories provide impetus to document the mechanisms in single-celled prokaryotes and multi-celled eukaryotes of the response to these minute differences in ionizing radiation and to identify the organismal response apparatus. In our future work, we will continue to put paradigms in Physics (short-term, 1–100 nGy/hr gamma radiation cannot evoke a near-field response in biological targets), Biology (background and below background radiation effects are biologically irrelevant) and Policy (all radiation is deleterious in a Linear, No-Threshold manner) to the test.

DATA AVAILABILITY STATEMENT

The datasets presented in this study can be found in online repositories. The names of the repository/repositories and accession number(s) can be found in the article/**Supplementary Material**.

AUTHOR CONTRIBUTIONS

All authors listed have made a substantial, direct and intellectual contribution to the work, and approved it for publication.

FUNDING

These results are based upon work supported by the U.S. Department of Energy (DOE) Office of Environmental Management under award number DE-EM0002423. This report was prepared as an account of work sponsored by an agency of the United States Government. Neither the United States Government or any agency thereof, nor any of their employees, makes any warranty, express or implied, or assumes any legal liability or responsibility for the accuracy, completeness or usefulness of any information, apparatus, product or process disclosed, or represents that its use would not infringe on privately owned rights. Reference herein to any specific commercial product, process or service by trade names, trademark, manufacturer or otherwise does not necessarily constitute or imply its endorsement. The views and the opinions of authors expressed herein do not necessarily state or reflect those of the United States Government or any agency thereof.

ACKNOWLEDGMENTS

We thank Los Alamos National Laboratory's Brian Dozier and Shawn Otto for their continued technical and safety support in the Waste Isolation Pilot Plant WIPP underground. We acknowledge the capable help of Jeremy Winder who set up the RT-PCR analyses and identified appropriate reference genes. Immo Hanson, Nguyen Vo, and Jennifer Lemon provided valuable editorial advise.

SUPPLEMENTARY MATERIAL

The Supplementary Material for this article can be found online at: https://www.frontiersin.org/articles/10.3389/fpubh.2020.581796/full#supplementary-material

REFERENCES

1. Cnossen I, Sanz Forcada J, Favata F, Witasse O, Zegers T, Arnold NF. Habitat of early life: Solar X-ray and UV radiation at Earth's surface 4–3.5 billion years ago. *J Geophys Res*. (2007) 112:E02008. doi: 10.1029/2006JE002784
2. Zimmer C. Origins. On *the origin of eukaryotes. Science.* (2009) 325:666–8. doi: 10.1126/science.325_666
3. Ghiassi-nejad M, Mortazavi SMJ, Cameron JR, Niroomand-rad A, Karam PA. Very high background radiation areas of Ramsar, Iran: preliminary biological studies. *Health Phys.* (2002) 82:87–93. doi: 10.1097/00004032-200201000-00011
4. Møller AP, Mousseau TA. The effects of natural variation in background radioactivity on humans, animals and other organisms. *Biol Rev Camb Philos Soc*. (2013) 88:226–54. doi: 10.1111/j.1469-185X.2012.00249.x
5. Hendry JH, Simon SL, Wojcik A, Sohrabi M, Burkart W, Cardis E, et al. Human exposure to high natural background radiation: what can it teach us about radiation risks? *J Radiol Prot*. (2009) 29:A29–42 doi: 10.1088/0952-4746/29/2A/S03
6. ICRP. The 2007 recommendations of the International Commission on Radiological Protection. In: *Ann ICRP*. ICRP Publication (2007). p. 37.
7. Sykes PJ. Until there is a resolution of the Pro-LNT/Anti-LNT Debate, we should head toward a more sensible graded approach for protection from low-dose ionizing radiation. *Dose-Response*. (2020) 18:1559325820921651. doi: 10.1177/1559325820921651
8. Tubiana M. Dose-effect relationship and estimation of the carcinogenic effects of low doses of ionizing radiation: the joint report of the academie des sciences (Paris) and of the academie nationale de medecine. *Int J Radiat Oncol Biol Phys*. (2005) 63:317–9. doi: 10.1016/j.ijrobp.2005.06.013
9. Feinendegen L. Evidence for beneficial low level radiation effects and radiation hormesis. *Br J Radiol.* (2014) 78:3–7. doi: 10.1259/bjr/63353075
10. Parsons PA. Metabolic efficiency in response to environmental agents predicts hormesis and invalidates the linear no-threshold premise: ionizing radiation as a case study. *Crit Rev Toxicol*. (2003) 33:443–9. doi: 10.1080/713611046
11. Elmore E, Lao XY, Kapadia R, Giedzinski E, Limoli C, Redpath JL. Low doses of very low-dose-rate low-LET radiation suppress radiation-induced

neoplastic transformation *in vitro* and induce an adaptive response. *Radiat Res*. (2008) 169:311–8. doi: 10.1667/RR1199.1
12. Okazaki R, Ootsuyama A, Norimura T. TP53 and TP53-related genes associated with protection from apoptosis in the radioadaptive response. *Radiat Res*. (2007) 167:51–7. doi: 10.1667/RR0623.1
13. Smith GB, Grof Y, Navarrette A, Guilmette RA. Exploring biological effects of low background radiation from the other side of the background. *Health Phys*. (2011) 100:263–5. doi: 10.1097/HP.0b013e318208cd44
14. Planel H, Soleilhavoup JP, Tixador R, Richoilley G, Conter A, Croute F, et al. Influence on cell proliferation of background radiation or exposure to very low, chronic gamma radiation. *Health Phys*. (1987) 52:571–8. doi: 10.1097/00004032-198705000-00007
15. Satta L, Augusti-Tocco G, Ceccarelli R, Esposito A, Fiore M, Paggi P, et al. Low environmental radiation background impairs biological defense of the yeast *Saccharomyces cerevisiae* to chemical radiomimetic agents. *Mutat Res*. (1995) 347:129–33. doi: 10.1016/0165-7992(95)00031-3
16. Satta L, Antonelli F, Belli M, Sapora O, Simone G, Sorrentino E, et al. Influence of a low background radiation environment on biochemical and biological responses in V79 cells. *Radiat Environ Biophys*. (2002) 41:217–24. doi: 10.1007/s00411-002-0159-2
17. Castillo H, Schoderbek D, Dulal S, Escobar G, Wood J, Nelson R, et al. Stress induction in the bacteria *Shewanella oneidensis* and *Deinococcus radiodurans* in response to below-background ionizing radiation. *Int J Radiat Biol*. (2015) 91:749–56. doi: 10.3109/09553002.2015.1062571
18. Castillo H, Smith GB. Below-background ionizing radiation as an environmental cue for bacteria. *Front Microbiol*. 8:177. doi: 10.3389/fmicb.2017.00177
19. Castillo H, Li X, Schilkey F, Smith GB. Transcriptome analysis reveals a stress response of *Shewanella oneidensis* deprived of background levels of ionizing radiation. *PLoS ONE*. (2018) 13:E0196472. doi: 10.1371/journal.pone.0196472
20. Morciano P, Cipressa F, Porrazzo A, Esposito G, Tabocchini MA, Cenci G. Fruit flys provide new insights in low-radiation background biology at the INFN Underground Gran Sasso National Laboratory (LNGS). *Radiat Res*. (2018) 190:217–25. doi: 10.1667/RR15083.1
21. Tharmalingam S, Etharan S, Kulesza AV, Boreham DR, Tai T. Low-dose ionizing radiation exposure, oxidative stress and epigenetic programing of health and disease. *Radiat Res*. (2017) 188:525–38. doi: 10.1667/RR14587.1
22. Choppin GR, Liljenzin JO, and Rydberg J. *Radiochemistry and Nuclear Chemistry*. 3rd Edn. Worburn, MA: Butterworth-Heinemann (2002).
23. USEPA map of Radon zones –New Mexico document number 402-R-93-051. Available online at: https://www.epa.gov/radon/epa-map-radon-zones
24. Van Voorhies W. *Genetic and environmental conditions that increase longevity in Caenorhabditis elegans decrease metabolic rate. Proc Natl Acad Sci USA*. (1999) 96:11399–403. doi: 10.1073/pnas.96.20.11399
25. Stiernagle T. *Maintenance of C. elegans. WormBook ed. The C. elegans Research Community*. Minneapolis, MN: WormBook (2006).
26. Beguet B. The persistence of processes regulating the level of reproduction in the hermaphrodite nematode *Caenorhabditis elegans*, despite the influence of parental ageing, over several consecutive generations. *Expl Geront*. (1972) 7:207–18. doi: 10.1016/0531-5565(72)90027-7
27. Byerly L, Cassada RC, Russell RL. The life cycle of the nematode *Caenorhabditis elegans. Dev Biol*. (1976) 51:23–33. doi: 10.1016/0012-1606(76)90119-6
28. Angelo G, Van Gilst MR. Starvation protects germline stem cells and extends reproductive longevity in *C. elegans. Science*. (2009) 326:954–8. doi: 10.1126/science.1178343
29. Klosin A, Casas E, Hidalgo-Carcedo C, Vavouri T, Lehner B. Transgenerational transmission of environmental information in *C. elegans. Science*. (2017) 356:320–3. doi: 10.1126/science.aah6412
30. Kaletsky R, Moore RS, Parsons LL, Murphy CT. Cross kingdom recognition of bacterial small RNAs induces transgenerational pathogenic avoidance. *bioRxiv*. (2019) 697888. doi: 10.1101/697888
31. Teshiba E, Miyahara K, Takeya H. Glucose-induced abnormal egg-laying rate in *Caenorhabditis elegans*. *Biosci Biotechnol Biochem*. (2016) 80:1436–9. doi: 10.1080/09168451.2016.1158634
32. Schafer WR. *WormBook: The Online Review of C. elegans Biology*. Pasadena, CA: WormBook 2005-2018 (2005).
33. Waggoner LE, Hardaker LA, Golik S, Schafer WR. Effect of a neuropeptide gene on behavioral states in *Caenorhabditis elegans* egg-laying. *Genetics*. (2000) 154:1181–92.
34. Benjamini Y, Hochberg Y. Controlling the false discovery rate: a practical and powerful approach to multiple hypothesis testing. *J R Stat Soc B*. (1995) 57:289–300. doi: 10.1111/j.2517-6161.1995.tb02031.x
35. Reimand J, Kull M, Peterson H, Hansen J, Vilo J. g:Profiler—a web-based toolset for functional profiling of gene lists from large-scale experiments. *Nucleic Acids Res*. (2007) 35:W193–200. doi: 10.1093/nar/gkm226
36. Supek F, BosÏnjak M, SĬkunca N, SĬmuc T. REVIGO summarizes and visualized long lists of gene ontology terms. *PLoS ONE*. (2011) 6:e21800. doi: 10.1371/journal.pone.0021800
37. Holdorf AD, Higgins DP, Hart AC, Boag PR, Pazour GJ, Walhout A, et al. WormCat: an online tool for annotation and visualization of *Caenorhabditis elegans* genome-scale data. *Genetics*. (2020) 214:279–94. doi: 10.1534/genetics.119.302919
38. Pfaffl MW, Horgan GW, Dempfle L. Relative expression software tool REST for group-wise comparisonand statistical analysis of relative expression results in real-time PCR. *Nucleic Acids Res*. (2002) 30:e36. doi: 10.1093/nar/30.9.e36
39. Andersen CL, Jensen JL, Ørntoft TF. *Normalization of real-time quantitative RT-PCR data: a model based variance estimation approach to identify genes suited for normalization - applied to bladder- and colon-cancer data-sets. Cancer Res*. (2004) 64:5245–50. doi: 10.1158/0008-5472.CAN-04-0496
40. Pfaffl MW, Tichopad A, Prgomet C, Neuvians TP. Determination of stable housekeeping genes, differentially regulated target genes and sample integrity: bestKeeper—excel based tool using pair-wise correlations. *Biotechnol Lett*. (2004) 26:509–15. doi: 10.1023/B:BILE.0000019559.84305.47
41. Zhikrevetskaya S, Peregudova D, Danilov A, Plyusnina E, Krasnov G, Dmitriev A, et al. Effect of low doses (5-40 cGy) of gamma-irradiation on lifespan and stress-related genes expression profile in *Drosophila melanogaster*. *PLoS ONE*. (2015) 10:e0133840. doi: 10.1371/journal.pone.0133840
42. Wood WB. *The Nematode Caenorhabditis elegans*. Cold Spring Harbor, NY: Cold Spring Harbor Laboratory Press (1988).
43. Riddle DL, Blumenthal T, Meyer BJ, Priess JR. Introduction to *C. elegans*. In: Riddle DL, Blumenthal T, Meyer BJ, Priess JR, editors. *C. elegans II*. Cold Spring Harbor, NY: Cold Spring Harbor Laboratory Press. (1997). *p*. 1–22.
44. Jung S-K, Qu X, Aleman-Meza B, Wang T, Riepe C, Liu Z, et al. Multi-endpoint, high-throughput study of nanomaterial toxicity in *Caenorhabditis elegans*. *Environ Sci Technol*. (2015) 49:2477–85. doi: 10.1021/es5056462
45. Hartman P, Herman R. Radiation-sensitive mutants of *Caenorhabditis elegans*. *Genetics*. (1982) 102:159–78.
46. Johnson T, Hartman P. Radiation Effects on Life Span in *Caenorhabditis elegans*. *J Gerontol*. (1988) 43:B137–41. doi: 10.1093/geronj/43.5.B137
47. van Voorhies WA, Ward S. Broad oxygen tolerance in the nematode *Caenorhabditis elegans*. *J Exp Biol. (2000) 203:2467–78*.
48. Cui F, Ma N, Han X, Chen N, Xi Y, Yuan W, et al. Effects of 60Co γ irradiation on the reproductive function of *Caenorhabditis elegans. Dose Res*. (2019) 17:1559325818820981. doi: 10.1177/1559325818820981
49. Pender C, Horvitz R. Hypoxia-inducible factor cell non-autonomously regulates *C. elegans* stress responses and behavior via a nuclear receptor. *eLife*. (2018) 7:e36828. doi: 10.7554/eLife.36828
50. Hodgkin J, Barnes TM. More is not better: brood size and population growth in a self-fertilizing nematode. *Proc Biol Sci*. (1991) 246:19–24. doi: 10.1098/rspb.1991.0119
51. McGovern M, Yu L, Kosinski M, Greenstein D, Savage-Dunn C. A role for sperm in regulation of egg-laying in the nematode *C. elegans. BMC Dev Biol*. (2007) 7:41. doi: 10.1186/1471-213X-7-41
52. Carbone MC, Pinto M, Antonelli F, Amicarelli F, Balata M, Belli M, et al. The cosmic silence experiment: on the putative adaptive role of environmental ionizing radiation. *Radiat Environ Biophys*. (2009) 48:189–96. doi: 10.1007/s00411-008-0208-6
53. Kawanishi M, Okuyama K, Shiraishi K, Matsuda Y, Taniguchi R, Shiomi N, et al. Growth retardation of paramecium and mouse cells by shielding them from background radiation. *J Radiat Res*. (2012) 53:404–10. doi: 10.1269/jrr.11145

54. Calabrese EJ, Baldwin LA. Chemical hormesis: its historical foundations as a biological hypothesis. *Hum Exp Toxicol*. (2000) 19:2–31. doi: 10.1191/096032700678815585
55. L'Hernault SW. Spermatogenesis. In: Riddle DL, editor. *C. elegans II*. Cold Spring Harbor, NY: Cold Spring Harbor Laboratory Press (1997). p. 271–94.
56. Miller MA, Nguyen VQ, Lee MH, Kosinski M, Schedl T, Caprioli RM, et al. A sperm cytoskeletal protein that signals oocyte meiotic maturation and ovulation. *Science*. (2001) 291:2144–7. doi: 10.1126/science.1057586
57. Miller MA, Ruest PJ, Kosinski M, Hanks SK, Greenstein D. An Eph receptor sperm-sensing control mechanism for oocyte meiotic maturation in *Caenorhabditis elegans*. *Genes Dev*. (2003) 17:187–200. doi: 10.1101/gad.1028303
58. Kuwabara PE. The multifaceted *C. elegans* major sperm protein: an ephrin signaling antagonist in oocyte maturation. *Genes Dev*. (2003) 17:155–61. doi: 10.1101/gad.1061103
59. Schwarz EM, Kato M, Sternberg PW. Functional transcriptomics of a migrating cell in *Caenorhabditis elegans*. *Proc Natl Acad Sci USA*. (2012) 109:16246–51. doi: 10.1073/pnas.1203045109
60. Maremonti E, Eide DM, Oughton DH, Salbu B, Grammes F, Kassaye YA, et al. Gamma radiation induces life stage-dependent reprotoxicity in *Caenorhabditis elegans* via impairment of spermatogenesis. *Sci Total Environ*. (2019) 695:133835. doi: 10.1016/j.scitotenv.2019.133835
61. Lampe N, Breton V, Sarramia D, Sime-Ngando T, Biron DG. Understanding low radiation background biology through controlled evolution experiments. *Evol Appl*. (2017) 10:658–66. doi: 10.1111/eva.12491
62. Katz JI. Comment on Castillo et al. (2015). *Inter. J Rad Biol*. (2016) 92:169–70. doi: 10.3109/09553002.2016.1135265
63. Castillo H, Schoderbek D, Dulal S, Escobar G, Wood J, Nelson R, et al. Response to Dr Katz. *Int. J. Radiat. Biol*. (2016) 92:169–70.

Conflict of Interest: The authors declare that the research was conducted in the absence of any commercial or financial relationships that could be construed as a potential conflict of interest.

frontiers in Public Health

ORIGINAL RESEARCH
published: 30 October 2020
doi: 10.3389/fpubh.2020.584964

Proteomic Characterization of Proliferation Inhibition of Well-Differentiated Laryngeal Squamous Cell Carcinoma Cells Under Below-Background Radiation in a Deep Underground Environment

Jifeng Liu[1,2], Tengfei Ma[1,2], Mingzhong Gao[3], Yilin Liu[4], Jun Liu[1], Shichao Wang[2], Yike Xie[2], Qiao Wen[1], Ling Wang[2], Juan Cheng[2], Shixi Liu[1], Jian Zou[1,2]*, Jiang Wu[2], Weimin Li[2] and Heping Xie[2,3,5]*

[1] Department of Otolaryngology Head and Neck Surgery, West China Hospital, Sichuan University, Chengdu, China, [2] Deep Underground Space Medical Center, West China Hospital, Sichuan University, Chengdu, China, [3] College of Water Resources and Hydropower, Sichuan University, Chengdu, China, [4] Department of Ophthalmology, West China Hospital, Sichuan University, Chengdu, China, [5] Institute of Deep Earth Science and Green Energy, Shenzhen University, Shenzhen, China

OPEN ACCESS

Edited by:
Geoffrey Battle Smith,
New Mexico State University,
United States

Reviewed by:
Narongchai Autsavapromporn,
Chiang Mai University, Thailand
Ken Raj,
Public Health England,
United Kingdom

***Correspondence:**
Jun Liu
hxheadneckjunl@163.com
Jian Zou
zoujian926@163.com

Specialty section:
This article was submitted to Radiation and Health, a section of the journal Frontiers in Public Health

Received: 19 July 2020
Accepted: 06 October 2020
Published: 30 October 2020

Citation:
Liu J, Ma T, Gao M, Liu Y, Liu J, Wang S, Xie Y, Wen Q, Wang L, Cheng J, Liu S, Zou J, Wu J, Li W and Xie H (2020) Proteomic Characterization of Proliferation Inhibition of Well-Differentiated Laryngeal Squamous Cell Carcinoma Cells Under Below-Background Radiation in a Deep Underground Environment. Front. Public Health 8:584964. doi: 10.3389/fpubh.2020.584964

Background: There has been a considerable concern about cancer induction in response to radiation exposure. However, only a limited number of studies have focused on the biological effects of below-background radiation (BBR) in deep underground environments. To improve our understanding of the effects of BBR on cancer, we studied its biological impact on well-differentiated laryngeal squamous cell carcinoma cells (FD-LSC-1) in a deep underground laboratory (DUGL).

Methods: The growth curve, morphological, and quantitative proteomic experiments were performed on FD-LSC-1 cells cultured in the DUGL and above-ground laboratory (AGL).

Results: The proliferation of FD-LSC-1 cells from the DUGL group was delayed compared to that of cells from the AGL group. Transmission electron microscopy scans of the cells from the DUGL group indicated the presence of hypertrophic endoplasmic reticulum (ER) and a higher number of ER. At a cutoff of absolute fold change ≥ 1.2 and $p < 0.05$, 807 differentially abundant proteins (DAPs; 536 upregulated proteins and 271 downregulated proteins in the cells cultured in the DUGL) were detected. KEGG pathway analysis of these DAPs revealed that seven pathways were enriched. These included ribosome ($p < 0.0001$), spliceosome ($p = 0.0001$), oxidative phosphorylation ($p = 0.0001$), protein export ($p = 0.0001$), thermogenesis ($p = 0.0003$), protein processing in the endoplasmic reticulum ($p = 0.0108$), and non-alcoholic fatty liver disease ($p = 0.0421$).

Conclusion: The BBR environment inhibited the proliferation of FD-LSC-1 cells. Additionally, it induced changes in protein expression associated with the ribosome, gene spliceosome, RNA transport, and energy metabolism among others. The changes

in protein expression might form the molecular basis for proliferation inhibition and enhanced survivability of cells adapting to BBR exposure in a deep underground environment. RPL26, RPS27, ZMAT2, PRPF40A, SNRPD2, SLU7, SRSF5, SRSF3, SNRPF, WFS1, STT3B, CANX, ERP29, HSPA5, COX6B1, UQCRH, and ATP6V1G1 were the core proteins associated with the BBR stress response in cells.

Keywords: deep-underground, below background radiation, proteomics, cell proliferation, stress, ribosome, FD-LSC-1 cell

INTRODUCTION

Humans are exposed to radiation that originates from natural and man-made sources (1). There has been a considerable concern about cancer induction in response to radiation exposure, which is one of the potential harmful effects of radiation (2). A linear no-threshold (LNT) relationship, which is an assumption model, was formed between dose and risk values to estimate the risk of cancer induced by low doses of radiation (1). However, increasing evidence suggests that the risks of low doses of radiation might not strictly conform to an LNT (2). In particular, the relevant biological research data has been collected from experiments conducted in deep underground laboratories (DUGLs), which were originally used to conduct particle, astroparticle, or nuclear physics experiments that require an environment with significantly low interference by cosmic ray particles (3). Biological experiments conducted in DUGLs revealed the detrimental effects of an environment with low background radiation on cultures (3). However, the limited number of studies that focus on this issue has made it difficult to draw a meaningful conclusion about the biological effects of below-background radiation (BBR).

To better serve the national interests of China related to the exploration of deep underground spaces and resources, a deep underground medical laboratory was established at Erdaogou Mine, Jiapigou Minerals Limited Corporation (CJEM) of China National Gold Group Corporation in northeast China (3). Owing to the rocky cover of 1,470 m, the cosmic radiation exposure in the DUGL at CJEM was negligible (4). The terrestrial γ-ray dose rate radiation in the DUGL (0.04 μSv/h) was only one-third of that in the above-ground laboratory (AGL; 0.15 μSv/h), which was constructed as a control laboratory in an office building near the entrance of the CJEM facility (4). We determined the environmental characteristics and tested the feasibility of conducting experiments at the DUGL at CJEM in December 2017 (3). The other environmental parameters showed that relative humidity (DULG/AGL = 99%/57.2%) ($p < 0.001$), air pressure (DULG/AGL = 1118.2 hPa/951.9 hPa) ($p < 0.001$), and concentration of CO_2 (DULG/AGL = 951.9 ppm/540.11 ppm] and radon gas (DULG/AGL = 4.0 pCi/L/1.25 pCi/L) ($p < 0.001$) were significantly higher in the DUGL compared to the AGL (4). However, O_2 concentration in the DUGL (20.8%) and AGL (20.6%) was not significantly different (4).

Initial studies showed that Chinese hamster V79 cells could be successfully cultured in the DUGL and presented with proliferation inhibition (3). In addition, quantitative proteomic analyses revealed that the differentially abundant proteins (DAPs) in V79 cells from the DUGL and AGL groups were associated with the ribosome pathway, RNA transport, and oxidative phosphorylation (OXPPL) among others. The alteration in protein expression might form the basis for V79 cell growth delay and stress response under BBR in the deep underground environment. However, the cells studied in the DUGL were normal cells. Only a limited number of studies have investigated the responses in cancer cells under such environments, in which background radiation is shielded.

We selected well-differentiated laryngeal squamous cell carcinoma cells (FD-LSC-1), which are moderately sensitive to radiation (4), to observe the biological effect of BBR in the DUGL at the CJEM facility. The growth curve, morphological, and quantitative proteomic experiments were performed on FD-LSC-1 cells cultured in the DUGL and AGL. These data might provide novel insights into the relationship between radiation and cancers in a BBR environment.

MATERIALS AND METHODS

The methods followed for cell culture, growth curve, transmission electron microscopy (TEM), tandem mass tag (TMT) protein quantification, and parallel reaction monitoring (PRM) experiments have been presented in one of our previous studies (4).

Cell Culture

Briefly, FD-LSC-1 cells were purchased from the Shanghai branch of the Chinese Academy of Science. The frozen FD-LSC-1 cells were revived and cultured in Dulbecco's modified Eagle medium (Gibco, USA) supplemented with 10% fetal calf serum (Gemini, USA), 50 U dm^{-3} penicillin, and streptomycin (Gibco, USA). Once the cells reached above 80% confluence, they were passaged. Next, the cultures were divided among four bottles. Two bottles were assigned randomly for culturing in the DUGL or AGL. The bottles for DUGL were transferred from AGL to DUGL in an incubator, which took about 1.5–2 h from the AGL to DUGL. Then the cells were maintained in incubators at the two locations at 37°C and 5% CO_2. The culture from one bottle from each laboratory was used to analyze the proliferation ability and morphological changes. The culture from the second bottle from each laboratory was used for passage when the cells were more than 80% confluent. After 4 days of culture in the DUGL or AGL,

three bottles of the cell samples cultured in each location were collected on site for proteomic analyses. The flow chart for the study is presented in **Figure 1**.

Growth Curve

Cell Counting Kit-8 (CCK-8) (MCE, USA) was used to compare the proliferative potential of FD-LSC-1 cells from the DUGL and AGL groups. Briefly, 200 μL of cell suspension at a concentration of 5×10^5 cells/mL, was added to each well in a 96-well plate. The cells were cultured in the incubator. The CCK-8 reagent was added to the five replicate wells (10 μL/well) every day for the following 7 days; then, the plates were incubated for 4 h in the incubator at both the locations. The absorbance of each well was measured at 450 nm (OD_{450}). On each day and at each location, the absorbance of cultures in the five replicate wells was measured to analyze the proliferation potential of the cells. The average value of five replicate absorbance values recorded each day was used to construct the growth curve.

TEM

The FD-LSC-1 cells cultured in the DUGL or AGL for 2 days were harvested for transmission electron microscopy (TEM) analysis. The cells were fixed with 2.5% glutaraldehyde at both the locations. Similar to V79 cells (4), the cell samples from both the laboratories were washed with pre-chilled phosphate buffered saline and fixed using 1% OsO_4. The cells were then dehydrated in ethanol and embedded in epoxy resin. Ultra-thin sections of 80 nm were cut and stained using 3% uranyl acetate and lead citrate. A Hitachi H7650 TEM (Hitachi, Japan) was used to observe the sections.

Quantification of TMT Protein

The FD-LSC-1 cells were lysed using a lysis buffer [7 M urea, 4% sodium dodecyl sulfate, 30 mM 2-[4-(2-hydroxyethyl) piperazin-1-yl]ethanesulfonic acid, 1 mM phenylmethanesulfonyl fluoride, 2 mM ethylenediaminetetraacetic acid, 10 mM dithiothreitol, and 1 × protease inhibitor cocktail (Sigma-Aldrich, USA)]. The protein lysates were sonicated on ice (5 s pulse on, 15 s pulse off, 180 W power, 10 min). After centrifugation at 10,000 × *g* and 4°C for 10 min, the protein concentrations in the supernatants were determined using a bicinchoninic acid protein assay kit (Fisher Scientific, USA). Hundred microgram of protein from each sample was then reduced using 10 mM dithiothreitol and alkylated using 35 mM iodoacetamide under dark conditions for 30 min. The samples were incubated in pre-chilled (at −20°C) acetone for 3 h and centrifuged at 20,000 × *g* and 4°C for 30 min. The samples were then washed twice with a 50% acetone and 50% ethanol mix and centrifuged at 20,000 × *g* and 4°C for 30 min. The precipitates were resuspended in 100 μL of 100 mM tetraethylammonium bromide and digested twice with trypsin (Promega, USA) at 37°C. The enzyme-protein ratio was 1:100 (w/w).

The digested samples were labeled with 6-plex TMT tag (Thermo Scientific, USA) for 2 h at room temperature, equilibrated to room temperature, and dissolved in 41 μL of anhydrous acetonitrile. The samples from the DUGL groups were labeled with TMT-126, −127, and −128. The samples from the AGL group were labeled with TMT-129, −130, and −131. The samples were then combined and lyophilized. Subsequently, the samples were desalted in a Sep-Pak C18 column (100 mg, 1 cc, Waters, USA) (4).

The labeled samples were fractionated by high performance liquid chromatography in a BEH C18 column (2.1 × 150 mm, 1.7 μm, 130 Å) (Acquity UPLCBEH C18, Waters Corporation, Eschborn, Germany) and a two-mobile-phase gradient elution system (mobile phase A: 10 mM ammoniumformate, pH 10; mobile phase B: 10 mM ammoniumformate and 90% acetonitrile, pH 10). The eluted fractions were collected using an automated fraction collector and combined into twelve fractions.

Peptide analyses were performed using an Orbitrap Fusion mass spectrometer (Thermo Scientific, San Jose, CA, USA) in positive ionization mode using the data-dependent acquisition (DDA) strategy. The full spectrum MS mode was used with the following settings: ESI voltage, 2 kV; capillary temperature, 300°C; automatic gain control target, 5×10^5 ions at a resolution of 70,000; scan range, 350–1,600 m/z; maximum injection time, 50 ms. The MS/MS data were acquired using the top 15 intense parent ions. The resolving power was set to 17,500 at an m/z value of 200. The MS/MS minimum ionic strength was 50,000, and the maximum injection time was 150 ms. The automatic gain control target for MS/MS was 2×10^5 with a 2 Da isolation window.

Protein Identification and Quantification

Raw data were initially processed using Proteome Discoverer (version 1.4.0.288, Thermo Fisher Scientific, USA), and protein identification was performed using MASCOT (Version 2.3.2, Matrix Science). MASCOT was configured to scan the UniProt database (taxonomy: *Homo sapiens*, total 161,584 entries) assuming digestion by trypsin. The protein identification parameters were the same as those in our previous study: Carbamidomethyl (C), TMT 6-plex (K), and (N-term) were defined as fixed modifications in MASCOT. Oxidation (M) was defined as a variable modification.

Relative quantification of the identified proteins was performed using the weighted ratios of the uniquely identified peptides belonging to a specific protein. The parameters for protein identification and quantification were the same as those in a previous report (4). Fisher's test was used for statistical analysis with a false discovery rate $\leq$ 1%. Proteins with a $p < 0.05$ and an absolute fold change ≥ 1.2 were considered differentially abundant.

PRM

The DAPs of TMT with high abundance and fold change were selected for verification. The verification was conducted using a Triple TOF 6,600+ LC-MS/MS system. Protein extraction, lysis, and desalting were performed as described above. The raw DDA files were analyzed using MaxQuant (version 1.3.0.5). The search for the resulting data was performed using the UniProt-cricetulus+griseus fasta database Protein Pilot. The PRM validation data were analyzed using Skyline. The peak shapes of the target peptides were identified by manual inspection.

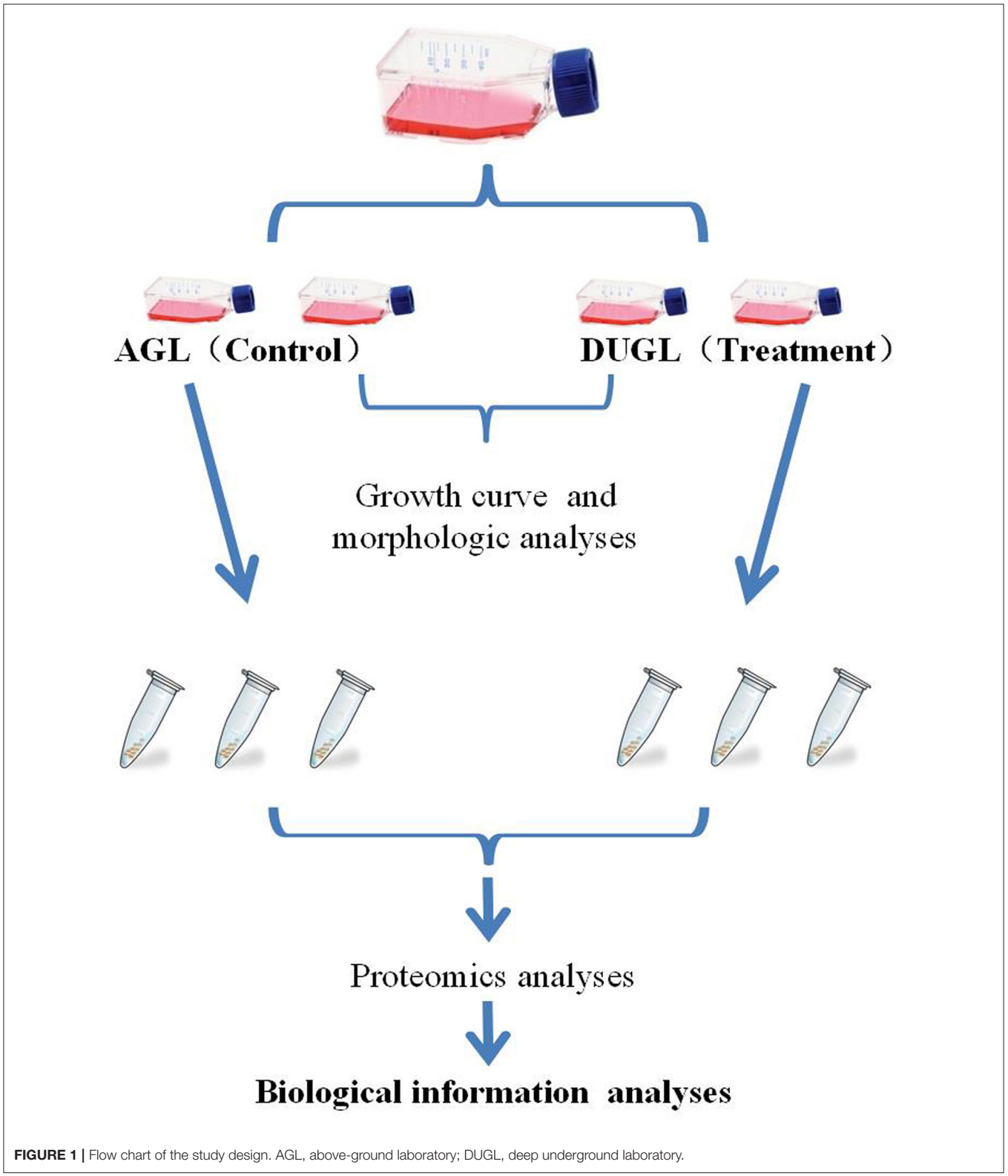

FIGURE 1 | Flow chart of the study design. AGL, above-ground laboratory; DUGL, deep underground laboratory.

Biological Function

The DAPs were functionally annotated using the OmicsBean software (http://www.omicsbean.com:88/). Fisher's exact test was used for the statistical analyses of Gene Ontology (GO) terms and Kyoto Encyclopedia of Genes and Genomes (KEGG) pathways. A corrected $p < 0.05$ was considered to represent significant

enrichment. With a confidence cutoff of 400, protein-protein interaction network analyses were performed to further reveal the functional interactions between the DAPs.

Statistical Analysis

The differences between the OD values of cultures from the DUGL and AGL groups were compared using Student's *t*-test. A $p < 0.05$ was considered statistically significant.

RESULTS

Cell Growth and Morphology

The proliferation potential of FD-LSC-1 cells cultured in the DUGL was significantly inhibited compared to that of cells cultured in the AGL. After 2 days of culture, the OD_{450} value of FD-LSC-1 cells cultured in the AGL (OD value: AGL/DUGL = $0.763 \pm 0.045/0.557 \pm 0.049$, $p < 0.001$) increased by 37.73%, whereas that of cells cultured in the DUGL increased only by 7.53%. On the third day, the OD value of FD-LSC-1 cells cultured in the AGL doubled, whereas that of cells cultured in the DUGL only increased by 76.25% (AGL/DUGL = $1.126 \pm 0.136/0.913 \pm 0.056$, $p < 0.001$). The FD-LSC-1 cultures from the AGL reached maximum saturation density (AGL/DUGL = $1.586 \pm 0.13/1.26 \pm 0.042$, $p < 0.001$) in the 96-well plate on the fourth day, whereas the cultures from the DUGL attained the same (AGL/DUGL = $1.360 \pm 0.159/1.558 \pm 0.140$) on the fifth day (**Figures 2**, **3C**).

The TEM scans showed that cells cultured in the DUGL contained hypertrophic endoplasmic reticulum (ER) as well as a higher number of ER compared to the cells cultured in the AGL (**Figure 4**).

Quantitative Proteomic Analyses

In the quantitative proteomic analyses, 37,202 unique spectra were matched to 29,719 unique peptides. In addition, 4,094 unique proteins were identified in FD-LSC-1 cells cultured in the DUGL and AGL. Eight hundred and seven DAPs were detected with a relative abundance absolute fold change cutoff ≥ 1.2 and $p < 0.05$. Of these, 536 proteins were upregulated (from 1.2 to 8.5-fold) and 271 proteins were downregulated (from 0.83 to 0.43-fold) in the FD-LSC-1 cells cultured in the DUGL compared to those cultured in the AGL (**Figure 3B**, **Supplementary Table 1**). One hundred and forty-five DAPs were identified with a absolute fold change cutoff ≥ 1.5 and $p < 0.05$ (118 upregulated and 27 downregulated in cells cultured in the DUGL). The protein names, accession numbers, and abbreviations used in our proteomic analyses were obtained from the UniProtKB/Swiss-Prot database. Proteomic data were deposited in the ProteomeXchange Consortium (Subproject: IPX0002120001).

Functional Analysis of DAPs

GO term enrichment and KEGG pathway analyses were performed to investigate the biological functions of the DAPs in FD-LSC-1 cells from the DUGL and AGL groups.

At a false discovery rate (*p*-adjusted) < 0.05, the GO term enrichment analysis of DAPs revealed that the top five enriched GO terms were cellular component organization or biogenesis, cellular component organization, cellular component biogenesis, macromolecular complex subunit organization, and mRNA metabolic process in the biological process (BP) category; extracellular vesicle, organelle, exosome, membrane-bounded organelle, membrane-bounded vesicle in the cellular components (CC) category; and protein binding, poly(A) RNA binding, RNA binding, binding, and enzyme binding in the molecular functions (MF) category (**Figure 5A**, **Supplementary Table 2**). The GO enrichment analysis of upregulated DAPs in cells cultured in the DUGL showed that the top five GO terms from the BP category were cellular component organization or biogenesis, cellular component organization, cellular component biogenesis, macromolecular complex subunit organization, and RNA processing. The terms in the CC category were extracellular vesicle, organelle, exosome, membrane-bounded organelle, and region part (**Figure 6A**, **Supplementary Table 3**). The terms in the MF category were protein binding, poly(A) RNA binding, RNA binding, binding, and structural molecule activity. In contrast, the top five GO terms for downregulated DAPs in cells cultured in the DUGL were protein folding, cellular catabolic process, amide biosynthetic process, cellular amide metabolic process, and cellular protein metabolic process in the BP category (**Figure 6B**, **Supplementary Table 4**); extracellular membrane-bounded organelles, exosomes, vesicles, organelles, and cytosol in the CC category; and poly(A) RNA binding, RNA binding, protein binding, cadherin binding, and small molecule binding in the MF category.

With a *p*-adjusted value < 0.05, the KEGG pathway analysis of these DAPs revealed that seven pathways were enriched. The significantly enriched pathways were ribosome ($p < 0.0001$), spliceosome ($p = 0.0001$), oxidative phosphorylation (OXPPL) ($p = 0.0001$), protein export ($p = 0.0001$), thermogenesis ($p = 0.0003$), protein processing in the endoplasmic reticulum ($p = 0.0108$), and non-alcoholic fatty liver disease ($p = 0.0421$) (**Figure 5B**, **Table 1**).

PRM Verification of DAPs

Out of the DAPs identified by PRM, 77.14% (27/35) were consistent with those identified in the TMT proteomic analysis. This indicated that the TMT proteomic analyses yielded reliable results (**Figure 3A**, **Table 2**).

Protein-Protein Interaction Network Construction and Module Analysis

To further ascertain the functional interactions between the DAPs, the Cytoscape software was used to construct the protein-protein interaction networks with a confidence cutoff of 400 (**Figure 7**). The findings showed that ribosome-related proteins were highly interrelated and played central roles across the network.

DISCUSSION

To our knowledge, this is the first study to investigate the biological effects of cancer cells cultured in a deep underground environment, and provide novel insights into cancer. Although relative humidity, air pressure, and concentration of CO_2 and

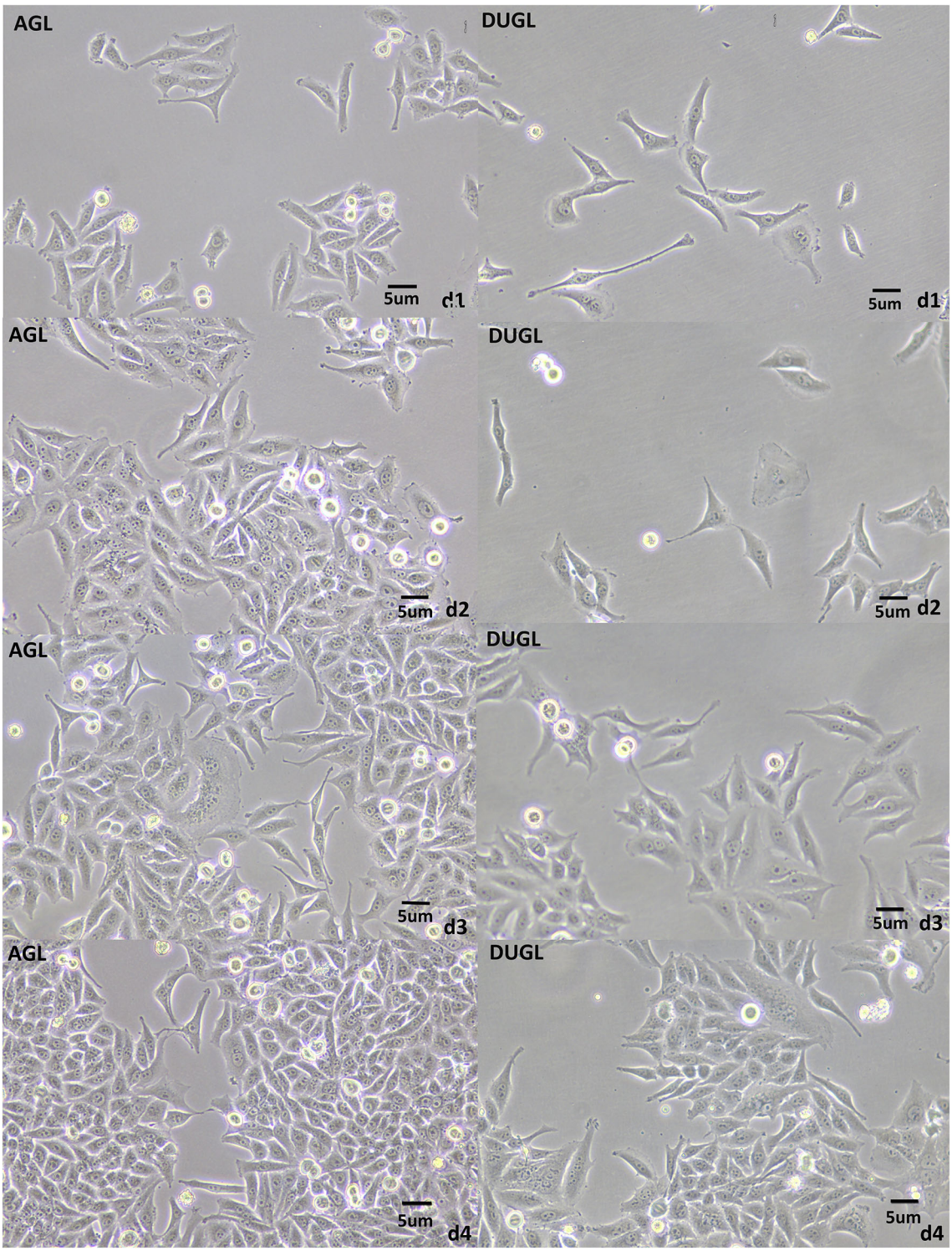

FIGURE 2 | FD-LSC-1 cells cultured for 4 days in the DUGL or AGL observed using light microscopy (at 10 × magnification). AGL, above-ground laboratory; DUGL, deep underground laboratory. The cell density in the DUGL group was observably lower than that in the AGL group on the corresponding day.

radon gas were significantly different between DUGL and AGL, the cell culture incubators at both the locations had the same level of relative humidity, temperature, and concentration of CO_2 (4). The air pressure (1.2–6 bar) could enhance cell growth rate (5, 6). Air pressure in the DUGL (1118.2 hPa) was slightly higher than that in the AGL (951.9 hPa); however, the difference was

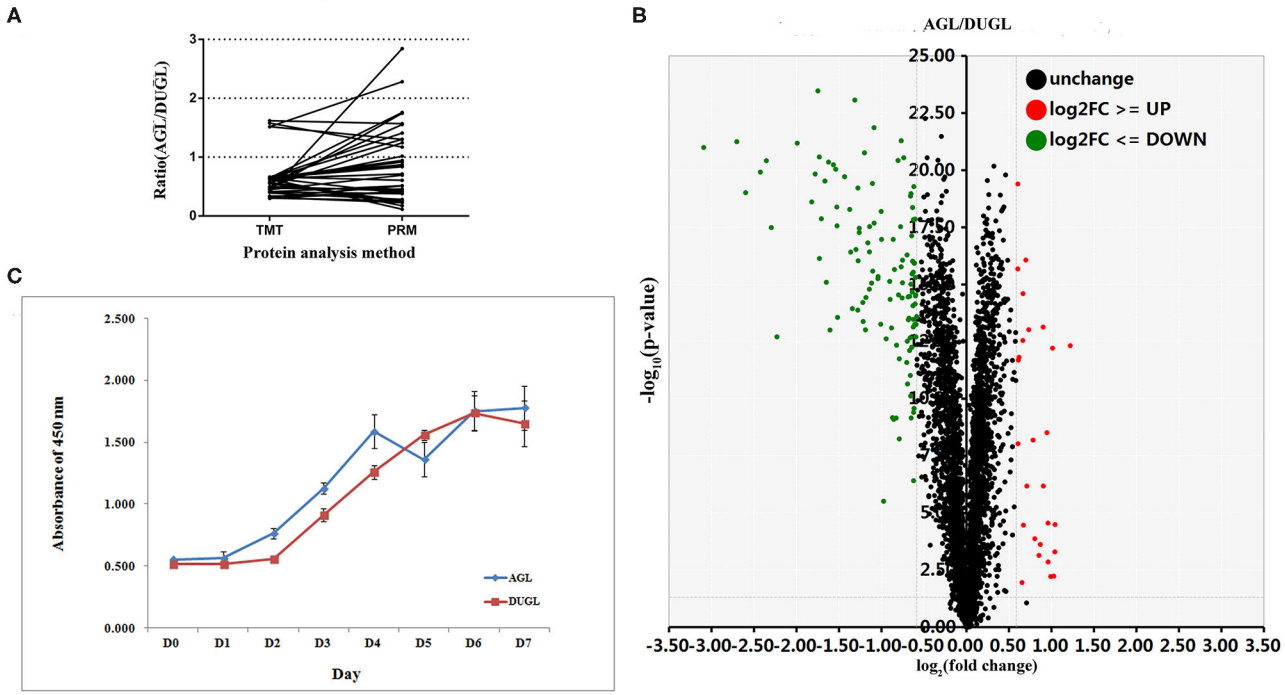

FIGURE 3 | (A) PRM verification results of the selected DAPs (AGL/DUGL); **(B)** Growth curves of FD-LSC-1 cells cultured in the DUGL or AGL; **(C)** Volcano plot (red, upregulated DAPs; black, unchanged DAPs; green, downregulated DAPs [AGL/DUGL]). DAPs, differentially abundant proteins; DUGL, deep underground laboratory; AGL, above-ground laboratory; PRM, parallel reaction monitoring.

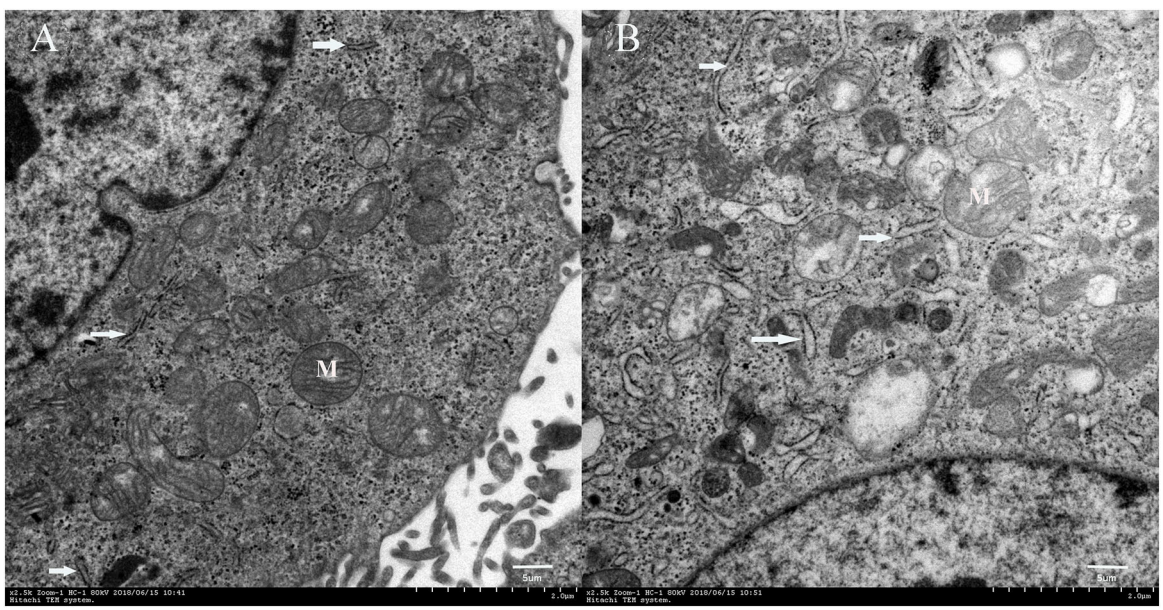

FIGURE 4 | Transmission electron microscopy images of FD-LSC-1 cells cultured in the AGL **(A)** and DUGL **(B)** (at 2,500 × magnification). White arrows, endoplasmic reticulum; M, mitochondria; AGL, above-ground laboratory; DUGL, deep underground laboratory.

dramatically reduced by the shift in gas and liquid (4). After all, the cells were cultured in liquid medium in the incubators. The 1,400-m rocky cover over of the DUGL shields almost all the cosmic radiation (7). Moreover, the terrestrial radiation in DUGL (0.04 μSv/h) was significantly lower than that in AGL (0.15 μSv/h) (4). Radon concentration (1.5 pCi/L) of the DUGL

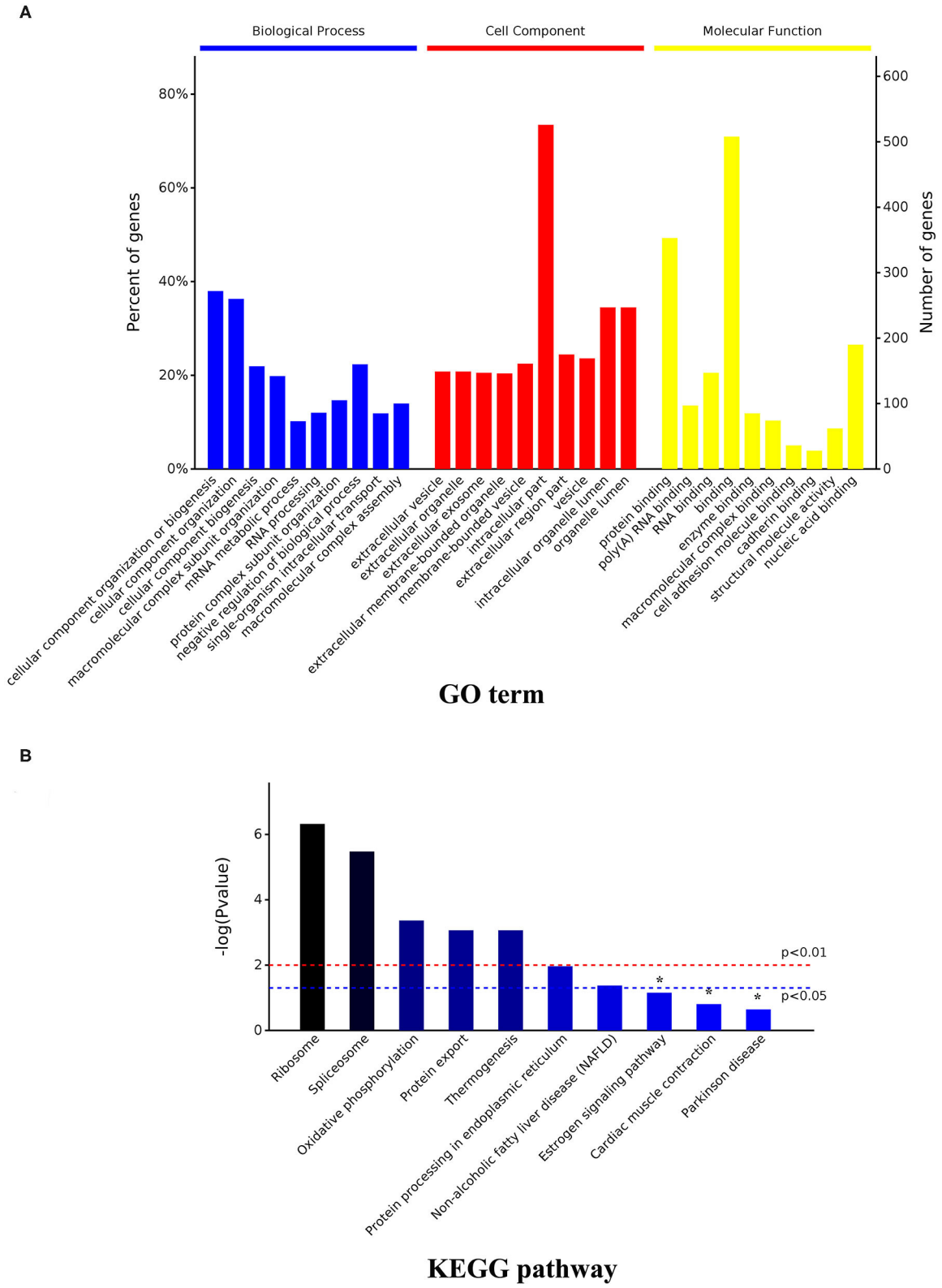

FIGURE 5 | GO and KEGG enrichment analysis of the total DAPs. **(A)** GO analysis result; **(B)** KEGG pathway analysis result. DAPs, differentially abundant proteins.

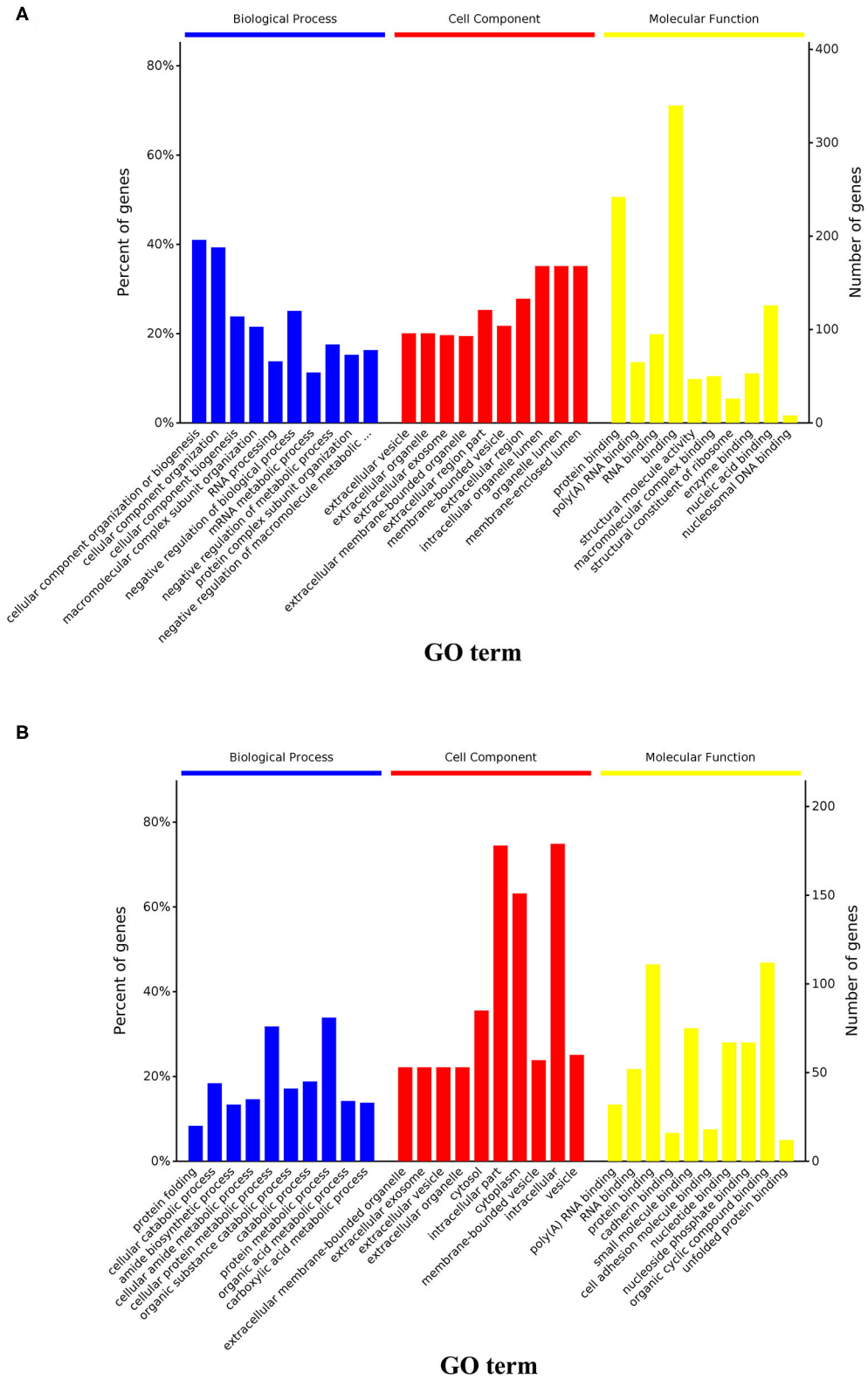

FIGURE 6 | GO and KEGG enrichment analysis of the upregulated and downregulated DAPs. **(A)** Results of GO analysis of upregulated DAPs in cells from the DUGL group; **(B)** Results of GO analysis of downregulated DAPs in cells from the DUGL group. DAPs, differentially abundant proteins.

TABLE 1 | KEGG pathway enrichment result.

Pathway	*p*-value (adjusted)	Number of upregulated proteins (n)	Upregulated DAPs	Number of downregulated proteins (n)	Downregulated DAPs
Ribosome	$p < 0.0001$	17	RPL39, RPS28, RPL30, RPL37A, RPL22, RPL38, RPL35A, RPS12, RPL34, RPS25, RPS27, RPL36, RPL26, MRPS17, RPS26, RPLP2, RPL36A	3	RPL7, RPS2, RPL4
Spliceosome	0.0001	13	SF3A2, SNRPF, DDX46, SLU7, ZMAT2, TRA2A, SMNDC1, LSM6, LSM5, SRSF3, SRSF5, SNRPD2, LSM2	5	HSPA8, PRPF40A, ISY1, PCBP1, HNRNPA1
Oxidative phosphorylation	0.00043	14	COX6C, UQCR10, ATP5ME, NDUFB3, NDUFAB1, NDUFS5, UQCRH, NDUFB1, ATP5PF, ATP5F1E, COX4I1, NDUFA2, COX6B1, ATP6V1G1	0	
Protein export	0.00086	2	SEC61B, SRP19	4	SRPRA, SRPRB, HSPA5, SRP72
Thermogenesis	0.00086	17	COX6C, UQCR10, COX19, COA7, ATP5ME, KDM3B, SMARCD2, NDUFB3, COX20, NDUFAB1, NDUFS5, UQCRH, NDUFB1, ATP5PF, ATP5F1E, NDUFA2, COX6B1	1	PRKACA
Protein processing in endoplasmic reticulum	0.00108	3	RBX1, SEC61B, WFS	10	EDEM3, HSPA8, ERP29, DNAJA1, P4HB, CANX, HSPA5, STT3B, HSP90AA1, HSP90AB1
Non-alcoholic fatty liver disease	0.0421	11	COX6C, UQCR, NDUFB, NDUFAB1, BID, NDUFS5, UQCRH, NDUFB1, COX4I1, NDUFA, COX6B1	0	

was similar to that at Gran Sasso National Laboratory (LNGS) and less than the normal background (1.7 nGy/h:0.04 μSv/h) (4). Herein, we speculate that BBR, as the main environmental factor, affected the cultures in the DUGL at the CJEM.

Consistent with previous reports, the present study confirmed that BBR exposure in a deep underground environment can reduce the growth rates of cells, even cancer cells, within a short duration (8–11). Additionally, we identified 807 DAPs (536 proteins upregulated and 271 proteins downregulated in FD-LSC-1 cells cultured in the DUGL) with a 1.2 absolute fold change, and 145 DAPs (118 upregulated and 27 downregulated in cells cultured in the DUGL) with a 1.5 absolute fold change. The upregulated DAPs underwent fold change ranging from 1.2- to 8.5-fold, while the downregulated DAPs underwent fold change ranging from 0.83- to 0.43-fold. Meanwhile, the ER was observed to be hypertrophic and present at a greater number in FD-LSC-1 cells cultured in the DUGL as observed using TEM. The changes in the proteomics profile and morphology of ER were also similar to those of V79 cells cultured in the DUGL (4), which strongly suggested that BBR could promote protein synthesis in cultures within a short duration.

The GO enrichment analyses helped us elucidate the functions of the DAPs (12). In the BP category, cellular component organization or biogenesis, macromolecular complex subunit organization, and mRNA metabolic process were the top three enriched terms. In addition, the upregulated DAPs were significantly enriched for negative regulation of biological and metabolic processes, which might explain the increased protein expression and delayed growth of FD-LSC-1 cells cultured in the DUGL. In the MF category, the poly(A) RNA binding, RNA binding, protein binding, and binding terms were enriched significantly, consistent with our observations in V79 cells used in our previous research. This suggested that BBR exposure in a deep underground environment primarily affected the macromolecular functions of the cultures by initiating binding dysregulation, especially in RNAs and proteins. The FD-LSC-1 cells cultured in DUGL exhibited enrichment in extracellular terms (e.g., vesicle, organelle, exosome, and membrane-bounded organelle) in the CC category, contrary to the V79 cells, which exhibited enrichment in intracellular terms. This implied that different cells exhibited similar or different responses at the molecular level under BBR exposure in a deep underground environment.

KEGG pathway analyses have been widely used to systematically identify the functions of large-scale proteins and/or genes in cells. Consistent with the observations in V79 cells in our previous research (4), the KEGG analyses of FD-LSC-1 DAPs showed that ribosome and spliceosome were the two most significantly enriched pathways. Meanwhile, most DAPs enriched in the two pathways were upregulated in both V79 and FD-LSC-1 cells cultured in the DUGL. Extracellular stimulation can induce ribosomal stress, disturb ribosome biogenesis, and affect cell proliferation (13). Similar to that in V79 cells, both RPL26, and RPS27, which regulate p53 expression and cell cycle arrest, were upregulated in cells cultured in the DUGL groups. These findings further indicate that ribosomal

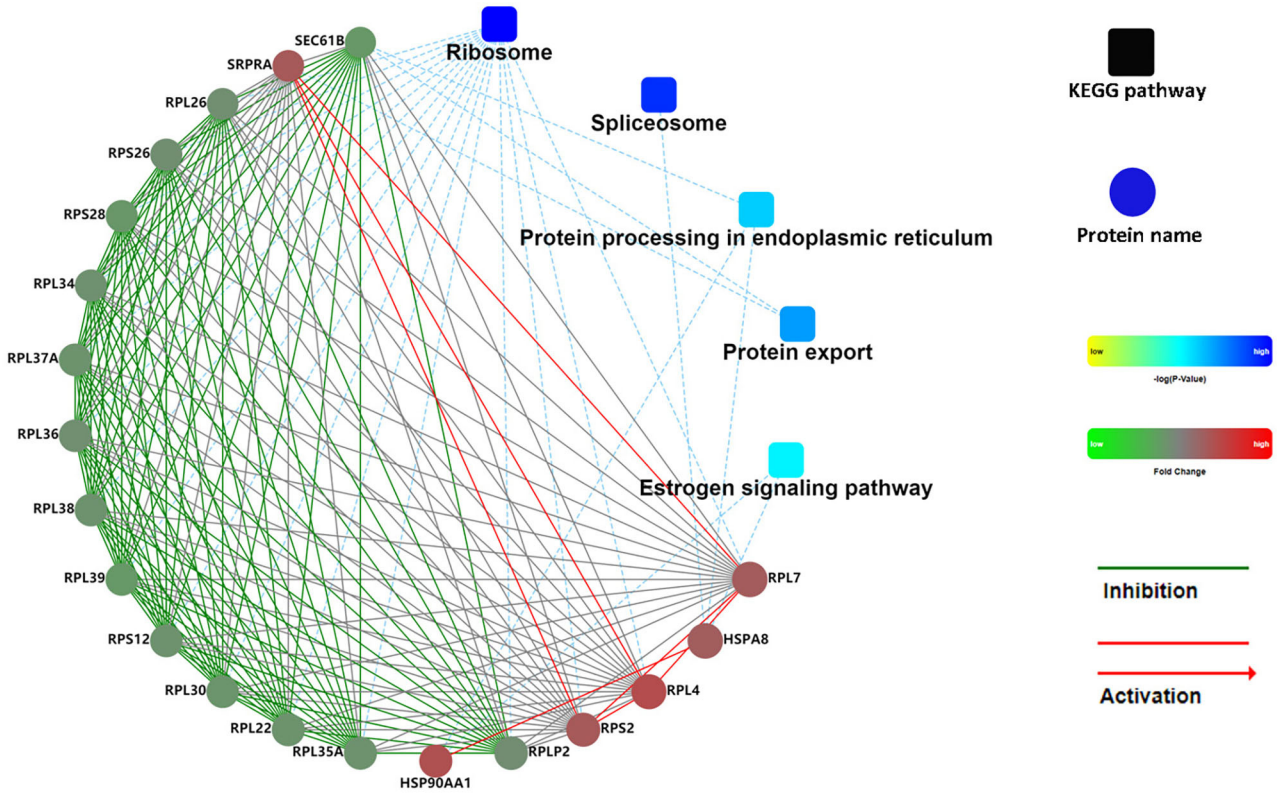

FIGURE 7 | PPI network of DAPs in FD-LSC-1 cells. Coloration with gradient: from yellow (lower *p*-value) to blue (higher *p*-value). The proteins with different abundances are indicated in red (upregulation in the AGL group) and green (downregulation in the AGL group). The default confidence cutoff value was fixed at 400. The red solid lines represent activation. The blue dashed lines indicate the KEGG pathway. PPI, protein-protein interaction; DAPs, differentially abundant proteins.

proteins, especially RPL26, and RPS27, play a significant role in the cellular stress response induced upon exposure to BBR in a deep underground environment and inhibit the proliferative potential of cells through p53 (14).

Spliceosome is an essential cellular organelle for cell growth and division that regulates gene expression and protein synthesis (15). The catalysis of precursor mRNA splicing by spliceosomes, a multi-megadalton ribonucleoprotein complex (16), is a vital step in the flow of genetic information from DNA to proteins in eukaryotes (17). We observed that 15/28 DAPs enriched in the spliceosome pathway were upregulated in cells cultured in the DUGL. Among the upregulated DAPs, seven proteins (ZMAT2, PRPF40A, SNRPD2, SLU7, SRSF5, SRSF3, and SNRPF) followed the same expression model as that in V79 cells (4). Pre-mRNA processing factor 40 homolog A (PRPF40A) plays a crucial role in the initiation of pre-mRNA splicing (18), while the splicing regulator SLU7 serves as an essential factor for the maintenance of cell viability (19). These findings further indicate that BBR could induce protein expression by enhancing spliceosome function, which might be advantageous for cell survival in an altered environment.

The ER has multiple functions, including the synthesis, folding, quality control, and transport of one-third of all cellular proteins (20, 21). In addition, the ER is a critical site for calcium homeostasis and can respond to exogenous stimuli by perceiving environmental signals (22). In the present study, 10/13 proteins enriched in protein processing in the ER pathway were downregulated in cells cultured in the DUGL, which was consistent with the findings from our previous analyses conducted on V79 cells (4). Notably, five proteins (WFS1, STT3B, CANX, ERP29, and HSPA5) were downregulated both in V79 and FD-LSC-1 cells cultured in the DUGL. Wolfram syndrome 1 gene (WFS1), an ER-resident transmembrane protein, regulates the cellular response to ER stress (23). The knockdown of WFS1 can render cells vulnerable to oxidative stress and induce alterations in mitochondrial homeostasis (24). Post-translational N-glycosylation mediated by STT3B plays an important role in the quality control of non-glycosylated proteins. The knockdown of STT3B was observed to delay cell proliferation (25). As an integral chaperon protein of the ER, calnexin (CANX) promotes cancer cell growth and proliferation. Endoplasmic reticulum protein 29 (ERp29), which plays a role in protein unfolding and secretion, is associated with the ER stress response (26). Heat shock protein 5 (HSPA5/GRP78/BiP) protects cells against ER stress and damage caused by reactive oxygen species, and helps cells survive by regulating calcium signaling in mitochondria-associated ER membranes (27). These findings strongly indicate that the ER plays a central role in the BBR stress response, and the downregulation of major ER stress proteins might explain the reduction in stress tolerance potential observed in previous

TABLE 2 | Results of DAP verification by parallel reaction monitoring.

UniProt ID	Gene name	TMT (AGL/DUGL)	PRM (AGL/DUGL)
A0A087WW43	ITIH3	0.4017319	2.844
A0A0G2JPA8	SERPINF2	0.3238109	0.512
A8MZH8	PTTG1IP	0.665582	0.86
E9PES6	HMGB3	0.6464124	0.944
E9PIT3	F2	0.6469235	0.383
E9PS74	SLC43A3	1.519244	1.302
F8W696	APOA1	0.3153911	0.227
I3L4G8	CHMP6	0.6435466	1.76
O00622	CYR61	0.4987531	0.427
P01023	A2M	0.411034	0.514
P01024	C3	0.390117	0.282
P02461	COL3A1	0.4081448	0.378
P05543	SERPINA7	0.3045479	0.259
P09669	COX6C	0.6596789	0.87
P09923	ALPI	1.57784	1.171
P13645	KRT10	0.4975399	1.243
P13647	KRT5	0.6197494	0.174
P14324	FDPS	1.619579	1.568
P17096	HMGA1	0.6389323	0.714
P35527	KRT9	0.4700966	0.457
P35908	KRT2	0.5715737	0.253
P43652	AFM	0.2987056	0.418
P60903	S100A10	0.5489479	0.246
P61769	B2M	0.633045	0.113
P81605	DCD	0.6339814	0.917
P98179	RBM3	0.4456107	0.694
Q01469	FABP5	0.6432707	1.304
Q15428	SF3A2	0.6603566	1.41
Q4KMP7	TBC1D10B	0.4632966	1.747
Q5T985	ITIH2	0.3368894	0.393
Q6ZVX7	NCCRP1	1.517451	2.281
Q8WXA9	SREK1	0.5544262	1.554
Q96B23	C18orf25	0.6465517	0.837
Q9BXV9	GON7	0.6654836	0.607
Q9UPY3	DICER1	0.574236	1.017

studies (28). Additionally, the downregulation of proliferation-promoting proteins might further contribute to the delay in the growth of cells cultured under low background radiation in the DUGL.

The activation of ribosomes and spliceosomes requires energy (29). Mitochondria can supply energy for cellular survival and development. Mitochondrial OXPPL is the primary pathway for energy synthesis in all cell types (30). In the current study, we characterized 14 DAPs that were upregulated in FD-LSC-1 cells cultured in the DUGL. The DAPs that underwent maximum upregulation were associated with energy metabolism related to thermogenesis and non-alcoholic fatty liver disease pathways. These results suggested that under BBR stress, FD-LSC-1 cells could activate the OXPPL pathway and enhance energy supply for cell survival. In support of this proposition, we observed that the expression of ubiquinol cytochrome c reductase hinge (UQCRH) and ATP6V1G1 also increased in V79 cells cultured under BBR (4). UQCRH upregulation suggests an increase in mitochondrial OXPPL activity (31). However, the findings of this study are contrasting to those of a previous study showing that some of the proteins enriched in the OXPPL pathway were downregulated in V79 cells and *Shewanella oneidensis* along with downregulation of ATPase mRNA (32). Cytochrome oxidase subunit 6B1 (COX6B1), which protects cells against injury (33, 34), was downregulated in V79 cells and upregulated in FD-LSC-1 cells cultured under BBR. The inconsistent results indicate that different cells express the same proteins as well as different proteins at different time points to counter BBR stress. UQCRH and ATP6V1G1 might be critical for cellular stress response under BBR. Notably, Carbone et al. (1) reported the inhibition in the activity of superoxide dismutase in TK6 cells cultured in the BBR environment in LNGS. This indicated the inhibition of superoxide dismutase expression, as observed through proteomic analyses in our study.

CONCLUSION

BBR exposure in a deep underground environment could inhibit the proliferation of FD-LSC-1 cells. In response, the FD-LSC-1 cells presented with changes in the proteomic profile related to the ribosome, gene spliceosome, RNA transport, and energy metabolism among others. The alterations in protein expression might constitute the molecular basis of proliferation inhibition and enhanced survivability in cells adapting to BBR in a deep underground environment. RPL26, RPS27, ZMAT2, PRPF40A, SNRPD2, SLU7, SRSF5, SRSF3, SNRPF, WFS1, STT3B, CANX, ERP29, HSPA5, COX6B1, UQCRH, and ATP6V1G1 were the major proteins associated with the BBR stress response in cells. Our findings provide novel insights into the response of cancer cells from a different perspective, in which the usual levels of radiation were reduced drastically in a deep underground environment.

LIMITATIONS

Similar to our previous reports, our present study has certain limitations. First, the growth curve obtained after culturing cells in the deep underground environment represented data recorded only for a week, and the samples used for the proteomic analyses were cultured for only 4 days in the DUGL. Second, the functions of DAPs should be verified in knockdown and overexpression studies. Third, it is necessary to use a normal cell line as a control in future studies. Fourth, some of the environmental factors could not be regulated to the desired levels owing to the challenge of ventilation in deep mines.

DATA AVAILABILITY STATEMENT

The datasets presented in this study can be found in online repositories. The names of the repository/repositories

and accession number(s) can be found in the article/**Supplementary Material**.

AUTHOR CONTRIBUTIONS

JiL, HX, SL, JZ, MG, JW, and JuL conceived and designed the project. TM, SW, YX, JC, LW, YL, and QW performed all the experiments. LJ wrote the manuscript and prepared the figures. JW, MG, WL, and HX reviewed and revised the manuscript. All authors reviewed and approved the manuscript.

FUNDING

This research was supported by grants from the special fund for deep-underground medical research (Grant no. YB2018002) and 1.3.5 project for disciplines of excellence (Grant no. ZYJC18016) provided by the West China Hospital, Sichuan University; Sichuan International Technological Innovation Cooperation Project (Grant no. 2018HH0159), Open Fund of the Key Laboratory of Deep Earth Science and Engineering, Ministry of Education (Grant no. DESEYU 201902) and the National Natural Science Foundation of China (Grant no. 51822403), the research fund of Health commission of Sichuan province (Grant no. 20PJ029).

ACKNOWLEDGMENTS

The authors sincerely thank Chairman Zhiliang Wu and his colleagues at Jiapigou Minerals Limited Corporation of China National Gold Group Corporation for their help providing an experimental site and their assistance in conducting research. We express our gratitude to Professor Aixiang Wu of the University of Science and Technology, Beijing for his guidance and help in searching for this experimental site. We thank Suzhou Bionovogene and Shanghai Oebiotech Co., Ltd. for their help with the proteomic analyses.

SUPPLEMENTARY MATERIAL

The Supplementary Material for this article can be found online at: https://www.frontiersin.org/articles/10.3389/fpubh.2020.584964/full#supplementary-material

REFERENCES

1. Carbone MC, Pinto M, Antonelli F, Amicarelli F, Balata M, Belli M, et al. The cosmic silence experiment: on the putative adaptive role of environmental ionizing radiation. *Radiat Environ Biophys.* (2009) 48:189–96. doi: 10.1007/s00411-008-0208-6
2. Huang L, Kim PM, Nickoloff JA, Morgan WF. Targeted and nontargeted effects of low-dose ionizing radiation on delayed genomic instability in human cells. *Cancer Res.* (2007) 67:1099–104. doi: 10.1158/0008-5472.CAN-06-3697
3. Liu J, Ma T, Liu Y, Zou J, Gao M, Zhang R, et al. History, advancements, and perspective of biological research in deep-underground laboratories: a brief review. *Environ Int.* (2018) 120:207–14. doi: 10.1016/j.envint.2018.07.031
4. Liu J, Ma T, Gao M, Liu Y, Liu J, Wang S, et al. Proteomics provides insights into the inhibition of Chinese hamster V79 cell proliferation in the deep underground environment. *Sci Rep.* (2020) 10:14921. doi: 10.1038/s41598-020-71154-z
5. Pinheiro R, Belo I, Mota M. Growth and beta-galactosidase activity in cultures of Kluyveromyces marxianus under increased air pressure. *Lett Appl Microbiol.* (2003) 37:438–42. doi: 10.1046/j.1472-765X.2003.01429.x
6. Pinheiro R, Belo II, Mota M. Air pressure effects on biomass yield of two different Kluyveromyces strains. *Enzyme Microb Technol.* (2000) 26:756–62. doi: 10.1016/S0141-0229(00)00168-X
7. Thome C, Tharmalingam S, Pirkkanen J, Zarnke A, Laframboise T, Boreham DR. The REPAIR project: examining the biological impacts of sub-background radiation exposure within SNOLAB, a deep underground laboratory. *Radiat Res.* (2017) 188:470–4. doi: 10.1667/RR14654.1
8. Planel H, Soleilhavoup JP, Tixador R, Richoilley G, Conter A, Croute F, et al. Influence on cell proliferation of background radiation or exposure to very low, chronic gamma radiation. *Health Phys.* (1987) 52:571–8. doi: 10.1097/00004032-198705000-00007
9. Smith GB, Grof Y, Navarrette A, Guilmette RA. Exploring biological effects of low level radiation from the other side of background. *Health Phys.* (2011) 100:263–5. doi: 10.1097/HP.0b013e318208cd44
10. Castillo H, Schoderbek D, Dulal S, Escobar G, Wood J, Nelson R, et al. Stress induction in the bacteria Shewanella oneidensis and deinococcus radiodurans response to below-background ionizing radiation. *Int J Radiat Biol.* (2015) 91:749–56. doi: 10.3109/09553002.2015.1062571
11. Kawanishi M, Okuyama K, Shiraishi K, Matsuda Y, Taniguchi R, Shiomi N, et al. Growth retardation of Paramecium and mouse cells by shielding them from background radiation. *J Radiat Res.* (2012) 53:404–10. doi: 10.1269/jrr.11145
12. Camon E, Magrane M, Barrell D, Lee V, Dimmer E, Maslen J, et al. The gene ontology annotation (GOA) database: sharing knowledge in uniprot with gene ontology. *Nucleic Acids Res.* (2004) 32:D262–6. doi: 10.1093/nar/gkh021
13. Zhou X, Liao WJ, Liao JM, Liao P, Lu H. Ribosomal proteins: functions beyond the ribosome. *J Mol Cell Biol.* (2015) 7:92–104. doi: 10.1093/jmcb/mjv014
14. Ma XR, Sim UH, Ling TY, Tiong TS, Khoo SB. Expression trend of selected ribosomal protein genes in nasopharyngeal Carcinoma. *Malays J Med Sci.* (2012) 18:23–30.
15. Li F, Zhao D, Yang S, Wang J, Liu Q, Jin X, et al. ITRAQ-based proteomics analysis of triptolide on human A549 lung adenocarcinoma cells. *Cell Physiol Biochem.* (2018) 45:917–34. doi: 10.1159/000487286
16. Will CL, Lührmann R. Spliceosome structure and function. *Cold Spring Harbor Perspect Biol.* (2011) 3:a003707. doi: 10.1101/cshperspect.a003707
17. Shi Y. Mechanistic insights into precursor messenger RNA splicing by the spliceosome. *Nat Rev Mol Cell Biol.* (2017) 18:655–70. doi: 10.1038/nrm.2017.86
18. Huo Z, Zhai S, Weng Y, Qian H, Tang X, Shi Y, et al. PRPF40A as a potential diagnostic and prognostic marker is upregulated in pancreatic cancer tissues and cell lines: an integrated bioinformatics data analysis. *OncoTargets Ther.* (2019) 12:5037–51. doi: 10.2147/OTT.S206039
19. Urtasun R, Elizalde M, Azkona M, Latasa MU, García-Irigoyen O, Uriarte I, et al. Splicing regulator SLU7 preserves survival of hepatocellular carcinoma cells and other solid tumors via oncogenic miR-17-92 cluster expression. *Oncogene.* (2016) 35:4719–29. doi: 10.1038/onc.2015.517
20. Turnham RE, Scott JD. Protein kinase A catalytic subunit isoform PRKACA; history, function and physiology. *Gene.* (2016) 577:101–8. doi: 10.1016/j.gene.2015.11.052
21. Wang Z, Feng Y, Li J, Zou J, Fan L. Integrative microRNA and mRNA analysis reveals regulation of ER stress in the Pacific white shrimp litopenaeus vannamei under acute cold stress. *Comp Biochem Physiol Part D Genomics Proteomics.* (2019) 33:100645. doi: 10.1016/j.cbd.2019.100645
22. Ryan D, Carberry S, Murphy ÁC, Lindner AU, Fay J, Hector S, et al. Calnexin, an ER stress-induced protein, is a prognostic marker and potential therapeutic target in colorectal cancer. *J Transl Med.* (2016) 14:196. doi: 10.1186/s12967-016-0984-8

23. Sakakibara Y, Sekiya M, Fujisaki N. Knockdown of wfs1, a fly homolog of Wolfram syndrome 1, in the nervous system increases susceptibility to age- and stress-induced neuronal dysfunction and degeneration in Drosophila. *PLoS Genet.* (2018) 14:e1007196. doi: 10.1371/journal.pgen.1007196
24. Cagalinec M, Liiv M. Role of mitochondrial dynamics in neuronal development: mechanism for wolfram syndrome. *PLoS Biol.* (2016) 14:e1002511. doi: 10.1371/journal.pbio.1002511
25. Sato T, Sako Y, Sho M, Momohara M, Suico MA, Shuto T, et al. STT3B-dependent posttranslational N-glycosylation as a surveillance system for secretory protein. *Mol Cell.* (2012) 47:99–110. doi: 10.1016/j.molcel.2012.04.015
26. Guo L, Ma L, Liu C, Lei Y, Tang N, Huang Y, et al. ERp29 counteracts the suppression of malignancy mediated by endoplasmic reticulum stress and promotes the metastasis of colorectal cancer. *Oncol Rep.* (2019) 41:1603–15. doi: 10.3892/or.2018.6943
27. Kim SY, Kim HJ, Kim HJ, Kim DH, Han JH, Byeon HK, et al. HSPA5 negatively regulates lysosomal activity through ubiquitination of MUL1 in head and neck cancer. *Autophagy.* (2018) 14:385–403. doi: 10.1080/15548627.2017.1414126
28. Carbone MC, Pinto M, Antonelli F, Balata M. Effects of deprivation of background environmental radiation on cultured human cells. *Il Nuovo Cimento.* (2010) 125:469–77. doi: 10.1393/ncb/i2010-10889-y
29. Shi Y. The spliceosome: a protein-directed metalloribozyme. *J Mol Biol.* (2017) 429:2640–53. doi: 10.1016/j.jmb.2017.07.010
30. Yan G, Li X, Cheng X, Peng Y, Long B, Fan Q, et al. Proteomic profiling reveals oxidative phosphorylation pathway is suppressed in longissimus dorsi muscle of weaned piglets fed low-protein diet supplemented with limiting amino acids. *Int J Biochem Cell Biol.* (2016) 79:288–97. doi: 10.1016/j.biocel.2016.08.024
31. Huang YP, Chang NW. PPARα modulates gene expression profiles of mitochondrial energy metabolism in oral tumorigenesis. *BioMedicine.* (2016) 6:3. doi: 10.7603/s40681-016-0003-7
32. Castillo H, Li X, Schilkey F, Smith GB. Transcriptome analysis reveals a stress response of Shewanella oneidensis deprived of background levels of ionizing radiation. *PLoS ONE.* (2018) 13:e0196472. doi: 10.1371/journal.pone.0196472
33. Zhang W, Wang Y, Wan J, Zhang P, Pei F. COX6B1 relieves hypoxia/reoxygenation injury of neonatal rat cardiomyocytes by regulating mitochondrial function. *Biotechnol Lett.* (2019) 41:59–68. doi: 10.1007/s10529-018-2614-4
34. Yang S, Wu P, Xiao J, Jiang L. Overexpression of COX6B1 protects against I/R-induced neuronal injury in rat hippocampal neurons. *Mol Med Rep.* (2019) 19:4852–62. doi: 10.3892/mmr.2019.10144

Conflict of Interest: The authors declare that the research was conducted in the absence of any commercial or financial relationships that could be construed as a potential conflict of interest.

frontiers in Public Health

BRIEF RESEARCH REPORT
published: 12 January 2021
doi: 10.3389/fpubh.2020.594789

Low Radiation Environment Switches the Overgrowth-Induced Cell Apoptosis Toward Autophagy

Mariafausta Fischietti[1,2], Emiliano Fratini[1,3], Daniela Verzella[2], Davide Vecchiotti[2], Daria Capece[2], Barbara Di Francesco[2], Giuseppe Esposito[3,4], Marco Balata[5], Luca Ioannuci[5], Pamela Sykes[6], Luigi Satta[1], Francesca Zazzeroni[2], Alessandra Tessitore[2], Maria Antonella Tabocchini[1,3,4†] and Edoardo Alesse[2†]*

[1] Museo Storico della Fisica e Centro Studi e Ricerche Enrico Fermi, Rome, Italy, [2] Department of Biotechnological and Applied Clinical Sciences, L'Aquila University, L'Aquila, Italy, [3] Istituto Superiore di Sanità, National Center for Innovative Technologies in Public Health, Rome, Italy, [4] Istituto Nazionale di Fisica Nucleare (INFN) Sezione Roma, Rome, Italy, [5] INFN-Gran Sasso National Laboratory, Assergi L'Aquila, Italy, [6] Flinders Center for Innovation in Cancer, Flinders University, Adelaide, SA, Australia

OPEN ACCESS

Edited by:
Claudio Pioli, Italian National Agency for New Technologies, Energy and Sustainable Economic Development (ENEA), Italy

Reviewed by:
Francis A. Cucinotta, University of Nevada, Las Vegas, United States
Paul Gottlob Layer, Darmstadt University of Technology, Germany

***Correspondence:**
Alessandra Tessitore
alessandra.tessitore@univaq.it

† These authors have contributed equally to this work

Specialty section:
This article was submitted to Radiation and Health, a section of the journal Frontiers in Public Health

Received: *14 August 2020*
Accepted: *26 November 2020*
Published: *12 January 2021*

Citation:
Fischietti M, Fratini E, Verzella D, Vecchiotti D, Capece D, Di Francesco B, Esposito G, Balata M, Ioannuci L, Sykes P, Satta L, Zazzeroni F, Tessitore A, Tabocchini MA and Alesse E (2021) Low Radiation Environment Switches the Overgrowth-Induced Cell Apoptosis Toward Autophagy. Front. Public Health 8:594789. doi: 10.3389/fpubh.2020.594789

Low radiation doses can affect and modulate cell responses to various stress stimuli, resulting in perturbations leading to resistance or sensitivity to damage. To explore possible mechanisms taking place at an environmental radiation exposure, we set-up twin biological models, one growing in a low radiation environment (LRE) laboratory at the Gran Sasso National Laboratory, and one growing in a reference radiation environment (RRE) laboratory at the Italian National Health Institute (Istituto Superiore di Sanità, ISS). Studies were performed on pKZ1 A11 mouse hybridoma cells, which are derived from the pKZ1 transgenic mouse model used to study the effects of low dose radiation, and focused on the analysis of cellular/molecular end-points, such as proliferation and expression of key proteins involved in stress response, apoptosis, and autophagy. Cells cultured up to 4 weeks in LRE showed no significant differences in proliferation rate compared to cells cultured in RRE. However, caspase-3 activation and PARP1 cleavage were observed in cells entering to an overgrowth state in RRE, indicating a triggering of apoptosis due to growth-stress conditions. Notably, in LRE conditions, cells responded to growth stress by switching toward autophagy. Interestingly, autophagic signaling induced by overgrowth in LRE correlated with activation of p53. Finally, the gamma component of environmental radiation did not significantly influence these biological responses since cells grown in LRE either in incubators with or without an iron shield did not modify their responses. Overall, *in vitro* data presented here suggest the hypothesis that environmental radiation contributes to the development and maintenance of balance and defense response in organisms.

Keywords: low radiation environment, LRE, apoptosis, autophagy, PARP1, p53

INTRODUCTION

Life has evolved on Earth for more than three billion years in ecosystems characterized by different levels of environmental radiation. This abiotic factor, acting as a natural tiny but constant daily stimulus, is at the heart of the development of life and has been incorporated within the biology of organisms during evolution (1). However, very little is known about molecular mechanisms

underpinning the effects of this influencing factor on living beings. To this aim, analysis of differences between two parallel biological systems, one kept in a reference radiation environment (RRE) and one in a very low radiation environment (LRE), helps to enhance knowledge in this field. During the last decades, studies performed in underground laboratories highlighted that biological models could react to background radiation changes in different ways. It was demonstrated that behavior of living systems under low radiation dose exposure can lead to interesting, and often unexpected, results. Several effects, such as genomic instability, with increase of DNA changes through generations; transgenerational effects, with hereditary alterations; bystander effect, which causes damage of healthy cells near to those irradiated, have been observed (2–4).

The peculiar location of the underground Gran Sasso National Laboratory (LNGS) of the Italian Institute of Nuclear Physics (INFN), characterized by very low-radiation conditions, makes it particularly suitable for implementing not only studies in the field of physics, such as proton decay or solar neutrino detection, but also in that of biology. In this location, shielded by more than 1400 meters of carbonate (dolomia) rock, cosmic radiation is almost completely absent (5). Furthermore, due to the nature of the rocks, Uranium and Thorium are barely detected, and the neutron flux is reduced by a factor of 10^3 with respect to external values (6). In addition, radon concentration is kept at a very low level by an efficient ventilation system that pumps air from the outside into the laboratory.

Accordingly, the low LET components, especially photons, are predominant at LRE. On the other hand, at RRE, there are both low LET and high LET components.

Previous researches demonstrated the influence of different environmental radiation on biological systems of different origin (yeast, mouse, and human), indicating that cell cultures maintained in LRE, compared to those in RRE, developed a different biochemical response, being less preserved from DNA damage and showing reduced Reactive Oxygen Species (ROS) scavenging power (1, 7–9).

In this study, we took advantage of the Gran Sasso National Laboratory to further show the core mechanisms putatively responsible for different cellular behaviors attributable to LRE. In particular, we investigated the molecular response of the pKZ1 A11 mouse hybridoma cells (10, 11), cultured in parallel in LRE (at LNGS) and in RRE (at ISS) laboratories, to overgrowth stress conditions, in which cells undergo nutrient deprivation, hypoxia, and pH unbalance. We found that radiation environment does not affect cell proliferation both in exponentially growing cells and in overgrowth conditions. On the contrary, cells overgrowing in LRE were prone to respond to this stress by inducing autophagy instead of apoptosis, which was not observed in cells parallelly cultured in RRE.

MATERIALS AND METHODS

Cell Lines and Proliferation Curve

The hybridoma A11 mouse cell line, which contains a pKZ1 chromosomal inversion cassette (10, 11) was used for the experiments. Cells were cultured under identical conditions in RPMI 1640 (Gibco) supplemented with 5% FBS, L-glutamine, and penicillin-streptomycin at 37°C in a 5% CO_2 humidified incubator. For the evaluation of the role of gamma component, cells were further cultured in parallel in two different incubators, with or without an iron shield, which is able to reduce the gamma component of the radiation spectrum by a factor of about four. For each experiment, parallel cell cultures were plated at 2×10^4 cells/mL in 25 mL of complete medium in 75 cm^2 flasks and grown in quadruplicate for up to 4 weeks at the LNGS Gran Sasso underground laboratory and at the ISS, under low (LRE) and reference (RRE) environmental radiation, respectively. Cells were passaged every Monday (72 h of culture) and every Friday (96 h of culture). An aliquot of 0.5 mL of cells was diluted 1:10 with Isoton Diluent (Beckman Coulter) and counted using an automatic cell counter (Coulter Counter). At every cell passage (every 72 h and 96 h), cells were seeded at 2×10^4 cells/ mL in 25 mL of complete medium in 75 cm^2 flasks. Aliquots of the cell suspension were also used to construct a growth curve along a period of 11 days.

After 4 weeks of culture in LRE, cells were moved to the RRE laboratory and grown for 2 more weeks in RRE.

Protein Extraction and Western Blot

Cells were centrifuged at 1,200 RPM, and protein extracts were prepared at +4°C in RIPA buffer (1x phosphate buffer, 1% NP40, 0.5% sodium deoxycholate, 0.1% SDS, 10 μL/mL PMSF, 30 μL/ml aprotinin; 10 μL/mL sodium orthovanadate) containing complete mini EDTA-free protease inhibitors (Roche Molecular Biochemicals, Mannheim, Germany). Protein concentration was determined by the BCA assay (Pierce, Thermo Fisher). Forty micrograms of proteins were loaded onto a SDS-PAGE and subjected to electrophoresis, and then proteins were electro-transferred to a nitrocellulose membrane (Whatmann, Dassel, Germany) and hybridized to anti-PARP1 (1:1,000; Cell Signaling Technology, cat #9542), anti-p53 (1:1,000; Cell Signaling Technology, cat #2524), anti-P-Ser392-p53 (1:1,000; Cell Signaling Technology, cat #9281), anti-P-Ser15-p53 (1:1,000, Cell Signaling Technology, cat #9284), anti-HSP70 (1:1,000 Cell Signaling Technology, cat #4876), anti-Caspase 3 (1:1,000, Cell Signaling Technology, cat #9662), anti-LC3B (1:1,000, Thermofisher, cat. #PA5-32254, which recognizes both LC3BI and II), anti-actin (1:2,000 Santa Cruz Biotech, cat sc-8432). Membranes were then incubated with specific horseradish peroxidase-conjugated secondary antibodies (Santa Cruz Biotech). Protein bands were visualized using a chemiluminescent detection system (Thermo Scientific, Rockford, USA).

Densitometric Analysis and Statistics

Densitometric analysis of immunoblotting was performed by using the ImageJ software (Rasband, W.S., ImageJ, U.S. National Institutes of Health, Bethesda, Maryland, USA, https://imagej.nih.gov/ij/, 1997–2018). All densitometries were expressed as a ratio of analyzed protein to endogenous control expression. Due to the demanding and very peculiar underground working conditions, it was possible to iterate just some immunoblotting experiments (i.e., anti-P-p53 Ser392, anti-PARP-1, anti-Caspase 3) for which statistical elaboration was provided. Results were

expressed as mean of two independent experiments ± SD. Data were analyzed using the GraphPad Prism (7.0 version) software and statistical analysis of the results was performed using the 2-tailed Student's *t*-test. $P < 0.05$ were considered statistically significant.

RESULTS

Setting Up of Experimental Conditions

In order to evaluate the effect of LRE on cell behaviors, such as cell proliferation and stress-induced cell death, a pKZ1 A11 hybridoma cell line was chosen as a model. This cell line was obtained by fusion of splenic lymphocytes of pKZ1 mouse with murine multiple myeloma cells P3653 (10). The pKZ1 mouse model has been extensively used to study the effects of low dose radiation on the adaptive response and to identify hormetic mutation responses (12–20). In order to set up the experimental conditions, pKZ1 A11 hybridoma cells were cultured in the RRE laboratory in Rome at the ISS (**Figure 1A**). Cell proliferation curve displayed a linear growth between 24 to 72 h, showing an inflection at 96 h and reaching a plateau at 123 h (**Figure 1A**). Interestingly, after 96 h, we observed a strong cleavage of PARP1, a known marker of apoptosis (**Figures 1B,C**) (21–23). Increase of PARP1 cleavage was detected in a time-dependent manner, reaching high level after 96 h, when cells initiated to enter to the proliferation plateau and began to stay in overgrowth stress conditions, due to nutrient and growth factor deprivation, pH changes of medium, higher oxygen need and consumption. These data indicated that, in RRE, pKZ1 A11 cells are prone to initiate and progress through apoptosis in response to the onset of overgrowth stress conditions.

Growth of pKZ1 A11 Cells Is Not Impaired in Low Radiation Environment

In order to assess the existence of differential behaviors potentially due to the environmental radiation levels, a twin culture of pKZ1 A11 cells was maintained in parallel in LRE and RRE, exactly under the same conditions, for 4 weeks and split twice a week, every 72 and 96 h. As shown in **Figure 2A**, no differences were observed in terms of proliferation rate in such conditions between cells grown in RRE and LRE. In accordance with data shown in **Figures 1A,B**, cell count at 72 h of each week of culture displayed a number of cells consistent with a linear growth rate, and cell count at 96 h of each week of culture showed a number of cells consistent with an initial overgrowth plateau state (**Figure 2A**). Moreover, to evaluate the effect of RRE on cells cultured for 1 month in LRE, pKZ1 A11 cells grown for 4 weeks in LRE were moved to the RRE laboratory and cultured for two more weeks (**Figure 2A**, weeks 5 and 6). No differences in proliferation were observed. These data showed that LRE does not influence the cell growth behavior of pKZ1 A11 cells.

PARP1 Cleavage Is Strongly Reduced in LRE-Overgrown Cells

To evaluate the effect of LRE at the molecular levels, cells grown as described in **Figure 2A** were collected twice a week (after 72 and 96 h of culture) for 6 weeks and analyzed for PARP1 cleavage. As expected, levels of PARP1 cleavage increased in a time-dependent manner, consistent with that described above (**Figure 1B**). At the same way, similar behavior was detected in terms of PARP1 expression and cleavage in RRE and LRE under conditions of linear growth (72 h). Interestingly, lower levels of PARP1 cleaved form were detected in LRE overgrown cells (96 h) compared to those cultured in RRE (**Figures 2B,C**). PARP1 cleaved protein was reduced approximately by half in LRE compared to RRE (**Figure 2C**). Interestingly, this effect globally reverted when, after 4 weeks of underground culture, cells were moved to the RRE laboratories for 2 more weeks (**Figures 2B,C**, weeks 5 and 6), indicating a plasticity of cells toward their response to low environmental radiation.

Low Radiation Environment Switches pKZ1 A11 Mouse Hybridoma Response to Overgrowth From Apoptosis Toward Autophagy

To further shed light on the molecular response of overgrown cells cultured in LRE vs. RRE, we performed the western blot analysis of proteins known to be implicated in cell stress response, such as Heat Shock Protein (HSP) 70; genomic stability control and cell death regulation, such as p53; markers of apoptosis, such as caspase 3; and markers of autophagy, such as LC3B. As shown in **Figure 3**, HSP70 levels did not differ between LRE- and RRE-cultured cells upon stress stimulation due to overgrowth (96 h of culture). As expected, the total p53 levels were not significantly modulated, whereas the active form of p53, evaluated as phosphorylation in both Ser15 and Ser392, was strongly induced in LRE overgrowth conditions. A canonical function of p53 is the induction of apoptotic response when cells cannot efficiently repair acquired DNA damage (24, 25). In addition to this function, p53 has been shown to be a modulator of the autophagic process (26), which is known to promote survival upon starvation stress and maintain metabolic homeostasis through degradation and recycling of intracellular components. Literature showed that autophagy suppresses p53 and, also, p53 activates autophagy as part of its protective function (26). In our experimental settings, expression of active p53 correlated with the conversion of LC3B-I to the lower migrating form LC3B-II which is used as an indicator of autophagy especially in condition of nutrient starvation (27, 28), showing that, in LRE conditions, the cell response to overgrowth stress is to switch toward autophagy (**Figure 3**). Finally, in accordance with PARP1 cleavage data (**Figures 2B**, **3**), apoptotic cell induction in RRE overgrowing cells was confirmed by caspase 3 induction. These data suggest an alternative mechanism of response and defense toward stress/damage induced by long-term cell culture in strongly reduced radiation background.

Gamma Component of Radiation Does Not Affect LRE Overgrowth Cell Response

To analyze the putative contribution of gamma component in inducing the above-described effects, cells were further grown in parallel in the LRE laboratory in two incubators, with or without iron shield. The iron (Fe) shield can reduce the gamma

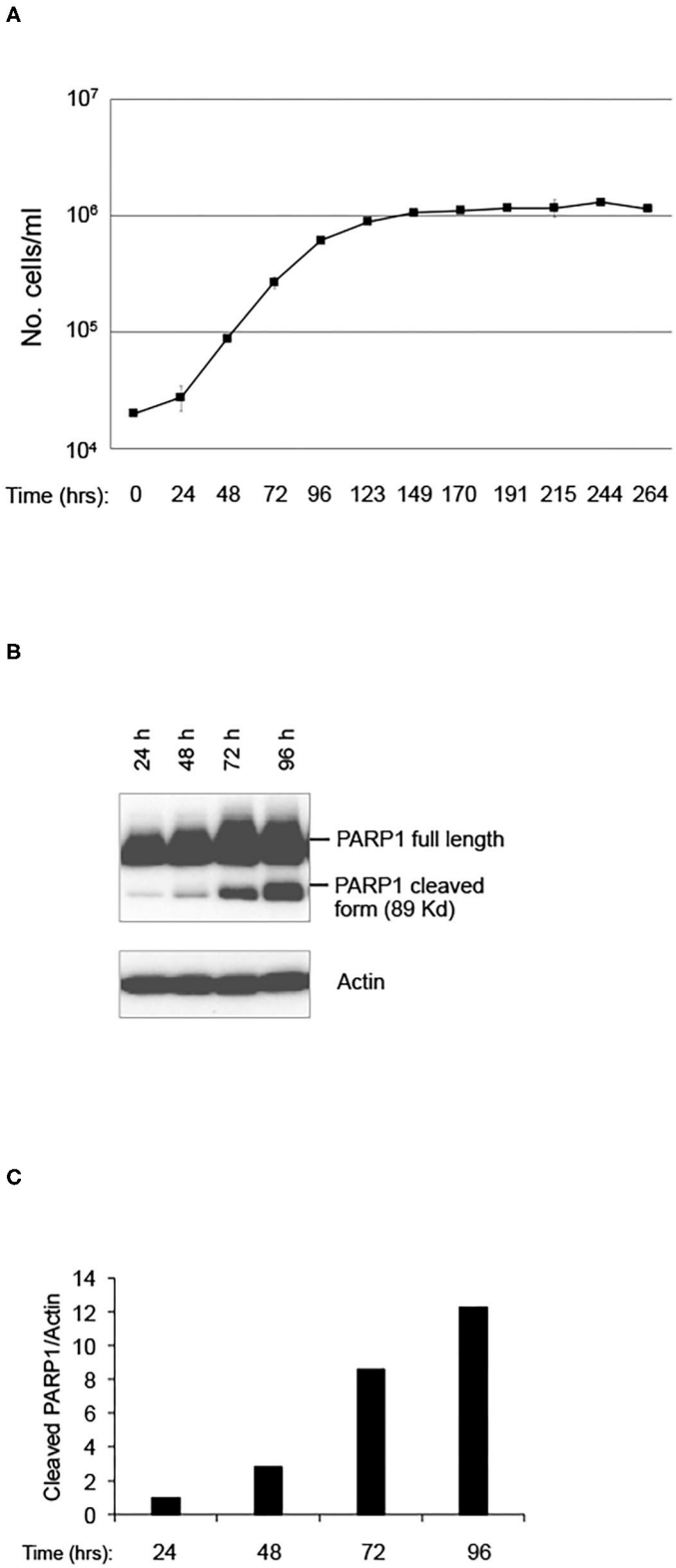

FIGURE 1 | Setting up of pKZ1 A11 mouse hybridoma cells growth condition. **(A)** Proliferation curve of pKZ1 A11 mouse hybridoma cells cultured at the ISS reference laboratory in Rome. Cells were counted in triplicate. Values are means ± SD. **(B)** pKZ1 A11 mouse hybridoma cells cultured as in **(A)** and analyzed for PARP1 cleavage by western blotting. **(C)** Densitometry analysis of western blot shown in **(B)**.

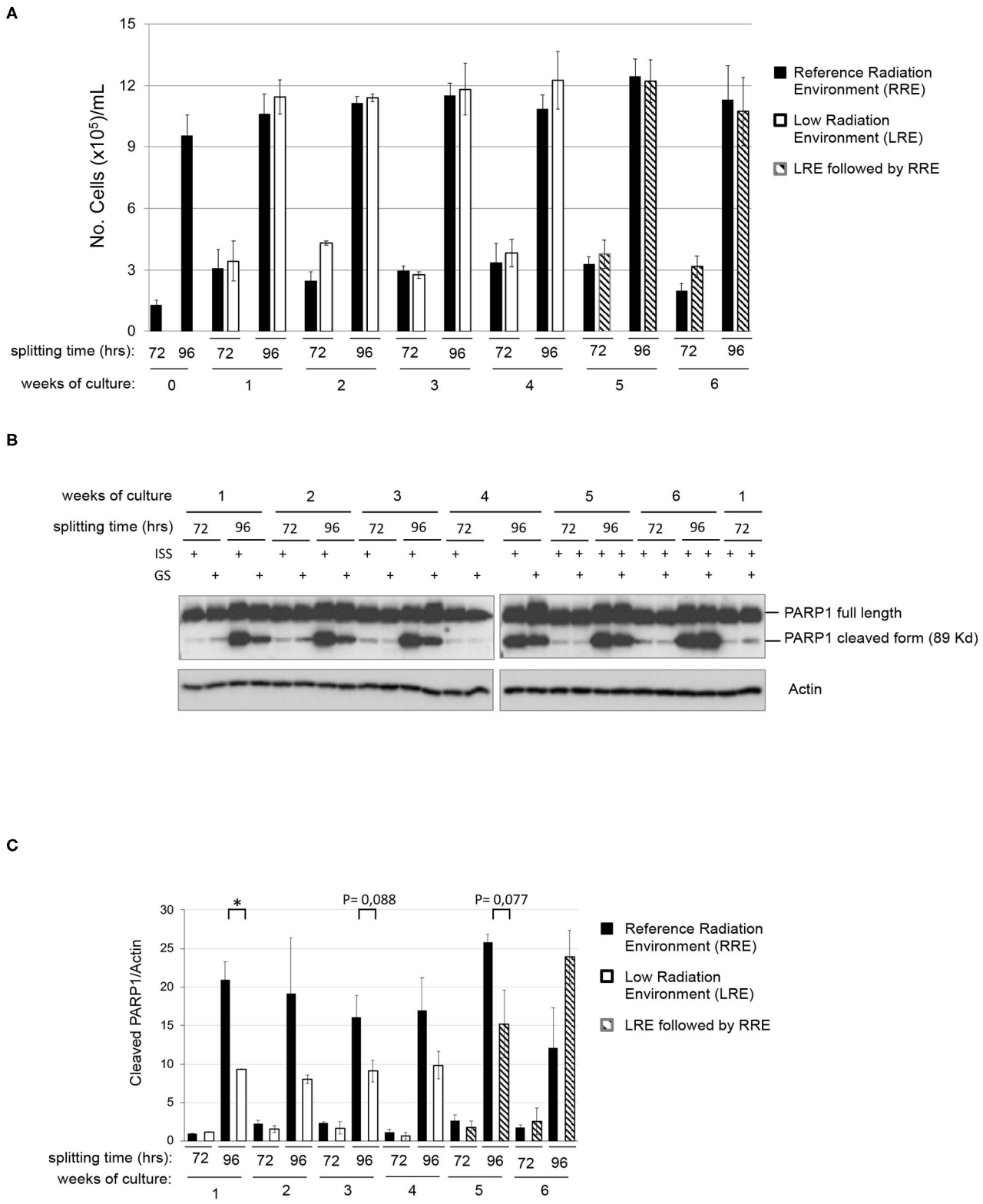

FIGURE 2 | Effects of low radiation environment on pKZ1 A11 mouse hybridoma cell proliferation and overgrowth-induced apoptosis. **(A)** A twin culture of pKZ1 A11 mouse hybridoma cells was set up in quadruplicate at the ISS reference laboratory in Rome and at the Gran Sasso underground laboratory. Cells were counted and

(Continued)

FIGURE 2 | split twice a week (after 72 h and after 96 h) for 4 weeks. After 4 weeks of underground cell growth, cells were moved to the ISS-Rome reference lab and grown for additional 2 weeks (weeks 5 and 6). Each cell culture was counted in triplicate. Values are means ± SD. **(B)** Western blots showing PARP1 cleavage in pKZ1 A11 mouse hybridoma cells grown as in **(A)**. ISS, Istituto Superiore di Sanità, RRE; GS, Gran Sasso National Laboratory, LRE. **(C)** Densitometric analysis of anti-PARP1 western blots. Values are means of two independent experiments ± SD. $^*P < 0.05$.

component of the radiation spectrum by a factor of about four. As shown in **Figure 4A**, proliferation of pKZ1 A11 cells was very similar in both conditions. In addition, in presence or absence of iron shielding, a globally comparable protein expression of phospho-p53, PARP1 cleavage and caspase 3 activation, and LC3-II induction was observed (**Figures 4B,C**), suggesting a negligible role of the gamma component in such cell responses and behavior.

DISCUSSION

In the last two decades, several efforts have been made by researchers to clarify the roles of low environmental radiations on cell response to stress stimuli. The linear no-threshold (LNT) model was first used in the radioprotection field to predict cell and DNA damage induced by ionizing radiation (Ann. ICRP, 2007). Several studies have, indeed, shown that risk assessment for low radiation dose does not follow a linear curve (29). Interestingly, Non-Target Effects (NTEs) are particularly evident at low doses and include the role of cell communication and responses at the tissue and systemic levels. Among the NTEs, it is possible to highlight the genomic instability and the Bystander Effect (BE), which seem to have a role in increasing the risk of developing cancer above the estimates made by extrapolation of the LNT model, and the Adaptive Response (AR), which, on the contrary, would be a protection against the development of cancer (30). In any case, a common feature of these phenomena is, however, the lack of dose linearity (31). Therefore, shedding light on the molecular mechanisms underlying cell response to low doses of radiation is particularly relevant in the radioprotection field.

In this work, we showed that cells grown in a LRE at the underground Gran Sasso National Laboratory (LNGS) of the Italian Institute of Nuclear Physics (INFN) display a qualitatively different response to stress induced by overgrowth, condition characterized by nutrient and growth factor deprivation, pH changes of medium, higher oxygen need and consumption. We did not find any difference in the growth of cells cultured in LRE compared to cells cultured in the RRE laboratory. On the other hand, after 96 h of growth in RRE, we noted an increase of PARP1 cleavage. This was described as an early marker of apoptosis (21). Interestingly, we observed a switch from apoptosis toward autophagy in LRE cultured cells, which appears to be mediated by p53.

Autophagy is an evolutionarily conserved catabolic pathway involved in many physiological and pathological mechanisms. It induces lysosomal degradation and recycling of non-functional cytoplasm components or organelles, generating substrates which promote stress adaptation and survival. However, autophagy is not intended as just a protective mechanism, as it can lead to an autophagy-associated and autophagy-mediated death, where autophagy occurs by accompanying or inducing apoptosis, or to an autophagy-dependent cell death, which is independent of both apoptosis and necrosis processes (32–34). Nevertheless, molecular mechanisms at the base of connections between autophagy, cell death, and cell fate decision are still unrevealed. Autophagy is increased by cell stress (e.g., DNA damage, hypoxia, starvation, or growth factor deprivation) and depends on complicated signaling networks which include mediators of relevant cell responses, such as p53, NF-κB, and STAT3 (35). It has been described that, in cancer, autophagy provides a sort of self-eating process to recruit nutrients in a condition where they become unavailable (36). Several studies indicate that stress can induce autophagy through two ways: an early response which takes place within minutes to hours and is essentially mediated by protein post-translational modifications, and a second, delayed response, which is based on specific activation of transcription (37). Moreover, an interesting relationship between p53 and autophagy has been reported, based on the use of *in vitro* and *in vivo* preclinical models (26): whereby autophagy can suppress p53 and p53 can activate autophagy. The tumor suppressor p53 usually acts as a tetrameric nuclear transcription factor, inducing genes coding for proteins involved in cell cycle arrest, apoptosis, or autophagy. On the other hand, it was described that cytoplasmic p53 can also promote cell death at the mitochondrial level and suppress autophagy (38). Furthermore, under stress conditions, p53 undergoes post-translation modifications able to avoid mdm-2-driven proteasomal degradation or, alternatively, mdm-2 can be degraded or sequestered by ARF, thus inhibiting the autophagic process. Ser392 is one of the highly conserved phospho-acceptor sites involved in p53 tumor-suppressor activities by enhancing p53 tetramers and DNA binding stabilization (39). Ser392 phosphorylation occurs not only after UV damage, but also after a range of different stimuli, such as etoposide, mdm-2 inhibitors or ionizing radiations (40). Since p53 is a well-known regulator of the apoptotic process too, further experiments will be needed to clarify, in particular, the specific signaling pathway and mechanisms through which p53 induces autophagy instead of apoptosis in our experimental settings.

Data here reported highlight different responses of cells reaching overgrowth stress conditions in RRE or LRE, respectively leading to apoptosis or autophagy, and characterized by the induction of specific mediators/markers involved in those pathways. Those novel results open to further investigations to examine in depth the molecular functional mechanisms specifically activated in RRE or LRE.

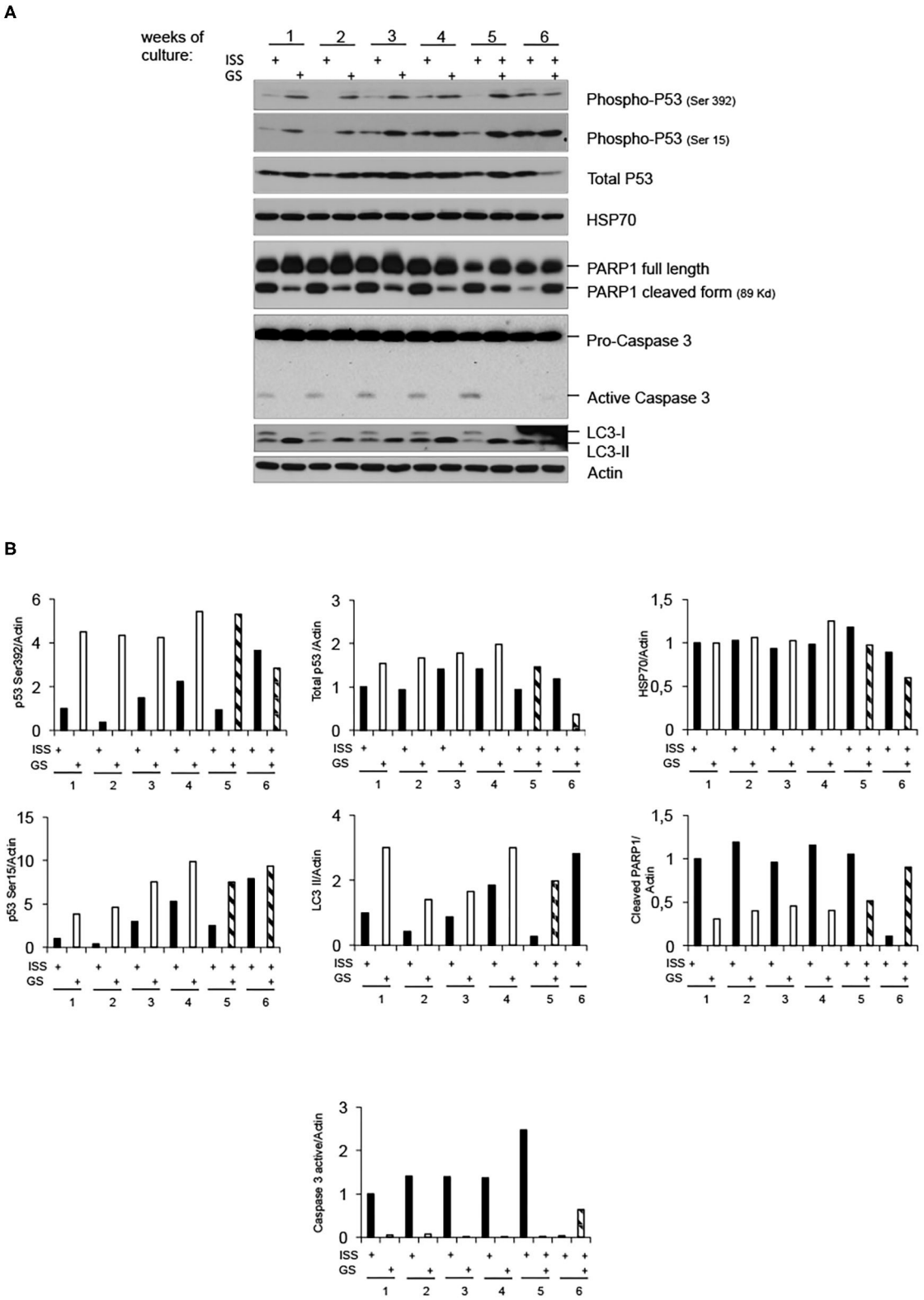

FIGURE 3 | Low radiation environment switches pKZ1 A11 mouse hybridoma overgrowth cell response from apoptosis toward autophagy. **(A)** Western blots showing activation of p53 and induction of LC3B-II in LRE (LNGS)-grown pKZ1 A11 mouse hybridoma cells and activation of PARP1 and caspase 3 in RRE (ISS) grown pKZ1 A11 mouse hybridoma cells. **(B)** Densitometry analysis of western blots shown in **(A)**.

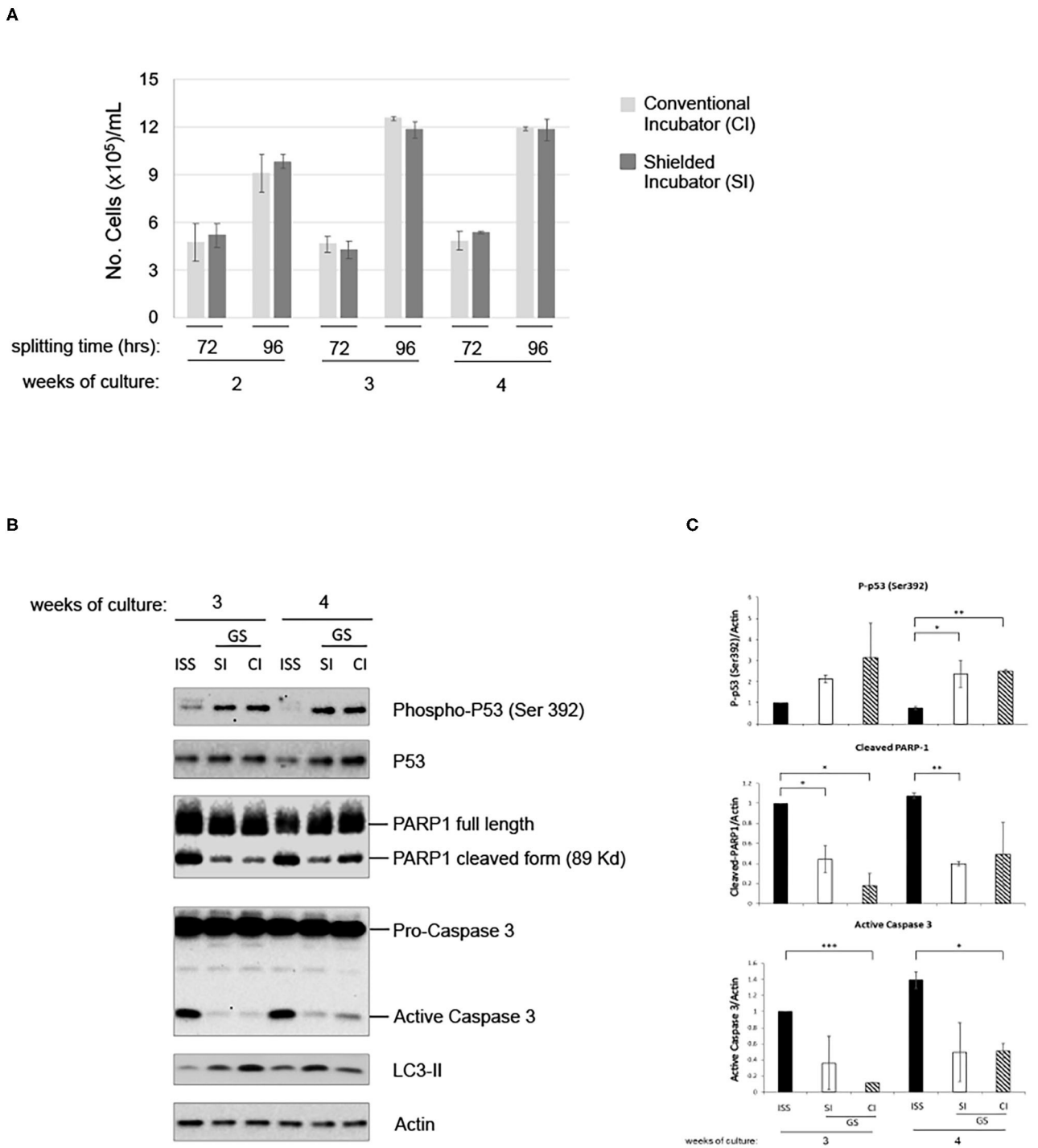

FIGURE 4 | Gamma radiation does not influence pKZ1 A11 mouse hybridoma cell response to overgrowth in low radiation environment. **(A)** Three cultures of pKZ1 A11 mouse hybridoma cells were set-up in quadruplicate and grown at the ISS reference laboratory in Rome (ISS) and at the Gran Sasso underground laboratory (GS) in a conventional incubator (CI) and in a γ-radiation shielded incubator (SI). Cells were counted and split twice a week (after 72 h and after 96 h) for 4 weeks. Cells were counted in triplicate. Values are means ± SD. **(B)** Cells grown as in **(A)** were collected after 3 and 4 weeks of cultures (at 96 h splitting time) and analyzed for apoptotic and autophagic markers by western blots. **(C)** Densitometric analysis of anti-P-p53 (Ser392), anti-PARP1, anti-caspase3 western blots. Values are means of two different experiments ± SD. $^*P < 0.05$, $^{**}P < 0.005$, $^{***}P < 0.0005$.

In particular, our findings draw attention to a p53-mediated autophagic cell response in a condition of almost absence of environmental radiation (Gran Sasso National Laboratory) instead of the apoptotic response observed in normal radiation environment. This is particularly fascinating and leaves to hypothesize that environmental radiation levels at the Earth's surface might represent a constitutive low-level stress able to sensitize cells to a prompt response in case of different acute stresses, which could produce further propagation of DNA damage in the case of inefficiently induced apoptosis.

Of further interest is to understand the role of both low and high LET components, both present in the external environment, in determining the response of the biological system. To answer this question, experiments are ongoing at the LNGS, presently focused on the role of the gamma component in the biological response(s) of fruit flies.

DATA AVAILABILITY STATEMENT

The raw data supporting the conclusions of this article will be made available by the authors, without undue reservation.

AUTHOR CONTRIBUTIONS

MF, DVer, DVec, and DC performed the LRE experiments. EF and GE performed the RRE experiments. BD performed the western blot. MB and LI contributed to LRE experiments' setup. PS and LS conceived the study. AT analyzed the data, wrote, and revised the manuscript. FZ, MT, and EA conceived the study, elaborated data, and wrote and revised the manuscript. All authors contributed to the article and approved the submitted version.

FUNDING

MF and EF were funded by the Centro Studi e Ricerche Enrico Fermi, Rome. This work was supported by the INFN-CSN5 COSMIC SILENCE Experiment.

ACKNOWLEDGMENTS

The authors would like to thank LNGS and all technical Services for their skilled assistance and support for the experiments.

REFERENCES

1. Fratini E, Carbone C, Capece D, Esposito G, Simone G, Tabocchini MA, et al. Low-radiation environment affects the development of protection mechanisms in V79 cells. *Radiat Environ Biophys*. (2015) 54:183–94. doi: 10.1007/s00411-015-0587-4
2. Mothersill C, Seymour C. Radiation-induced bystander effects: evidence for an adaptive response to low dose exposures? *Dose-Response*. (2006) 4:283–90. doi: 10.2203/dose-response.06-111.Mothersill
3. Morgan WF. Radiation induced genomic instability. *Health Phys*. (2011) 100:280–1. doi: 10.1097/HP.0b013e3182082f12
4. Mothersill C, Rusin A, Seymour C. Low doses and non-targeted effects in environmental radiation protection; where are we now and where should we go? *Environ Res.* (2017) 159 484–90. doi: 10.1016/j.envres.2017.08.029
5. MACRO Collaboration, Ahlen SP, Ambrosio M, Auriemma G, Baldini A, Barbarino GC, et al. Study of penetrating cosmic ray muons and search for large scale anisotropies at the Gran Sasso Laboratory. *Phys Lett B*. (1990) 249:149–56. doi: 10.1016/0370-2693(90)90541-D
6. Rindi A, Celani F, Lindozzi M, Miozzi S. Underground neutron flux measurement. *Nucl Instrum Methods A*. (1988) 272:871–4. doi: 10.1016/0168-9002(88)90772-3
7. Satta L, Augusti-Tocco G, Ceccarelli R, Esposito A, Fiore M, Paggi P, et al. Low environmental radiation background impairs biological defence of the yeast Saccharomyces cerevisiae to chemical radiomimetic agents. *Mutat Res*. (1995) 347:129–33. doi: 10.1016/0165-7992(95)00031-3
8. Satta L, Antonelli F, Belli M, Sapora O, Simone G, Sorrentino E, et al. Influence of a low background radiation environment on biochemical and biological responses in V79 cells. *Radiat Environ Biophys*. (2002) 41:217–24. doi: 10.1007/s00411-002-0159-2
9. Carbone MC, Pinto M, Antonelli F, Amicarelli F, Balata M, Belli M, et al. The Cosmic Silence experiment: on the putative adaptive role of environmental ionizing radiation. *Radiat Environ Biophys*. (2009) 48:189–96. doi: 10.1007/s00411-008-0208-6
10. Hooker AM, Horne R, Morley AA, Sykes PJ. Dose-dependent increase or decrease of somatic intrachromosomal recombination produced by etoposide. *Mutation Res*. (2002) 500:117–24. doi: 10.1016/s0027-5107(02)00007-6
11. Capece D, Fratini E. The use of pKZ1 mouse chromosomal inversion assay to study biological effects of environmental background radiation. *Eur Phys J Plus.* (2012) 127:37. doi 10.1140/epjp/i2012-12037-7
12. Sykes PJ, Day TK, Swinburne SJ, Lane JM, Morley AA, Hooker AM, et al. *In vivo* mutagenic effect of very low dose radiation. *Dose Response*. (2006) 4:309–16. doi: 10.2203/dose-response.06-004.Sykes
13. Day TK, Zeng G, Hooker AM, Bhat M, Scott BR, Turner DR, et al. Extremely low priming doses of X radiation induce an adaptive response for chromosomal inversions in pKZ1 mouse prostate. *Radiat Res*. (2006) 166:757–66. doi: 10.1667/RR0689.1
14. Sykes PJ, Morley AA, Hooker AM. The PKZ1 recombination mutation assay: a sensitive assay for low dose studies. *Dose Response*. (2006) 4:91–105. doi: 10.2203/dose-response.05-035.Sykes
15. Zeng G, Day TK, Hooker AM, Blyth BJ, Bhat M, Tilley WD, et al. Non-linear chromosomal inversion response in prostate after low dose X-radiation exposure. *Mutat Res*. (2006) 602:65–73. doi: 10.1016/j.mrfmmm.2006.08.002
16. Sykes PJ, Day TK. Requirements for identification of low dose and non-linear mutagenic responses to ionising radiation. *Dose Response*. (2007) 5:308–14. doi: 10.2203/dose-response.07-018.Sykes
17. Day TK, Zeng G, Hooker AM, Bhat M, Turner DR, Sykes PJ. Extremely low doses of X-radiation can induce adaptive responses in mouse prostate. *Dose Response*. (2007) 5:315–22. doi: 10.2203/dose-response.07-019.Day
18. Day TK, Zeng G, Hooker AM, Bhat M, Scott BR, Turner DR, et al. Adaptive response for chromosomal inversions in pKZ1 mouse prostate induced by low doses of X radiation delivered after a high dose. *Radiat Res*. (2007) 167:682–92. doi: 10.1667/RR0764.1
19. Ormsby RJ, Staudacher AH, Blyth BJ, Bezak E, Sykes PJ. Temporal responses to X-radiation exposure in spleen in the pKZ1 mouse recombination assay. *Radiat Res*. (2016) 185:623–9. doi: 10.1667/RR14390.1
20. Bannister L, Serran M, Bertrand L, Klokov D, Wyatt H, Blimkie M, et al. Environmentally relevant chronic low-dose tritium and gamma exposures do not increase somatic intrachromosomal recombination in pKZ1 mouse spleen. *Radiat Res*. (2016) 186:539–48. doi: 10.1667/RR14564.1
21. Kaufmann SH, Desnoyers S, Ottaviano Y, Davidson NE, Poirier GG. Specific proteolytic cleavage of poly(ADP-ribose) polymerase: an early marker of chemotherapy-induced apoptosis. *Cancer Res.* (1993) 53:3976–85.
22. Tewari M, Quan LT, O'Rourke K, Desnoyers S, Zeng Z, Beidler DR, et al. Yama/CPP32 beta, a mammalian homolog of CED-3, is a CrmAinhibitable protease that cleaves the death substrate poly (ADP-ribose) polymerase. *Cell*. (1995) 81:801–9. doi: 10.1016/0092-8674(95)90541-3
23. Fischer U, Janicke RU, Schulze-Osthoff K. Many cuts to ruin: a comprehensive update of caspase substrates. *Cell Death Differ*. (2003) 10:76–100. doi: 10.1038/sj.cdd.4401160

24. Aubrey BJ, Kelly GL, Janic A, Herold MJ, Strasser A. How does p53 induce apoptosis and how does this relate to p53-mediated tumour suppression? *Cell Death Differ*. (2018) 25:104–13. doi: 10.1038/cdd.2017.169
25. Fischer M. Census and evaluation of p53 target genes. *Oncogene*. (2017) 36:3943–56. doi: 10.1038/onc.2016.502
26. White E. Autophagy and p53. *Cold Spring Harb Perspect Med*. (2016) 6:a026120. doi: 10.1101/cshperspect.a026120
27. Tanida I, Minematsu-Ikeguchi N, Ueno T, Kominami E. Lysosomal turnover, but not a cellular level, of endogenous LC3 is a marker for autophagy. *Autophagy*. (2005) 1:84–91. doi: 10.4161/auto.1.2.1697
28. Tanida I, Takashi U, Kominami E. LC3 and autophagy. *Methods Mol Biol*. (2008) 445:77–88. doi: 10.1007/978-1-59745-157-4_4
29. Mullenders L, Atkinson M, Paretzke H, Sabatier L, Bouffler S. Assessing cancer risks of low-dose radiation. *Nat Rev Cancer*. (2009) 9:596–604. doi: 10.1038/nrc2677
30. Tubiana M. Radiation risks in perspective: radiation-induced cancer among cancer risks. *Radiat Environ Biophys*. (2000) 39:3–16. doi: 10.1007/pl00007682
31. Mothersill C, Seymour C. Radiation-induced non-targeted effects of low doses-what, why and how? *Health Phys*. (2011) 100:302. doi: 10.1097/hp.0b013e3182080f0c
32. Yonekawa T, Thorburn A. Autophagy and cell death. *Essays Biochem*. (2013) 55:105–17. doi: 10.1042/bse0550105
33. Bialik S, Dasari SK, Kimchi A. Autophagy-dependent cell death—where, how and why a cell eats itself to death. *J Cell Sci*. (2018) 131:jcs215152. doi: 10.1242/jcs.215152
34. Denton D, Kumar S. Autophagy-dependent cell death. *Cell Death Differ*. (2019) 26:605–16. doi: 10.1038/s41418-018-0252-y
35. Verzella D, Pescatore A, Capece D, Vecchiotti D, Ursini MV, Franzoso G, et al. Life, death, and autophagy in cancer: NF-kB turns up everywhere. *Cell Death Dis*. (2020) 11:210. doi: 10.1038/s41419-020-2399-y
36. Lacroix M, Riscal R, Arena G, Linares LK, Le Cam L. Metabolic functions of the tumor suppressor p53: Implications in normal physiology, metabolic disorders, and cancer. *Mol Metab*. (2020) 33:2–22. doi: 10.1016/j.molmet.2019.10.002
37. Pietrocola F, Izzo V, Niso-Santano M, Vacchelli E, Galluzzi L, Maiuri MC, et al. Regulation of autophagy by stress-responsive transcription factors. *Semin Cancer Biol*. (2013) 23:310–22. doi: 10.1016/j.semcancer.2013.05.008
38. Maiuri MC, Galluzzi L, Morselli E, Keep O, Malik SA, Kroemer G. Autophagy regulation by p53. *Curr Opin Cell Biol*. (2010) 22:181–5. doi: 10.1016/j.ceb.2009.12.001
39. MacLaine NJ, Hupp TR. How phosphorylation controls p53. *Cell Cycle*. (2011) 10:916–21. doi: 10.4161/cc.10.6.15076
40. Cox ML, Meek DW. Phosphorylation of serine 392 in p53 is a common and integral event during p53 induction by diverse stimuli. *Cell Signal*. (2010) 22:564–71. doi: 10.1016/j.cellsig.2009.11.014

Conflict of Interest: The authors declare that the research was conducted in the absence of any commercial or financial relationships that could be construed as a potential conflict of interest.

Advantages of publishing in Frontiers

OPEN ACCESS
Articles are free to read for greatest visibility and readership

FAST PUBLICATION
Around 90 days from submission to decision

HIGH QUALITY PEER-REVIEW
Rigorous, collaborative, and constructive peer-review

TRANSPARENT PEER-REVIEW
Editors and reviewers acknowledged by name on published articles

Frontiers
Avenue du Tribunal-Fédéral 34
1005 Lausanne | Switzerland

Visit us: www.frontiersin.org
Contact us: frontiersin.org/about/contact

REPRODUCIBILITY OF RESEARCH
Support open data and methods to enhance research reproducibility

DIGITAL PUBLISHING
Articles designed for optimal readership across devices

FOLLOW US
@frontiersin

IMPACT METRICS
Advanced article metrics track visibility across digital media

EXTENSIVE PROMOTION
Marketing and promotion of impactful research

LOOP RESEARCH NETWORK
Our network increases your article's readership